Design, Fabrication and Applications of Soft and Crystalline Metal-Organic Materials

Ph.D. Thesis

By

NOVINA MALVIYA

DISCIPLINE OF CHEMISTRY

INDIAN INSTITUTE OF TECHNOLOGY INDORE

APRIL 2019

Design, Fabrication and Applications of Soft and Crystalline Metal-Organic Materials

A THESIS

Submitted in partial fulfillment of the
requirements for the award of the degree
of
DOCTOR OF PHILOSOPHY

by

NOVINA MALVIYA

DISCIPLINE OF CHEMISTRY
INDIAN INSTITUTE OF TECHNOLOGY INDORE
APRIL 2019

INDIAN INSTITUTE OF TECHNOLOGY INDORE

CANDIDATE'S DECLARATION

I hereby certify that the work which is being presented in the thesis entitled **DESIGN, FABRICATION AND APPLICATIONS OF SOFT AND CRYSTALLINE METAL-ORGANIC MATERIALS** in the partial fulfillment of the requirements for the award of the degree of **DOCTOR OF PHILOSOPHY** and submitted in the **DISCIPLINE OF CHEMISTRY, Indian Institute of Technology Indore**, is an authentic record of my own work carried out during the time period from **July 2014** to **April 2019** under the supervision of Dr. Suman Mukhopadhyay, Professor, Discipline of Chemistry, Indian Institute of Technology Indore.

The matter presented in this thesis has not been submitted by me for the award of any other degree of this or any other institute.

signature of the student with date
(NAME OF THE PhD STUDENT)

This is to certify that the above statement made by the candidate is correct to the best of my/our knowledge.

Signature of Thesis Supervisor #1 with date
(NAME OF THESIS SUPERVISOR)

Signature of Thesis Supervisor #2 with date
(NAME OF THESIS SUPERVISOR)

MS. NOVINA MALVIYA has successfully given his/her Ph.D. Oral Examination held on **<Date of PhD Oral Examination>**.

Signature of Chairperson (OEB)
Date:

Signature of External Examiner
Date:

Signature(s) of Thesis Supervisor(s)
Date:

Signature of PSPC Member #1
Date:

Signature of PSPC Member #2
Date:

Signature of Convener, DPGC
Date:

Signature of Head of Discipline
Date:

ACKNOWLEDGEMENTS

I am grateful to God Almighty for the blessings and for giving me the strength and wisdom to achieve this dream. I dedicate this work to my beloved parents and brother, who are the persons of motivation and with their encouragement, initiated this research venture.

This doctoral thesis is in its current form due to the assistance and encouragement of several people. It is a pleasure to express my sincere thanks to all those who helped me for the success of this study and made it an unforgettable experience.

First and foremost, I am fortunate to express my sincere heartfelt thanks and deepest gratitude to my supervisor Professor Suman Mukhopadhyay for his constant encouragement, support, understanding, care, and guidance throughout my work. I am grateful for his attention to the smallest detail of my thesis and ensuring the sheer perfection of a doctoral thesis. I appreciate his politeness, simplicity, and art of feeding knowledge patiently to bring out the researching capability and deliver my research product successfully all through the endeavor. I will always cherish the valuable lessons and suggestions received from him.

I wish to express my gratitude to Prof. Pradeep Mathur, Director, IIT Indore, for his continuous support in every aspect. I would like to thanks to IIT Indore and Ministry of Human Resource Development (MHRD) for financial support during my Ph.D. I am grateful to Sophisticated Instrument Centre (SIC), IIT Indore for instrumentation facility. I express my sincere thanks to my PSPC members Dr. Biswarup Pathak and Dr. Rajesh Kumar for their valuable suggestions and guidance. I would like to thank my collaborators, Dr. Rakesh Ganguly, Dr. Shaikh M Mobin, and Dr. Krishna Pada Bhabak, for their active supports for solid-state characterization and computational study. I would like to thank all faculty members of the Discipline of Chemistry, IIT Indore for their guidance and help during various activities. I am also thankful for the support received from all the teaching and non-teaching staff. I would also thanks to Ms. Sarita Batra, Mr. Kinny Pandey, Mr. Nitin, Mr. Ghanshyam Bhavsar, Rameshwar Dohare, and Mr. Manish Kushwaha.

It has been a wonderful experience to work with many friends at IIT Indore during my Ph.D. who really helped me in many aspects. I personally extend my hearties gratitude to my senior Dr. Rajender Nasani and my friend Mr. Pramod Kumar Gavel for their constant guidance, help, and support at all ups and downs during my Ph.D.

I am thankful to my former and present group members Dr. Rajender Nasani, Dr. Komal Vyas, Dr. Manideepa Saha, Dr. Mriganka Das, Dr. Poulami Mandal, Mr. Bidyut Kumar Kundu, Ms. Chanchal Sonkar, Mr. Rishi Ranjan, Ms. Reena Kyarikwal, Ms. Pragti Porwal, Mr. Kripa Shankar Pandey, Mr. Arun Kumar, Ms. Mahima Rajput, Mr. Nitish. I would personally like to extend my sincere thanks to my room-mate cum friend Ms. Priyanka Garg, who was always there whenever required and never let me down during these Ph.D. days. I would also like to express my heartiest gratitude to my friends Ms. Swati Choubey, Dr. Kuber Singh Rawat, Ms. Kavita Soni, Dr. Yuvraj Patil, Dr. Ambikesh Dwivedi, Ms. Shikha Khandelwal, Mr. Suresh Mali, Ms. Vijay Laxmi Pandey, Ms. Chinky Binnani, Ms. Anubha Yadav, Ms. Pratibha Kumari, Mr. Amit Pandit, Mr. Siddarth Jain. I am also thankful to Dr. Anupam Das, Dr. Bhagwati Sharma, Dr. Thaksen Jadhav, Dr. Arpan Bhattacharya, Dr. Kavita Gupta, Mr. Sourabh Kumar, Mr. Soumya Kanti De, Mr. Mahendra Awasthi, Ms. Jamuna Vaishnav, Mr. Sandeep Das, Mr. Vikash Mishra for their generous cooperation and help.

I would like to take this opportunity to express my respect, love and gratitude to especially my teacher Mr. Satish Jaiswal and all other teachers from my School Jawahar Navodaya Vidyalaya, Khargone and my college School of Chemical Science, DAVV, Indore.

Most importantly, none of this would have been possible without the support of my family. I am extremely fortunate to have such caring and loving parents, Mr. B. L. Malviya and Mrs. Rekha Malviya and supportive brother, Mr. Tushar Malviya. My dream of completing this work would not have blossomed without their wholehearted support, sacrifice, and prayers. They deserve special mention for providing me with all the opportunities to explore my potentials and pursue my dreams ever since I was a child.

Finally, I would like to thanks all others who helped and supported me directly or indirectly.

Dedicated to

My Beloved Parents

and

Elder Brother

ABSTRACT

Serendipitous formation of many gel-based materials with possibility of versatile applications initiated significant efforts to rationally design molecules with gelation ability to understand the gelation mechanism. Many π-conjugated gelators form gels after self-assembly, which involves certain non-covalent interactions between the molecules but the synthesis of π-conjugated gelators is challenging to the environment. To overcome these challenges, supramolecular chemistry has gained extensive importance as an alternative approach for designing π-conjugated molecules. It is evident that the design and fabrication of low molecular weight (LMW) (M<3000 Da) gels is the best bottom-up approach for the formation of gel materials. LMW gels have non-covalent interactions with low binding strength, which can restrain high amounts of solvents. The mechanical strength of LMW gels is quite different because of the involvement of the weak bonds than polymeric gels (covalent bond) which indicates several advantages such as thermo-reversible nature, hierarchical aggregates structured by the spontaneous organization of small molecules with probability to tailor the gel properties. Introduction of metal ions in gel materials opens the possibility for more diverse structures and versatile applications.

To date, the development of BTA and tetrazole based crystalline and soft metal-organic materials are in great demand due to their unique behavior like aggregate induced enhanced emission (AIEE), swelling capacity, and self-healing property. So, these kinds of molecules can be exploited to generate smart materials to apply as materials to biology.

This thesis work includes the LMW gelators based on:

- ✓ Nitrile derivatives of BTA
- ✓ Tetrazole derivatives
- ✓ Transition and inner-transition metallogels based on nitrile derivatives of BTA and tetrazole derivatives

The objective of the present work is to design and fabricate LMW based soft and crystalline metal-organic materials which can be explored for a range of applications in various inter-disciplinary areas.

Summary of research work

The contents of each chapter included in the thesis are discussed briefly as follows:

Chapter 1: General Introduction and Background

A brief insight and recent scientific development towards the designing, fabrication, and properties of LMW gelators and their soft and crystalline metal-organic materials. Although, introduced about their potential applications in various inter-disciplinary areas. Finally, a brief summary of the research work reported in this thesis and the relevance in the prospects of recent development have been put forward.

Chapter 2: A Smart Organic Gel Template as Metal Cation and Inorganic Anion Sensor

In this report, synthesis and characterization of a smart carboxamide based gelator *N1*, *N3*,*N5*-tris(4-cyanophenyl)benzene-1,3,5-tricarboxamide (**G1**) with additional coordination binding sites have been reported. The gelator molecule can form supramolecular organogel in the presence of water in DMF or DMSO. The gel thus formed has shown intense aggregation-induced enhanced emission (AIEE). The synthesized gel can selectively sense $\mathbf{Fe^{2+}}$ and $\mathbf{Fe^{3+}}$ by completely switching off the AIEE. Furthermore, upon induction of several metal ions, the formation of different metallogels (MGs) has been observed. Among them, **Cu(II)G1** can sense $\mathbf{SCN^-}$, **Zn(II)G1** can sense $\mathbf{Br^-}$, **Ni(II)G1** can sense $\mathbf{CN^-}$ and **Fe(II)G1/ Fe(III)G1** can sense $\mathbf{S^{2-}}$, selectively, by an abrupt change in the fluorescence property of the metallogels with high selectivity and sensitivity (Figure 1).

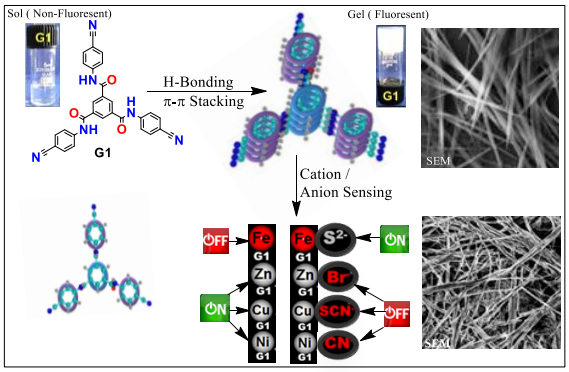

Figure 1. *Gelator* ***G1*** *and the selective sensing of cation and anion by abrupt change in aggregation-induced fluorescence enhanced emission (AIEE).*

Chapter 3: Discotic Organic Gelators in Ion Sensing, Metallogel Formation, and Bioinspired Catalysis

Herein, the synthesis and gelation property of two isomeric carboxamides, nitrile-based gelators *N1*, *N3*, *N5*-tris(3-cyanophenyl)benzene-1,3,5-tricarboxamide (**G2**) and *N1*, *N3*, *N5*-tris(2-cyanophenyl)benzene-1,3,5-tricarboxamide (**G3**) have been reported. Gelator **G2** has shown exquisite sensing property toward certain cations (**Ag^{+}**, **Fe^{2+}**, and **Fe^{3+}**) by switching off the aggregation-induced enhanced emission (AIEE). The **G3** organogel shows a similar behavior with the **Fe^{2+}** ion. Remarkably, the formation of metallogels such as **Ni(II)G2** and **Co(II)G2** leads to selective sensing of **sulfide ion** and **Cu(II)G2** has been found effective for sensing of **iodide ion** by switching off the fluorescence even in multianalyte conditions. Also, the copper-based metallogel [**Cu(II)G2**] mimics as a bio-inspired catalyst for the conversion of catechol to quinone by aerobic oxidation in the gel state at room temperature and pressure (Figure 2).

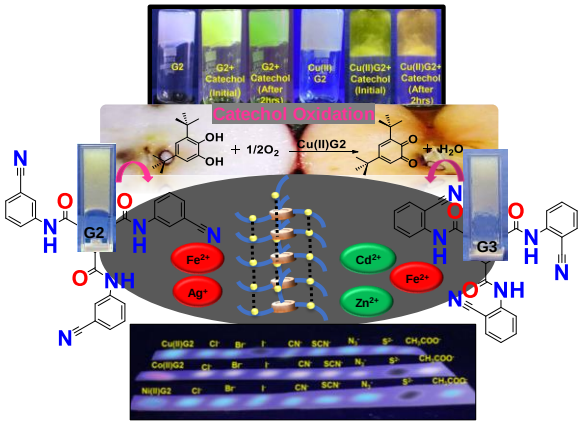

Figure 2. *Self-Assembled Gelators **G2** and **G3** and various applications.*

Chapter 4: **Cobalt Metallogel Interface for Selectively Sensing L-Tryptophan among Essential Amino Acids**

A cobalt-based metallogel has been designed and synthesized utilizing the gelator *N1*, *N3*,*N5*-tris(4-cyanomethyl-phenyl)benzene-1,3,5-tricarboxamide **G4**. The compound **G4** has been successfully crystallized**,** and various non-covalent interactions in the solid state have been explored through X-ray crystallographic study. Application of the cobalt metallogel interface has been explored as it can sense L-tryptophan selectively in a gel

state by drastic quenching of AIEE. Interestingly, the cobalt-based metallogel can also sense tryptophan amino acid residue present in a complex structure like BSA protein which is observable even by naked eyes. This work also reports the role of water as a solvent in sol-gel transformation. These experimental findings have the potential to become a facile, robust and cost-effective approach for tryptophan sensing in the various areas of material chemistry to biology (Figure 3).

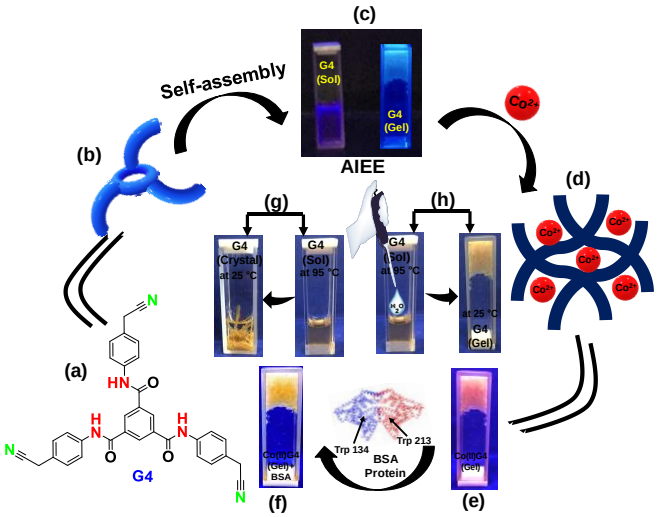

Figure 3. *Colorimetric sensing of L-tryptophan by* ***Co(II)G4****: the role of water in transition between Sol-Gel & Crystal of* ***G4*** *gelator. [(a) Chemical structure of* ***G4****. (b) Pictorial representation of* ***G4****. (c) Image of AIEE of* ***G4*** *gelator after self-assembly under UV light. (d) Self-assembly of* ***Co(II)G4*** *(e) Optical photograph of* ***Co(II)G4****. (f) Optical photograph of* ***Co(II)G4+BSA*** *protein lead to colorimetric change. (g) Cooling of* ***G4*** *solution leads to the crystallization. (h) Addition of water into* ***G4*** *solution leads to the gel formation at room temperature].*

Chapter 5: Novel Approach to Generate Self-Deliverable Anticancer Ru(II) agent in the Self-Reacting Confined Gel Space

D**e**signing and synthesis of 3,5-bis((4-cyanoethyl)phenyl)carbonyl)benzoic acid (**G5**) gelator and methyl 3,5-bis((4-cyanoethyl)phenyl)carboxyl benzoate (**Me-G5'**) where **G5'**= G5-H have been contemplated and accomplished. **G5** gelator has been used for the formation of ruthenium-based metallogel [**Ru(II)G5**] and utilized as a self-deliverable anticancer drug through collapsing of the gel by pH variation (Figure 4).

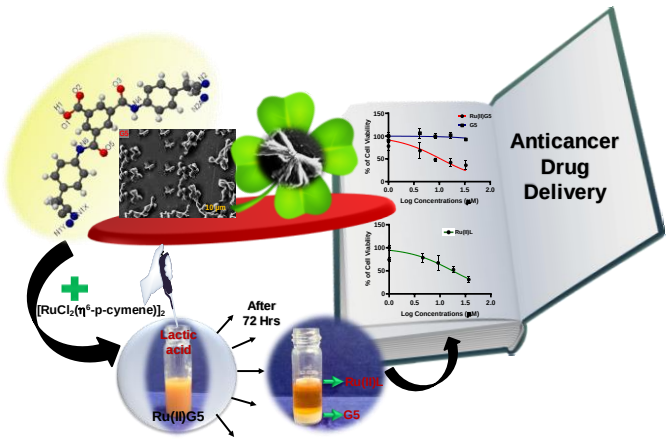

Figure 4. *Clover leaf-like morphology of* ***G5,*** *formation of ruthenium-based metallogel with* ***G5****, conversion of ruthenium [****$Ru_2(p\text{-}cym)_2Cl_4$****] complex in gel phase and delivery of the ruthenium-Drug [****Ru(II)****L] in the cancerous cell through gel collapse in the presence of lactic acid, anticancer cell cytotoxicity.*

Chapter 6: Self-Healable Lanthanoid Based Photoluminescent Metallogel and Confined Gel Space Crystallization

In this work design and synthesis of lanthanoids based metallogels *viz*. [**La(III)G6-Cl**, **La(III)G6-NO3**, **Pr(II)G6-Cl**, **Gd(III)G6-NO_3**] have been performed by using di(1*H*-tetrazole-5-yl) methane (**G6**). Interestingly **La(III)G6-Cl** metallogel has shown self-healing property. Furthermore, it is noteworthy to mention that the single crystals of gadolinium tetrazole complex have been obtained from the metallogel stage of **Gd(III)G6-NO_3** and the solid state molecular structure of the metallogel have been elucidated (Figure 5).

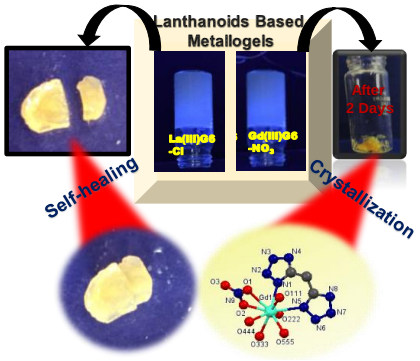

Figure 5. *Photoluminescent lanthanoid based metallogels, their self-healing property and crystallization from Confined metallogel space.*

Chapter 7: Nickel Tetrazolato Complexes Synthesized by Microwave Irradiation: Catecholase Like Activity and Interaction with Biomolecules

In this work two tetrazole based nickel complexes [NiL(5-phenyltetrazolato)] (**complex 1**) and [NiL{5-(4-pyridyl)-tetrazolato}] (**complex 2**) [HL = 3-(2-diethylamino-ethyl imino)-1-phenyl-butan-1-one] have been synthesized by microwave irradiation. These metal tetrazole complexes show protein binding and bioinspired catechol oxidation (Figure 6).

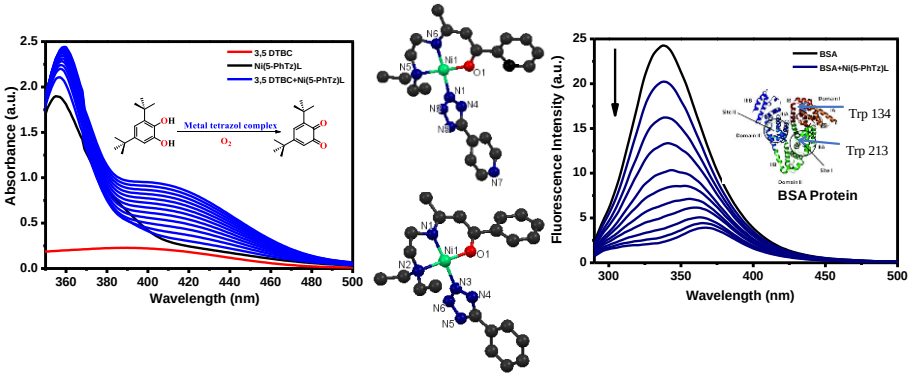

Figure 6. *Nickel tetrazole complex interacts with proteins and bioinspired catechol oxidation.*

Chapter 8: General Conclusions

In this thesis work, synthesized LMW soft and crystalline metal-organic materials have shown AIEE property and Self-healing property which permit their utilization in sensing of cations, anions, biomolecules, and as smart self-healing materials. Introduction of metal ions in gels make them suitable to explore for bioinspired catalysis, anticancer properties, and efficient drug-delivery system.

LIST OF PUBLICATIONS

Publications from Ph.D. thesis work:

1. **Malviya N.**, Sonkar C., Ganguly R., Mukhopadhyay S. (2019), Cobalt Metallogel Interface for Selectively Sensing L-Tryptophan among Essential Amino Acids *Inorg. Chem.*, 58, 7324-7334 (10.1021/acs.inorgchem.9b00455)
2. **Malviya N.**, Sonkar C., Kundu B. K., Mukhopadhyay S. (2018), Discotic Organic Gelators in Ion Sensing, Metallogel Formation and Bioinspired Catalysis, *Langmuir*, 25, 8451-8456 (DOI: 10.1021/acs.langmuir.8b02352)
3. **Malviya N.**, Das M.; Mandal P., Mukhopadhyay S. (2017), A Smart Organic Gel Template as Metal Cation and Inorganic Anion Sensor, *Soft Matter*, 13, 6243-6249. (**Impact factor** 3.89) (DOI: 10.1039/C7SM01199G)
4. **Malviya N.**, Mondal P., Das M., Ganguly R., Mukhopadhyay S. (2017), Nickel tetrazolato complexes synthesized by microwave irradiation: catecholase like activity and interaction with biomolecules, *J. Coord. Chem.*, 70, 261-278 (DOI: 10.1080/00958972.2016.1260121)
5. **Malviya N.**, Sonkar C., Ganguly R., Bhattacherjee D., Bhabak K., Mukhopadhyay S., Novel Approach to Generate Self-Deliverable Anticancer Ru(II) agent in the Self-Reacting Confined Gel Space (Manuscript submitted)
6. **Malviya N.**, Shaikh M Mobin., Mukhopadhyay S. Self-Healable Lanthanoid Based Photoluminescent Metallogel and Confined Gel Space Crystallization (Manuscript submitted)

Other publications during Ph.D.:

7. **Malviya N.**, Rajput M., Nasani R., Fluorometric determination of solvent percentage and solvent sensing by 2-aminobenzonitrile derivatives and their cobalt complex template for selective sensing of sulfide ion (Manuscript under preparation)
8. Mukhopadhyay S.; Kundu B. K.; **Malviya N.**, Tetrazoles as versatile ligands: from materials to biology (Review article submitted)
9. Kundu B. K., Chhabra V., **Malviya N.**, Ganguly R., Mishra G. S, Mukhopadhyay S. (2018), Zeolite encapsulated host-guest Cu(II) Schiff base complexes: superior

activity towards oxidation reactions over homogenous catalytic systems, *Microporous Mesoporous Mater.*, 271, 100-117 (DOI: 10.1016/j.micromeso.2018.05.046)

10. Mandal P., **Malviya N.**, Kundu B. K., Dhankhar S. S., Nagaraja C. M., Mukhopadhyay S. (2018), RAPTA complexes containing N-substituted tetrazole scaffolds: synthesis, characterization and antiproliferative activity, *Appl. Organomet. Chem*., 32**,** 4179 (DOI: 10.1002/aoc.4179)

11. Saha M., **Malviya N.**, Das M., Choudhuri I., Mobin S. M., Pathak B., Mukhopadhyay S. (2017), Effect on catecholase activity and interaction with biomolecules of metal complexes containing differently tuned 5-substituted ancillary tetrazolato ligands, *Polyhedron*, 121, 155-171 (DOI: 10.1016/j.poly.2016.09.035)

12. Mandal P., **Malviya N.**, Guedes da Silva M. F. C., Dhankhar S. S., Nagaraja C. M., Mobin S. M., Mukhopadhyay S. (2016), Fine tuning through valence bond tautomerization of ancillary ligand in ruthenium(II) arene complex for better anticancer activity and enzyme inhibition property, *Dalton Trans*., 45, 19277-19289 (DOI: 10.1039/C6DT02969H)

13. Das M., Mandal P., **Malviya N.**, Choudhuri I., Charmier M. A. J., Morgado S., Mobin S. M., Pathak B., Mukhopadhyay S. (2016), Copper complexes with flexible piperazinyl arm: nuclearity driven catecholase activity and interactions with biomolecules, *J. Coord. Chem.*, *69*, 3619-3637 (DOI: 10.1080/00958972.2016.1236193)

LIST OF CONFERENCES

1. Oral presentation in CHEM 2019 In-House Chemistry Symposium organized by IIT Indore, February 28, 2019.
2. Poster presentation in IIT Indore-RSC Symposium on Advances in Chemical Sciences, held at IIT Indore, India on 30th January 2018.
3. GIAN Course entitled "Metal-Ligand Interplay in Advance Coordination Chemistry" From February 5-9, 2018.
4. Poster presentation in EuCheMS Inorganic Chemistry Conference (EICC-4) **Copenhagen**, **Denmark** July 2-5, 2017.
5. Poster presentation in 6th International Conference on Metals in Genetics, Chemical Biology and Therapeutics (ICMG-2016), held in IISc Bangalore.
6. Attend Symposium on "Advances in Chemistry with Biological and Industrial Relevance" organized by MP Council of Science and Technology (MPCST) at B.M. College Indore, February 1, 2016.
7. Participated in Workshop on "Intellectual Property Rights" organized by MP Council of Science and Technology (MPCST) at B.M. College Indore, September 22, 2015.
8. Participated in one-day "Researcher Connect Program" organized by Wiley in collaboration with Indian Institute of Technology Indore on October 26, 2015.
9. Participated in "National Seminar on Emerging in Chemical Science (ETCS-2012)" held at School of Chemical Science Indore on March 20, 2012.

TABLE OF CONTENTS

List of Nomenclature

α	Alpha
β	Beta
γ	Gama
τ	Fluorescence Lifetime
Å	Angstrom
χ	Chi
λ	Wavelength
μ	Micro
Π	Pi
nm	Nanometer
ns	Nanosecond
mM	Milli Molar
μM	Micro Molar
K_{sv}	Stern Volmer Quenching Constant
K_{cat}	Turnover frequency values
K_M	Michaelis-Menten constant
ε	Molar Extinction coefficient
cm	Centimeter
°	Degree
mL	Milliliter
μL	Microliter
a. u.	Arbitrary Unit
λ_{ex}	Excitation Wavelength
λ_{em}	Emission Wavelength
pH	The negative logarithm of hydronium-ion concentration
η	Eta (Efficiency)

K_a	Binding Constant
Φ	Quantum Yield
G′	Storage Modulus
G″	Loss Modulus
Pa	Pascle
T_{gel}	Gel-sol phase transition temperatures
V_{max}	Maximum initial rate
δ	Chemical sift

List of Acronyms

AIEE	Aggregation Induced Enhanced Emission
ACQ	Aggregation Caused Quenching
3,5-DTBC	3,5-di-tert-butylcatechol
3,5-DTBQ	3,5-di-tert-butylbenzoquinone
BSA	Bovine Serum Albumin
BTA	1,3,5-Benzene Tricarboxamide
CCDC	Cambridge Crystallographic Data Centre
CD	Circular Dichroism
CDCl3	Chloroform - *d*
CGC	Critical Gel Concentrations
DMF	Dimethylformamide
DMPC	1,2-dimyristoyl-sn-glycero-3-phosphocholine
DMSO-d_6	Dimethyl sulfoxide-d_6
DNA	Deoxyribonucleic acid
EB	Ethidium Bromide
EDC	1-Ethyl-3-(3′-dimethylaminopropyl) carbodiimide
ESI-MS	Electron Spin Ionization Mass Spectroscopy
FE-SEM	Field Emission Scanning Electron Microscope
FT-IR	Fourier Transforms Infrared
FS	Frequency Sweep
IC_{50}	Inhibitory Concentration
LMW	Low Molecular Weight
LA	Lactic Acid
LVE	Linear Visco Elastic
NMR	Nuclear Magnetic Resonance
MOF	Metal Organic Framework
MTT	3-(4,5-Dimethylthiazol-2-yl)-2,5-diphenyl Tetrazolium bromide
MCT	Monocarboxylate transporter

PXRD	Powder X-Ray Diffraction
PPM	Part Per Milian
TEM	Transmission Electron Microscopy
THF	Tetrahydrofuran
Trp	Tryptophan
TCSPC	Time Correlated Single Photon Counting

List of Figures

Chapter 1

Chapter 2

Chapter 3

Chapter 6

Chapter 7

Chapter 8

List of Schemes

List of Tables

Chapter 1

General Introduction and Background

Chapter 1

General Introduction and Background

1.1 Introduction

Metal-organic compounds are spread in the diverse areas from metal-coordination complexes to soft materials and have applications in various fields like material science, medicinal science, catalysis, nanomaterials, cosmetics materials, food industries and so on.[1,2] The limitless combinations between inorganic and organic building blocks enable researchers to synthesize metal-coordination complex as well as soft materials with versatile structural properties. The coordination complexes of transition and inner transition metal ions are well explored and used extensively in the fields like catalysis, gas storage, separation, sensing, heat transformation, and drug delivery.[3,4] Besides, soft materials are found to be an engrossing novel class of materials, and the use of the metal-organic compounds to design as desired soft material is emerging as a fruitful approach. Though there are ample of literature reports in which designing and application of metal-based soft material have been explored; there is wide scope to come up with diverse low molecular weight gelators and metal-based soft materials and to explore their exciting properties. Soft materials are the class of materials which can be easily deformed by thermal stresses or thermal fluctuations at room temperature.[5] It includes liquids, polymers, foams, gels, colloids, granular materials, as well as most soft biological materials.[5] Gels belong to one of the important class of soft material and found in our daily life, although we are often not aware of it. When the materials look like in a phase between solid and liquid and feel to be jelly-like are known as gels (Figure 1.1). The gel can be easily distinguished by the inversion test tube method. In 1926, Jordan D. Lloyd well said that “we can recognize gel easily rather than define”.[6] However, Almdal *et al*. proposed that the gel is a soft, solid-like material in which loss modulus (G" *i.e.* Viscous portion of the viscoelastic behavior) is considerably smaller than the storage modulus (G' *i.e.* elastic portion of the viscoelastic behavior) in the plateau region.[7] Thus, gels usually

show viscoelastic properties with a flow behavior between that of an ideal fluid and an ideal solid.[8,9] Depending on the difference between the storage and the loss modulus, gels are classified as "strong" and "weak" gels.

Figure 1.1. *Examples of gels used in daily life.*

Through the examples as reported earlier, we can say gels consist of two parts: gelator and solvent. Generally, gels build up a 3D network in which gelator entraps the solvent molecules as a major component, and it can show as a good balance between crystallization and solution. During the process of solubility of gelator in the solvent, mainly three outcomes are observed.[10] First, when the molecules self-assemble in a highly ordered way, the outcome is crystal formation. Secondly, the self-assembly in a random way could give an amorphous precipitate. Third, the self-assembly in order way by entrapping the solvent leads to the formation of gel (Figure 1.2).[10]

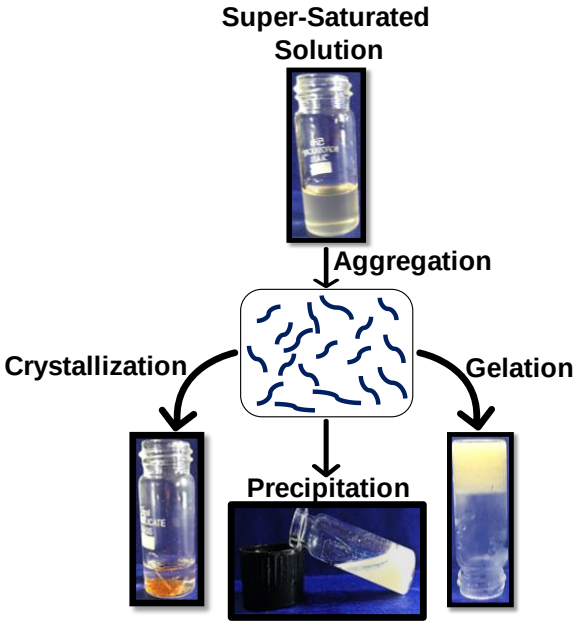

Figure 1.2. *Modes of aggregation.*

1.1.1 Classification of gels

Gel could be classified based on the presence and absence of metal centers. The gelator incorporated with metal complex or ion is called metallogels, whereas organogels or hydrogels are depending upon their major (solvent) components. Gels can be prepared in organic solvents (organogels), water (hydrogels) or aqueous organic mixtures. When the solvent is absent from the gels, it is known as xerogels or aerogels. Freundlich described the xerogel as "the porosity may still exist in the coherent framework of gel even in the absence of solvent molecules."[11] So usually, these terms are used for dried hydro- or organogels. Further, the gels can be distinguished by their origin. It could be natural gels (derived from nature like gelatin, chitosan, alginate, etc.) or artificial gels (designed in the laboratories). Furthermore, we can classify gels based on the driving forces for molecular aggregation. The crosslinked polymer formed by the covalent bonds which are unable to dissolve again are known as chemical gels whereas gels made of either low molecular weight (LMW)) molecules or polymers formed by non-covalent interactions like hydrogen bonding, van der Waals, charge-transfer, dipole-dipole, π-π stacking, coordination interactions and lead to reversible gel-to-sol phase transitions are known as physical gels.[10] Further, metallogels are classified into two categories. When ligand or metal exerted self-assembly through non-covalent interaction and form a fibrous network which entrapped the solvent molecules is known as a discrete metal complex gel.[12,13] In this case, no direct involvement of metal ion for the establishment of a fibrous network. On the other hand, a combination of metal ion (act as a node) and LMW gel (act as linker) in which solvent immobilizes is known as coordination polymer gel (CPG).[14] In this case, the metal ion is actively participating, and gelation gets induced by the coordination of metal with ligand (Figure 1.3).

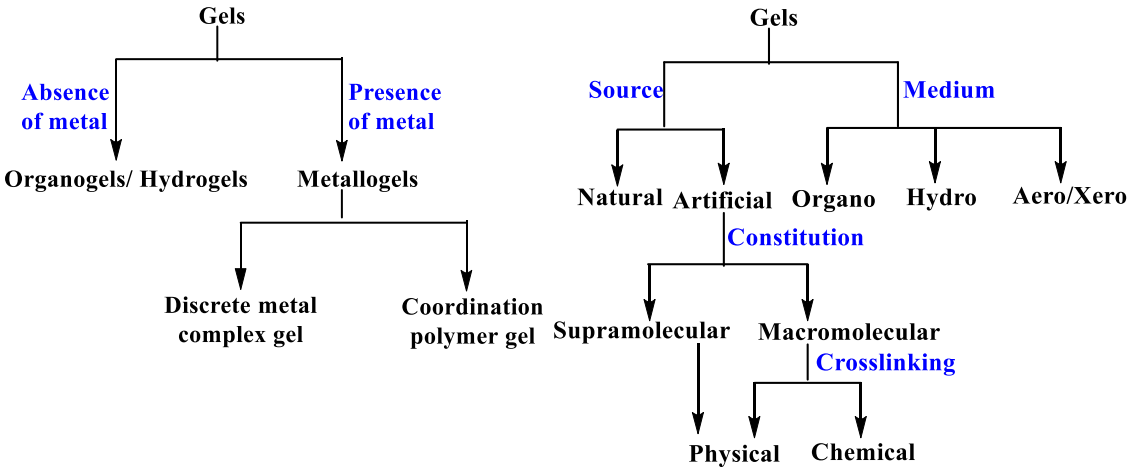

Figure 1.3. *Classifications of gels.* [15]

1.1.2 Characterizations and properties of gels

Various experimental techniques are used to study the properties and characterizations of gels. Nowadays, broad experimental techniques provide the solution to understanding the structure, bulk nature of gel, and the mechanism behind the gelation.[16] Gels are formed by self-assembly mechanism, which is primarily examined by their thermodynamic and rheological properties. It is also possible to predict the viscosity point with the help of some visual assessments like the inverted test tube method, dropping ball technique, bubble motion. However, the heating-cooling method indicates the thermo-reversibility of gel (Figure 1.4).[17]

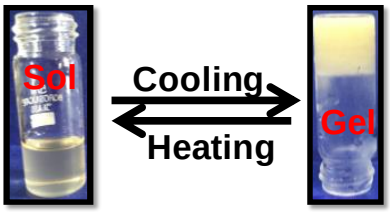

Figure 1.4. *Inversion test tube method represents the thermo-reversible nature of the gel.*

However, a wide range of skills and techniques are used to understand gelation (Figure 1.5).[1] The rheological experiments can assess the mechanical strength of the gel. The study of effect in flow and deformation of matter under the applied stress is known as rheology. The rheological experiment has been performed by placing gel under oscillatory stress, and obtained value of G′ (elastic storage modulus, *i.e.*, solid-like) and G″ (elastic loss modulus, *i.e.*, liquid-like) are used to measure the outcome of the strength of the gel. Though, the rheological experiment should indicate that the value of G′ is greater at least some order of magnitude than the value of G″ for considering the material as a gel.[18] Further, the structure of gel at the molecular level that is nano to microscale can be identified by several microscopic techniques. Particularly, scanning electron microscopy (SEM), transmission electron microscopy (TEM) can demonstrate the morphologies of gel, and small angle X-ray scattering (SAXS), small angle neutron scattering (SANS), single-crystal X-ray diffraction (SXRD) can suggest about correlation distances. Fourier transforms infrared (FTIR), powder X-ray diffraction (PXRD), nuclear magnetic resonance (NMR) spectroscopy are used to study the non-covalent interaction in the gel.

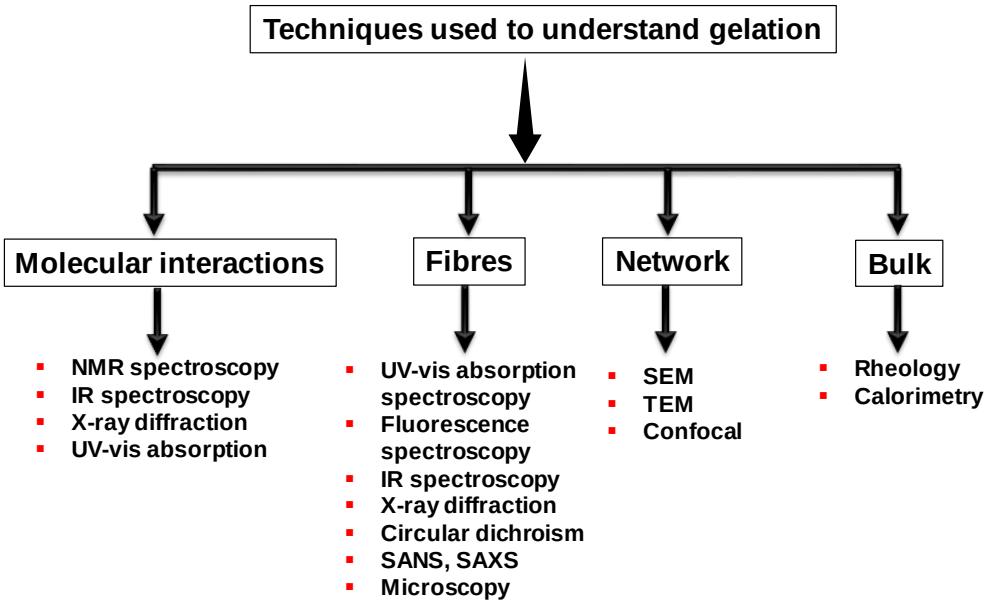

Figure 1.5. *Wide range of techniques used to understand gelation.*

Property of gel to respond towards a variety of external stimuli including pH, temperature, chemical stimuli, light, electro/magnetic fields, and mechanical action reveal some notable changes from the macroscopic to the molecular level. The most common gel formation after aggregation leads to aggregation-caused quenching (ACQ) property, which indicates the decrease in emission intensity from the molecule. In contrast, some gelator molecules show aggregation-induced enhanced emission (AIEE) property, which indicates the enhancement in emission intensity after aggregation (Figure 1.6).[19, 20,21]

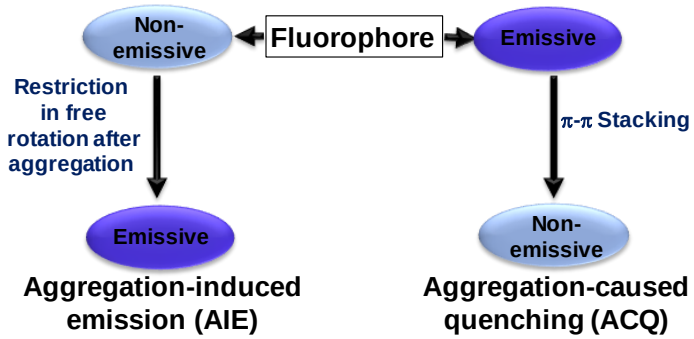

Figure 1.6. *Aggregation-induced emission (AIE) and aggregation caused quenching (ACQ).*

Furthermore, the most impressive property of gels is the self-healing, which indicates the ability to heal and regenerate after getting damaged by external stimuli. Thereby, the self-healing gels bear resemblance with some biological materials (e.g., merging of broken bones, cell-wall recovery upon deformation of wood).[22, 23]

1.2 Design strategies for low molecular weight gelators

Due to serendipitously formation of many gel-based materials, from the last few years, significant efforts have been made to rationally design the molecules which contain gelation ability and understanding their gelation mechanism. As we know, most of the molecule (π-conjugated gelators) formed a gel after self-assembly, which involves certain non-covalent interactions between the molecules but the synthesis of π-conjugated gelators is challenging to the environment.[24] To overcome these challenges,

supramolecular chemistry has gained extensive importance as an alternative approach for designing π-conjugated gelators. It is evident that the design and fabrication of low molecular weight (LMW) based gel is the best bottom-up approach for formation of gels.[24] LMW gels have non-covalent interactions with low binding strength which can restrain high amounts of solvents. The mechanical strength of LMW gels is quite different because of the involvement of the weak bonds than polymeric gels (covalently bound). This points at several advantages in selecting LMW gelators, such as thermo-reversible nature, hierarchical aggregates structured by the spontaneous organization of small molecules, and probability to tailor the gel properties. However, it is worthy of mentioning that it is not only about non-covalent interactions, but some other factors are also crucial for design LMW gels, *viz.* pH, ionic strength and temperature of the solvent.

LMW gel (M<3000 Da) attracted much attention in the last few years due to several reasons[25] like:

- Accessibility to gelators with a range of structural properties which could be produced by standard methods.
- Biocompatibility and natural sources like proteins, amino acids, sugars, etc.
- Sustainability of 3-D network due to the presence of non-covalent forces.
- Thermo-reversible nature providing the probability of re-establishing internal monomeric bonds after chain rupture.
- Operational even in low concentration.
- Thixotropic nature.

So far, there are some methods reported which can reinforce LMW gel[26] such as:

- Use of metal-ion coordination.
- Addition of polymers.
- Host-guest interactions.
- Post-polymerization.

Although numbers of publications are rapidly increasing day by day on the LMW based gels which have efficacy in many fields like sensing, drug delivery, regenerative medicine, catalysis, optoelectronics, biocompatible materials and so on. [24] Following are some earlier examples of LMWGs reported previously.

- Benzoyl-cystine as the first examples of LMW hydrogel reported in 1892.[27]
- *N*, *N'*-Dibenzoyl-L-cystine (DBC) LMW gel discovered by E. Goldmann and E. Baumann in the 19th Century. It formed both hydrogels as well as organogel and used in biomedicine as media for drug delivery. DBC with Eu^{3+} ion enhanced the luminescent property of gel.[28]
- There are also ample of examples where, amino acids, urea, fatty acid, sugar, pyrene, anthryl derivatives, and steroid behave like LMW gel.[29-32]
- Some other examples of LMW gels explored later on are dendrimers, C_3-symmetric cyclohexane derivatives, resorcin-based gelators, azobenzene and trinuclear Cu(II) complex of inositol.[33-36]
- Ability of 1,3,5-benzene tricarboxamide (BTA) derivatives and tetrazoles to form gels have explored in recent years.

In this thesis, BTA derived organogels with nitrile functional groups and tetrazoles as LMWGs, and their metallogels have been explored.

1.2.1 1,3,5-Benzenetricarboxamide (BTA)

There are certain specificities in the structure of 1,3,5-benzene tricarboxamide (BTA) and its derivatives (Scheme 1.1)[37] which perhaps make them very much suitable as LMGs:

- Planar benzene cores
- Three C-centered amide groups in the positions 1, 3, and 5 leading to a C_3-symmetry of the molecule.
- Lateral functional moieties or substituents R that are attached to the amide units.

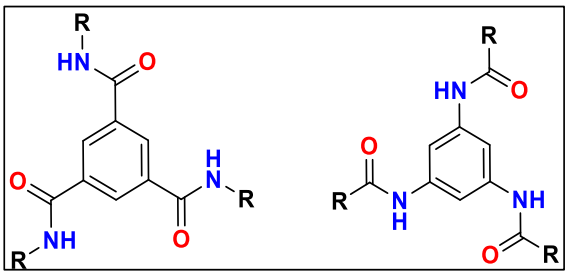

Scheme 1.1. *Representation of general chemical structures of C=O- and N-centered BTA molecules.*[37]

The first 1,3,5-benzene tricarboxamide (BTA) was synthesis near-century ago (Scheme 1.2).[38]

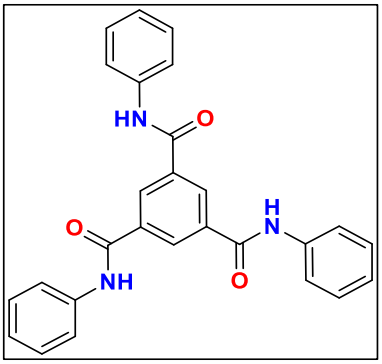

Scheme 1.2. *First published example of BTA.*[38]

The basic molecular structure of BTA shows supramolecular columnar aggregation where the benzene cores are set on top of each other with π-π distances ranging from 0.33 nm to 0.38 nm.[37, 39] The R substituents and the amide group of BTA contain staggered conformation which indicates the 60° rotation in the adjacent molecules. In between adjacent molecules with amide moieties, a triple hydrogen bond is formed which manages the helicity in the aggregate column. In case of a skew or straight columnar aggregates molecular packing, it is important to note the deviation angle of three amide unit (range from about 10° to about 45°). The proper arrangement in BTA molecule is recognized by substituents type, solvent system, temperature, and environmental conditions. In BTA molecule, amide moieties arranged in the same direction and acted as hydrogen bonding

units which influence the aggregation nature (Figure 1.7).[37,40,41] The amide moiety constituted in the way of N-centered, C-centered, or a combination of both but the term 1,3,5-benzene tricarboxamide used for C-centered derivatives. However, almost endless possibilities arise out of the derivatization by substitution in the three side arms of BTA with multifold properties and applications. However, in this work, the study is restricted to C-centered BTA.

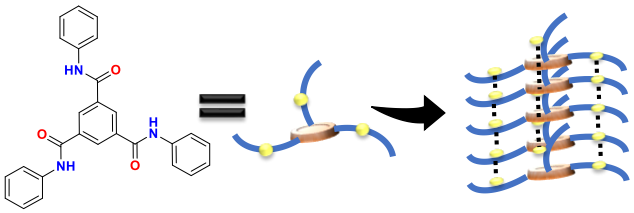

Figure 1.7. *Pictorial representation of self-assembly in derivatives of benzene-1,3,5-tricarboxamide (BTA).*

Following is a summary of the factors which influence the self-assembly in BTA derivatives by a unique combination of interactions [41]:

- **BTAs as a trivalent building block in the synthesis and metal ion coordination:** BTA acts as an attractive trivalent ligand for the metal ion coordination, for example, zinc metal ion stabilizes by BTA based structure has been published.[42] BTA based metal-organic framework (MOF) acts as porous material in which BTA molecule assemble into sheet-like aggregates with structures which similar to honeycombs. [43]
- **Self-assembly of BTA derivatives in various environments:**
  The main environmental factors are the bulk aggregation, polymer additives, and different solvent (polar, nonpolar, protic, and aprotic organic) combination influence the self-assembly of BTA. [44]

1.2.1.1 Nitrile

The nitrile derivatives of BTA are an important class of gelators because of the electron-withdrawing tendency of nitrile groups which endow strong non-covalent interaction

between aromatic rings. The nitrile functionality found in a number of pharmaceuticals and natural products.[45, 46] The nitrile derivatives coordinated to metal centers due to their higher charge density and nucleophilicity.[47] The nitrile containing adjacent negative charge endows the powerful inductive stabilization, which is the main reason behind excellent nucleophilicity with tiny steric demand. Inductive stabilization is the key to the interpretation of metal nitriles reactivity. It reveals two potential metal nitrile coordination sites: *N*-metalation at the nitrile nitrogen and *C*-metalation at anionic carbon depending closely on the ligands, temperature, counter-ion, and solvent (Scheme 1.3). The *C*- and *N*-metallated nitriles have either sp^3 or sp^2 hybridization at the nucleophilic carbon.

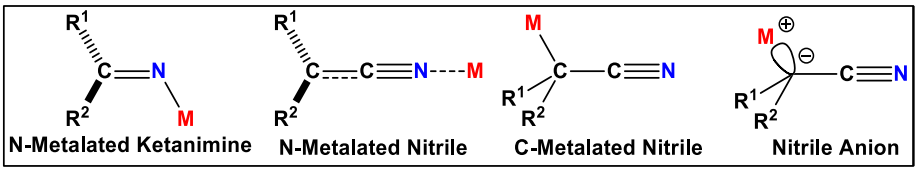

Scheme 1.3. *General representation of metal-nitrile coordination.*

1.2.2 Tetrazole

The nitrogen-rich tetrazoles belongs to azole family which contains a 5-membered ring with four nitrogen. All 5-substituted tetrazoles have one proton on the nitrogen atom of the ring and exist in two tautomeric forms (1-*H* and 2-*H*) in almost 1:1 ratio and their chemical and physical properties are dissimilar (Scheme 1.4). The unsubstituted N-H tetrazoles interestingly participate in N-H···N hydrogen bonding which influences their molecular packing substantially.[48]

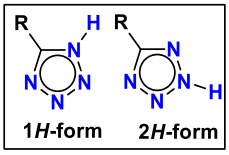

Scheme 1.4. *Representing the tautomeric nature of 5-substituted tetrazole.*[48]

Tetrazoles can act as very good gelator and are being proved as suitable candidates as a versatile ligand in coordination chemistry, [49-51] because:

- Tetrazole is being nitrogen-rich, considered as a unique linker in coordination chemistry. It allows all its nitrogen atoms to participate in coordination with metal ions based on the conditions and nature of the metal center.
- Nine possible binding modes of the tetrazole have been commonly observed, where it can bind in μ_1 to μ_4 modes (Scheme 1.5).
- Presence of N-H bond makes them acidic with pk_a around 4-5 for a wide range of 5-substituted tetrazoles ranging from aliphatic to aromatic groups.
- The ring can be easily deprotonated on treatment with base and ends up with a respective tetrazolato anion.
- The negative charge on the generated tetrazolato anion distributes all over the ring, including carbon atom and stabilizes the anion. These anions are stable even against hydrolysis and present predominately in the anionic form in aqueous solutions. These anions can be easily generated from aqueous-alcoholic solutions as they have higher capabilities to form hydrogen bonding with these solvents compared to their neutral analog.
- It can act as π-acceptor and they're capable of forming metal complexes and coordination polymers with great thermal stability.

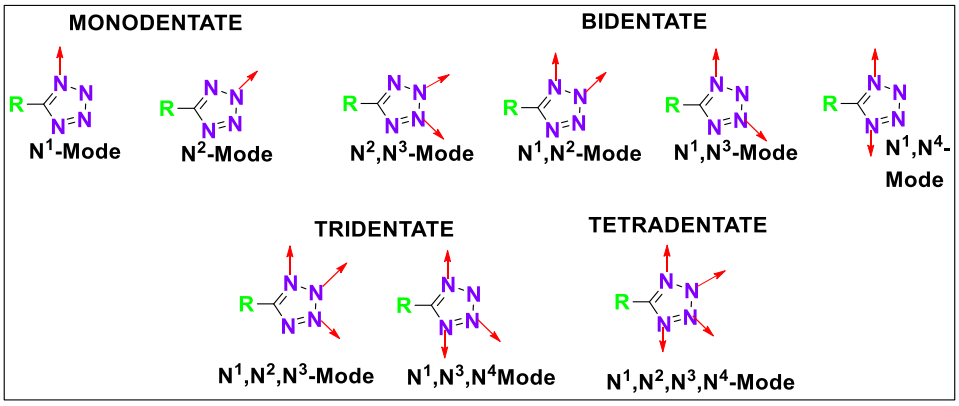

Scheme 1.5. *Displaying multi-dentate nature of tetrazole ligand with metal centers.*[51]

However, it is important to note that due to versatile coordination ability of tetrazoles they have been extensively utilized to generate transition metal complexes with various topologies and with applications in catalysis, gas adsorptions, magnetic materials,

fluorescent materials, metal-based drugs, and energetic materials. [52-54] A scrutiny of those tetrazole complexes revealed that there are limited examples where tetrazole based complexes have been utilized for bio-inspired catalytic reactions.[55,56] Therefore, it is worthy to further investigate biomimetic catalytic abilities of tetrazole based transition metal complexes.

1.2.3 Examples of BTA and tetrazole based gels

Over the past few years a range of BTA and tetrazole derivatives are reported which play significant role in the field of soft materials. BTA derivatives like alkyl derivatives[57,58], aryl derivatives[59-61], pyridyl derivative[62,63], bipyridyl derivatives[64,65], porphyrinyl derivatives[66], triphenylyl derivatives[67], oligo(p-phenylenevinylene) derivatives[68], derivatives with 1, 2 and 3 hydrophilic side-arms[69], 4-benzoic acid derivative[60], 2 and 3- hydroxy-4-benzoic acid derivatives[70], 3-benzoic acid and naphthoic acid derivatives[70], amino-acid derivatives[71-75], dipeptide derivatives[76,77], oligopeptide[78], oligo(ethyleneoxy) [79,80], benzocrown ethers[81] are reported so far which formed organogel, hydrogels and metallogels with number of applications. In addition tetrazole derivatives like bis(tetrazole)-appended pyridine derivative[82], 5-(2-Mercaptoethyl)-1*H*-tetrazole[83], 1,3-Bis(5-tetrazolyl)benzene[84], 5-methyltetrazole[84,85], 5-dodecyl tetrazole[84], 5-phenyltetrazole[84], 1,3-bis(1-methyl-5-tetrazolyl)benzene[84], 1,4-di(1*H*-tetrazol-5-yl)benzene[85,86], 1,3,5-tri(1*H*-tetrazol-5-yl)benzene[85], 1,2,4,5-tetra substituted phenyl tetrazole[86], tetrazole derivative of 2,5-dicarboxamide pyridine[87], N-substituted 5-methyltetrazole[88,89], tetrazole moiety containing cefpiramide (CPM) [90] are being explored and their involvement in formation of organogel, hydrogels and metallogels with number of applications have been investigated.

1.2.4 Strategy adopted for the formation of BTA and tetrazole based organogels/ hydrogels and metallogels

Formation of the gel is serendipitous. There is no optimized process developed by which it can be predicted when the gel will form. However, there are some general strategies

reported previously for gelation. Gelation gets induced by various factors like maintaining particular pH condition, temperature, and solvent combination, through sonication or refluxing and so on.

In general, organogel/ hydrogel based on BTA and tetrazole is formed by dissolving gelator molecules into an organic solvent and addition of water on it.[91, 92] The resultant solution left in an undisturbed condition. After a few minutes, gelations get induce.

On the other hand, metallogel is prepared by using three common processes [93]:

a) Metallogel is formed after the addition of metal in a solution of gelator molecule is known as self-supported metallogel.
b) Metallogel is formed on addition of metal in organogel or hydrogel.
c) Metallogel is formed by the process in which metal and gelator molecule both get dissolved in the solvent and resultant solution left undisturbed. This type of gel is known as an organometallic gel.

1.3 Uniqueness behind LMW soft materials and their applications

The inspiring flexibility of LMW gel and their metallogels offers scientists to find its applications in various fields. To date, the development of BTA and tetrazole based inspirational soft materials are in great demand due to their unique behavior like AIEE, swelling capacity, and self-healing property. So, this kind of molecules can be exploited to generate smart materials to apply in materials to biology.

1.3.1 Smart gel template for sensing: Anions, cations, and biomolecules

The LMW gels like nitrile derivatives of BTA and their metallogels interestingly show AIEE during the sol-gel transition. The non-fluorescent solution of gelator (nitrile derivatives of BTA) become fluorescent in the gel state due to AIEE[91, 92, 94] (Figure 1.8).

So, it can be very promising smart gelator material for sensing of cations, anions, biomolecules.

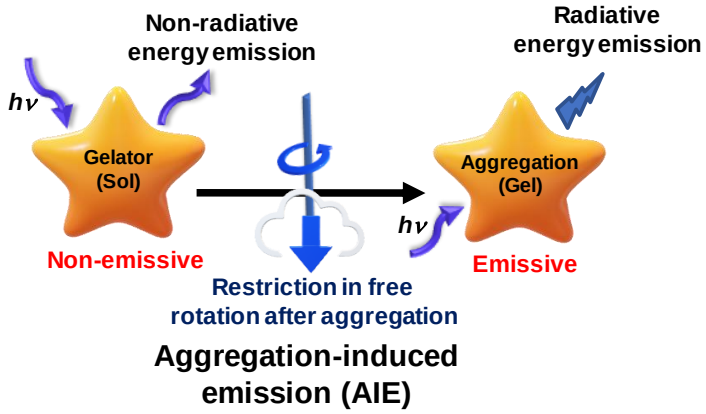

Figure 1.8. *Pictorial representation of AIE during sol-gel conversion.*

In many instances, the presence of a particular cation or anion or a chemical substance influences the network structure in a great way to bring about significant changes in the associated properties. This characteristic of soft material to discriminate a particular entity from similar other motifs can endow special power to the material for enormous sensing capacity. There are ample reports where LMWGs, in a gel state, particularly with the help of a drastic change in the aggregate induced emission property, are capable of sensing various cationic and anionic species.[95-100] Sometimes it is also possible to create a smart template which can sense metal ions by switching off or on the aggregation-induced emission property and in turn, the metallogels formed can be utilized further in sensing of anions. The metallogels have been proved to be quite effective in sensing certain anions when assembled with different gelators.[101,102] There were also numerous reports when metallogel acted as a sensor for ammonia, hydrogen sulfide, triethylamine, pyridine, and picric acid through different spectroscopic methodology as well as colorimetric detection.[103-106] The sensing and recognition of important biological substrates, for example, an amino acid is very promising for the amino acid pool which is responsible for doing a balanced metabolism and can act as potential biomarkers and precursor for various key biological substances.[105] Though the interaction of metal ions

with different amino acids has been explored extensively; however, metallogel getting utilized as sensor come up as a new approach for discrimination of amino acid.

1.3.2 Self-healing materials: Novel to biomimetic

The self-healing mean reformation of the bond after the breakage. The self-healing materials have the ability to repair itself after damage.[106] It is very much similar to the properties of tissues during wound healing and can generate novel materials (like self-healing polymers and elastomers, self-healing coatings, self-healing cementitious materials, self-healing ceramics, self-healing organic dyes).[107,108]

Self-healing materials can be classified based on the nature of the self-healing process and triggered requirements. Self-healing materials are mainly two type based on their nature, *i.e*. extrinsic self-healing material in which healing ability is due to some external healing components while intrinsic self-healing material not required any external component, it can inherently reform the bond after damage with reversibility.[109] Furthermore, the self-healing mechanism based on:

- Release of healing agents upon damage in which repetitive healing is usually not possible.
- Addition of molecular functionalities which triggered repetitive healing includes association by non-covalent interaction, metal coordination, dynamic chemical bonds, or molecular diffusion and entanglement.

The self-healing gel is a smart material. It has the potential to solve the problem of interface connection between gels and biological tissues as well as maintain the material performance with lower costs. As it is known that gel is formed through self-assembly by covalent and non-covalent interaction; thereby, it is no wonder that several gels have been designed which can show excellent self-healing property by self-assembly approach. In this thesis, tetrazole based self-healable gels and their metallogel based on inner-transition metal has been explored extensively. There are several reports of metallogels

based on inner transition metals as well as LMW tetrazoles with self-healing nature.[110-114] However, the role of inner-transition metal containing metallogels of LMW tetrazole in formation self-healing materials is one of the objectives of this thesis.

1.3.3 Anticancer activity and drug delivery

In recent years, LMW gels have been found to be associated with anticancer activity. Globally, cancer is the second leading cause of death. Cancer can affect all ages of persons, and with age, the risk of developing cancer gets increased. Cancer or neoplasm (in term of medical language) is uncontrolled cell division, mutation, and ability to spread. It can be malignant, benign, or metastatic. There are different modes of cancer treatments: surgery, radiation therapy, hormonal therapy, immunotherapy, stem cell transplantation therapy, chemotherapy. Chemotherapeutic reagents have been classified in various categories depending upon their mode of actions that are an intercalating agent, alkylating agents, antimetabolites, topoisomerase inhibitors, and metal-based chemotherapeutic drugs.[115,116] The measure of cell viability is one of the basic methodology adopted to get an idea about the potential of a molecule as an anticancer agent. Trypan blue stain is used most commonly for the measurement of cell viability, and cell counting is measured by hemocytometer. [117,118] The cell viability is examined by MTT assay (a sensitive, quantitative, and reliable colorimetric assay that measures viability, proliferation, and activation of cells). It is based on the capacity of mitochondrial dehydrogenase enzyme in living cells to convert the yellow water-soluble substrate 3-(4,5-dimethylthiazol-2-yl)-2,5-diphenyl tetrazolium bromide (MTT) into dark blue formazan product which is insoluble in water. The amount of formazan produced is directly proportional to cell number in the range of cell lines.[117, 118] The DNA labeling assay gets carried out by Hoechst stain.[117, 118] It indicates the morphological changes in the cells. Apoptosis cells feature the shrinkage of cells, condensed chromatin, whereas necrotic cells indicate the swelling of the cell, non-condensed chromatin.[115, 116] Anticancer drugs are designed to target the signaling and associated molecules. Cancer cells considerably need more energy than healthy cells, and their metabolism require a large number of micronutrients,

particularly iron.[117,119] Ruthenium can bind albumin and transferrin. As we know, cancer cells need more iron; transferrin receptors are overexpressed. So allowing a ruthenium-based drug to be more efficiently delivered to cancer cells.[119,120]

However, to improve the anti-cancer efficacy and to counteract the side effects, a variety of drug delivery systems have been invented in the past few years. Drug delivery is an important phenomenon as it can affect the rate of release, pharmacokinetic, and side effect profile. Drug release follows a mechanism like affinity-based, diffusion, degradation, and swelling.[121, 122] Current efforts in the area of drug delivery include the development of targeted delivery in which the drug is only released in the target area of the body like cancerous cells. Cancer is a dynamic and heterogeneous disease with high mortality. Its treatment is largely dependent upon chemotherapy and efficient delivery of the therapeutic agent.[117, 123] Various drug delivery systems are getting utilized clinically to deliver a wide variety of chemotherapeutic drugs.[124] Recently, LMW gelators that self-assemble *via* non-covalent interactions have attracted significant attention due to their good biocompatibility, low toxicity, inherent biodegradability as well as the convenience to design them.

The possible advantages of LMW gelators over other drug delivery systems are:

- Its drug loading capacity is high at approx. 10% more than normal delivery systems.
- The encapsulation of anti-cancer drugs into gel or formation of the gel by a drug derivative itself which can eliminate the unexpected adverse effects from excipients.
- It can be designed to undergo controllable and sustained release of drugs by incorporating enzyme cleavable sites in the gelators.

These advantages suggest the huge potential of LMW gelators for the delivery of anti-cancer drugs. The LMW Nitrile substituted BTA and tetrazole based gelators have

swelling capacity after the formation of gel which encapsulating the drug and play promising role for anticancer drug delivery towards cancer cells (Figure 1.9).

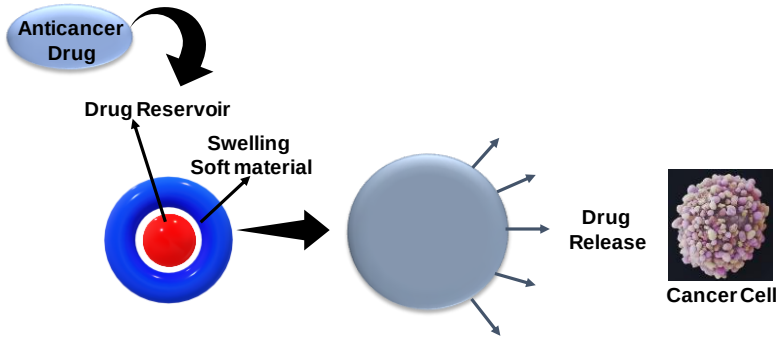

Figure 1.9. *Pictorial representation of drug release mechanism of soft materials.*

1.3.4 Metallogel: Bio-inspired catalysis

Utilization of metallogels as a prospective catalyst is an area where the examples are limited and have not been fully explored. The literature data which is available indicates mostly utilization of palladium and silver (cation/nanoparticle) based metallogels which have been utilized for organic reactions like Suzuki-Miyura coupling reactions[125,126], reductions of aromatic nitro groups to amine [127] or degradation of dye molecules. [128,129] Limited examples are available where $Ca^{2+,}$ $Cr^{3+,}$ or Cu^{+} based metallogels are explored for another kind of organic catalytic reactions.[130-132] However, several metalloenzymes to catalyze the controlled and selective oxidation of organic compounds are found in nature. Among them, an important enzyme is catecholase. Catecholase is a dinuclear Cu^{2+} containing an enzyme with a type-3 active site which is responsible for catechol oxidation in the higher plant which oxidizes catechol to *o*-quinone. In 1988, the "met form" enzyme crystal structure was found and revealed that the active site consists of a hydroxo bridged di-Cu^{2+} center. Three histidine nitrogen atoms coordinate Cu^{2+} center. The coordination sphere of each copper has a trigonal pyramidal environment with His109 and His240 at the apical site [133] (Figure 1.10).

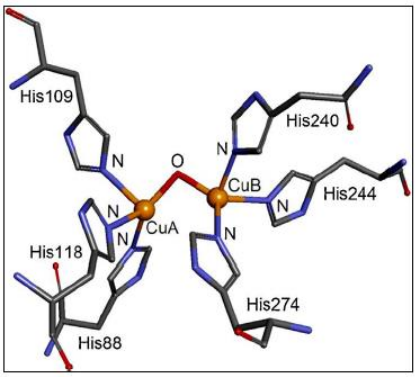

Figure 1.10. *Crystal structure of the met state of the enzyme (PDB ID: 1BT3).*

Catecholase activity is the oxidation of a broad range of catechol's to quinones through the four-electron reduction of molecular oxygen to water undertaken by catechol oxidase. Catechol is present in the vacuoles of cells of most of the plant tissues. Catechol oxidase is present in the cell cytoplasm. If the plant tissues are damaged, the catechol is released, and the enzyme converts the catechol to ortho-quinone, which is a natural antiseptic.[134] As per the report, mechanistic studies catecholase activity studied by mainly four approaches that are substrate-binding studies, structure-activity relationship. This thesis work focused on the catecholase activity of copper-based metallogel. It can act as a reaction medium as well as a catalyst for aerobic oxidation of catechol to quinone in the gel state at room temperature and pressure, mimicking a bioinspired catalytic reaction in the presence of metalloenzymatic catechol oxidase.

1.4 Metal tetrazole complex in bioinspired oxidation catalysis: Catechol oxidation

Naturally found metalloenzymes are involve in bioinspired oxidation catalysis by using molecular oxygen. This selective oxidation is important for life as well as industrial purpose. Thereby, designing of the bioinspired oxidation catalyst is a safer and simple strategy. These types of catalyst have some advantage over the metalloenzymes system as they might increase selectivity, specificity, productivity, and their scope. The

bioinspired approach does not aim at imitating exact details of an active site but instead exploits its basic chemical principles to enrich chemistry with new catalysts. However, the catalytic properties are dependent on the tunable constituents and their cooperation. Thereby, metal complex based on tetrazole has shown promising role in bioinspired catechol oxidation due to their nitrogen-rich environment with multiple binding sites. So far, the bioinspired catechol oxidation is one of the interesting types of bioinspired oxidation catalysis in which catechol is oxidized into o-quinone by using metal tetrazole complex (Scheme 1.6). Although, some examples of metal tetrazole based complex are already reported in previous years which can be utilized in bioinspired catechol oxidation. *[55,56]*

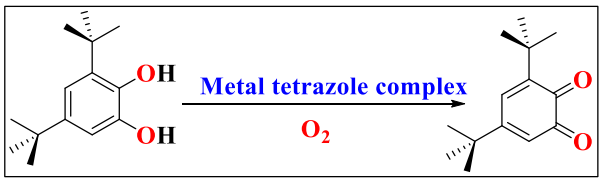

Scheme 1.6. *Schematic representation of catechol oxidation.*

1.5 Purpose and Span of Present Investigation

The purpose of present work is to design, fabrications, and explore the application of soft materials containing LMW gelators based on:

- ✓ Nitrile derivatives of BTA
- ✓ Tetrazole derivatives
- ✓ Transition and inner-transition metallogels based on nitrile derivatives of BTA and tetrazole derivatives.

The dynamic interactions of these soft-materials with the transition and inner-transition metals which make them able to enhance their applications in the various area from material to biology have been also explored. In this thesis work, synthesized soft materials have shown AIEE and self-healing properties which make them able to be utilized in

sensing of cations, anions, biomolecules and as smart self-healing materials. Introduction of metal ions in gels make them suitable to explore for bioinspired catalysis, anticancer properties, and efficient drug-delivery system.

Chapter 1 provide insight about the designing, fabrication, and properties of LMW gel and applications.

Chapter 2 illustrates the designing and synthesis of *N1*,*N3*,*N5*-tris(4-cyanophenyl)benzene-1,3,5-tricarboxamide (**G1**) gelator and their metallogels based on Fe^{2+}, Fe^{3+}, Cu^{2+}, Zn^{2+}, Co^{2+}, Ni^{2+}, Ag^{+}, Cd^{2+}, Ca^{2+}. The gelator **G1** and their metallogels remarkably show AIEE assisted cations and anions sensing.

Chapter 3 demonstrates the designing and synthesis of *N1*,*N3*,*N5*-tris(3-cyanophenyl)benzene-1,3,5-tricarboxamide (**G2**) and *N1*, *N3*, *N5*-tris(2-cyanophenyl)benzene-1,3,5-tricarboxamide (**G3**). LMWGs and their metallogels have been taken up which show the application in sensing of cations and anions through AIEE. Also, the copper-based metallogel mimics the bio-inspired catalysis reaction of conversion of catechol to quinone by aerobic oxidation in the gel state at room temperature and pressure.

Chapter 4 presents the designing and synthesis of *N1*, *N3*, *N5*-tris(4-cyanoethyl-phenyl)benzene-1,3,5-tricarboxamide (**G4**) gelator, and their metallogels which show the application in sensing of biomolecules by selectively sensing of L-tryptophan amino acid in the free state as well as in BSA protein.

Chapter 5 show the d**e**signing and synthesis of 3,5-bis((4-cyanoethyl)phenyl)carbonyl)benzoic acid (**G5**) gelator and methyl 3,5-bis((4-cyanoethyl)phenyl)carboxyl benzoate (**Me-G5'**) where G5'= G5-H has been contemplated and executed. **G5** gelator has been used for the formation of ruthenium-based metallogel and utilized in anticancer drug delivery through collapsing of the gel by pH variation.

Chapter 6 talks about the designing and synthesis of lanthanoid ($LaCl_3.7H_2O$, $PrCl_3.6H_2O$, $La(NO_3)_3.6H_2O$, $Gd(NO_3)_3.6H_2O$) based metallogels [**La(III)G6-Cl**, **La(III)G6-NO3**, **Pr(II)G6-Cl**, **Gd(III)G6-NO$_3$**] by using di(1H-tetrazole-5-yl) methane (**G6**). This metallogel can show self-healing property as well as anticancer activity against different cancers cell lines.

Chapter 7 illustrate the synthesis of nickel tetrazole complexes [NiL(5-phenyltetrazolato)] (**complex 1**) and [NiL{5-(4-pyridyl)-tetrazolato}] (**complex 2**) [HL = 3-(2-diethylamino-ethylimino)-1-phenyl-butan-1-one] by microwave irradiation. These metal tetrazole complex show protein binding, DNA binding and bioinspired catechol oxidation.

1.6 References

[1] Piepenbrock M. O. M., Lloyd G. O., Clarke N., Steed J. W. (2009), Metal and anion binding supramolecular gels, Chem. Rev., 110, 1960-2004 (DOI: 10.1021/cr9003067)

[2] Zhang J., Su C. Y. (2013), Metal-organic gels: From discrete metallogelators to coordination polymers, Coord. Chem. Rev, 257, 1373-1408 (DOI: 10.1016/j.ccr.2013.01.005)

[3] Wu H., Zheng J., Kjøniksen A. L., Wang W., Zhang Y., Ma J. (2019), Metallogels: Availability, Applicability, and Advanceability, Ad. Mater, 31, 1806204 (DOI: 10.1002/adma.201806204)

[4] Jung J. H., Lee J. H., Silverman J. R., John G. (2013), Coordination polymer gels with important environmental and biological applications, Chem. Soc. Rev, 42, 924-936 (DOI: 10.1039/C2CS35407A)

[5] Chen D. T., Wen Q., Janmey P. A., Crocker J. C. Yodh, A. G. (2010), Rheology of soft materials, Annu. Rev. Condens. Matter Phys., 1, 301-322 (DOI: 10.1146/annurev-conmatphys-070909-104120)

[6] Lloyd D. J., Alexander J. (1926), Colloid Chemistry, 1st edition, Chemical Catalogue Company, New York, USA.

[7] Almdal K., Dyre J., Hvidt S., Kramer O. (1993), Towards a phenomenological definition of the term 'gel', Polym. Gels Netw., 1, 5-17 (DOI:10.1016/0966-7822(93)90020-I)

[8] De Loos M., Feringa B. L., van Esch J. H. (2005), Design and application of self-assembled low molecular weight hydrogels, Eur. J. Org. Chem, 2005, 3615-3631 (DOI:10.1002/ejoc.200400723)

[9] Estroff L. A., Hamilton A. D. (2004), Water gelation by small organic molecules, Chem. Rev, 104, 1201-1218 (DOI: 10.1021/cr0302049)

[10] Sangeetha N. M., Maitra U. (2005), Supramolecular gels: Functions and uses, Chem.Soc. Rev, 34, 821-836 (DOI: 10.1039/B417081B)

[11] McNaught ed. A. D., Wilkinson A. (1997), Xerogel - definition in compendium of chemical terminology, Blackwell Science, 2nd edition, Oxford, Malden, MA, England, USA.

[12] Tam A. Y. Y., Yam V. W. W. (2013), Recent advances in metallogels, Chem. Soc. Rev, 42, 1540-1567 (DOI: 10.1039/C2CS35354G)

[13] Saha S., Das G., Thote J., Banerjee R. (2014), Photocatalytic metal–organic framework from CdS quantum dot incubated luminescent metallohydrogel, J. Am. Chem. Soc, 136, 14845-14851 (DOI: 10.1021/ja509019k)

[14] Jung J. H., Lee J. H., Silverman J. R., John G. (2013), Coordination polymer gels with important environmental and biological applications, Chem. Soc. Rev, 42, 924-936 (DOI: 10.1039/C2CS35407A)

[15] Sutar P., Maji T. K. (2016), Coordination polymer gels: Soft metal–organic supramolecular materials and versatile applications, Chem. Commun, 52, 8055-8074 (DOI: 10.1039/C6CC01955B)

[16] Hamley I. W. (2003), Nanotechnology with soft materials, Angew. Chem. Int. Ed, 42, 1692-1712 (DOI: 10.1002/anie.200200546)

[17] Chung Y. M., Simmons K. L., Gutowska A., Jeong B. (2002), Sol-gel transition temperature of PLGA-g-PEG aqueous solutions, Biomacromolecules, 3, 511-516 (DOI: 10.1021/bm0156431)

[18] Draper E. R., Adams, D. J. (2017), Low-molecular-weight gels: the state of the art, Chem, 3, 390-410 (DOI: 10.1016/j.chempr.2017.07.012)

[19] Castilla A. M., Dietrich B., Adams D. J. (2018), Using aggregation-induced emission to understand dipeptide gels, Gels, 4, 17 (DOI:10.3390/gels4010017)

[20] Mei J., Leung N. L., Kwok R. T., Lam J. W., Tang B. Z. (2015), Aggregation-induced emission: Together we shine, united we soar, Chem. Rev, 115, 11718-11940 (DOI: 10.1021/acs.chemrev.5b00263)

[21] Hong Y., Lam J. W., Tang B. Z. (2009), Aggregation-induced emission: phenomenon, mechanism and applications, Chem. Commun., 29, 4332-4353 (DOI: 10.1039/B904665H)

[22] Haering M., Díaz D. D. (2016), Supramolecular metallogels with bulk self-healing properties prepared by in situ metal complexation. Chem. Commun, 52, 13068-13081. (DOI: 10.1039/C6CC06533C)

[23] Fang Y., Wang C. F., Zhang Z. H., Shao H., Chen S. (2013), Robust self-healing hydrogels assisted by cross-linked nanofiber networks, Sci. Rep, 3, 2811 (DOI: 10.1038/srep02811).

[24] Babu S. S., Praveen V. K., Ajayaghosh A. (2014), Functional π-gelators and their applications, Chem. Rev, 114, 1973-2129 (DOI: 10.1021/cr400195e)

[25] Stupp S. I., Palmer L. C. (2013), Supramolecular chemistry and self-assembly in organic materials design, Chem. Mater, 26, 507-518 (DOI: 10.1021/cm403028b)

[26] De Loos M., van Esch J., Stokroos I., Kellogg R. M., Feringa B. L. (1997), Remarkable stabilization of self-assembled organogels by polymerization, J. Am. Chem. Soc, 119, 12675-12676 (DOI: 10.1021/ja972899z)

[27] Brenzinger K. (1892), Zur Kenntniss des Cystins und des Cystëins. (Mitgetheilt von E. Baumann.), Zeitschrift Für Physiologische Chemie, 16, 552-58810 (DOI:1515/bchm1.1892.16.6.552)

[28] Goldmann E., Baumann E. (1888), Zur kenntniss der schwefelhaltigen verbindungen des Harns, Zeitschrift Für Physiologische Chemie, 12, 254-261 (DOI: 10.1515/bchm1.1888.12.3.254)

[29] Fatás P., Bachl J., Oehm S., Jiménez A. I., Cativiela C., Díaz Díaz D. (2013), Multistimuli-responsive supramolecular organogels formed by low-molecular-weight peptides bearing side-chain azobenzene moieties, Chem. Eur. J, 19, 8861-8874 (DOI: 10.1002/chem.201300796)

[30] Terech P., Pasquier D., Bordas V., Rossat C. (2000), Rheological properties and structural correlations in molecular organogels, Langmuir, 16, 4485-4494 (DOI: 10.1021/la991545d)

[31] Yan N., Xu Z., Diehn K. K., Raghavan S. R., Fang Y., Weiss R. G. (2013), Pyrenyl-linker-glucono gelators correlations of gel properties with gelator structures and characterization of solvent effects, Langmuir, 29, 793-805 (DOI: 10.1021/la304957n)

[32] Jadhav S. R., Vemula P. K., Kumar R., Raghavan S. R., John G. (2010), Sugar-derived phase-selective molecular gelators as model solidifiers for oil spills, Angew. Chem. Int. Ed, 49, 7695-7698 (DOI: 10.1002/anie.201002095)

[33] Boekhoven J., Koot M., Wezendonk T. A., Eelkema R., van Esch J. H. (2012), A self-assembled delivery platform with post-production tunable release rate, J. Am. Chem. Soc, 134, 31, 12908-12911 (DOI: 10.1021/ja3051876)

[34] Haines S. R., Harrison R. G. (2002), Novel resorcinarene-based pH-triggered gelator, Chem. Commun., 23, 2846-2847 (DOI: 10.1039/B203462J)

[35] Lee S., Oh S., Lee J., Malpani Y., Jung Y.-S., Kang B., Lee J. Y., Ozasa K., Isoshima T., Lee S. Y., Hara M., Hashizume D., Kim J.-M. (2013), Stimulus-responsive azobenzene supramolecules: Fibers, gels, and hollow spheres, Langmuir, 29, 19, 5869-5877 (DOI: 10.1021/la400159m)

[36] Ray S., A. Das K., Banerjee A. (2007), pH-Responsive, bolaamphiphile-based smart metallo-hydrogels as potential dye adsorbing agents, water purifier, and vitamin B12 carrier, Chem. Mater, 19, 7, 1633-1639 (DOI: 10.1021/cm062672f)

[37] Cantekin S., de Greef T. F., Palmans A. R. (2012), Benzene-1,3,5-tricarboxamide: A versatile ordering moiety for supramolecular chemistry, Chem. Soc. Rev, 41, 8, 6125-6137 (DOI: 10.1039/C2CS35156K)

[38] Curtius T. (1915), Hydrazide und azide organischer säuren. XXX. Abhandlung. Bildung von Hydrazihydraziden und Hydraziaziden dreibasischer Säuren, Journal Für Praktische Chemie, 91, 39-102 (10.1002/prac.19150910102)

[39] Lightfoot M. P., Mair F. S., Pritchard R. G., Warren J. E. (1999), New supramolecular packing motifs: π-stacked rods encased in triply-helical hydrogen bonded amide strands. Chem. Commun, 1945-1946. (DOI: 10.1039/A905245C)

[40] Palmans A., Meijer E. (2007), Amplification of chirality in dynamic supramolecular aggregates, Angew. Chem. Int. Ed, 46, 47, 8948-8968 (DOI: 10.1002/anie.200701285)

[41] Nagarajan V., Pedireddi V. R. (2014), Gelation and structural transformation study of some 1, 3, 5-Benzenetricarboxamide derivatives, Cryst. Growth Des, 14, 4, 1895-1901 (DOI: 10.1021/cg500026t)

[42] Lee H., Noh T.H., Jung O.S. (2014), Halogen effects on photoluminescence and catalytic properties: a series of spatially arranged trimetallic zinc (II) complexes, Dalton Trans., 43, 10, 3842-3849 (DOI: 10.1039/C3DT53137F)

[43] Tang K., Yun R., Lu Z., Du L., Zhang M., Wang Q., Liu, H. (2013), High CO_2/N_2 Selectivity and H_2 adsorption of a novel porous yttrium metal-organic framework based on N, N′, N ″-tris (isophthalyl)-1, 3, 5-benzenetricarboxamide, Crys. Growth Des., 13, 1382-1385 (DOI: 10.1039/C3DT53137F)

[44] Kim E., Lee H., Noh T.H., Jung O.S. (2014), Suprachannels via a molecular array of 2D networks: Solvent effects, anion exchange, and physicochemical properties of silver (I) complexes bearing N, N′, N ″-tris (2-pyridinylethyl)-1, 3, 5-benzenetricarboxamide, Cryst. Growth Des., 14, 1888-1894 (DOI: 10.1021/cg500025k)

[45] Fleming F. F., Yao L., Ravikumar P. C., Funk L., Shook B. C. (2010), Nitrile-containing pharmaceuticals: efficacious roles of the nitrile pharmacophore, J. Med. Chem, 53, 7902-7917 (DOI: 10.1021/jm100762r)

[46] Fleming F. F. (1999), Nitrile-containing natural products, Nat. Prod. Rep, 16, 597-606 (DOI:10.1039/A804370A)

[47] Yang X., Fleming F. F. (2017), C-and N-metalated nitriles: The relationship between structure and selectivity, Acc. Chem. Res., 50, 2556-2568 (DOI: 10.1021/acs.accounts.7b00329)

[48] Peters L., Froehlich R., Boyd A. S. F., Kraft A. (2001), Noncovalent interactions between tetrazole and an N,N'-diethyl-substituted benzamidine, J. Org. Chem, 66, 3291-3298 (DOI: 10.1021/jo005632i)

[49] Herr R. J. (2002), 5-Substituted-1H-tetrazoles as carboxylic acid isosteres: Medicinal chemistry and synthetic methods, Bioorg. Med. Chem, 10, 3379-3393 (DOI: 10.1016/S0968-0896(02)00239-0)

[50] Jeong S., Song X., Jeong S., Oh M., Liu X., Kim D., Moon D., Lah M. S. (2011), Metal-organic frameworks based on unprecedented trinuclear and pentanuclear metal-tetrazole clusters as secondary building units, Inorg. Chem, 50, 12133-12140 (DOI: 10.1021/ic201883f)

[51] Liu B., Qiu Y.-C., Peng G., Deng H., (2010), In situ solvothermal syntheses of a heteronuclear copper(I)-alkaline metallic tetrazole-based coordination polymer, Cryst. Eng. Comm., 12, 270-276 (DOI: 10.1039/b910418f)

[52] Liu Y., Eubank J. F., Cairns A. J., Eckert J., Kravtsov V. C., Luebke R., Eddaoudi M. (2007), Assembly of metal-organic frameworks (MOFs) based on indium-trimer building blocks: A porous MOF with soc topology and high hydrogen storage, Angew. Chem., Int. Ed., 46, 3278-3283 (DOI: 10.1002/anie.200604306)

[53] Horike S., Dincă M., Tamaki K., Long J. R., (2008), Size-selective Lewis acid catalysis in a microporous metal-organic framework with exposed Mn^{2+} coordination sites, J. Am. Chem. Soc., 130, 5854–5855 (DOI: 10.1021/ja800669j)

[54] Mota A. J., Rodríguez-Diéguez A., Palacios M. A., Herrera J. M., Luneau D., Colacio E., (2010), Theoretical and experimental study of the effectiveness of the 5-pyrimidyl-tetrazolate bridging ligand in mediating magnetic exchange interactions, Inorg. Chem., 49, 8986-8996 (DOI: 10.1021/ic101322s)

[55] Saha M., Vyas K. M., Martins L. M., Martins N. M., Pombeiro A. J., Mobin S. M., Bhattacherjee D., Bhabak K. P., Mukhopadhyay S. (2017), Copper(II)

tetrazolato complexes: Role in oxidation catalysis and protein binding, Polyhedron, 132, 53-63 (DOI: 10.1016/j.poly.2017.04.016)

[56] Saha M., Das M., Nasani R., Choudhuri I., Yousufuddin M., Nayek H. P., Shaikh M. M., Pathak B., Mukhopadhyay S. (2015), Targeted water-soluble copper-tetrazolate complexes: Interactions with biomolecules and catecholase like activities, Dalton Trans., 44, 20154-20167.

[57] Matsunaga Y., Miyajima N., Nakayasu Y., Sakai S., Yonenaga M. (1988), Design of Novel Mesomorphic Compounds: N,N′,N″-Trialkyl-1,3,5-benzenetricarboxamides, Bull. Chem. Soc. Jpn, 61, 207-210 (DOI: doi.org/10.1246/bcsj.61.207)

[58] Stals P. J., Everts J. C., de Bruijn R., Filot I. A., Smulders M. M., Martín-Rapún R., Pidko E. A., de Greef T. F., Palmans A. R., Meijer E. W. (2010), Dynamic supramolecular polymers based on benzene-1,3,5-tricarboxamides: The influence of amide connectivity on aggregate stability and amplification of chirality, Chem. Eur. J, 16,810-821 (DOI: 10.1002/chem.200902635).

[59] Van Gorp J. J., Vekemans J. A. J. M., Meijer E. W. (2002), C_3-Symmetrical supramolecular architectures: Fibers and organic gels from discotic trisamides and trisureas, J. Am. Chem. Soc, 124, 14759-14769 (DOI: 10.1021/ja020984n)

[60] Bernet A., Albuquerque R. Q., Behr M., Hoffmann S. T., Schmidt H.-W. (2012), Formation of a supramolecular chromophore: A spectroscopic and theoretical study, Soft Matter, 8, 66-69 (DOI: 10.1039/C1SM06789C)

[61] Chang J. Y., Baik J. H., Lee C. B., Han M. J. (1997), Liquid crystals obtained from disclike mesogenic diacetylenes and their polymerization, J. Am. Chem Soc, 119, 3197–3198 (DOI: 10.1021/ja961193m)

[62] Palmans A. R. A., Vekemans J. A. J. M., Meijer E. W., Kooijmans H., Spek A. L. (1997), Benzene-1,3,5-tricarboxamide: A versatile ordering moiety for supramolecular chemistry, Chem. Commun., 2247-2248 (DOI: 10.1039/C2CS35156K)

[63] Kumar D. K., Jose D. A., Dastidar P., Das A. (2004), Nonpolymeric hydrogelators derived from trimesic amides, Chem. Mater, 16, 12, 2332-2335 (DOI: 10.1021/cm049881p)

[64] Palmans A. R., Vekemans J. A., Fischer H., Hikmet R. A., Meijer, E. W. (1997), Extended-core discotic liquid crystals based on the intramolecular H-bonding in N-acylated 2, 2′-bipyridine-3, 3′-diamine moieties, Chem. Eur. J, 3, 300-307 (DOI: 10.1002/chem.19970030220)

[65] Brunsveld L., Zhang H., Glasbeek M., Vekemans J. A. J. M., Meijer E.W. (2000), Hierarchical growth of chiral self-assembled structures in protic media, J. Am. Chem. Soc, 122, 6175-6182 (DOI: 10.1021/ja0005237)

[66] Van Hameren R., Schön P., Van Buul A. M., Hoogboom J., Lazarenko S. V., Gerritsen J. W., Engelkamp H., Christianen P. C., Heus H. A., Maan J. C., Rasing T. (2006), Macroscopic hierarchical surface patterning of porphyrin trimers via self-assembly and dewetting, Science, 314, 1433-1436 (DOI: 10.1126/science.1133004)

[67] Paraschiv I., Giesbers M., van Lagen B., Grozema F. C., Abellon R. D., Siebbeles L. D. A., Marcelis A. T. M., Zuilhof H., E. Sudho¨ lter J. R. (2006), H-bond-stabilized triphenylene-based columnar discotic liquid crystals, Chem. Mater., 18, 968-974 (DOI:10.1021/cm052221f)

[68] Van Herrikhuyzen J., Jonkheijm P., Schenning A. P., Meijer E. W. (2006), The influence of hydrogen bonding and π-π stacking interactions on the self-assembly properties of C_3-symmetrical oligo (p-phenylenevinylene) discs, Org. Biomol. Chem., 4,1539-1545 (DOI: 10.1039/B517993A)

[69] Leenders C. M., Mes T., Baker M. B., Koenigs M. M., Besenius P., Palmans A.R., Meijer E.W. (2014), From supramolecular polymers to hydrogel materials. Mater.Horizons, 1,116-120 (DOI: 10.1039/C3MH00103B)

[70] Howe R. C. T., Smalley A. P., Guttenplan A. P. M., Doggett M. W. R., Eddleston M. D., Tan J. C., Lloyd G. O. (2013), A family of simple benzene 1,3,5-tricarboxamide (BTA) aromatic carboxylic acid hydrogels, Chem. Commun., 49, 4268–4270 (DOI: 10.1039/C2CC37428E)

[71] Gong B., Zheng C., Yan Y. (1999), Structure of N, N′, N ″-tris (carboxymethyl)-1, 3, 5-benzenetricarboxamide trihydrate, J. Chem. Crystallogr., 29,649-652 (DOI: 10.1023/A:1009511501537)

[72] Bose P. P., Drew M. G. B., Das A. K., Banerjee A. (2006), Structure of N, N′,N″-tris(carboxymethyl)-1,3,5-benzenetricarboxamide trihydrate. Chem. Commun, 3196–3198 (DOI: 10.1023/A:1009511501537)

[73] Besenius P., Portale G., Bomans P. H. H., Janssen H. M., Palmans A. R. A., Meijer E. W. (2010), Controlling the growth and shape of chiral supramolecular polymers in water, Proceedings of the National Academy of Sciences of the United States of America, 107, 17888–17893 (DOI: 10.1073/pnas.1009592107)

[74] Gelinsky M., Vogler R., Vahrenkamp H. (2002), Tripodal pseudopeptides with three histidine or cysteine donors: Synthesis and zinc complexation, Inorg. Chem., 41, 2560–2564 (DOI: 10.1021/ic011263c)

[75] De Loos M., van Esch J. H., Kellogg R. M., Feringa B. L. (2007), C_3-Symmetric, amino acid based organogelators and thickeners: A systematic study of structurr-property relations, Tetrahedron, 63, 7285-7301 (DOI: 10.1016/j.tet.2007.02.066)

[76] Veld M. A. J., Haveman D., Palmans A. R. A., Meijer E. W. (2011), Sterically demanding benzene-1,3,5-tricarboxamides: Tuning the mechanisms of supramolecular polymerization and chiral amplification, Soft Matter, 7, 524–531 (DOI: 10.1039/C0SM00516A)

[77] Van den Hout K.P., Martín-Rapún R., Vekemans J. A., Meijer E. E. (2007), Tuning the stacking properties of C_3-symmetrical molecules by modifying a dipeptide motif, Chem. Eur. J, 13, 8111-8123 (DOI:10.1002/chem.200700630)

[78] Matsuura K., Murasato K., Kimisuka N. (2005), Artificial peptide-nanospheres self-assembled from three-way junctions of β-sheet-forming peptides, J. Am. Chem. Soc, 127, 10148-10149 (DOI: 10.1021/ja052644i)

[79] Akiyama M., Katoh A., Ogawa, T. (1989), N-hydroxy amides. part 8. synthesis and iron (III)-holding properties of di-and tri-hydroxamic acids extending from benzene-di-and-tri-carbonyl units through oligo (ethyleneoxy) arms, J. the Chem. Soc., Perkin Trans., 2, 1989, 1213-1218 (DOI: 10.1039/P29890001213)

[80] Stals P. J. M., Haveman J. F., Martı´n-Rapu´ n R., Fitie´C. F. C., Palmans A. R. A., Meijer E. W. (2009), The influence of oligo(ethylene glycol) side chains on the self-assembly of benzene-1,3,5-tricarboxamides in the solid state and in solution, J. Mater. Chem, 19, 124-130 (DOI: 10.1039/B816418E)

[81] Lee S., Lee J.-S., Lee C. H., Jung Y.-S., Kim J.-M. (2011), Nonpolymeric thermosensitive benzene tricarboxamides, Langmuir, 27, 1560-1564 (DOI: 10.1021/la104568c)

[82] Lee J. H., Baek Y. E., Kim K. Y., Choi H., Jung J. H. (2016), Metallogel of bis (tetrazole)-appended pyridine derivative with $CoBr_2$ as a chemoprobe for volatile gases containing chloride atom, Supramol. Chem., 28,870-873 (DOI: 10.1080/10610278.2016.1142088)

[83] Voitekhovich S. V., Wolf A., Guhrenz C., Lyakhov A. S., Ivashkevich L. S., Adam M., Gaponik N., Kaskel S., Eychmüller A. (2016), 5-(2-Mercaptoethyl)-1H-tetrazole: Facile synthesis and application for the preparation of water soluble nanocrystals and their gels, Chem. Eur. J, 22, 14746-14752 (DOI: 10.1002/chem.201602980)

[84] Yan L., Gou S., Ye Z., Zhang S., Ma, L. (2014), Self-healing and moldable material with the deformation recovery ability from self-assembled supramolecular metallogels. Chem. Commun., 50, 12847-12850 (DOI: 10.1039/C4CC06154C)

[85] Yan L., Liu C., Shen L., Li J., Liu X., Lv M., Su C., Ye Z. (2018), Visual discrimination of 2-picolinic acid by a supramolecular metallogel, Chem. Lett., 47,640-642 (DOI:10.1246/cl.180065)

[86] Howlader P., Mukherjee P.S. (2016), Face and edge directed self-assembly of Pd12 tetrahedral nano-cages and their self-sorting, Chem. Sci, 7, 5893-5899 (DOI: 10.1039/c6sc02012g)

[87] Lee H., Kang S., Lee J.Y., Jung J.H. (2012), Coordination polymer gel derived from a tetrazole ligand and Zn^{2+}: Spectroscopic and mechanical properties of an amorphous coordination polymer gel, Soft Matter, 8, 2950-2955 (DOI: 10.1039/C2SM07231A)

[88] Lee J. H., Kang S., Lee J. Y., Jung J. H. (2012), A tetrazole-based metallogel induced with Ag^{+} ion and its silver nanoparticle in catalysis, Soft Matter, 8, 6557-6563 (DOI: 10.1039/C2SM25316J)

[89] Liwei Yan., Linghong Shen., Mingqian Lv., Wenkun Yu., Jie Chen., Shuang Wang., Xiaofang Fu., Zhongbin Ye. (2015), Self-healing supramolecular heterometallic gels based on the synergistic effect of the constituent metal ions, Chem. Commun., 2015, 51, 17627 (DOI: 10.1039/c5cc08421k)

[90] Guo M., Yin Q., Li Y., Huang Y., Zhang Z., Zhou L. (2017), Gel-crystal transition during crystallization of cefpiramide, Chem. Lett, 46, 1292-1295 (DOI:10.1246/cl.170465)

[91] Malviya N., Sonkar C., Kundu B. K., Mukhopadhyay S. (2018), Discotic organic gelators in ion sensing, metallogel formation and bioinspired catalysis, Langmuir, 34, 11575-11585 (DOI: 10.1021/acs.langmuir.8b02352)

[92] Malviya N., Das M., Mandal P., Mukhopadhyay S. (2017), A smart organic gel template as metal cation and inorganic anion sensor, Soft Matter, 13, 6243-6249 (DOI: 10.1039/C7SM01199G)

[93] Escuder B., Rodrı F., guez-Llansola., JF Miravet. (2010), Supramolecular gels as active media for organic reactions and catalysis, New J. Chem, 34, 1044-1054 (DOI: 10.1039/b9nj00764d)

[94] Gupta A., Kumar N. (2016), A review of mechanisms for fluorescent ‘‘turn-on’’ probes to detect Al^{3+} ions, RSC Adv., 6, 106413-106434 (DOI: 10.1039/C6RA23682K)

[95] Terech P., Weiss R. G. (1997), Low molecular mass gelators of organic liquids and the properties of their gels, Chem. Rev, 97, 3133-3160 (DOI: 10.1021/cr9700282)

[96] Zhao Z., Lam J. W., Tang B. Z. (2013), Self-assembly of organic luminophores with gelation-enhanced emission characteristics, Soft Matter, 9, 4564-4579 (DOI: 10.1039/C3SM27969C)

[97] Babu S. S., Praveen V. K., Ghosh A. (2014), Functional π-gelators and their applications, Chem. Rev., 114, 1973-2129 (DOI: 10.1021/cr400195e)

[98] Xue P., Ding J., Shen Y., Gao H., Zhao J., Sun J., Lu R. (2017), Aggregation-induced emission nanofiber as a dual sensor for aromatic amine and acid vapor, J. Mater. Chem. C, 5, 11532-41 (DOI: 10.1039/C7TC03192K)

[99] Feng Y., Liu Z. X., Chen H., Yan Z. C., He Y. M., Liu C. Y., Fan Q. H. (2014), Systematic study of peripherally multiple aromatic ester-functionalized poly(benzyl ether) dendrons for the fabrication of organogels: Structure-property relationships and thixotropic property, Chem.-Eur. J, 20, 7069-7082 (DOI: 10.1002/chem.201400157)

[100] Chen H., Feng Y., Deng G. J., Liu Z. X., He Y. M., Fan Q. H. (2015), Fluorescent dendritic organogels based on 2-(2′-Hydroxyphenyl) benzoxazole: Emission enhancement and multiple stimuli-responsive properties, Chem.-Eur. J., 21, 11018-11028 (DOI: 10.1002/chem.201500849)

[101] Lin Q., Lu T. T., Zhu X., Sun B., Yang Q. P., Wei T. B., Zhang Y. M. (2015), A novel supramolecular metallogel-based high-resolution anion sensor array, Chem. Commun., 51, 1635-1638 (DOI:10.1016/j.inoche.2016.07.013)

[102] Lin Q., Lu T. T., Zhu X., Wei T. B., Li H., Zhang Y. M. (2016), Rationally introduce multi-competitive binding interactions in supramolecular gels: A simple and efficient approach to develop a multi-analyte sensor array, Chem. Sci., 7, 5341-5346 (DOI: 10.1039/C6SC00955G)

[103] Xue P., Ding J., Shen Y., Gao H., Zhao J., Sun J., Lu R. (2017), Aggregation-induced emission nanofiber as dual sensor for aromatic amine and acid vapor, J. Mater. Chem. C, 5, 11532-11541 (DOI: 10.1039/C7TC03192K)

[104] Lee J. H., Baek Y. E., Kim K. Y., Choi H., Jung J. H. (2016), Metallogel of bis (tetrazole)-appended pyridine derivative with $CoBr_2$ as a chemoprobe for volatile gases containing chloride atom, Supramol. Chem, 28, 870-873 (DOI: 10.1080/10610278.2016.1142088)

[105] Hyeaná Kim B. (2006), An insulin-sensing sugar-based fluorescent hydrogel, Chem. Commun., 1842-1844 (DOI: 10.1039/B516632B)

[106] Feldner T., Häring M., Saha S., Esquena J., Banerjee R., Díaz D. D. (2016), Supramolecular metallogel that imparts self-healing properties to other gel

networks, Chem. Mater, 28, 3210-3217 (DOI: 10.1021/acs.chemmater.6b01144)

[107] Biswas P., Ganguly S., Dastidar P. (2018), Stimuli-responsive metallogels for synthesizing Ag nanoparticles and sensing hazardous gases, Chem. Asian J., 13, 1941-1949 (DOI: 10.1002/asia.201800743)

[108] Borghei Y. S., Hosseini M., Khoobi M., Ganjali M. R. (2017), Copper Nanocluster-Enhanced Luminol Chemiluminescence for High-Selectivity Sensing of Tryptophan and Phenylalanine. Luminescence, 32, 1045-1050. (DOI: 10.1002/bio.3289)

[109] Hager M. D., Greil P., Leyens C., van der Zwaag, S., Schubert U. S. (2010), Self-healing materials, Adv. Mater., 22, 5424-5430 (DOI:10.1002/adma.201003036)

[110] Haering M., Díaz D. D. (2016), Supramolecular metallogels with bulk self-healing properties prepared by in situ metal complexation, Chem. Commun., 52, 13068-13081 (DOI: 10.1039/C6CC06533C)

[111] N Yan L., Gou S., Ye Z., Zhang S., Ma, L. (2014), Self-healing and moldable material with the deformation recovery ability from self-assembled supramolecular metallogels, Chem. Commun., 50, 12847-12850 (DOI: 10.1039/c4cc06154c)

[112] Martínez-Calvo M., Kotova O., Möbius M. E., Bell A. P., McCabe T., Boland J. J., Gunnlaugsson T. (2015), Healable luminescent self-assembly supramolecular metallogels possessing lanthanide (Eu/Tb) dependent rheological and morphological properties, J. Am. Chem. Soc., 137, 1983-1992 (DOI: 10.1021/ja511799n)

[113] Haering M., Díaz, D. D. (2016), Supramolecular metallogels with bulk self-healing properties prepared by in situ metal complexation, Chem. Commun., 52, 13068-13081 (DOI: 10.1039/c6cc06533c)

[114] Feldner T., Häring M., Saha S., Esquena J., Banerjee R., Díaz D. D. (2016), Supramolecular metallogel that imparts self-healing properties to other gel networks, Chem. Mater., 28, 3210-3217.

[115] Lee Y. T., Tan Y. J., Oon C. E. (2018), Molecular targeted therapy: Treating cancer with specificity, Eur. J. Pharmacol (DOI: 10.1016/j.ejphar.2018.07.034)

[116] Brown J. M., Attardi L. D. (2005), The role of apoptosis in cancer development and treatment response, Nat. Rev. Cancer, 5, 231 (DOI: 10.1038/nrc1560)

[117] Fotakis G., Timbrell J. A. (2006), In vitro cytotoxicity assays: Comparison of LDH, neutral red, MTT and protein assay in hepatoma cell lines following exposure to cadmium chloride, Toxicol. Lett., 160, 171-177 (DOI: 10.1016/j.toxlet.2005.07.001)

[118] Riss T. L., Moravec R. A., Niles A. L., Duellman S., Benink H. A., Worzella T.J., Minor L. (2016), Cell viability assays.

[119] Bergamo A., Sava G. (2011), Ruthenium anticancer compounds: myths and realities of the emerging metal-based drugs, Dalton Trans., 40, 7817-7823 (DOI: 10.1039/C0DT01816C)

[120] Peacock A. F., Sadler P. J. (2008), Medicinal organometallic chemistry: Designing metal arene complexes as anticancer agents, Chem. Asian J, 3, 1890-1899 (DOI: 10.1002/asia.200800149)

[121] Hoffman A. S. (2012), Hydrogels for biomedical applications, Adv. Drug Deliv. Rev., 64, 18-23 (DOI: 10.1016/j.addr.2012.09.010)

[122] Lu Z.-R., Qiao P. (2018), Drug delivery in cancer therapy, Quo Vadis?, Mol. Pharmacol, 15, 3603-3616 (DOI: 10.1021/acs.molpharmaceut.8b00037)

[123] Ndagi U., Mhlongo N., Soliman M. E. (2017), Metal complexes in cancer therapy-an update from drug design perspective, Drug Des. Dev. Ther, 11, 599 (DOI: 10.2147/DDDT.S119488)

[124] Cho K., Wang X. U., Nie S., Shin D.M. (2008), Therapeutic nanoparticles for drug delivery in cancer, Clin. Cancer Res., 14, 1310-1316 (DOI: 10.1158/1078-0432.CCR-07-1441)

[125] Huang J., He L., Zhang J., Chen L., Su C. Y. (2010), Dynamic functionalised metallogel: An approach to immobilised catalysis with improved activity, J. Mol. Catal. A: Chem., 317, 97-103 (DOI: 10.1016/j.molcata.2009.11.001)

[126] Liu Y. R., He L., Zhang J., Wang X., Su C. Y. (2009), Evolution of spherical assemblies to fibrous networked Pd(II) metallogels from a pyridine-based tripodal ligand and their catalytic property, Chem. Mater., 21, 557-63 (DOI: 10.1021/cm802841r)

[127] Sharma M., Sarma P. J., Goswami M. J., Bania K. K. (2017), Metallogel templated synthesis and stabilization of silver-particles and its application in the catalytic reduction of nitro-arene, J. Colloid Interface Sci, 490, 529-541 (DOI: 10.1016/j.jcis.2016.11.065)

[128] Wen X., Tang L. (2015), One-dimensional copolymer nanostructures loaded with silver nanoparticles fabricated via metallogel template copolymerization and their pH-dependent photocatalytic degradation of methylene blue, J. Mol. Catal. A: Chem, 399, 86-96 (DOI: 10.1016/j.molcata.2015.01.025)

[129] Wen X., Tang L., Li B. (2014), Metallogel template fabrication of pH-responsive copolymer nanowires loaded with silver nanoparticles and their photocatalytic degradation of methylene blue, Chem. Asian J., 9, 2975-83 (DOI: 10.1002/asia.201402575)

[130] Ye L., Wan L., Huang F. (2017), A class of polytriazole metallogels via CuAAC polymerization: Preparation and properties, New J. Chem., 41, 4424-4430 (DOI: 10.1039/C7NJ00610A)

[131] Mallick A., Schön E. M., Panda T., Sreenivas K., Díaz D. D., Banerjee R. (2012), Fine-tuning the balance between crystallization and gelation and enhancement of CO_2 uptake on functionalized calcium-based MOFs and metallogels, J. Mater. Chem, 22, 14951-14963 (DOI: 10.1039/C2JM30866E)

[132] Tang X. Q., Xiao B. W., Li C. M., Wang D. M., Huang C. Z., Li Y. F. (2017), Co-metal-organic-frameworks with pure uniform crystal morphology prepared *via* Co^{2+} exchange-mediated transformation from Zn-metallogels for luminol catalysed chemiluminescence, Spectrochim. Acta Part A, 175, 11-16 (DOI: 10.1016/j.saa.2016.12.014)

[133] Klabunde T., Eicken C., Sacchettini J. C., Krebs B. (1988), Crystal structure of a plant catechol oxidase containing a dicopper center, Nat. Struct. Mol. Biol, 5, 1084-1090 (DOI: 10.1038/4193).

[134] Marbach I., Mayer A. M. (1975), Change in catechol oxidase and permeability to water in seed coat of pisum elatiusduring seed development and maturation, Plant Physiol., 56, 93-96 (DOI:10.1104/pp.56.1.93)

Chapter 2

A Smart Organic Gel Template as Metal Cation and Inorganic Anion Sensor

Chapter 2

A Smart Organic Gel Template as Metal Cation and Inorganic Anion Sensor

2.1 Introduction

Molecular recognition is a powerful process in nature to arrange molecules in a definite way, imparting various physical states and, in consequence, inducing certain novel characteristics in the assembled structures[1-3] One of the most recent advances that have been made in material chemistry using the molecular recognition phenomena is the development of self-assembled supramolecular gel-phase materials, which have great applications in various scientific processes.[4,5] Entrapment of liquid in the interstices of a solid matrix through surface tension and capillary forces results in the formation of a gel-like structure. Based on the driving forces enticing the molecular assembly, gels are classified as chemical gels (cross-linked polymers formed by covalent bonds) and physical gels (small molecular weight compounds assembled by non-covalent interaction).[6-8] However, systems based on both types of interactions have also been documented. The self-assembly of the gelator molecules in gel state can induce changes in some behaviors of the bulk material *e.g.* luminescent property or how it responds to external stimuli like heat, sound, light (physical stimuli) and change in pH or addition of cations or anions (chemical stimuli).[9,10] Furthermore, some gels can also have self-healing property like similar smart materials.[11,12] All these interesting phenomena make the gels suitable candidates for applications in the area of sensors and actuators, cosmetics, foods, environmental remediation, catalysis, drug delivery materials, and regenerative medicines.[13-16] Among all these applications, the utilization of gel materials to sense inorganic cations and anions is relatively rare and unexplored.[17,18]

This chapter presents the synthesis and characterization of a smart 1,3,5-tricarboxamide (BTA) based gelator **G1** with coordination binding sites and fluorescent signal groups

attached to it. The gelator molecule can form supramolecular organogel in the presence of small amounts of water in DMF or DMSO. The gel thus formed has shown some interesting and intense aggregation-induced fluorescence enhanced emission (AIEE).[19,20]

The synthesized gel can selectively sense $\mathbf{Fe^{2+}}$ and $\mathbf{Fe^{3+}}$ by completely switching off the AIEE. Furthermore, upon induction of several metal ions, the gelator molecule shows the formation of different metallogels (MGs). Among them, **CuG1** can sense $\mathbf{SCN^-}$, **ZnG1** can sense $\mathbf{Br^-}$, **NiG1** can sense $\mathbf{CN^-}$ and **Fe(II)G1**/**Fe(III)G1** can sense $\mathbf{S^{2-}}$, selectively, by an abrupt change in the fluorescence property of the metallogels with high selectivity and sensitivity. To the best of our knowledge, there are only a few examples of gelator template molecules that can sense a particular cation selectively (zinc) and can form several metallogels that can detect an array of anions ($\mathbf{SCN^-}$, $\mathbf{CN^-}$, $\mathbf{S^{2-}}$ and $\mathbf{I^-}$).[17,18]

2.2 Experimental section

2.2.1 Material and method

All the reagents are commercially available and used as received. All solvents were of analytical grade, purchased from Merck chemicals, and used directly without further purification. Sodium or potassium salts of anions and perchlorate salts of cations were used, which were purchased from Sigma-Aldrich, USA. During the whole experiment, fresh Milli-Q water was used. Fourier-transform infrared (FTIR) spectroscopy was performed on KBr pellets on a Bruker Tensor 27 FTIR spectrophotometer. NMR spectra were recorded on an AVANCE III 400 Ascend Bruker BioSpin machine at ambient temperature using DMSO-d_6 as a solvent. Chemical shifts are reported in parts per million, downfield of tetramethylsilane; the peak multiplicities are reported as follows: singlet (s), doublet (d), doublet of doublets (dd), triplet (t), and multiplet (m). A Bruker-Daltonics microTOF-Q II mass spectrometer was used for mass spectrometric analyses.

2.2.2 Synthesis of gelator G1 [*N1, N3, N5*-tris(4-cynophenyl) benzene-1,3,5-tricarboxamide]

In a typical experiment, trimesic acid (1 equiv.) in tetrahydrofuran (THF) within a schlenk flask was degassed and purged with argon (Ar). To this, thionyl chloride (3.5 equiv.) was added dropwise under the continuous flow of Ar. The mixture was allowed to heat at 80 °C for 2 h. After cooling the mixture to room temperature, it was washed with dry THF several times resulting in trimesoyl chloride.

Trimesoyl chloride (1.25 g, 4.75 mmol) was treated slowly with excess (3.5 equiv.) 4-aminobenzonitrile and triethylamine in dry DMF at 0 °C and was stirred overnight at ambient conditions. The reaction mixture was kept at room temperature and then the solution layers were separated. The aqueous layer was extracted with EAA (100 mL). Combined organic layer was washed with dil. HCl (1 N, 100 mL), sat. Na_2CO_3 (100 mL), water (100 mL) and brine (100 mL). The resultant powder was dried at room temperature under vacuum. Yield: 75%. ^{1}H NMR (400 MHz, 298 K, DMSO-d_6): d 11.50 (3H, s), 8.96 (3H, s), 8.26 (6H, d), 7.88 (6H, d). ^{13}C NMR (100 MHz, 293 K, DMSO-d_6): d 165.28, 143.97, 134.96, 133.60, 131.35, 120.76, 119.55, 106.09. FT-IR (KBr): 3451, 2234, 1683 cm^{-1}. MS (ESI): *m/z* = 509 (in negative mode).

2.2.3 Preparation of gels

A 0.04 millimole of **G1** gelator was dissolve in 1.5 mL of dimethylformamide (DMF) or dimethyl sulfoxide (DMSO), and 500 μL of Milli-Q water was added in a 5 mL glass vial. The solution was left undisturbed for a couple of minutes, and a stable organogel formed spontaneously. However, metallogels were obtained by mixing 20 mM concentration of **G1** with 10 mM concentration of metal perchlorate salts (**G1**: $\mathbf{M^{n+}}$ molar ratio = 2:1 and solvent is 1 mL DMF/1 mL water).

2.2.4 Gel melting temperature

Gel melting temperature (T_{gel}) of **G1** has been measured by test tube inversion method. The steel ball (approximately 100 mg) was kept on the top of **G1** gel. The gel has been heated with the rate of 2 °C/5 min and the height of the steel ball was recorded with temperature. The steel ball starts moving downward direction of the vial after gradually melting of gel into sol form. However, the gel-melting temperature is the temperature where the gel starts melting.

2.2.5 Characterizations

UV-visible Spectroscopy. Absorption spectra have been analyzed by Varian Carry 100 Bio UV-vis spectrophotometer using quartz cuvette (10×10 mm^2).

Fluorescence Spectroscopy. Fluoromax-4 spectrofluorometer (HORIBA Jobin Yvon, model FM-100) has been used for recording of emission spectra of the gels in a quartz cuvette (10×10 mm^2). The excitation and emission slit width and data pitch were 2 and 1 nm, respectively. Excitation wavelength (λ_{ex}) 350 nm was set to record the emission spectra of organogel **G1**. The absolute fluorescence quantum yield of organogel **G1** has been calculated at λ_{ex} = 350 nm under ambient conditions by using standard *viz.*, quinine sulfate (ϕ = 0.53). The expression for the quantum yields is

$$Q_x = Q_r \left(\frac{K_r}{K_x}\right)\left(\frac{D_x}{D_r}\right)\left(\frac{\eta_{x^2}}{\eta_{r^2}}\right)$$

here, Q is the quantum yield; K denotes the average detector output per photon over the emission spectrum [Kr/Kx = 1 for estimates of yields for compounds emitting below 600 nm]; D represents the detector response; η is the refractive index of the solvent [η = 1.483 for DMSO, η = 1.439 for DMF and η = 1.33 for H_2O solvent]; x and r subscripts are the unknown and standard reference.

FT-IR Spectroscopy. Bruker (Tensor 27) FTIR spectrophotometer has been used for recording the FTIR spectrum with the help of KBr pellet. The range of wavenumber for the FTIR measurement has been taken around 500-4000 cm^{-1} over 64 scans at a resolution of 4 cm^{-1} and interval of 1 cm^{-1}.

Powder X-ray Diffraction (PXRD). Powder X-ray diffraction spectra (PXRD) has been taken with the help of Rigaku Smart Lab, automated multipurpose X-ray diffractometer with Cu Kα source (the wavelength of X-rays was 0.154 nm). The tube voltage and current were 40 kV and 30 mA. The XRD patterns have been taken in between 20-80° (2θ) with step size and scan speed of 0.02° and 2°/min, respectively.

Morphological Study. Field-emission scanning electron microscopy (FE-SEM, Carl Zeiss Microscope, model-Supra 55) has been used to observe the various morphology and sizes of the gels. For this experiment, sample has been prepared by diluting 100 μL of the gel in 400 μL of water. After this, small amount (50 μL) of the gel has to be placed on a glass coverslip. After drying the sample, the gold coating was used for analysis.

Rheological Properties. Mechanical properties of the **G1** organogel and their metallogels have been quantified via oscillating rheology. The rheology experiments were executed at 25 °C on an Anton Paar Physica MCR 301 rheometer. A 25 mm stainless steel parallel plate with a TruGap of 0.5 mm was used for rheology test. The mechanical strength of gels was measured at 0.5% strain by measuring the storage (G′) and loss (G″) modulus. Gels (1 mL) were transferred very carefully onto the rheometer plate using small spatula, and the solvent trap was used to keep the gel hydrated.

2.3 Results and discussion

The gelator molecule *N1*,*N3*,*N5*-tris(4-cynophenyl)benzene-1,3,5-tricarboxamide (**G1**) was prepared by treating trimesoyl chloride with an excess of 4-aminobenzonitrile (3.5 equiv.) in the presence of triethylamine (Scheme 2.1). The resultant compound was extracted with ethyl acetate, and the purified compound was characterized by ^{1}H and ^{13}C NMR, IR and ESI-MS spectroscopy.

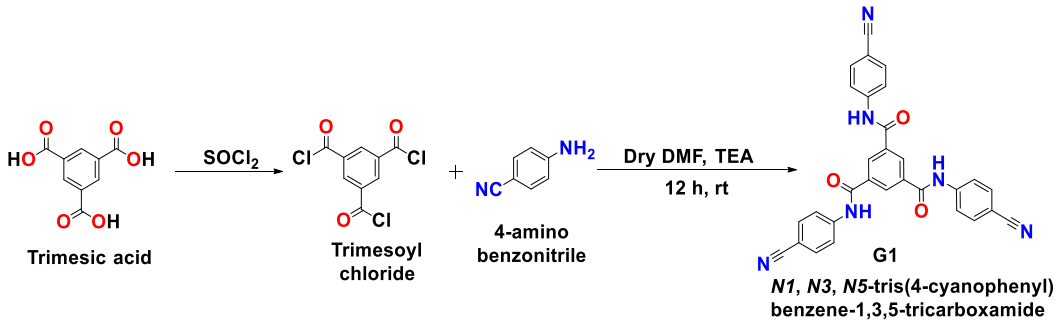

Scheme 2.1. *Systematic scheme for the synthesis of gelator* ***G1****.*

The IR spectrum of the molecule reveals characteristic band for carboxamide N-H at 3389 cm^{-1} as shoulder, for C=O stretching at 1683 cm^{-1}, and amide I at 1641 cm^{-1}.[21] The broadband at 3389 cm^{-1} for N-H stretching is indicative of possible hydrogen bonding. The nitrile group of the gelator molecule has shown a characteristic band at 2235 cm^{-1}. In ^{1}H NMR spectrum, the aromatic ring protons were observed within the range of 8.96-7.87 ppm (Figure 2.1). The carboxamide protons showed a peak at 11.50 ppm. In ^{13}C NMR, the carboxamide carbons were observed at 165.2 ppm, and the nitrile carbons were observed at 119.5 ppm (Figure 2.2). All the aromatic carbons are observable between 143.9 and 106.0 ppm. The ESI-MS spectrum has shown a molecular ion peak at 509.1 in the negative mode, confirming the formation of the gelator molecule (Figure 2.3).

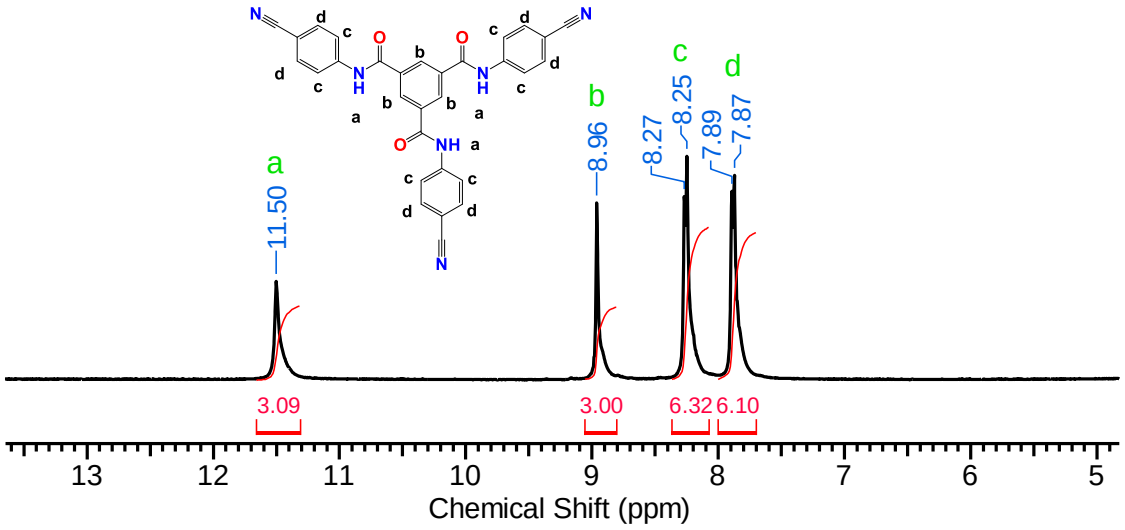

Figure 2.1. *^{1}H NMR spectrum of gelator* ***G1****.*

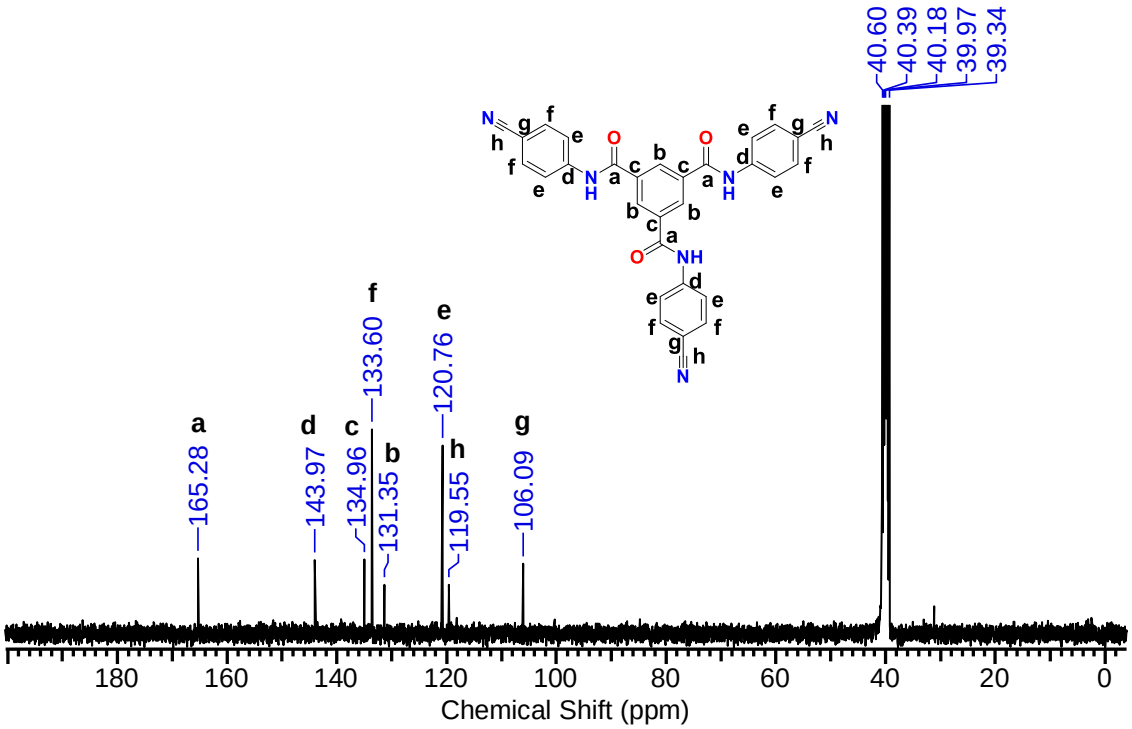

Figure 2.2. *^{13}C NMR spectrum of gelator* ***G1***.

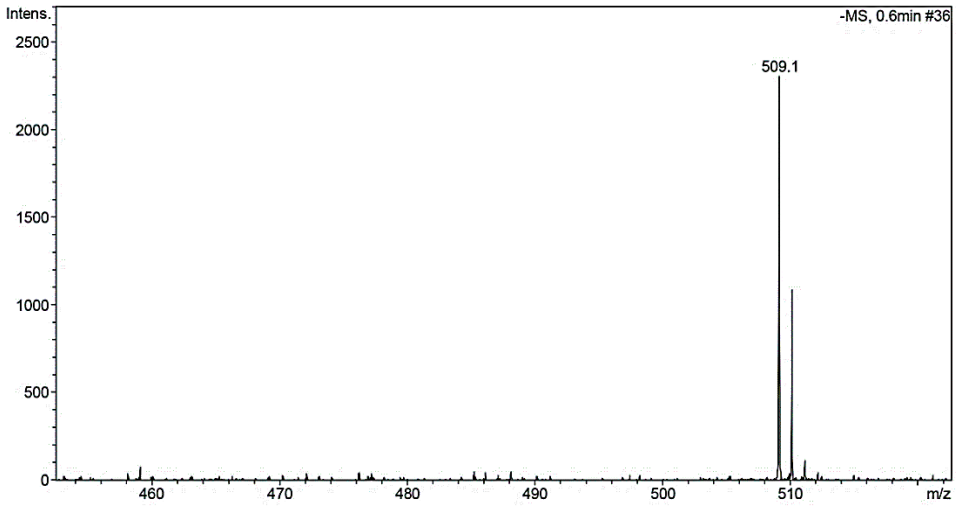

Figure 2.3. *ESI- Mass spectrum of gelator* ***G1***.

Different combinations of solvents were used to explore the propensity of the gelator molecule towards gel formation. The compound has shown solubility only in DMF and

DMSO. It is not soluble in common organic solvents like cyclohexane, THF, toluene, hexane, chloroform, dichloromethane, acetone, acetonitrile, methanol, ethanol, or isopropanol. The gelator showed a tendency in the formation of the gel upon addition of 500 μL of water in a 20 mM solution of DMF or DMSO like some similar compounds reported earlier.[21] The critical gel concentrations (CGCs) were found to be 10.18 mg mL^{-1} for DMF-water pair and 10.07 mg mL^{-1} for DMSO-water pair. The gel-sol phase transition temperatures (T_{gel}) were found to be 100 °C and 97 °C, respectively. The above-mentioned results indicate the stability of the gel at room temperature. The gel formation was ascertained by ‘‘test tube inversion’’ method (Figure 2.4).

Figure 2.4. *Optical image of gelator* ***G1*** *(Test tube inversion method).*

Further, the transition was investigated by temperature dependent emission spectroscopy. **G1** in an aqueous mixture of DMF reveals a feeble fluorescence band at 445 nm (excitation 350 nm) which may be associated with π^*-π or π^*-n transition at a high temperature around 100 °C in hot DMF. However, upon gradual cooling of the solution after the formation of the gel, the emission band enhances several folds, and a progressive blue-shift is observed where the emission maxima is detected at 434 nm (Figure 2.5). This significant fluorescence enhancement due to gelation is called aggregation induced enhanced emission (AIEE) phenomenon. During the organogel formation of **G1**, various non-covalent interactions might have played crucial roles. Among them, hydrogen bonding interactions between carboxamide and nitrile moieties, π-π stacking interactions between aromatic rings and van der Waals interaction between different molecules may act in tandem to stabilize the gel structure.[22] Additionally, AIEE was further corroborated

by the quantum yield (Φ) experiment. Quantum yields for the organogel **G1** has been found to be 0.04.

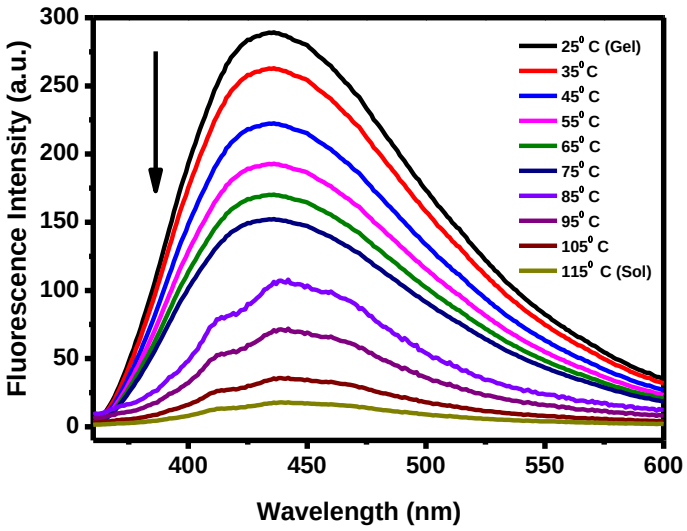

Figure 2.5. *Temperature-dependent fluorescence spectra of the organogel* ***G1*** *(in DMF) during the gelation process (λ_{ex} = 350 nm).*

To look into the possible role of hydrogen bonding in the formation of the gel, infrared and concentration-dependent ^{1}H NMR spectroscopy were utilized. A comparison between the IR spectra of the powder and xerogel obtained from DMF reveals a shift of the carboxamide N–H band from 3389 cm^{-1} to 3314 cm^{-1}, the C=O vibration peak from 1683 cm^{-1} to 1679 cm^{-1}, the amide I band from 1641 cm^{-1} to 1614 cm cm^{-1} and amide II band from 1545 to 1523 cm^{-1} (Figure 2.6). Shifting of these bands towards lower wavenumbers indicates the formation of stronger hydrogen bonds in the gel state with more ordered structure. Interestingly, the stretching frequency of nitrile group also shows a shift towards lower wavenumber from 2234 to 2226 cm^{-1}. It is also an indication of the formation of hydrogen bond.[23,24]

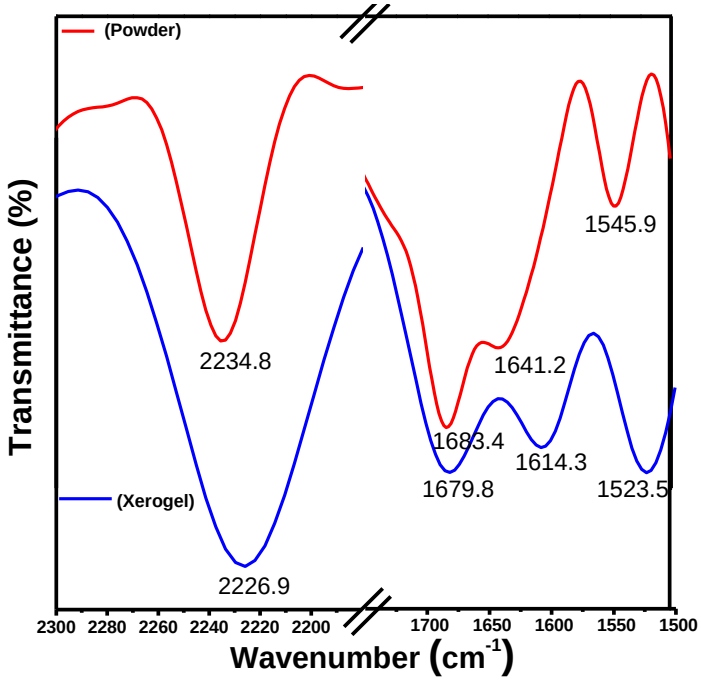

Figure 2.6. *FT-IR spectra of powder and xerogel of* ***G1****.*

Formation of hydrogen-bonded aggregation of gelator molecule **G1** is further investigated with concentration-dependent ^{1}H NMR spectra. Upon increasing the concentration of the gelator molecule from 20 mM to 150 mM, the NH protons show a downfield shift from 11.50 to 10.99 ppm (Figure 2.7).[25,26] Furthermore, with a gradual increase in concentration, the ^{1}H NMR signals of the aromatic rings also show a downfield shift, indicating a possible role of the aromatic protons in hydrogen bonding.

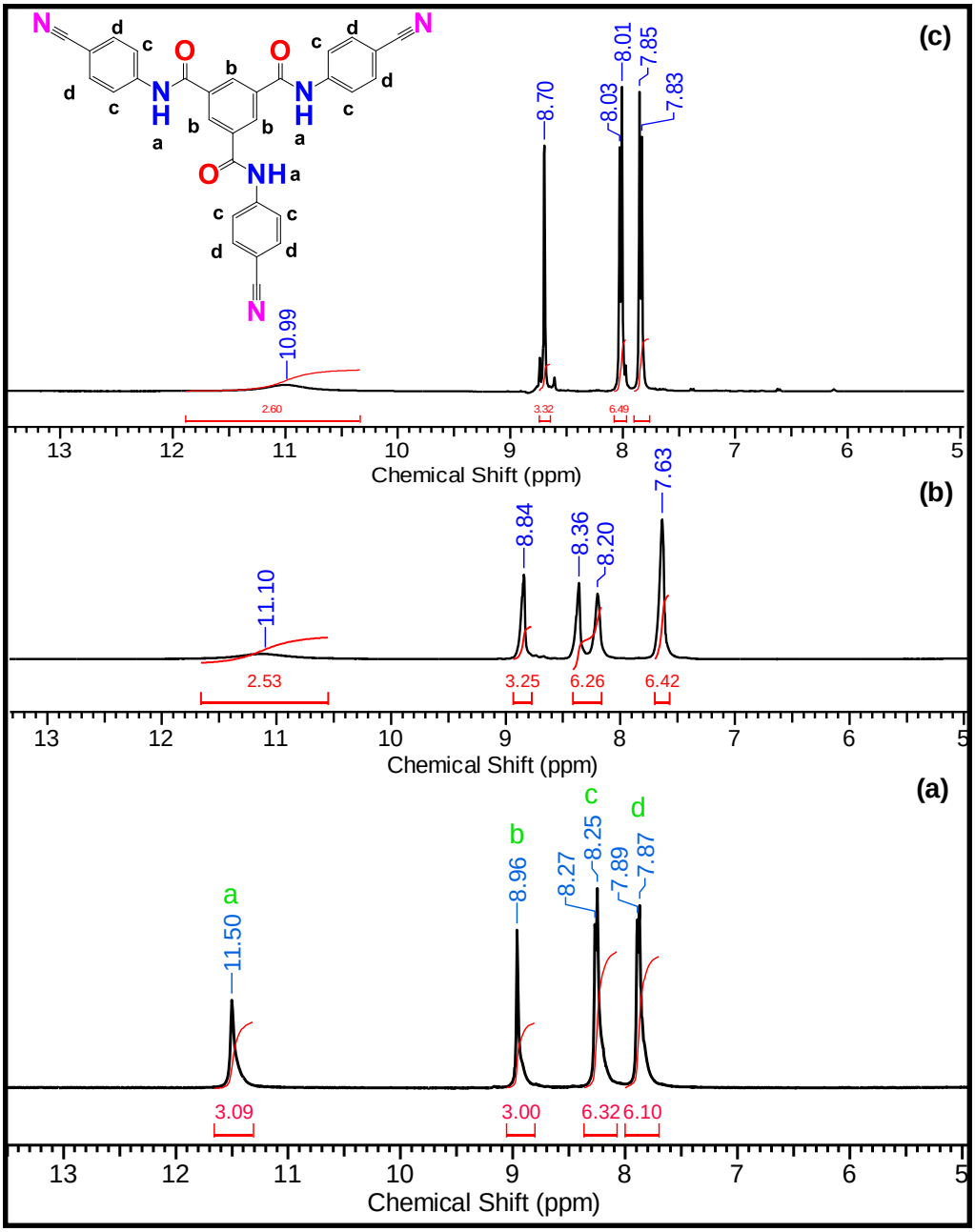

Figure 2.7. *^{1}H NMR spectra of* ***G1*** *in DMSO-d_6 at different concentrations:(a) 20 mM (b) 100 mM (c) 150 mM.*

Interestingly, powder XRD pattern of the xerogel shows peaks at 2θ = 21.60° corresponding to the *d*-spacing value of 4.1 Å, which corresponds to the intercolumnar stacking.[27] The peak at 2θ = 25.36° corresponding to the *d*-spacing value of 3.51 Å is

indicative of π-π stacking.[28,29] The peak at 2θ = 30.05° corresponding to the *d*-spacing value of 2.97 Å and at 2θ = 35.15° corresponding to the *d*-spacing value of 2.55 Å indicate the existence of hydrogen bonding in nitrile containing organic moiety, which is observable in the solid state (Figure 2.8).[30–32]

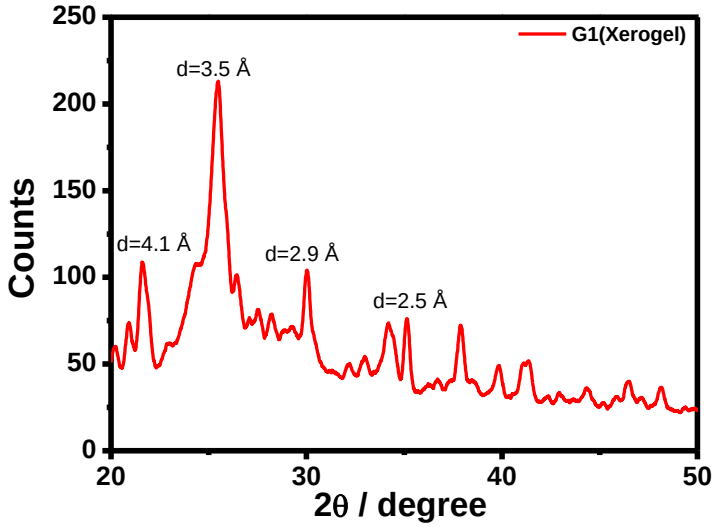

Figure 2.8. *Powder XRD spectra of* ***G1*** *xerogel.*

The influence of different metal ions on the emission properties of the gel was investigated by dissolving the gelator molecule **G1** and 0.5 equivalent of different metal perchlorate salt as the source of metal cations (Fe^{2+}, Fe^{3+}, Cu^{2+}, Zn^{2+}, Co^{2+}, Ni^{2+}, Ag^{+}, $Cd^{2+,}$ and Ca^{2+}) in DMF. Upon addition of a small amount of water, instantaneous metallogel formation was observed. Almost for all the ions, after the formation of the metallogel, quenching of fluorescence spectra and blue or red shift of the emission maxima were found. However, in the case of **Fe^{2+}** and **Fe^{3+}**, the fluorescence gets turned-off completely, paving the way to selectively detect iron ion in the aqueous solution with the naked eye using a handheld UV-lamp (Figure 2.9). Even in daylight, the presence of an iron ion in the metallogel is quite distinctive with respect to other ions (Figure 2.10).

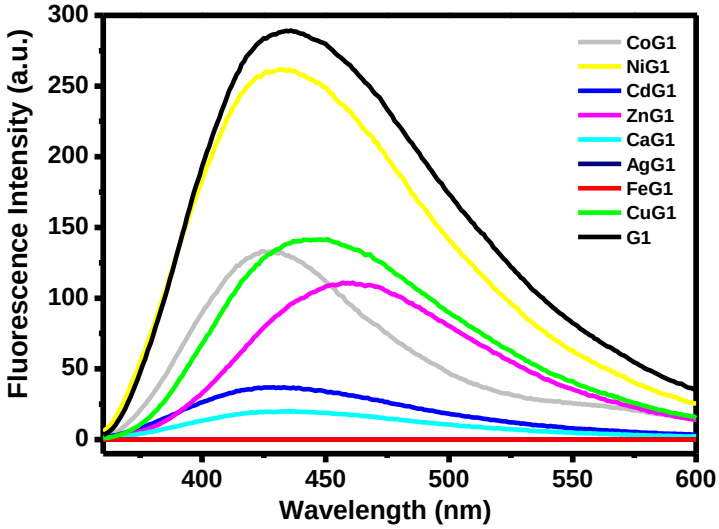

Figure 2.9. *Fluorescence spectra of organogel* ***G1*** *in the presence of several metal ions (in DMF) (with Sources of their perchloric salts) added in 2:1 molar ratio on* ***G1*** *(λ_{ex} = 350 nm).*

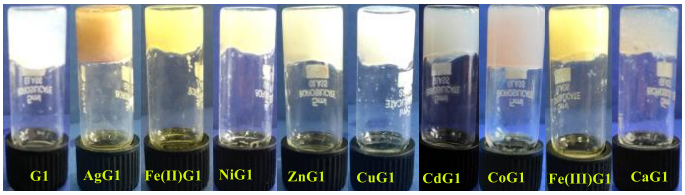

Figure 2.10. *Optical image of* ***G1*** *organogel and their metallogels under day light.*

To investigate the type of interaction between metal ions and the gelator molecule **G1**, the IR spectra of the metal xerogel of **CuG1**, **ZnG1**, **NiG1**, **Fe(II)G1** and **Fe(III)G1** were recorded. All the spectra showed a remarkable lowering of the C=O stretching frequency from the region 1630 cm^{-1} to 1600 cm^{-1}, indicating coordination of the gelator molecule to the metal centre through oxygen of the C=O group. The N–H stretching frequency was found to become sharper around 3339–3342 cm^{-1} indicating the removal of hydrogen bonds. The most intriguing observation was the shift of -C≡N stretching frequency from 2226 cm^{-1} to 2220 to 2205 cm^{-1}, observed for **CuG1**, **ZnG1,** and **NiG1**, respectively, indicating a weak interaction between the metal ion and the nitrile group through a π-

bond. However, in the case of **Fe(II)G1** and **Fe(III)G1**, the shifts were much more pronounced as the nitrile stretches were observed at 2159 cm^{-1} and 2171 cm^{-1}, respectively (Figure 2.11). These results indicate that nitrile gets attached to iron(II) and iron(III) centers through π-coordination,[33–35] which might be the origin of disruption in the aggregated structure, and hence the AIEE gets completely quenched after coordination to the iron centres.

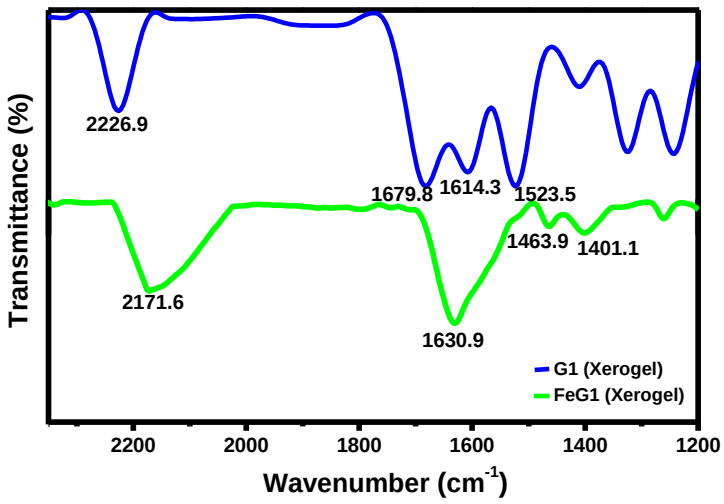

Figure 2.11. *FT-IR spectra of xerogels of* ***G1*** *and* ***FeG1****.*

Furthermore, all the metallogels were tested for anion response capability by adding various anions (Br^-, Cl^-, I^-, OAc^-, N_3^-, SCN^-, ClO_4^-, CN^- and S^{2-}) into the respective metallogels. Interestingly some of them have showed unique selection and sensing property according to the stimuli of the corresponding anion. While **ZnG1** showed selective sensing of **Br^-** ion by turning off the fluorescence, **CuG1** showed selective sensing of **SCN^-** by completely switching off the fluorescence. The nickel metallogel **NiG1** showed selective sensing of **CN^-** ion by drastic quenching of the fluorescence, and **FeG1** (both in +2 and in +3 state) gave the selective sensing of **S^{2-}** ion by fluorescence ‘‘turn-on’’ (Figure 2.12).

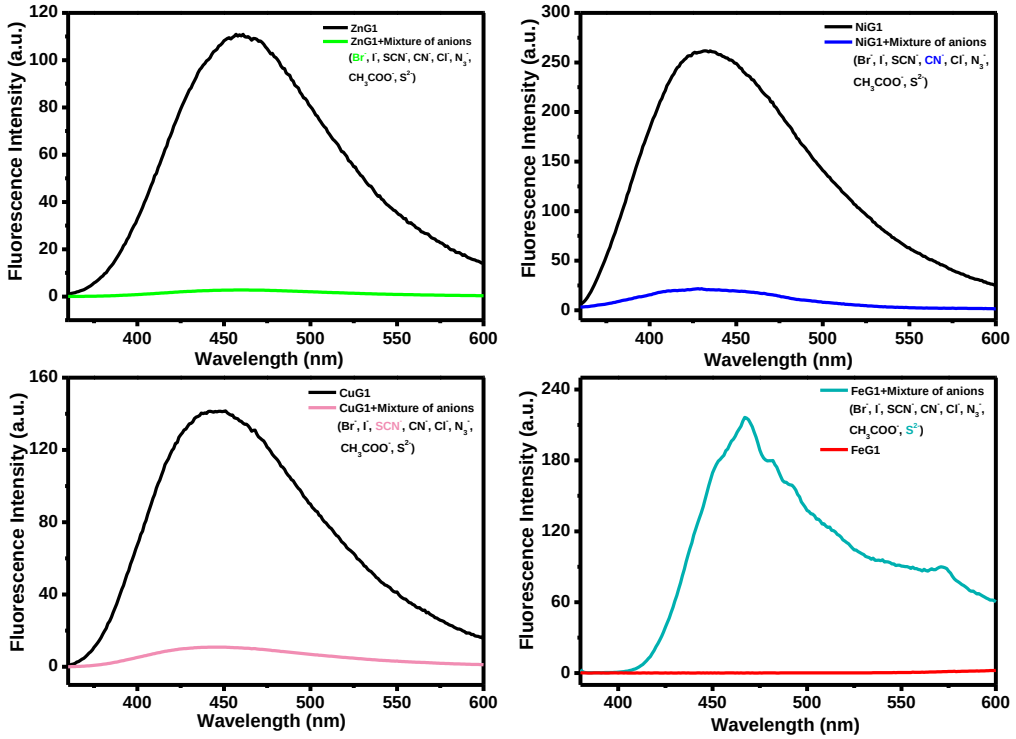

Figure 2.12. *Fluorescence spectra of MGs (in DMF) in the presence of various anions (λ_{ex} = 350 nm) [**ZnG1** and **ZnG1** treated with **Br⁻**; **CuG1** and **CuG1** treated with **SCN⁻**; **NiG1** and **NiG1** treated with **CN⁻**; **FeG1** and **FeG1** treated with **S²⁻**].*

However, the presence of specific anion, which affects the interaction between the metal ion and gelator molecule is further investigated through IR spectroscopy (Figure 2.13). It was observed that in the presence of the specific ion, the nitrile peak of the gelator molecule in the metallogel shifts towards the original position, *i.e.* around 2226 cm^{-1} for **ZnG1**, **CuG1,** and **NiG1**, indicating the non-interaction of nitrile group with the metal ions. Interestingly, in case of **FeG1** in the presence of S^{2-} the -C≡N stretching frequency further shifts towards the lower wavenumber region, which is a signature of stronger π-coordination. The IR stretching frequency for C=O group for all the metallogel was found to be in the range of 1658–1628 cm^{-1}, indicating a weaker interaction between the metal ions and the gelator molecule in the presence of selective ions. The N–H stretching frequency of the gelator molecule also shifts towards higher wavenumber and becomes

broader, indicating the restoration of hydrogen bonds. In case of **NiG1**, a sharp band at 2161 cm^{-1} indicates the presence of coordinated cyanide ion, whereas in case of **CuG1**, two bands at 2160 and 2074 cm^{-1} indicate the presence of two types of thiocyanate ions, presumably one is bridging and the other is terminal.[21,36]

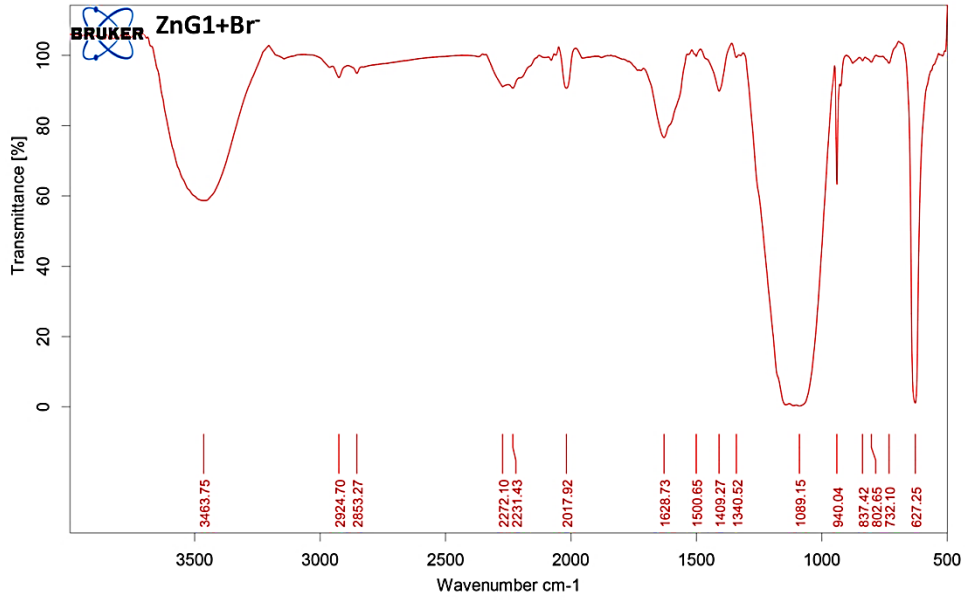

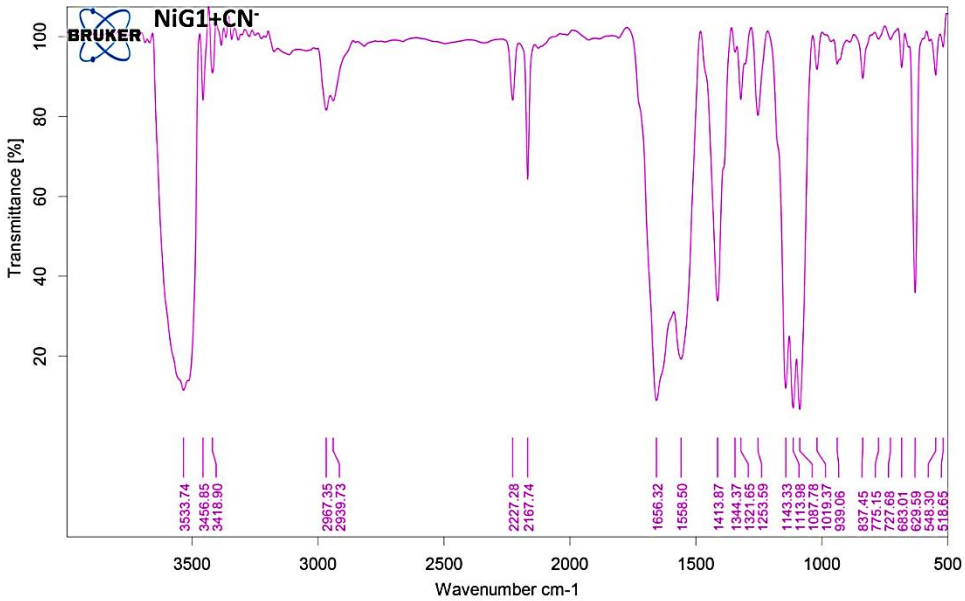

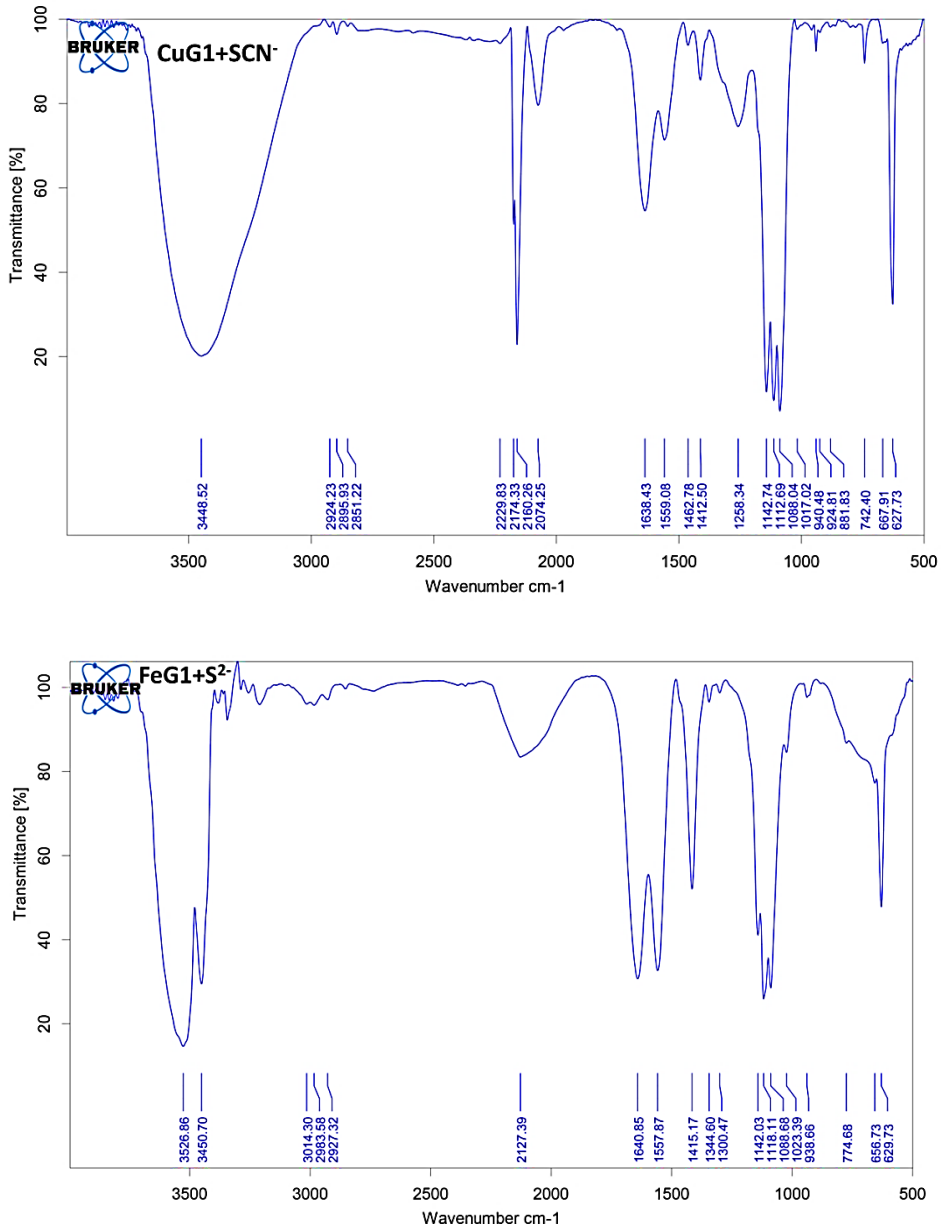

Figure 2.13. *FT-IR spectra of xerogels of* ***ZnG1+Br-***, ***NiG1+CN-***, ***CuG1+SCN-***, ***Fe(II)G1+S2-***.

The sensing results obtained can be combined to produce a metallogel based sensor system that can identify the presence of **Br-**, **SCN-**, **CN-** and **S2-** in water medium with high selectivity and sensitivity. To find out the efficacy of the system, the sensing experiment was carried out in a multi-analytical condition by the addition of a mixture of

Br^-, Cl^-, I^-, OAc^-, N_3^-, SCN^-, ClO_4^-, CN^- and S^{2-} to different metallogels. The metallogels responded in a way similar to when treated with a single target anion, confirming their efficacy to act as a sensor even in a multi-analytical condition in water. Furthermore, to explore the efficacy of the anion sensing property of metallogels, the fluorescent probe has been used to measure the change in intensity of fluorescence peaks with increasing concentration of different anions which are being detected. The detection limits of each metallogels were calculated using the following equation: detection limit = 3s/k, where 's' is the standard deviation of the blank measurement and 'k' is the slope between the fluorescence intensity *vs.* [anion]. The values obtained were 7.2 $\times 10^{-5}$ M for **Br^-** (**ZnG1**); 4.8×10^{-5} M for **CN^-** (**NiG1**); 2.2×10^{-7} M for **SCN^-** (**CuG1**) and 5.2×10^{-5} M for **S^{2-}** (**FeIIG1**).[37] TLC plates can be utilized as spot detectors for the anions in water solution. For this, the plate should be coated with the metallogel, and a drop of an aqueous solution of the corresponding anion should be placed over it. This strip can be reused further for one or two times more by making a coat of the corresponding metal ion with a brush on top of it (Figure 2.14).

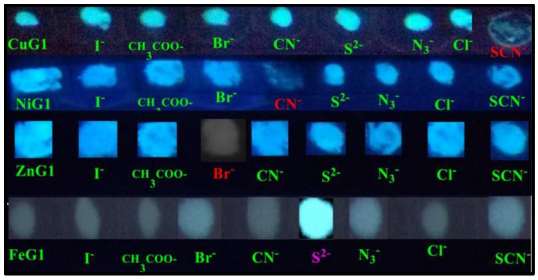

Figure 2.14. *Fluorescence responses of the metallogel-based sensor array in the presence of 1 equiv. of various anions (using 0.1 mol L^{-1} anion sodium or potassium salt water solution as anion source).*

The viscoelastic property of **G1** and other metallogels was explored by rheological studies.[38] The average storage modulus (G′) for gelator **G1** (Figure 2.15) was found to be 10 Pa, whereas induction of metal ions in the gelator showed a considerable increase in the average storage modulus value of 3×10^3, 9×10^2, 8×10^3 and 6×10^3 Pa for **CuG1**,

ZnG1, **NiG1** and **Fe(II)G1** (Figure 2.16), respectively. These results indicate the increase in stiffness upon the incorporation of the metal ions. It may lead to the formation of a network structure through the generation of MOF (Metal Organic Framework), and that might be the reason behind the increase in the average storage modulus value. It is also intriguing to note that the increase in stiffness is quite high for iron(II), which shows complete quenching of AIEE, hinting that the complete disruption of the gel structure may have been occurred by efficient MOF formation. In all the cases, storage modulus G′ was found to be higher than the loss modulus G″, and with an increase in stress both the values deviated from linearity and the stress crossover point was observed at 150, 100 and 50 Pa for **CuG1**, **Fe(II)G1**, and **ZnG1**, respectively, whereas no crossover point was detected for **G1** and **NiG1**. The shear stresses during the frequency sweep were found to be 70, 5×10^3, 7×10^3, 3×10^2 and 8×10^2 Pa. The G′-G″ value indicates the rigidity of the metallogels, and for all the samples, G′ was found to be higher than G″ in entire sweep range, showing the viscoelastic nature of the gels.

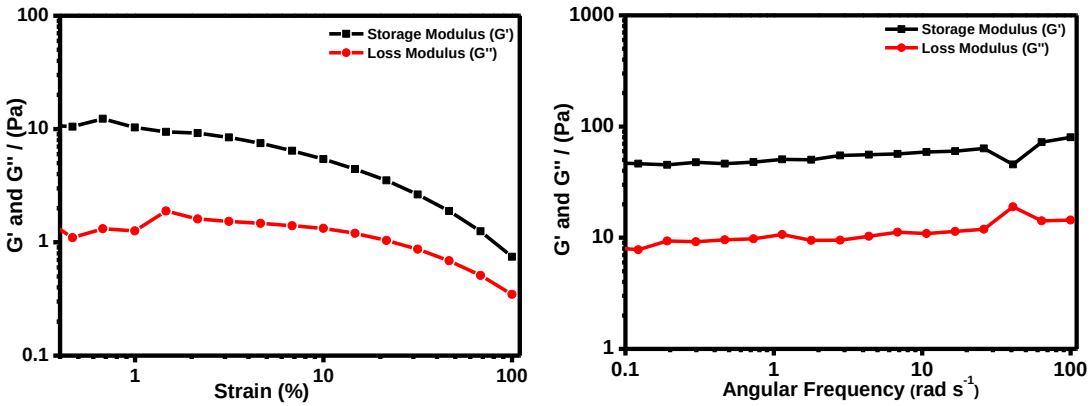

Figure 2.15. *Linear viscoelastic (LVE) and dynamic frequency sweep property of* ***G1*** *(storage modulus G′ is higher than the loss modulus G″).*

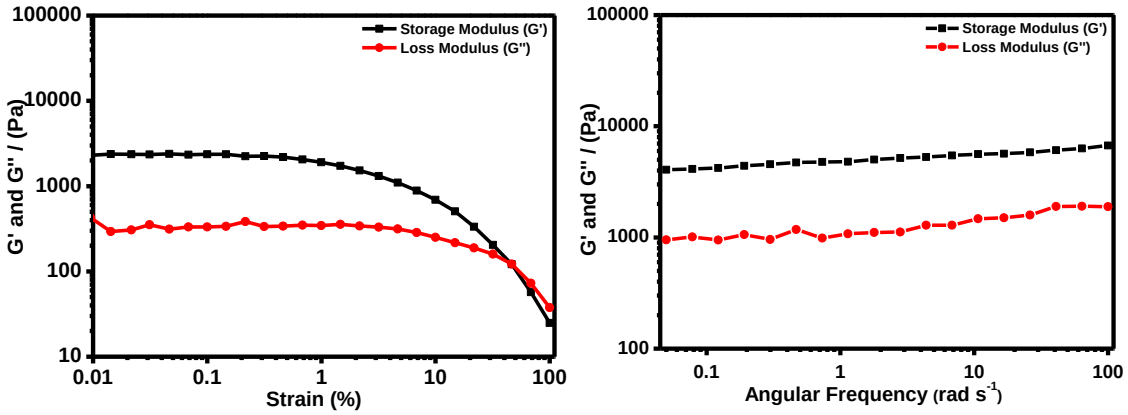

Figure 2.16. *Linear viscoelastic (LVE) and dynamic frequency sweep property of* ***FeG1*** *(storage modulus G′ is higher than the loss modulus G″).*

To have a better understanding of the morphological features of the gel formed by the gelator molecule **G1** and metallogels, the xerogels formed were investigated with SEM studies.[39] The SEM image of the **G1** organogel revealed a needle-like structure with a mean diameter of about 200 nm and length of about 20 mm (Figure 2.17). Further, **FeG1** metallogel has shown fibrous morphology with 2 μm diameter (Figure 2.17). However, incorporation of metal ion changes the morphology to a fibrous one with length in the order of micrometer and the width ranging from 50 nm to 100 nm.

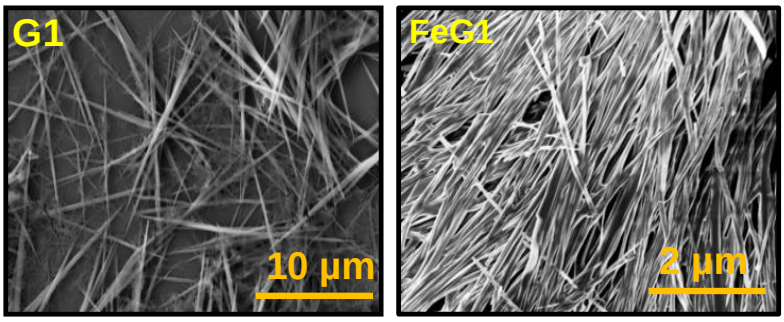

Figure 2.17. *SEM images of* ***G1*** *organogel and* ***FeG1*** *metallogel.*

Further, the PXRD pattern of the metal-containing xerogels reveals the absence of peaks around 2θ = 30° and 35°, indicating disruption in the hydrogen-bonded structure in the

organogel. However, a peak around 2θ = 25.5° corresponding to a *d*-spacing value of around 3.49 Å is retained, indicating the retention of π-π stacking even in the metallogel (Figure 2.18). Interestingly, upon introduction of $\mathbf{S^{2-}}$, the peak at 2θ = 35° reappears, which indicates the formation of extensive hydrogen bonds, which may be the driving force behind the regeneration of the fluorescence property. Not much difference is observed in PXRD patterns of **NiG1** and **ZnG1** upon introduction of selective anions. In the case of **CuG1**, upon the introduction of $\mathbf{SCN^-}$, the peak around 2θ = 35° reappears indicating the formation of H-bonds. However, despite that, the fluorescence gets switched off, which indicates that there might be some other reason behind the exclusive sensing property towards $\mathbf{SCN^-}$ exhibited by **CuG1**.

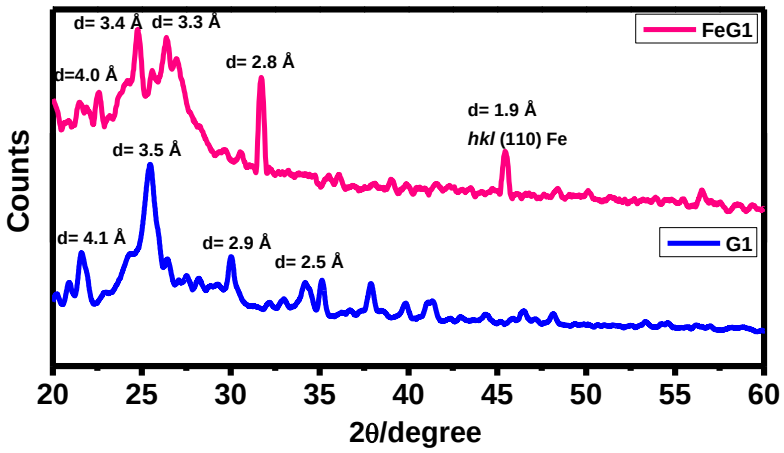

Figure 2.18. *Powder XRD spectra of xerogel of* ***G1*** *and* ***FeG1****.*

2.4 Conclusions

To summarize, a BTA based tri-nitrile molecule showed attractive gelation property in an aqueous mixture of DMF or DMSO. Upon gelation, it shows an aggregation induced enhanced fluorescence spectra. Inductions of various metal ions strengthen the gel property further without much disturbance to the fluorescence property. Interestingly $\mathbf{Fe^{2+}}$ and $\mathbf{Fe^{3+}}$ completely switch off the emission of the gel, and this can help the gel to act as an iron sensor. Detailed study through IR spectroscopy revealed a greater interaction of

the gelator molecule through the π-bonding of the nitrile group towards the center, which might be the cause behind the disruption of the aggregate-induced structure, thus switching off the fluorescence. Furthermore, induction of different metal ions individually produced anion sensing metallogel array, which could selectively bind and sense anions like **SCN^-**, **CN^-**, **Br^-** and **S^{2-}** with high precision by either switching off or switching on the aggregation induced emission property of the gel. Further investigations in this unusual anion sensing property of the metallogel might help to understand the key interactions, which are instrumental in bringing out such sensing feature and can help us to further fine tune the gelator molecule for futuristic applications in the realm of sensor chemistry.

2.5 References

[1] Zhang L., Wang X., Wang T., Liu M. (2015), Tuning soft nanostructures in self-assembled supramolecular gels: from morphology control to morphology-dependent functions, Small, 11, 1025-1038 (DOI: 10.1002/smll.201402075)

[2] Zhang L., Qin L., Wang X., Cao H. Liu M. (2014), supramolecular chirality in self-assembled soft materials: regulation of chiral nanostructures and chiral functions, Adv. Mater., 26, 6959-6964 (DOI: 10.1002/adma.201305422)

[3] Babu S. S., Praveen V. K., Ghosh A. (2014), Functional π-gelators and their applications, Chem. Rev., 114, 1973-2129 (DOI: 10.1021/cr400195e)

[4] Bhattacharya S., Samanta S. K. (2016), Soft-nanocomposites of nanoparticles and nanocarbons with supramolecular and polymer gels and their applications, Chem. Rev., 116,11967-12028 (DOI: 10.1021/acs.chemrev.6b00221)

[5] Okesola B. O., Smith D. K. (2016), Applying low-molecular weight supramolecular gelators in an environmental setting–self-assembled gels as smart materials for pollutant removal, Chem. Soc. Rev., 45, 4226-4251 (DOI: 10.1039/C6CS00124F)

[6] Thool G. S., Narayanaswamy K., Venkateswararao A., Naqvi S., Gupta V., Chand S., Vivekananthan V., Koner R. R., Krishnan V., Singh S. P. (2016), Highly directional 1D supramolecular assembly of new diketopyrrolopyrrole-

based gel for organic solar cell applications, Langmuir, 32, 4346-4351 (DOI: 10.1021/acs.langmuir.6b00846)

[7] Datta S., Bhattacharya S. (2015), Multifarious facets of sugar-derived molecular gels: molecular features, mechanisms of self-assembly and emerging applications, Chem. Soc. Rev., 44, 5596-5637 (DOI: 10.1039/C5CS00093A)

[8] Cui Y., Chen B., Qian G. (2014), Lanthanide metal-organic frameworks for luminescent sensing and light-emitting applications. Coord. Chem. Rev., 273, 76-86 (DOI: 10.1016/j.ccr.2013.10.023)

[9] Gómez-Valdemoro A., Trigo M., Ibeas S., García F. C., Serna F. García J. M. (2011), Acrylic copolymers with pendant 1, 2, 4-triazole moieties as colorimetric sensory materials and solid phases for the removal and sensing of cations from aqueous media, J. Polym. Sci. A Polym. Chem., 49, 3817-3825 (DOI: 10.1002/pola.24820)

[10] Gomes M. A., Lima A. S., Eguiluz K. I., Salazar-Banda G. R. (2016), Wet chemical synthesis of rare earth-doped barium titanate nanoparticles, J. Mater. Sci., 51, 4709-4727 (DOI: 10.1007/s10853-016-9789-7)

[11] Haering M., Díaz D. D. (2016), Supramolecular metallogels with bulk self-healing properties prepared by in situ metal complexation, Chem. Commun., 52, 13068-13081 (DOI: 10.1039/C6CC06533C)

[12] Taylor D. L. In het Panhuis M. (2016), Self-healing hydrogels, Adv. Mater., 28, 9060-9093 (DOI: 10.1002/adma.201601613)

[13] Hirst A. R., Escuder B., Miravet J. F., Smith D. K. (2008), High-tech applications of self-assembling supramolecular nanostructured gel-phase materials: from regenerative medicine to electronic devices, Angew. Chem., Int. Ed., 47, 8002-8018 (DOI: 10.1002/anie.200800022)

[14] Jung J. H., Lee J. H., Silverman J. R. John G. (2013), Coordination polymer gels with important environmental and biological applications, Chem. Soc. Rev., 42, 924-936 (DOI: 10.1039/C2CS35407A)

[15] Díaz D. D., Kühbeck D., Koopmans R. J. (2011), Stimuli-responsive gels as reaction vessels and reusable catalysts, Chem. Soc. Rev., 40, 427-448 (DOI: 10.1039/C005401C)

[16] Sutar P., Maji T. K. (2016), Coordination polymer gels: soft metal–organic supramolecular materials and versatile applications, Chem. Commun., 52, 8055-8074 (DOI: 10.1039/C6CC01955B)

[17] Lin Q., Lu T. T., Zhu X., Sun B., Yang Q. P., Wei T. B., Zhang Y. M. (2015), A novel supramolecular metallogel-based high-resolution anion sensor array, Chem. Commun., 51, 1635-1638 (DOI: 10.1039/C4CC07814D)

[18] Lin Q., Sun B., Yang Q. P., Fu Y. P., Zhu X., Zhang Y. M., Wei T. B. (2014), A novel strategy for the design of smart supramolecular gels: controlling stimuli-response properties through competitive coordination of two different metal ions, Chem. Commun., 50, 10669-10671 (DOI: 10.1039/C4CC03753G)

[19] Shen Z., Wang T., Liu M. (2014), Macroscopic Chirality of Supramolecular Gels Formed from Achiral Tris (ethyl cinnamate) Benzene-1, 3, 5-tricarboxamides, Angew. Chem., Int. Ed., 53, 13424-13428 (DOI: 10.1002/anie.201407223)

[20] Mei J., Leung N. L., Kwok R. T., Lam J. W., Tang B. Z. (2015), Aggregation-induced emission: together we shine, united we soar, Chem. Rev., 115, 11718-11940 (DOI: 10.1021/acs.chemrev.5b00263)

[21] Mehdi H., Pang H., Gong W., Dhinakaran M. K., Wajahat A., Kuang X. Ning G. (2016), A novel smart supramolecular organic gelator exhibiting dual-channel responsive sensing behaviours towards fluoride ion via gel–gel states, Org. Biomol. Chem., 14, 5956-5964 (DOI: 10.1039/C6OB00600K)

[22] Nagarajan V., Pedireddi V. R. (2014), Gelation and Structural Transformation Study of Some 1, 3, 5-Benzenetricarboxamide Derivatives, Cryst. Growth Des., 14, 1895-1901 (DOI: 10.1021/cg500026t)

[23] Sutton J. E., Zink J. I. (1976), Spectroscopic studies of perpendicular nitrile-metal interactions, Inorg. Chem., 15, 675-678 (DOI: 10.1021/ic50157a036)

[24] Jain S. C., Rivest R. (1967), Possible coordination between halides of Group IV elements and the triple bond of diethylaminoacetonitrile as ligand, Inorg. Chem., 6, 467-469 (DOI: 10.1021/ic50049a007)

[25] Farona M. F., Kraus K. F. (1970), Coordination of organonitriles through CN Π Systems, Inorg. Chem., 9, 1700-1704 (DOI: 10.1021/ic50089a018)

[26] Sun Y., Wang Y. X., Wu M., Yuan W., Chen, Y. (2017), p-Quaterphenylene as an aggregation-induced emission fluorogen in supramolecular organogels and fluorescent sensors, Chem. Asian J., 12, 52–59 (DOI: 10.1002/asia.201601388)

[27] Beltrán E., Garzoni M., Feringán B., Vancheri A., Barberá J., Serrano J. L., Pavan G. M., Giménez R., Sierra T. (2015), Self-organization of star-shaped columnar liquid crystals with a coaxial nanophase segregation revealed by a combined experimental and simulation approach, Chem. Commun., 51, 1811-1814 (DOI: 10.1039/C4CC08602C)

[28] Shen Z., Wang T., Shi L., Tang Z., Liu M. (2015), Strong circularly polarized luminescence from the supramolecular gels of an achiral gelator: tunable intensity and handedness, Chem. Sci., 6, 4267-4272 (DOI: 10.1039/C5SC01056J)

[29] Shen Z., Jiang Y., Wang T., Liu M. (2015), Symmetry Breaking in the Supramolecular Gels of an Achiral Gelator Exclusively Driven by π–π Stacking, J. Am. Chem. Soc., 137, 16109-16115 (DOI: 10.1021/jacs.5b10496)

[30] Zhang Y., Liang C., Shang H., Ma Y., Jiang S. (2013), supramolecular organogels and nanowires based on a V-shaped cyano-stilbene amide derivative with aggregation-induced emission (AIE) properties, J. Mater. Chem. C, 1, 4472-4480 (DOI: 10.1039/C3TC30545G)

[31] Ghosh A., Das P., Kaushik R., Damodaran K. K., Jose D.A. (2016), Anion responsive and morphology tunable tripodal gelators, RSC Adv., 6, 83303-83311 (DOI: 10.1039/C6RA16345A)

[32] Xu Y. L., Li C. T., Cao Q. Y., Wang B. Y. Xie Y. (2017), A pyrenyl-appended organogel for fluorescence sensing of anions, Dyes Pigm., 139, 681-687 (DOI: 10.1016/j.dyepig.2016.12.068)

[33] Howe R. C., Smalley A. P., Guttenplan A. P., Doggett M.W., Eddleston M. D., Tan J. C. Lloyd G. O. (2013), A family of simple benzene 1, 3, 5-tricarboxamide (BTA) aromatic carboxylic acid hydrogels, Chem. Commun., 49, 4268-4270 (DOI: 10.1039/C2CC37428E)

[34] Lin Q., Lu T. T., Zhu X., Wei T. B., Li H., Zhang Y. M. (2016), Rationally introduce multi-competitive binding interactions in supramolecular gels: a simple and efficient approach to develop multi-analyte sensor array, Chem. Sci., 7, 5341-5346 (DOI: 10.1039/C6SC00955G).

[35] Farona M. F., Bremer N. J. (1966), Succinonitrile derivatives of halogeno pentacarbonyl manganese(I), J. Am. Chem. Soc., 88, 3735-3737 (DOI: 10.1021/ja00968a011)

[36] Xu Y., Xue P., Xu D., Zhang X., Liu X., Zhou H., Jia J., Yang X., Wang F., Lu R. (2010), Multicolor fluorescent switches in gel systems controlled by alkoxyl chain and solvent, Org. Biomol. Chem., 8, 4289-4296 (DOI: 10.1039/C0OB00091D)

[37] Yu C., Li X., Zeng F., Zheng F., Wu S. (2013), Carbon-dot-based ratiometric fluorescent sensor for detecting hydrogen sulfide in aqueous media and inside live cells, Chem. Commun., 49, 403-405 (DOI: 10.1039/C2CC37329G)

[38] Piepenbrock M. O. M., Lloyd G. O., Clarke N., Steed J. W. (2010), Metal-and anion-binding supramolecular gels, Chem. Rev., 110, 1960-2004 (DOI: 10.1021/cr9003067)

[39] Foster J. A., Piepenbrock M. O. M., Lloyd G. O., Clarke N., Howard J. A., Steed J. W. (2010), Anion-switchable supramolecular gels for controlling pharmaceutical crystal growth, Nat Chem., 2, 1037-1043 (DOI:10.1038/nchem.859)

Chapter 3

Discotic Organic Gelators in Ion Sensing, Metallogel Formation, and Bioinspired Catalysis

Chapter 3

Discotic Organic Gelators in Ion Sensing, Metallogel Formation, and Bioinspired Catalysis

3.1 Introduction

Self-assembly of low-molecular-weight gelators (LMWGs) can generate soft materials, which can work wonders in the area of catalysis, tissue engineering, material sciences, cosmetics, drug delivery, regenerative medicines, and sensors.[1-9] Various noncovalent interactions can help to tune the supramolecular structure in definitive ways to bring out the potentiality of these soft materials for multiple applications. Among them, H-bonding interactions, π-π stacking, hydrophobic interaction, van der Waals interaction, and interaction through dipole-dipole are different essential tools to build the soft materials.[10-13] Introduction of metal ions in organogels can initiate formation of hybrid soft materials through the operative metal-ligand interaction and can enrich the properties of soft materials further in the form of unprecedented optical, magnetic, gas storage, electronic, sensing, and catalytic properties.[14-21] Utilization of metal ions to generate such materials can result in the formation of interesting nanostructures such as nanotubes, nanoballs, nanofibers, and vesicles.[22-24] Many of the soft materials can show a smooth reversible temperature-dependent transition between the sol and gel states. Interestingly, the three dimensional structure of the soft gels can get significantly influenced by various external stimuli such as temperature, shear stress, ultrasound, pH, redox reaction, and presence of other chemical entities.[25,26] In many instances, the presence of a particular cation or anion or a chemical substance influences the network structure in a great way to bring about significant changes in the associated properties.[27,28] This characteristic of a soft material to discriminate a particular entity from similar other motifs can endow special power to the material for enormous sensing capacity. There are several reports where LMWGs can sense different cations and anions in the gel state particularly with

the help of a drastic change in the aggregate induced emission property.[29-34] Sometimes, it is also possible to create a smart template which can sense metal ions by switching off or on the aggregation-induced emission property, and in turn, the metallogels formed can be utilized further in sensing of anions.[35-38] Utilization of metallogels as a prospective catalyst is another area where the examples are limited and have not been fully explored. Whatever literature data are available indicates mostly utilization of palladium and silver (cation/ nanoparticle)-based metallogels, which have been utilized for organic reactions such as Suzuki-Miyura coupling reactions,[39,40] reductions of aromatic nitro groups to amine,[41] or degradation of dye molecules.[42,43] Only limited examples are available where Ca^{2+}, Cr^{3+}, or Cu^{+} based metallogels are explored for another kind of organic catalytic reactions.[44-46] Herein, we report the synthesis and gelation property of two isomeric carboxamides, nitrile-based gelators **G2** and **G3**. While the gelator **G2** has shown exquisite sensing property toward certain cations by switching off the aggregation-induced enhanced emission, the gelator **G3** can sense some other cations in solution by switching on the fluorescence property. Interestingly, the gelator **G2** is capable of forming metallogels with different metal ions, and some of them have shown unique sensing properties of certain anions, which can be utilized as an effective metallogel-based sensor array. Furthermore, we have investigated the possibility of utilizing a copper-based metallogel **Cu(II)G2** as an effective catalyst for bioinspired oxidation of catechol. Catechol oxidase is a type-3 di-copper enzyme, which processes atmospheric dioxygen to carry out selective oxidation of catechol to ortho-quinones. Though there are reports of several copper-based complexes to act as a mimic of catechol oxidase enzyme, however no such report is available where a copper metallogel has been utilized as a catalyst to carry out the oxidation reaction in the gel state at room temperature, till date.

3.2 Experimental section

3.2.1 Material and method

All the required chemicals were purchased from Sigma and used without further purification. The specifications of all the instruments used for analysis purpose were same as described in the section 2.2.1 of the chapter 2.

3.2.2 Synthesis of gelator G2 [*N1, N3, N5*-tris(3-cynophenyl) benzene-1,3,5-tricarboxamide] and G3 [*N1, N3, N5*-tris(2-cynophenyl) benzene-1,3,5-tricarboxamide]

The gelators **G2** and **G3** were synthesized by the addition of trimesoyl chloride (1 g, 4.75 mmol) to 3.5 molar equivalent of substituted benzonitrile [i.e., 3-aminobenzonitrile (1.95 g, 16.5 mmol) in the case of **G2** and 2-aminobenzonitrile (1.95 g, 16.5 mmol) in the case of **G3**] in the presence of triethylamine (2.35 mL, 16.8 mmol) in dry DMF (8 mL) at 0 °C. It has been stirred overnight at ambient conditions. Ethylacetate (100 mL) was added in the solution mixture. The combined organic layer was washed with dil. HCl (1 N, 100 mL) and subsequently with saturated Na_2CO_3 (100 mL) aqueous solution and brine (100 mL). The organic layer was then dried over anhydrous sodium sulfate and evaporated under reduced pressure to obtain a resultant white colored powder. The isolated compound was then dried at room temperature under vacuum. Yield: 75% (for **G2**) and 78.6% (for **G3**). ^{1}H NMR of **G2** (400 MHz, 298 K, DMSO-d_6): δ 11.10 (3H, amide, s), 8.84 (3H, aromatic, s), 8.30 (6H, aromatic, d), 7.63 (6H, aromatic, s). ^{1}H NMR of **G3** (400 MHz, 298 K, DMSO-d_6): δ 9.14 (3H, amide, s), 9.05 (1H, aromatic, s), 8.48 (2H, aromatic, s), 8.10 (3H, aromatic, d), 7.98 (6H, aromatic, t), 7.66 (3H, aromatic, s). ^{13}C NMR of **G2** (100 MHz, 293 K, DMSO-d_6): δ 165.2 (amide), 140.4 (aromatic), 139.6 (aromatic), 135.4 (aromatic), 130.7 (aromatic), 127.9 (aromatic), 125.4 (aromatic), 123.5 (aromatic), 119.2 (nitrile), 112.0 (aromatic). ^{13}C NMR of **G3** (100 MHz, 293 K, DMSO-d_6): δ 167.3 (amide), 140.5 (aromatic), 140.1 (aromatic), 135.4 (aromatic), 130.7 (aromatic), 128.2 (aromatic), 125.4 (aromatic), 123.5 (aromatic), 119.2 (nitrile), 113.7 (aromatic). FTIR of **G2** (KBr): ν = 3480.7, 3370.9, 2254.9, 1681.3, 1641.9, 1543.4 cm^{-1},

FTIR of **G3** (KBr): ν = 3439.5, 3345.9, 2234.1, 1693.9, 1591.5 cm^{-1}. MS (ESI) of **G2** *m/z*: 509.10 and **G3** *m/z*: 509.12 (in negative mode).

3.2.3 Preparation of gels

The gel preparation method of **G2** and **G3** organogels and metallogels of **G2** were the same as described in the section 2.2.3 of chapter 2. However, metallogels of **G3** were obtained by mixing 20 mM concentration of **G2** with 5 mM concentration of metal perchlorate salts (**G3**: $\mathbf{M^{n+}}$ molar ratio = 2:0.5 and solvent is 1 mL DMF/1 mL water).

3.2.4 Gel melting temperature

Gel melting temperature (Tgel) of **G2** and **G3** has been investigated in the same method as described in section 2.2.4 of chapter 2.

3.2.5 Characterizations

Characterizations techniques like UV-visible Spectroscopy, Fluorescence Spectroscopy, FT-IR Spectroscopy, powder X-ray Diffraction (PXRD) and morphological Study, Rheological Properties of **G2** and **G3** and their metallogels have been same as described in the section 2.2.5 of chapter 2.

3.2.6 Catechol Oxidation by the Cu(II)G2 Metallogel

3,5-Ditertbutylcatechol (3,5-DTBC) was used to monitor the Catecholase activity of the **Cu(II)G2** metallogel. Gels were prepared by mixing a 0.2 mM solution of **Cu(II)G2** in DMSO (2 mL) with 100 equivalents of 3,5-DTBC and subsequent addition of 100 μL of water under aerobic conditions. The mixture was left undisturbed for 2 min, and the formation of the gel is observed. The gel (10 μL) was pipetted out instantaneously after the formation of a gel, and it was dissolved in 2 mL of DMSO. The resultant solution was subjected to the UV-vis experiment without any delay, and a peak was observed to develop at around 410 nm. This procedure was repeated in a time-dependent manner, and

the formation of a distinctive peak with time at 410 nm indicates the formation of the oxidized product, *viz.*, quinone (3,5-DTBQ). The dependence of the rate on various concentrations and different kinetic parameters were obtained by using a 0.1 mM **Cu(II)G2** metallogel with 100-500 equivalents of the substrate (3,5-DTBC) and by monitoring the upsurge in absorbance at 402 nm (the peak corresponding to the quinone band maxima) as a function of time.

3.3 Results and discussion

The synthesis of gelators **G2** and **G3** is straightforward. Condensation of trimesoyl chloride and excess of 3-amino benzonitrile (3.5 equiv) for **G2** and a 2-amino benzonitrile (3.5 equiv) for **G3**, in the presence of triethylamine, furnished the tricarboxamide compound (Scheme 3.1). The resultant compound was extracted with ethyl acetate, and the purified compound was characterized by ^{1}H, ^{13}C NMR, IR, and electrospray ionization mass spectrometry (ESI-MS) spectroscopy.

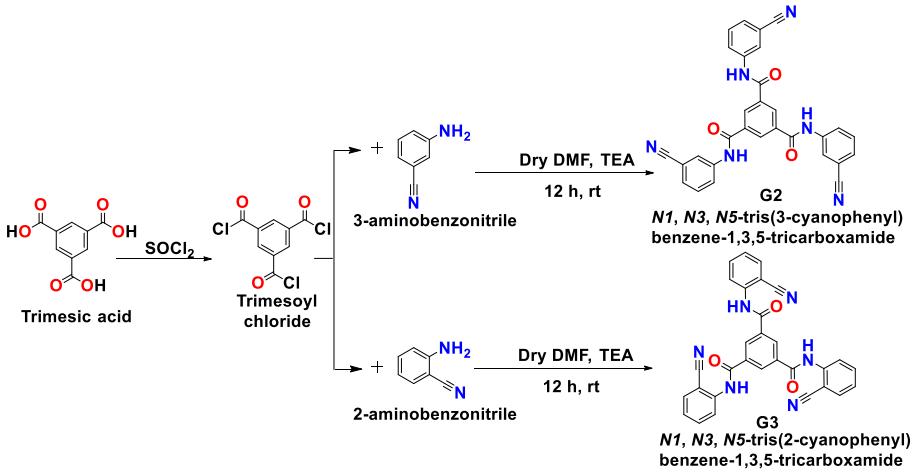

Scheme 3.1. *Systematic scheme for the synthesis of gelator **G2** and **G3**.*

The FTIR of the gelator **G2** reveals the characteristic band at 3370 cm^{-1} corresponding to carboxamide N−H as the shoulder. Whereas the bands at 1681, 1641, and 1543 cm^{-1} reveal the carboxamide C=O stretching and amides I and II stretching, respectively (Figure 3.1).[47] The FTIR spectrum of the gelator **G3** reveals the similar characteristic

bands at 3345, 1693, 1651, and 1591 cm^{-1}, respectively (Figure 3.1). The broadband in the range of 3370−3345 cm^{-1} indicates extensive hydrogen bonding through the carboxamide N-H group. The bands at 2254 and 2234 cm^{-1} indicate the presence of a nitrile group in the gelators **G2** and **G3**, respectively.[47]

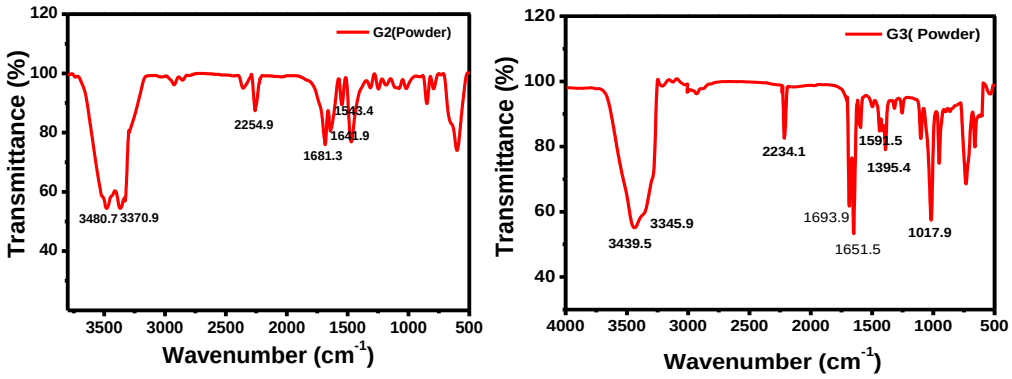

Figure 3.1. *FT-IR spectra of gelator **G2** and **G3**.*

The ^{1}H NMR and ^{13}C NMR spectra of the gelators **G2** and **G3** corroborate with the structure of the synthesized molecules. In the ^{1}H NMR spectrum, the aromatic ring protons are observed within the range of 8.3-7.6 ppm. The peak at 11.2 and 9.3 ppm has shown the presence of the carboxamide protons[48,49] (Figure 3.2, 3.3).

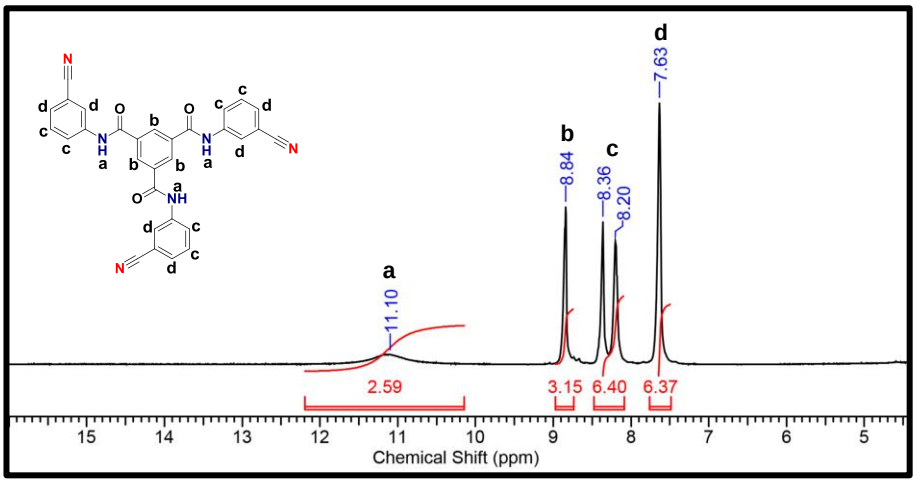

Figure 3.2. *^{1}H NMR spectrum of gelator **G2**.*

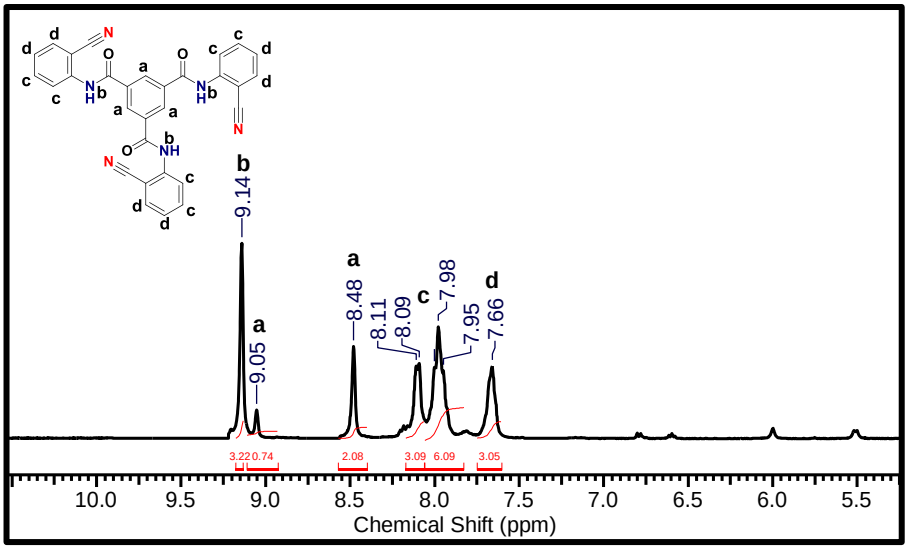

Figure 3.3. *^{1}H NMR spectrum of gelator **G3**.*

In ^{13}C NMR spectra, the peaks at 165 and 164 ppm reveal the characteristic peaks of the carboxamide carbons and the peaks for the nitrile carbons have been observed at 119-118 ppm.[50] All the aromatic carbons are observable between 140 and 103 ppm (Figure 3.4, 3.5).

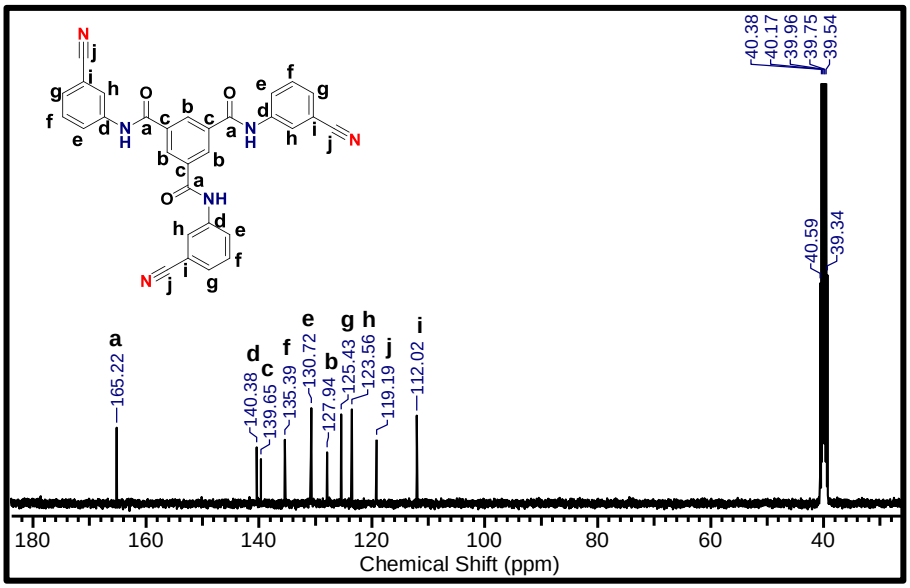

Figure 3.4. *^{13}C NMR spectrum of gelator **G2**.*

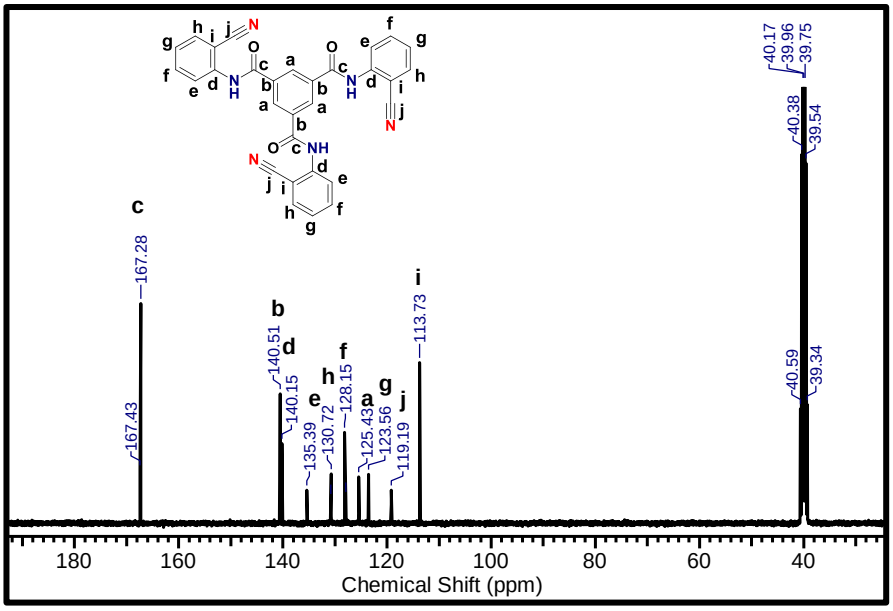

Figure 3.5. *^{13}C NMR spectrum of gelator **G3**.*

The ESI-MS spectra have displayed a molecular ion peak at 509.10 and 509.12 in a negative mode, indicating the formation of the gelators **G2** and **G3** (Figures 3.6, 3.7).

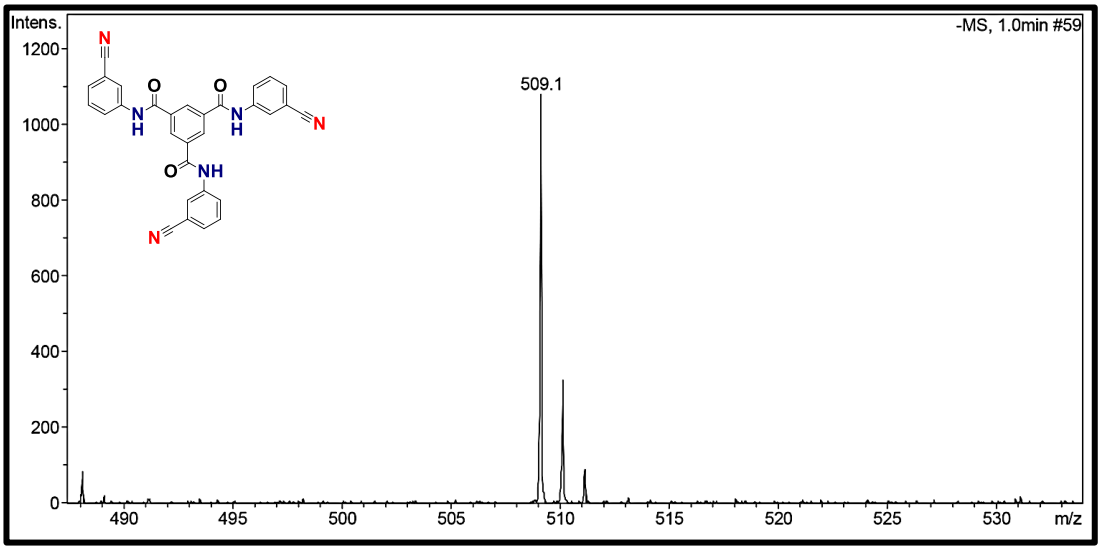

Figure 3.6. *ESI-Mass spectrum of gelator **G2**.*

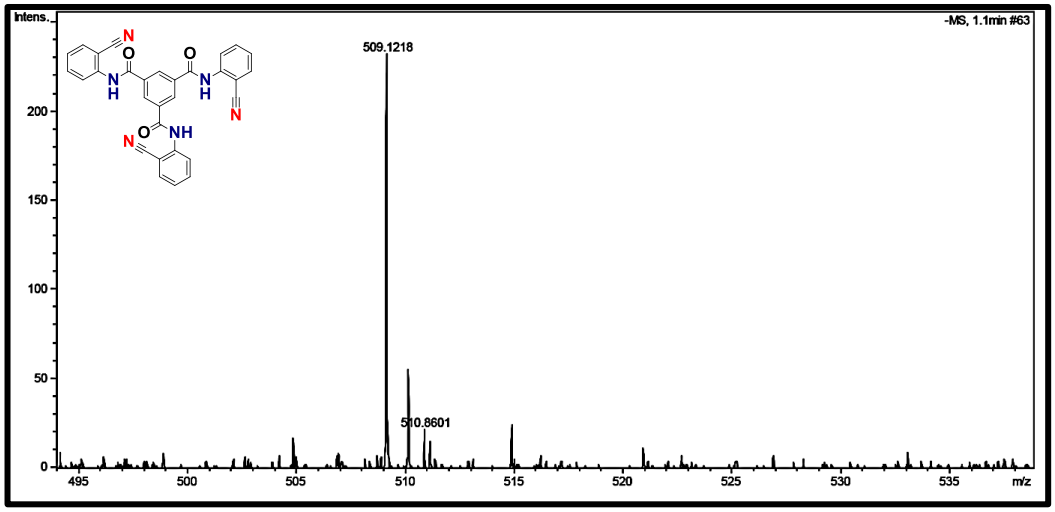

Figure 3.7. *ESI-Mass spectrum of gelator* ***G3****.*

Gelation Behavior. The standard heating and cooling method were used to explore the propensity of the gelation ability of **G2** and **G3** in organic solvents. Gelators **G2** and **G3** are insoluble in common organic solvents, even in heating. However, both of them are readily soluble in highly polar solvents such as DMF and DMSO. Upon addition of a small quantity of water in DMF or DMSO, the gel formation gets induced. The critical gel concentrations for both the gelators are found to be 20 mM in the solvent combination, that is, DMF/water and DMSO/water. It may be put forward that hydrogen bonding between the gelator and the solvent molecule plays a crucial role during the gelation process. The gelation nature of gelators **G2** and **G3** were further ascertained by the "test tube inversion" experiment (Figure 3.8). However, the heating-cooling experiment indicates the reversible nature of gelators during sol-gel transition. The phase transition temperatures (Tgel) of sol-gel have been found to be 100 °C for both the gelators, which prove the stability of the gel at room temperature.

Figure 3.8. *Optical image of gelator* ***G2*** *and* ***G3*** *(Test tube inversion method).*

Aggregation-Induced Enhanced Emission (AIEE) Phenomenon. The non-luminescent nature of the gelators in solution and significant fluorescence enhancement as a result of gelation occur because of the AIEE phenomenon. We have recorded UV-vis spectra to obtain insights into the absorption maxima of the supramolecular aggregates. The UV-vis spectrum of the gelator **G2** has shown peaks at 280 and 355 nm, whereas the peaks observed at 260 and 355 nm are for **G3**, respectively. These peaks might be associated with the intramolecular π-π^* transition between the aromatic moieties.[38] The gelation property was studied with the help of temperature-dependent fluorescence spectroscopic experiments where **G2** and **G3** in the gel state at 30 °C have shown intense emission at around 437 and 434 nm, respectively (in the solution state, the gelators are non-emissive). After gradual heating up to 100 °C, the emission maxima shifted toward 425 and 439 nm for **G2** and **G3**, respectively, may be due to the change in internal assembly because of the heating effect (Figure 3.9). The enhancement in the emission of gelators (**G2** and **G3**) was observed in the self-assembled state as compared to that in the solution state. The reason behind the AIEE during the self-assembly process could be due to the restrictions in the free rotations of gelators, which results in blocking the fast deactivation pathways in an excited state. The radiationless relaxation of blocked channels leads to the opening of radiative decay pathway in the aggregated state. However, in the solution state, these molecular rotations occur freely, which provide relaxation pathways of the excited state.[51,52] Additionally, AIEE was further investigated by the quantum yield (Φ) experiment. The standard and reported procedure was used in determining the absolute quantum yields of **G2** and **G3**.[53,54] Quantum yields for the organogels **G2** and **G3** are found to be 0.08 and 0.14, respectively. In the solution state, **G2** and **G3** were non-emissive with a negligibly low quantum yield of fluorescence. In the case of **G2** with slow cooling of the gel from 100 °C, the emission bands shift gradually to a higher wavelength, whereas it sticks at 437 nm when at room temperature. Curiously for the gelator **G3**, a progressive blue shift is observed with gradual cooling of the gel along with enhancement of the emission band.

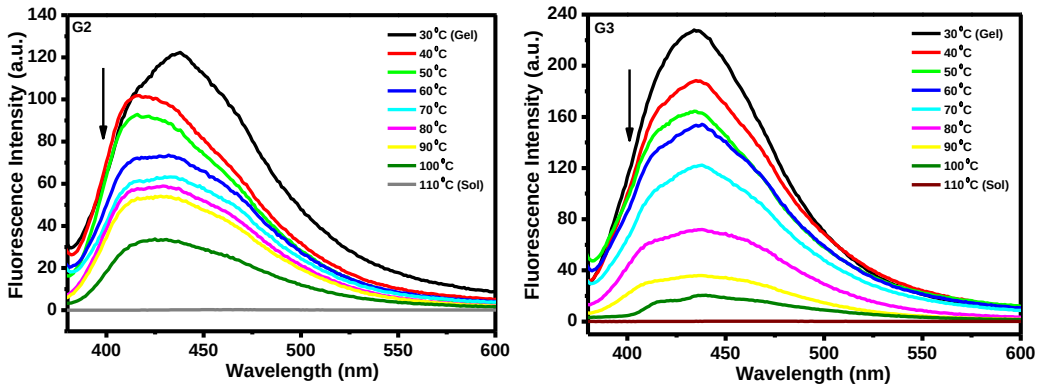

Figure 3.9. *Temperature-dependent fluorescence spectra for* ***G2*** *and* ***G3*** *(in DMF) during the gelation process (λ_{ex} = 355 nm).*

Self-Assembly Mechanism. The self-assembly mechanism of the discrete gelators leading to the formation of the gel has been examined through various spectroscopic techniques. Several noncovalent interactions play their part to induce gel formation through interactions such as H-bonding, π-π stacking, and weak supramolecular interactions.[7,8] Among them, it is assumed that the presence of carboxamide and nitrile moieties helps in hydrogen bond formation, whereas π-π and intercolumnar stacking between aromatic rings and van der Waals interactions may play crucial roles to establish the gel structure.[55] The mechanism of the gel formation has been further investigated through fluorescence, concentration-dependent ^{1}H NMR, and IR spectroscopy. PXRD and SEM studies have also been conducted to get a deeper insight. The fluorescence spectroscopy experiment suggests that the π-π stacking interactions between the aromatic moieties could play a decisive role in the self-assembly mechanism.[56] Gelators **G2** and **G3** do not show any emission peak when it is in a solution of DMF. However, even at 100 °C in a DMF/water mixture, the gel starts to set in. The emission spectra of a solution of **G2** and **G3** show emission peaks at around 425 and 439 nm. In the gel state, gelators **G2** and **G3** show sharp emission at around 437 and 434 nm, respectively (Figure 3.9). The red-shift in the gelator **G2** in the gel phase suggests an effective π-π stacking between the aromatic residues probably by the formation of *J*-aggregates.[57,58] However, interestingly a slight blue shift in the case of **G3** indicates the formation of probable *H*-aggregates.[57,58]

Self-assembly of gelators **G2** and **G3** is further inspected with the help of concentration-dependent ^{1}H NMR.[59-61] In ^{1}H NMR spectra, amide proton NH is not observable at low concentration, and it is only visible in very high concentration at around 150 mM. However, all the aromatic protons have shown a downfield shift with a gradual increase in the concentration, indicating their possible role in H-bonding.

The FTIR spectroscopic method has also been utilized to scrutinize the self-assembly mechanism. A comparison between the IR spectra of powder and xerogel of **G2** and **G3** revealed strong evidence of formation of self-assembly during gelation (Figures 3.10). The carboxamide N-H band for **G2** and **G3** at 3370 and 3345 cm^{-1}, respectively, shifts towards lower wavenumbers, that is, 3231 and 3259 cm^{-1}, after formation of the gel. The carboxamide C=O vibration band has also been shifted toward a lower wavenumber from 1681 to 1679 and 1697 to 1667 cm^{-1}, indicating the formation of strong hydrogen bonds during gelation.[62] Whereas the amide I, amide II, and C≡N stretching bands also shift toward lower wavenumber upon gelation as expected in a hydrogen-bonded network.[63,64] The amide I band shifted from 1641 cm^{-1} (powder) to 1617 cm^{-1} (gel) for **G2** and 1651 cm^{-1} (powder) to 1616 cm^{-1} (gel) for **G3**. Similarly, the amide II band shifted from 1543 cm^{-1} (powder) to 1509 cm^{-1} (gel) for **G2** and 1591 cm^{-1} (powder) to 1547 cm^{-1} (gel) for **G3**, whereas the C≡N stretching band shifted from 2254 cm^{-1} (powder) to 2230 cm^{-1} (gel) for **G2** and 2234 cm^{-1} (powder) to 2214 cm^{-1} (gel) for **G3** after formation of a gel.

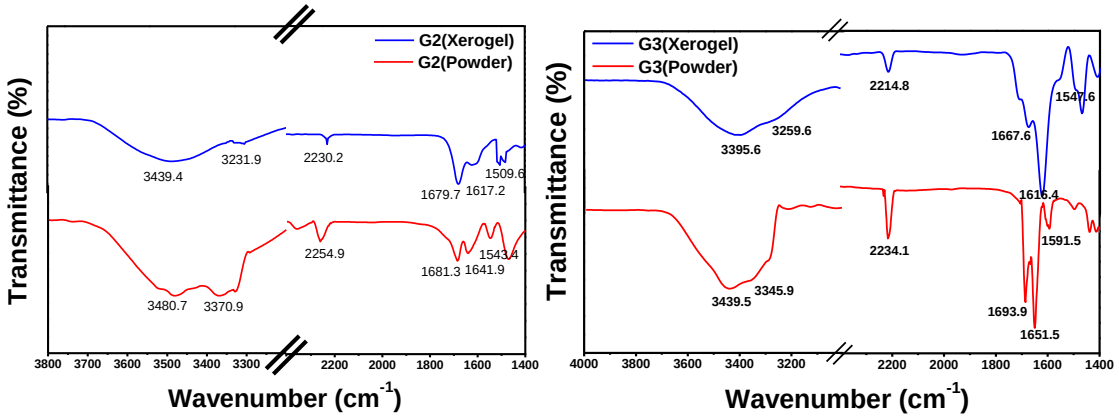

Figure 3.10. *FT-IR spectra of powder and xerogel of **G2** and **G3**.*

Interestingly, in xerogels of **G2** and **G3**, the PXRD experiment showed an intense peak at 2θ = 21.50° and 2θ = 21.09°, respectively, corresponding to the d-spacing value of 4.13 and 4.20 Å, which represents the intercolumnar stacking.[65] For **G2** and **G3**, the peaks with *d*-spacing at 2θ = 25.40° and 2θ = 25.63° corresponding to the *d*-spacing value of 3.50 and 3.47 Å reveal the *π*-*π* stacking between the aromatic moieties, whereas the *d*-spacing at 2θ = 34.10° and 2θ = 35.09° corresponding to the *d*-spacing value of peak at 2.62, and 2.55 Å suggests the hydrogen bonding between NH proton of amide and nitrile groups (Figure 3.11).[66–68] The peaks obtained in PXRD experiments invariably prove the importance of noncovalent interaction in the self-assembly of gelators, which shows a pivotal role in the formation of the ordered structure.

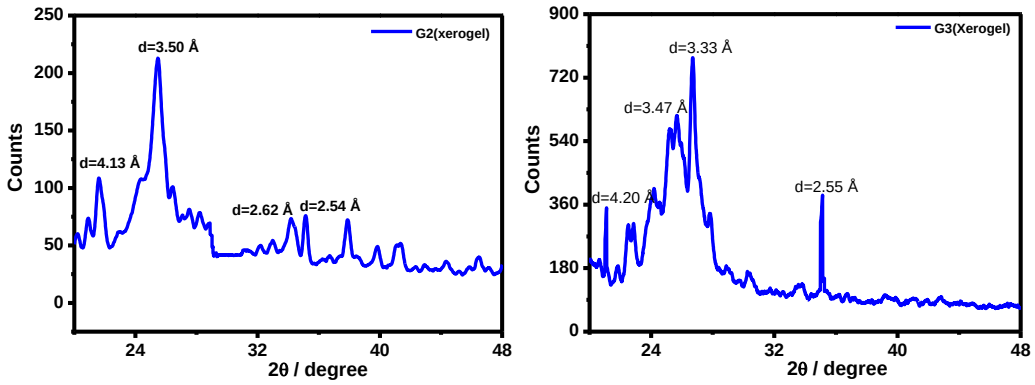

Figure 3.11. *Powder XRD spectra of* ***G2*** *and* ***G3*** *xerogel.*

To gain an insight into the aggregate morphological feature, the organogels **G2** and **G3** were examined through the FE-SEM technique.[69-72] The SEM image of **G2** showed a fibrous network with approximately 1 μm length in the gel state. Similarly, **G3** showed the aggregation of the material with a dendritic-like morphology (Figure 3.12).

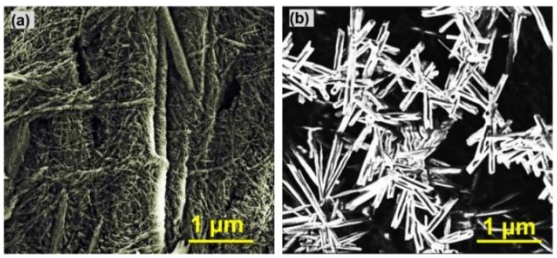

Figure 3.12. *FE-SEM images of organogels (a)* ***G2*** *and (b)* ***G3****.*

Fluorescence Response of Gelators G2 and G3 toward Different Metal Ions. The formation ability of metallogels and fluorescence response of gelators with different metal ions (Ag^{+}, Fe^{2+}, Fe^{3+}, Ni^{2+}, Cu^{2+}, Co^{2+}, Cd^{2+}, and Zn^{2+}) have been further inspected. The solution of gelators was treated with perchlorate salts of various metal ion precursors. In the case of the gelator **G2**, the treatment of gelators and the metal ion in a 2:1 molar ratio in the DMF/H_2O mixture produced corresponding supramolecular metallogels, most probably through the formation of a metal-organic (MOF) framework. Remarkably, in almost all cases, quenching of emission peak has been observed concerning free organogels; however, in the case of **Ag^{+}**, **Fe^{2+}**, and **Fe^{3+}**, the fluorescence gets entirely turned off (Figure 3.13). Similar exposure of the organo-gelator **G3** to different metal ions in a 2:1 molar ratio failed to form any metallogel, even when tried in DMF/water combination. The metal ion salts along with the gelator, formed a turbid solution without any change in fluorescence property. However, in the presence of Zn^{2+} and Cd^{2+} ions, the turbid solution became fluorescent with maxima observed at around 440 nm. Metallogel formation by aggregation has been observed when the gelator (**G3**) to metal ratio has been maintained at 2:0.5. In all cases, the metallogel showed quenching in emission intensity; however, only in the case of **Fe^{2+}**, the emission band quenched completely, furnishing a complete turn-off state (Figure 3.13). With the utilization of a hand-held UV lamp, **Fe^{2+}** can be selectively sensed in the naked eye. Therefore, both the organogelators have shown a remarkable ability to sense iron in the +2-oxidation state (Figure 3.14).

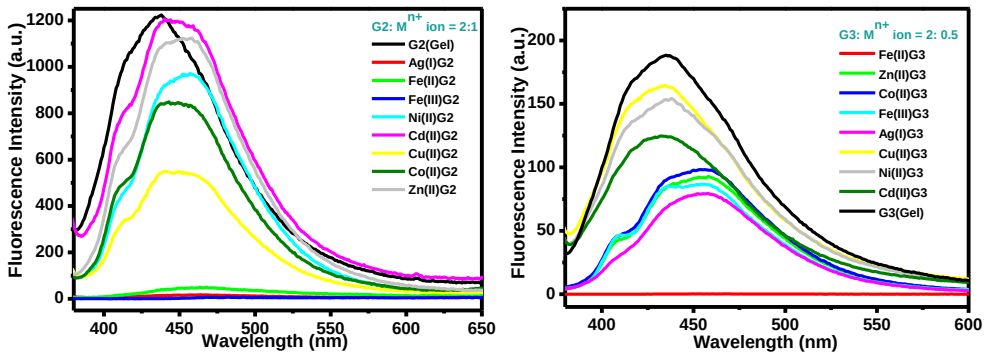

Figure 3.13. *Fluorescence spectra of organogel **G2** and **G3** in the presence of several metal ions (in DMF) (with sources of their perchlorate salts) (λ_{ex} = 355 nm).*

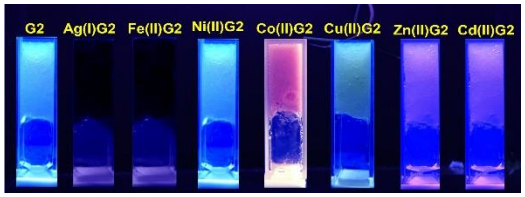

Figure 3.14. *Optical image of* ***G2*** *and their metallogels under UV lamp.*

Fluorescence Response of Metallogels toward Various Anions. As per the previous reports regarding sensing of anions using metallogels, we took the opportunity to study the response of the different metallogels upon treatment with various anions (Br^-, Cl^-, N_3^-, OAc^-, SCN^-, ClO_4^-, CN^-, I^-, and S^{2-}) with the help of fluorescence spectroscopy. Remarkably, some of the metallogels have shown unique selection and sensing property toward various anions as discussed below. Metallogels **Ni(II)G2** and **Co(II)G2** have shown selective sensing of $\mathbf{S^{2-}}$ and **Cu(II)G2** specifically detected $\mathbf{I^-}$ by turning off the emission band (Figure 3.15). During the investigation of responses by the fluorescence property, we found notable visible color change, particularly for the cobalt(II) ion upon interaction with the gelator **G2**. On addition of aqueous solution of the cobalt(II) ion in the organogelator **G2** in its gel phase, the **Co(II)G2** metallogel formed and the colorless organic gelator **G2** became visibly pink with a characteristic emission band. Upon gradual diffusion of the $\mathbf{S^{2-}}$ ion into the **Co(II)G2** metallogel, the pink color starts to get discharged, and a colorless gel was obtained where the fluorescence gets completely turned off.

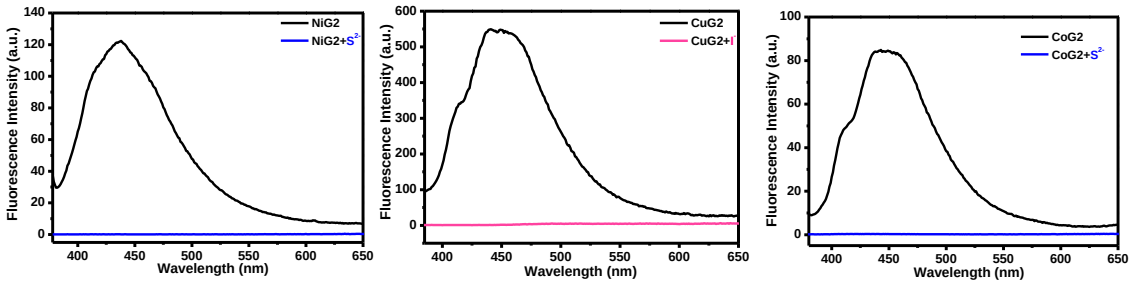

Figure 3.15. *Fluorescence spectra of MGs (in DMF) in the presence of various anions (λ_{ex} = 355 nm);* ***Ni(II)G2*** *and* ***Ni(II)G2+S^{2-}***; ***Co(II)G2*** *and* ***Co(II)G2+S^{2-}***; ***Cu(II)G2*** *and* ***Cu(II)G2+I$^-$***.

Selective sensing of certain anions helps us to design a sensor array, which could analyze a solution with multianalytes to detect the specific anions. The results obtained indicated that the metallogels could work with the same efficiency to detect S^{2-} and I^- in multianalyte conditions (Br^-, Cl^-, N_3^-, OAc^-, SCN^-, ClO_4^-, CN^-, $I^-$and S^{2-}). Additionally, to explore the anion-sensing efficiency of metallogels, separate experiments have been carried out with increasing concentration of different anions and their effect on the change in the intensity of emission peaks. The detection limit of the specific anions is calculated by using the same methodology described in chapter 2.[73,74] The values obtained are 4.2 × 10^{-6} M for S^{2-} in [**Ni(II)G2**], 5.8 × 10^{-6} M for S^{2-} in [**Co(II)G2**], and 8.3 × 10^{-7} M for I^- [**Cu(II)G2**] which is comparable to the previous reports.[33,75] Furthermore, the anion sensor array can work on thin-layer chromatography (TLC) plate, which has been utilized as a spot detector under UV light for the selective anions. The metallogel of the gelator **G2** is brushed on the TLC plate, and a drop of an aqueous solution of different anions under consideration is added on the top of the detection spots. Amazing color changes under UV light have been observed. The TLC strips can be reutilized few more times by making a coat of the corresponding metallogels (Figure 3.16).

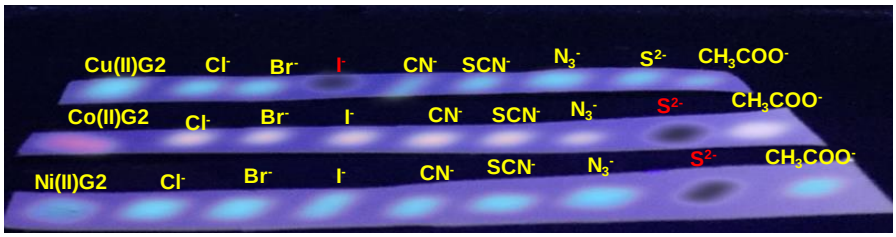

Figure 3.16. *Fluorescence responses of the metallogel-based sensor array under UV light using TLC plate in the presence of 1 equiv. of various anions (using 0.1 mol* L^{-1} *sodium or potassium salt water solution as anion source).*

Rheological Study of Gelators G2 and G3 and Their Metallogels. The metallogels of **G2** and **G3** were subjected to rheological studies to understand the viscoelastic properties. The average storage modulus (G′) for both the gelators was found to be around 10 Pa, and in all the cases, G′ was found to be higher than the loss modulus (G″). With the increase of strain, both the values deviated from linearity (Figure 3.17). The average

storage modulus increased dramatically upon induction of metal ions, indicating formation of more ordered MOF-type structures with values in the range of 10^4 to 10^5 Pa for **Ag(I)G2**, **Fe(II)G2**, **Fe(III)G2**, **Ni(II)G2**, **Co(II)G2**, **Cu(II)G2**, and **Fe(II)G3**. The crossover points with increasing strain for metallogels have been observed in the range of 1000-2000 Pa. During the frequency sweep, the shear stress has been found to be in the range of 1×10^4 to 5×10^4 Pa. The rigidity of the metallogel was observable from G′-G″ values, which remained positive in the entire sweep range.

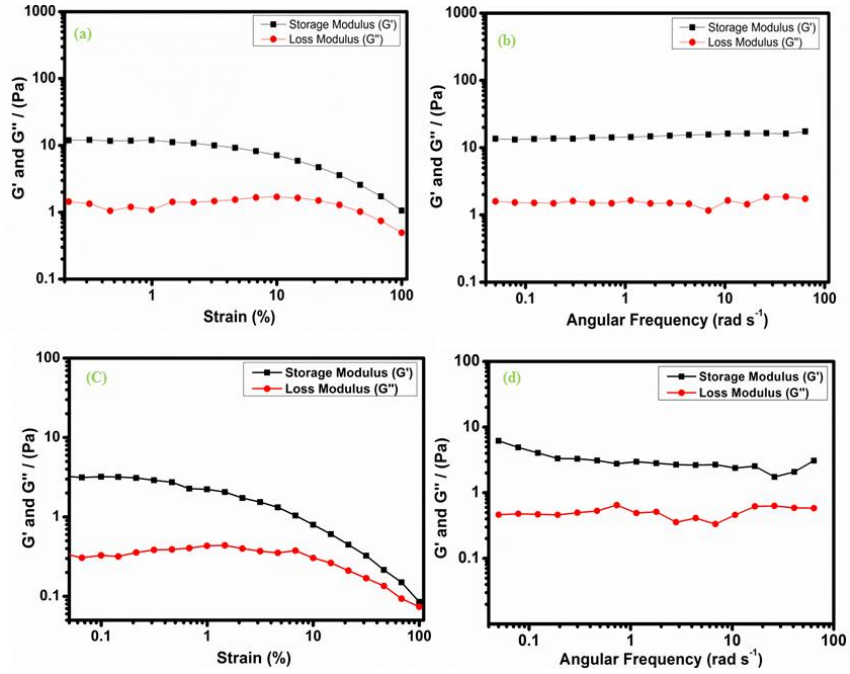

Figure 3.17. *(a) and (c) Linear viscoelastic (LVE) for organogel of **G2** and **G3**; (b) and (d) Dynamic frequency sweep for organogel of **G2** and **G3**.*

Metal-Gelator Interactions, Self-Assembly, and Selective Anion Sensing. To investigate the metal-gelator interaction, the UV-visible titration studies have been performed to verify the stoichiometry between various metal ions and gelators **G2** and **G3**. The stoichiometry of $\mathbf{Ag^+}$, $\mathbf{Fe^{2+}}$, and $\mathbf{Fe^{3+}}$ with **G2** and **G3** was confirmed by the continuous variation method (Job plots), and it revealed a 1:1 interaction in all cases among metal ions and gelators (Figure 3.18).

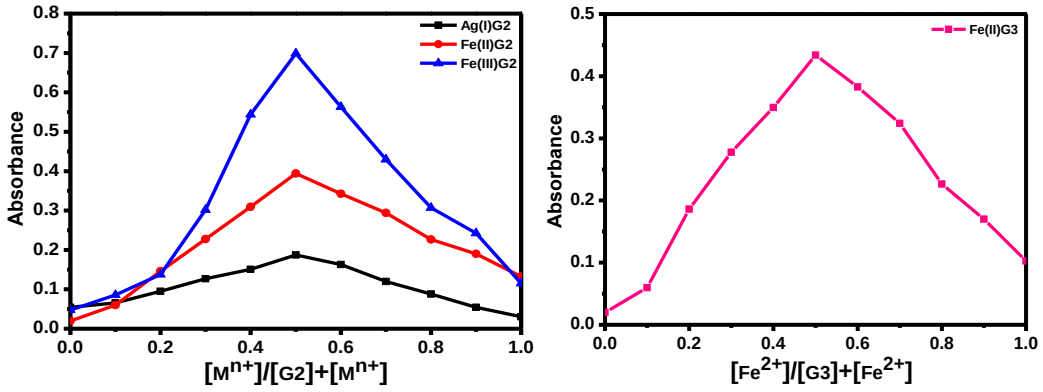

Figure 3.18. *Job plots of* ***G2*** *by addition of* ***Ag*** $^{+}$, ***Fe*** $^{2+}$, ***Fe*** $^{3+}$, *and* ***G3*** *by addition of* ***Fe*** $^{3+}$ *in DMF.*

Furthermore, the IR spectroscopic studies of the **Ag(I)G2**, **Fe(II)G2**, **Fe(III)G2**, **Ni(II)G2**, **Cu(II)G2**, **Co(II)G2**, and **Fe(II)G3** metallogels and **Cd(II)G3** and **Zn(II)G3** powders have been done to understand the interactions between the metal and the ligand. The FT-IR spectra of **G2** and **G3** organogels show amide bands at 1679 and 1667 cm^{-1}, respectively. The IR spectra of metallogels of **G2** and **G3** showed significant shifts of C=O stretching frequency toward the lower wavenumber in the range of 1660-1620 and 1630-1624 cm^{-1}, respectively. The significant band shifting indicated the coordination of the amide group to the metal center through the C=O group.[50] However, the most significant feature was observed in the case of nitrile stretching frequency. The FTIR data for **G2** and **G3** organogels showed nitrile stretching bands at 2236 and 2214 cm^{-1}, respectively. However, the metallogels **Ag(I)G2**, **Fe(II)G2**, and **Fe(III)G2** have shown shifting of the nitrile stretch slightly toward the lower wavenumber in the range of 2220-2228 cm^{-1}, indicating the interaction between the metal ion and the -C≡N group through π-bond.[62] Possibly this bond formation disturbs the self-assembled structure of the gel, and the aggregate-induced emission (AIE) gets turned off. However, all the other metallogels with **G2** have shown almost no deviation of the nitrile group stretching frequency. A similar observation has also been noticed for **G3**, where **Fe(II)G3** has shown a considerable deviation of nitrile stretching frequency toward the lower wavenumber at 2171.9 cm^{-1} (Figure 3.19). Furthermore, to determine the selective

interaction of metallogels with anions, we recorded the IR spectra of **Ni(II)G2** + S^{2-}, **Co(II)G2** + S^{2-}, and **Cu(II)G2** + I^-. Here, we observed the lowering of nitrile stretching frequency from 2232 to 2224, 2222, and 2223 cm^{-1} (Figures 3.19) respectively, indicating a stronger interaction of the nitrile group through π-bonding with metal, leading to certain adjustments to accommodate the anions in the structural framework.

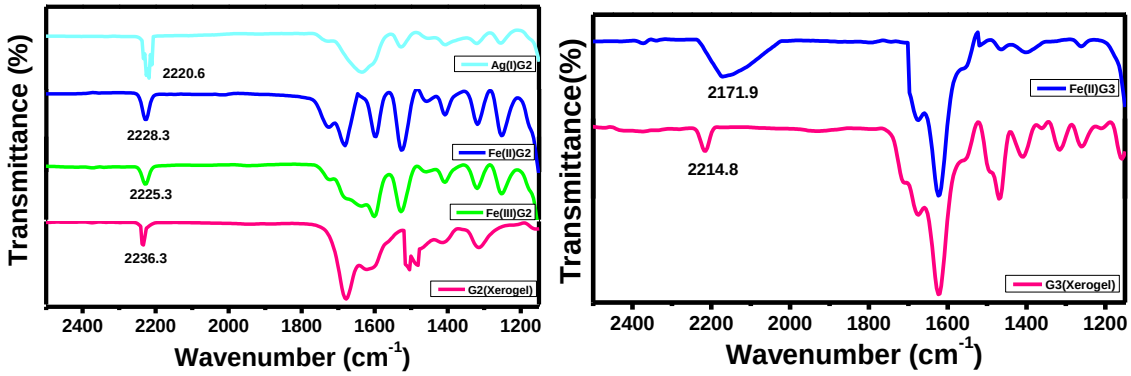

Figure 3.19. *FT-IR spectra for xerogel of* ***G2***, ***G3*** *and their metallogels.*

The PXRD investigation also showed some notable results. The PXRD peak for **G2** centered at 2θ = 25.40° corresponding to the *d*-spacing value of 3.50 Å becomes shifted to the range of 2θ = 33.66° and 2θ = 32.50° corresponding to 2.66 and 2.75 Å with a reduction in peak intensity in the case of **Ag(I)G2**, indicating disruption of π-π stacking. **Fe(II)G2** shows fractured peaks centered at 2θ = 31.62° corresponding to the *d*-spacing value of 2.82 Å signifying the alteration of π-π stacking. Likewise, the peaks around 2θ = 35° equivalent to the *d*-spacing value 2.5 Å also get shifted, indicating a disruption in the hydrogen-bonded self-assembled structure.[35,76,77] In the case of **Fe(II)G3**, the peak correlating to the hydrogen-bonded structure of the xerogel at around 2θ = 34.10° equivalent to the *d*-spacing value 2.62 Å gets almost vanished, revealing the probable disruption in hydrogen-bonded structure. Upon incorporation of metal ions, the self-assembled structure tends to dissociate that might be the reason behind the switching-off the AIEE. Whereas in the case of **Ni(II)G2**, **Cu(II)G2**, and **Co(II)G2** metallogels, the PXRD peak centered at 2θ = 42.70°-35.65° corresponding to the *d*-spacing value between 2.1 and 2.5 Å has been retained because of extensive hydrogen bonding, which may be

the driving force behind the retention of the emission property.[35,76,78] Moreover, a peak at around 2θ = 25.50° corresponding to a *d*-spacing value of 3.5 Å is maintained in the above metallogels specifying the retention of π-π stacking. Remarkably, gradual addition of the S^{2-} anion in **Ni(II)G2** and **Co(II)G2** metallogels and $\mathbf{I^-}$ in **Cu(II)G2** metallogels reveals the absence of a peak at around 2θ = 42.70°-35.60°, indicating a disruption in the hydrogen-bonded network, which might be the driving force to turn off the fluorescence particularly with $\mathbf{S^{2-}}$ and $\mathbf{I^-}$ anions. The morphological features of metallogels of **G2** and **G3** have been explored through the FE-SEM technique. The SEM images for the **G2** and **G3** organogels revealed a fibrous and dendritic-like morphology. Significant formation of the metallogel MOF disrupted the morphology to a great extent and changed it to the dense 3D network.[79-81]

Catechol Oxidase-like Activity of Cu(II)G2 in Gel Assembly. To determine the possible catecholase-like activity of **Cu(II)G2** in the gel assembled state, 100 equivalents of 3,5- DTBC were taken with 0.2 mM solution of **Cu(II)G2** in DMSO (2 mL), and subsequent addition of 100 μL of water under aerobic conditions leads to the formation of the gel after leaving it for 2 min in the uninterrupted state. After that, 10 μL of the gel was taken out and completely dissolved in 2 mL of DMSO. UV-vis spectroscopy monitored the solution for the possible formation of the oxidized product, that is, quinone. This procedure was repeated at different time intervals to monitor the progress of the reaction. The experiments revealed that a peak at around 402 nm instantaneously appeared upon the formation of the gel on the addition of catechol, indicating the oxidation of the catechol. The peak became more intense with the time, and a slight bathochromic shift in the maxima was observed, which settled at around 410 nm with time. It indicated that the **Cu(II)G2** metallogel can act as an efficient catalyst for the oxidation of 3,5-DTBC to 3,5-DTBQ (Figure 3.20). Similar experiments have been done in the absence of copper ions with the only organogel, and catechol showed very slow oxidation in the presence of aerobic oxygen (Figure 3.20).

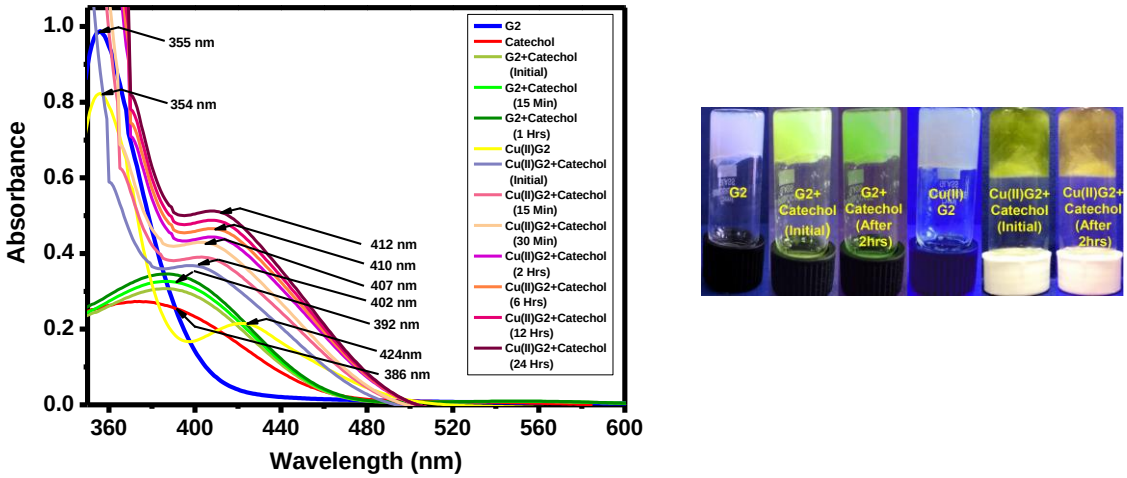

Figure 3.20. *UV-visible spectra of catechol Oxidase activity of* ***Cu(II)G2*** *in gel assembly and visible changes* ***Cu(II)G2+3,5-DTBC*** *at different intervals of time.*

To further confirm the formation of the oxidized product, that is, 3,5-di-*tert*-butyl-quinone, and to examine the probable mechanism, first the xerogel of **Cu(II)G2** was exposed to an ESI mass spectrometer in the methanol solution, which displayed two assignable peaks at 533.1 and 573.1 arising out of [**G2**+**Na**]$^+$ and [**Cu(II)G2**]$^+$, respectively. The Job plot also indicated the formation of a 1:1 metal complex with the ligand. For the determination of a possible metallogel-substrate intermediate, an ESI-MS positive spectrum was taken for a mixture of **Cu(II)G2** and 3,5-DTBC in a 1:100 molar ratio and the spectra were recorded in 5 min intervals. A lot of peaks in the resultant spectra showed extensive fragmentation of the **Cu(II)G2** metallogel into the substrate or complex-substrate intermediate. However, the appearance of a peak at 243.1 unequivocally confirmed the formation of a quinone-sodium aggregate [(3,5-DTBQ)Na]$^+$. The resultant peak at 463.3 could be identified as [(3,5-DTBQ)$_2$Na]$^+$, whereas the peak at 815.7 specifies the formation of [Cu(II)G2(3,5-DTBQ)2Na]$^+$, which could be the probable intermediate for catecholase mimicking activity. The rate constant for the catalytic reaction was calculated by the initial rate method to comprehend the kinetic feature of catalysis for the **Cu(II)G2** metallogel. The Michaelis-Menten approach of enzymatic kinetics then analyzed the observed rate versus substrate concentration data. This approach was used to find the Lineweaver-Burk plot, Michaelis-Menten constant

(K_M), and the maximum initial rate (V_{max}) (Figure 3.21).[82] Turnover frequency values (K_{cat}) were obtained by dividing the Vmax values by the concentration of the copper ion in the metallogel system. The kinetic parameters regarding the potential activity of the **Cu(II)G2** metallogel are represented in Table 3.1.

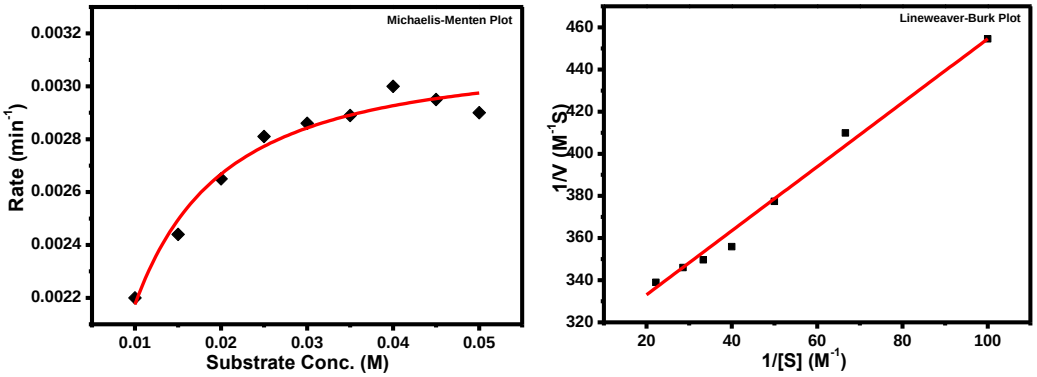

Figure 3.21. *Michaelis–Menten plot and Lineweaver–Burk plot for* ***Cu(II)G2****.*

Table 3.1. *Various kinetic parameters of Catecholase activity of* ***Cu(II)G2*** *metallogel.*

Catalyst Conc. (M)	**V_{max} (M min^{-1})**	**Std. Error**	**K_M (M)**	**Std. Error**	**K_{cat} / TOF (h^{-1})**
0.0001	0.00312	1.1659×10^{-4}	0.00541	6.4×10^{-4}	1.872×10^{3}

3.4 Conclusions

Two carboxamide nitrile-based gelators **G2** and **G3** have been synthesized and characterized thoroughly through different spectroscopic techniques. They have shown a tendency to form gels in an aqueous mixture of DMF or DMSO. Both the gelators have not shown any fluorescence peaks in solution. However, on gel formation, it showed inherent AIEE phenomena. Addition of different metal ions in the 2:1 ligand metal ratio strengthens the gel property generally without much affecting the fluorescence behavior. However, in the presence of $\mathbf{Ag^{+}}$, $\mathbf{Fe^{2+}}$, and $\mathbf{Fe^{3+}}$, the AIEE gets completely switched off, inducing the silver- and iron-sensing nature of the gelator in the gel state. **G3** in the same ligand-to-metal ratio remained in solution; however, with the lower concentration of metal ions, that is, 2:0.5 ratio, it also senses ferrous ions by turning off the fluorescence

in the gel state. Remarkably, other metallogels such as **Ni(II)G2** and **Co(II)G2** can sense sulfide ion and **Cu(II)G2** can sense iodide ion by switching off the fluorescence, which can work even in the presence of multianalytes. In this work, the copper-based metallogel can act as a reaction medium as well as a catalyst for aerobic oxidation of catechol to quinone in the gel state at room temperature and pressure, mimicking a bioinspired catalytic reaction in the presence of metalloenzymatic catechol oxidase. As per the literature survey, this is the first example where a metallogel material has been successfully utilized to demonstrate the catalytic activity for this kind of bioinspired catalysis.

3.5 References

[1] Bhattacharya S., Samanta S. K. (2016), Soft-nanocomposites of nanoparticles and nanocarbons with supramolecular and polymer gels and their applications, Chem. Rev., 116, 11967-12028 (DOI: 10.1021/acs.chemrev.6b00221)

[2] Okesola B. O., Smith D. K. (2016), Applying low-molecular weight supramolecular gelators in an environmental setting self-assembled gels as smart materials for pollutant removal. Chem. Soc. Rev., 45, 4226-4251 (DOI: 10.1039/C6CS00124F)

[3] Hirst A. R., Escuder B., Miravet J. F., Smith D. K. (2008), High-tech applications of self-assembling supramolecular nanostructured gel phase materials: from regenerative medicine to electronic devices, Angew. Chem. Int. Ed., 47, 8002-8018 (DOI:10.1002/anie.200800022)

[4] Sutar P., Maji T. K. (2016), Coordination polymer gels: soft metalorganic supramolecular materials and versatile applications, Chem. Commun., 52, 8055-8074 (DOI: 10.1039/C6CC01955B)

[5] Lin Q., Lu T.-T., Zhu X., Sun B., Yang Q.-P. Wei T.-B., Zhang Y.-M. (2015), A novel supramolecular metallogel-based higher solution anion sensor array, Chem. Commun, 51, 1635-1638 (DOI: 10.1039/C4CC07814D)

[6] Lin Q., Sun B., Yang Q.-P., Fu Y.-P., Zhu X., Zhang Y.-M., Wei T.-B. (2014), A novel strategy for the design of smart supramolecular gels: controlling stimuli-

response roperties through competitive coordination of two different metal ions, Chem. Commun., 50, 10669-10671 (DOI: 10.1039/C4CC03753G)

[7] Hu Y., Xie D., Wu Y., Lin N., Song A., Hao J. (2017), Hydrogels based on Ag+ -modulated assembly of 5′-adenosine monophosphate for enriching biomolecules Chem.-Eur. J., 23, 15721-15728 (DOI:10.1002/chem.201703180)

[8] Zhang F., Xu Z., Dong S., Feng L., Song A., Tung C.-H., Hao J. (2014), Hydrogels formed by enantioselective self-assembly of histidine-derived amphiphiles with tartaric acid, Soft Matter., 10, 4855-4862 (DOI: 10.1039/C4SM00479E)

[9] Wang H., Xu W., Song S., Feng L., Song A., Hao J. (2014), Hydrogels facilitated by monovalent cations and their use as efficient dye adsorbents, J. Phys. Chem. B., 118, 4693-4701 (DOI: 10.1021/jp500113h)

[10] Nagarajan V., Pedireddi V. R. (2014), Gelation and structural transformation study of some 1, 3, 5-Benzenetricarboxamide derivatives, Cryst. Growth Des., 14, 1895-1901 (DOI: 10.1021/cg500026t)

[11] Thool G. S., Narayanaswamy K., Venkateswararao A., Naqvi S., Gupta V., Chand S., Vivekananthan V., Koner R. R., Krishnan V., Singh S. P. (2016), Highly directional 1D supramolecular assembly of new diketopyrrolopyrrole-based gel for organic solar cell applications, Langmuir, 32, 4346-4351, (DOI: 10.1021/acs.langmuir.6b00846)

[12] Datta S., Bhattacharya S. (2015), Multifarious facets of sugar-derived molecular gels: molecular features, mechanisms of self-assembly and emerging applications, Chem. Soc. Rev., 44, 5596-5637 (DOI: 10.1039/C5CS00093A)

[13] Cui Y., Chen B., Qian G. (2014), Lanthanide metal-organic frameworks for luminescent sensing and light-emitting applications, Coord. Chem. Rev., 273, 76-86 (DOI: 10.1016/j.ccr.2013.10.023)

[14] Aiyappa H. B., Saha S., Wadge P., Banerjee R., Kurungot S. (2015), Fe(III) phytate metallogel as a prototype anhydrous, intermediate temperature proton conductor, Chem. Sci., 2015, 6, 603-607 (DOI: 10.1039/C4SC02294G)

[15] McCarney E. P., Byrne J. P., Twamley B., Martínez-Calvo M., Ryan G., Möbius M. E., Gunnlaugsson T. (2015), Self-assembly formation of a healable lanthanide

luminescent supramolecular metallogel from 2,6-bis(1,2,3-triazol-4-yl)pyridine (btp) ligands, Chem. Commun., 51, 14123-14126 (DOI: 10.1039/C5CC03139G)

[16] Dastidar P., Ganguly S., Sarkar K. (2016), Metallogels from coordination complexes, organometallic, and coordination Polymers. Chem.-Asian J., 11, 2484-2498 (DOI:10.1002/asia.201600814)

[17] Xing B., Choi M.-F., Zhou Z., Xu B. (2002), Spontaneous enrichment of organic molecules from aqueous and gas phases into a stable metallogel, Langmuir, 18, 9654-9658 (DOI: 10.1021/la0256580)

[18] Sarkar S., Dutta S., Bairi P., Pal T. (2014), Redox-responsive copper(I) metallogel: a metal-organic hybrid sorbent for reductive removal of chromium(VI) from aqueous solution, Langmuir., 30, 7833-7841 (DOI: 10.1021/la501309m)

[19] Cong H.-P., Ren X.-C., Wang P., Yu S.-H. (2012), Macroscopic multifunctional graphene-based hydrogels and aerogels by a metal ion induced self-assembly process, ACS Nano., 6, 2693-2703 (DOI: 10.1021/nn300082k)

[20] Zhu C.-H., Hai Z.-B., Cui C.-H., Li H.-H., Chen J.-F., Yu S.- H. (2012), In situ-controlled synthesis of thermosensitive poly(nisopropylacrylamide)/Au nanocomposite hydrogels by gamma radiation for catalytic application, Small., 8, 930-936 (DOI: 10.1002/smll.201102060)

[21] Cong H.-P., Wang P., Yu S.-H. (2013), Stretchable and self-healing graphene oxide-polymer composite hydrogels: a dual-network design, Chem. Mater., 25, 3357-3362 (DOI: 10.1021/cm401919c)

[22] Ganta S., Chand D. K. (2015), Nanoscale metallogel via self-assembly of self-assembled trinuclear coordination rings: multi-stimuli-responsive soft materials, Dalton Trans., 44, 15181-15188 (DOI: 10.1039/C4DT03715D)

[23] Paul M., Sarkar K., Dastidar P. (2015), Metallogels derived from silver coordination polymers of C3-symmetric tris (pyridylamide) tripodal ligands: synthesis of Ag nanoparticles and catalysis, Chem.-Eur. J., 21, 255-268 (DOI:10.1002/chem.201404959)

[24] Bhattacharjee S., Samanta S. K., Moitra P., Pramoda K., Kumar R., Bhattacharya S., Rao C. N. R. (2015), Nanocomposite made of an oligo(p-phenylenevinylene)-based trihybrid thixotropic metallo- (organo)gel comprising nanoscale metal-organic particles, carbon nanohorns, and silver nanoparticles, Chem.-Eur. J., 21, 5467-5476 (DOI:10.1002/chem.201405522)

[25] Gómez-Valdemoro A., Trigo M., Ibeas S., García F. C., Serna F., García J. M. (2011), Acrylic copolymers with pendant 1, 2, 4- triazole moieties as colorimetric sensory materials and solid phases for the removal and sensing of cations from aqueous media, J. Polym. Sci., Part A: Polym. Chem., 49, 3817-3825 (DOI:10.1002/pola.24820)

[26] Gomes M. A., Lima Á. S., Eguiluz K. I. B., Salazar-Banda G. R. (2016), Wet chemical synthesis of rare earth-doped barium titanate nanoparticles, J. Mater. Sci., 51, 4709-4727 (DOI 10.1007/s10853-016-9789-7)

[27] Biswas A., Dubey M., Mukhopadhyay S., Kumar A., Pandey D. S. (2016), Anion triggered metallogels: demetalation and crystal growth inside the gel matrix and improvement in viscoelastic properties using Au-NPs. Soft Matter, 12, 2997-3003 (DOI: 10.1039/C5SM02464A)

[28] Zhong J.-L., Jia X.-J., Liu H.-J., Luo X.-Z., Hong S.-G., Zhang N., Huang J.-B. (2016), Self-assembled metallogels formed from *N*,*N*′,*N*″-tris(4-pyridyl)trimesic amide in aqueous solution induced by Fe(III)/Fe(II) ions, Soft Matter, 2016, 12, 191-199 (DOI: 10.1039/C5SM01513H)

[29] Terech P., Weiss R. G. (1997), Low molecular mass gelators of organic liquids and the properties of their gels, Chem. Rev., 97, 3133-3160 (DOI: 10.1021/cr9700282)

[30] Zhao Z., Lam J. W. Y., Tang B. Z. (2013), Self-assembly of organic luminophores with gelation-enhanced emission characteristics, Soft Matter, 9, 4564-4579, (DOI: 10.1039/C3SM27969C)

[31] Babu S. S., Praveen V. K., Ajayaghosh A. (2014), Functional π-gelators and their applications, Chem. Rev., 114, 1973-2129 (DOI: 10.1021/cr400195e)

[32] Xue P., Ding J., Shen Y., Gao H., Zhao J., Sun J., Lu R. (2017), Aggregation-induced emission nanofiber as a dual sensor for aromatic amine and acid vapor, J. Mater. Chem. C., 5, 11532-11541 (DOI: 10.1039/C7TC03192K)

[33] Feng Y., Liu Z.-X., Chen H., Yan Z.-C., He Y.-M., Liu C.-Y.;Fan. (2014), Q.-H. A systematic study of eripherally multiple aromatic ester-functionalized poly (benzyl ether) dendrons for the fabrication of organogels: structure-property relationships and thixotropic property, Chem.-Eur. J., 20, 7069-7082 (DOI:10.1002/chem.201400157)

[34] Chen H., Feng Y., Deng G.-J., Liu Z.-X., He Y.-M., Fan Q.- H. (2015), Fluorescent dendritic organogels based on 2-(2′-Hydroxyphenyl)benzoxazole: emission enhancement and multiple stimuli-responsive properties, Chem.-Eur. J., 21, 11018-11028 (DOI: 10.1002/chem.201500849)

[35] Lin Q., Lu T.-T., Zhu X., Sun B., Yang Q.-P., Wei T.-B., Zhang Y.-M. (2015), A novel supramolecular metallogel-based high resolution anion sensor array, Chem. Commun., 51, 1635-1638 (DOI: 10.1039/C4CC07814D)

[36] Lin Q., Lu T.-T., Zhu X., Wei T.-B., Li H., Zhang Y.-M. (2016), Rationally introduce multi-competitive binding interactions in supramolecular gels: a simple and efficient approach to develop multi-analyte sensor array, Chem. Sci., 7, 5341-5346 (DOI: 10.1039/C6SC00955G)

[37] Piepenbrock M.-O. M., Clarke N., Steed J. W. (2009), Metal ion and anion- based "tuning" of a supramolecular metallogel, Langmuir. 25, 8451-8456 (DOI: 10.1021/la900145n)

[38] Malviya N., Das M., Mandal P., Mukhopadhyay S. (2017), A smart organic gel template as metal cation and inorganic anion sensor, Soft Matter, 2017, 13, 6243-6249 (DOI: 10.1039/C7SM01199G)

[39] Huang J., He L., Zhang J., Chen L., Su C.-Y. (2010), Dynamic functionalized metallogel: an approach to immobilised catalysis with improved activity, J. Mol. Catal. A: Chem., 317, 97-103 (DOI: 10.1016/j.molcata.2009.11.001)

[40] Liu Y.-R., He L., Zhang J., Wang X., Su C.-Y. (2009), Evolution of spherical assemblies to fibrous networked Pd (II) metallogels from a pyridine-based

tripodal ligand and their catalytic property, Chem. Mater., 21, 557-563 (DOI: 10.1021/cm802841r)

[41] Sharma M., Sarma P. J., Goswami M. J., Bania K. K. (2017), Metallogel templated synthesis and stabilization of silver-particles and its application in catalytic reduction of nitro-arene, J. Colloid Interface Sci., 490, 529-541 (DOI: 10.1016/j.jcis.2016.11.065)

[42] Wen X., Tang L. (2015), One-dimensional copolymer nanostructures loaded with silver nanoparticles fabricated via metallogel template copolymerization and their pH dependent photocatalytic degradation of methylene blue, J. Mol. Catal. A: Chem., 399, 86-96 (DOI: 10.1016/j.molcata.2015.01.025)

[43] Wen X., Tang L., Li B. (2014), Metallogel template fabrication of pH-responsive copolymer nanowires loaded with silver nanoparticles and their photocatalytic degradation of methylene blue, Chem.-Asian J., 9, 2975-2983 (DOI:10.1002/asia.201402575)

[44] Ye L., Wan L., Huang F. (2017), A class of polytriazole metallogels via CuAAC polymerization: preparation and properties, New J. Chem., 2017, 41, 4424-4430 (DOI: 10.1039/C7NJ00610A)

[45] Mallick A., Schön E.-M., Panda T., Sreenivas K., Díaz D. D., Banerjee R. (2012), Fine-tuning the balance between crystallization and gelation and enhancement of CO_2 uptake on functionalized calcium-based MOFs and metallogels., J. Mater. Chem., 22, 14951-14963 (DOI: 10.1039/C2JM30866E)

[46] Tang X. Q., Xiao B. W., Li C. M., Wang D. M., Huang C. Z., Li Y. F. (2017), Co-metal-organic-frameworks with pure uniform crystal morphology prepared via Co^{2+} exchange-mediated transformation from Zn-metallogels for luminol catalyzed chemiluminescence, Spectrochim. Acta, Part A., 175, 11-16 (DOI: 10.1016/j.saa.2016.12.014)

[47] Mehdi H., Pang H., Gong W., Dhinakaran M. K., Wajahat A., Kuang X., Ning G. (2016), A novel smart supramolecular organic gelator exhibiting dual-channel responsive sensing behaviours towards fluoride ion via gel-gel states, Org. Biomol. Chem., 14, 5956-5964, (DOI: 10.1039/C6OB00600K)

[48] Farona M. F., Kraus K. F. (1970), Coordination of organonitriles through CN.π systems, Inorg. Chem., 9, 1700-1704 (DOI: 10.1021/ic50089a018)

[49] Sun Y., Wang Y.-X., Wu M., Yuan W., Chen Y. (2017), p-quaterphenylene as an aggregation-induced emission fluorogen in supramolecular organogels and fluorescent sensors, Chem.-Asian J., 12, 52-59 (DOI:10.1002/asia.201601388)

[50] Lin Q., Sun B., Yang Q.-P., Fu Y.-P., Zhu X., Wei T.-B., Zhang Y.-M. (2014), Double metal ions competitively control the guest-sensing process: a facile approach to stimuli-responsive supramolecular gels, Chem.-Eur. J., 20, 11457-11462 (DOI:10.1002/chem.201403327)

[51] Castilla A., Dietrich B., Adams D. (2018), Using aggregation-induced emission to understand dipeptide gels, Gels, 4, 17 (DOI:10.3390/gels4010017)

[52] Mei J., Leung N. L. C., Kwok R. T. K., Lam J. W. Y., Tang B. Z. (2015), Aggregation-induced emission: together we shine, united we soar, Chem. Rev., 115, 11718-11940 (DOI: 10.1021/acs.chemrev.5b00263)

[53] Crosby G. A., Demas J. N. (1971), Measurement of photoluminescence quantum yields review, J. Phys. Chem., 75, 991-1024 (DOI: 10.1021/j100678a001)

[54] Li X.-Q., Zhang X., Ghosh S., Würthner F. (2008), Highly fluorescent lyotropic mesophases and organogels based on J-aggregates of ore-twisted perylene Bisimide dyes, Chem.-Eur. J., 14, 8074-8078 (DOI:10.1002/chem.200800915)

[55] Feng Y., Liu Z., Wang L., Chen H., He Y., Fan Q. (2012), Poly(benzyl ether) dendrons without conventional gelation motifs as a new kind of effective organogelators, Chin. Sci. Bull., 57, 4289-4295 (DOI: 10.1007/s11434-012-5479-2)

[56] Liyanage, W.; Nilsson, B. L. (2016), Substituent effects on the selfassembly/ coassembly and hydrogelation of phenylalanine derivatives, Langmuir, 2016, 32, 787-799. (DOI: 10.1021/acs.langmuir.5b03227)

[57] Yan X., Cui Y., He Q., Wang K., Li J. (2008), Organogels based on self-assembly of diphenylalanine peptide and their application to immobilize quantum dots, Chem. Mater., 20, 1522-1526 (DOI: 10.1021/cm702931b)

[58] Yan X., Zhu P., Li J. (2010), Self-assembly and application of diphenylalanine-based nanostructures, Chem. Soc. Rev., 39, 1877-1890 (DOI: 10.1039/B915765B)

[59] Lin Q., Zhong K.-P., Zhu J.-H., Ding L., Su J.-X., Yao H., Wei T.-B., Zhang Y. M. (2017), Iodine controlled pillar[5]arene-based multi responsive supramolecular polymer for fluorescence detection of cyanide, mercury, and cysteine, Macromolecules, 2017, 50, 7863-7871 (DOI: 10.1021/acs.macromol.7b01835)

[60] Lin Q., Fan Y.-Q., Mao P.-P., Liu L., Liu J., Zhang Y.-M., Yao H., Wei T.-B. (2018), Pillar [5] arene-based supramolecular organic framework with multi-guest detection and recyclable separation properties, Chem.-Eur. J., 24, 777-783 (DOI:10.1002/chem.201705107)

[61] Lin Q., Mao P.-P., Fan Y.-Q., Liu L., Liu J., Zhang Y.-M., Yao H., Wei T.-B. (2017), A novel supramolecular polymer gel based on naphthalimide functionalized-pillar[5]arene for the fluorescence detection of Hg^{2+} and I^{-} and recyclable removal of Hg^{2+} via cation-π interactions, Soft Matter, 2017, 13, 7085-7089 (DOI: 10.1039/C7SM01447C)

[62] Nakamoto, K.; Nakamoto, K. (1977), Infrared and Raman Spectra of Inorganic and Coordination Compounds, Wiley

[63] Sutton J. E. Zink, J. I. (1976), Spectroscopic studies of perpendicular nitrile-metal interactions, Inorg. Chem., 15, 675-678 (DOI: 10.1021/ic50157a036)

[64] Jain S. C., Rivest R. (1967), Possible coordination between halides of Group IV elements and the triple bond of diethylaminoacetonitrile as ligand, Inorg. Chem., 6, 467-469 (DOI: 10.1021/ic50049a007)

[65] Beltrán E., Garzoni M. Feringán B., Vancheri A., Barberá J., Serrano J. L., Pavan, G. M., Giménez R., Sierra T. (2015), Self-organization of star-shaped columnar liquid crystals with a coaxial nanophase segregation revealed by a combined experimental and simulation approach, Chem. Commun., 51, 1811-1814 (DOI:10.1021/jacs.6b06792)

[66] Zhang Y., Liang C., Shang H., Ma Y., Jiang S. (2013), Supramolecular organogels and nanowires based on a V-shaped cyanostilbene amide derivative with aggregation-induced emission (AIE) properties, J. Mater. Chem. C., 1, 4472-4480 (DOI:10.1039/C3TC30545G)

[67] Ghosh A., Das P., Kaushik R., Damodaran K. K., Jose D. A. (2016), Anion responsive and morphology tunable tripodal gelators, RSC Adv., 6, 83303-83311 (DOI: 10.1039/C6RA16345A)

[68] Xu Y.-L., Li C.-T., Cao Q.-Y., Wang B.-Y., Xie Y. A. (2017), Pyrenylappended organogel for fluorescence sensing of anions, Dyes Pigm., 139, 681-687 (DOI: 10.1016/j.dyepig.2016.12.068)

[69] Mears L. L. E., Draper E. R., Castilla A. M., Su H., Zhuola., Dietrich B., Nolan M. C., Smith G. N., Doutch J., Rogers S., Akhtar R., Cui H., Adams D. J. (2017), Drying affects the fiber network in low molecular weight hydrogels, Biomacromolecules, 18, 3531-3540 (DOI: 10.1021/acs.biomac.7b00823)

[70] Adams D. (2018), Does Drying Affect Gel Networks?, Gels, 4, 32 (DOI:10.3390/gels4020032)

[71] Du X., Zhou J., Shi J., Xu B. (2015), Supramolecular hydrogelators and hydrogels: from soft matter to molecular biomaterials, Chem. Rev., 115, 13165-13307 (DOI: 10.1021/acs.chemrev.5b00299)

[72] Kartha K. K., Babu S. S., Srinivasan S., Ajayaghosh A. (2012), Attogram sensing of trinitrotoluene with a self-assembled molecular gelator, J. Am. Chem. Soc., 134, 4834-4841 (DOI: 10.1021/ja210728c)

[73] Yu C., Li X., Zeng F., Zheng F., Wu S. (2013), Carbon-dot-based ratiometric fluorescent sensor for detecting hydrogen sulfide in aqueous media and inside live cells, Chem. Commun., 49, 403-405 (DOI: 10.1039/C2CC37329G)

[74] Masih D., Aly S. M., Alarousu E., Mohammed O. F. (2015), Photoinduced triplet-state electron transfer of platinum porphyrin: a one-step direct method for sensing iodide with an unprecedented detection limit, J. Mater. Chem. A., 3, 6733-6738 (DOI: 10.1039/C4TA07033J)

[75] Choi M. G., Cha S., Lee H., Jeon H. L., Chang S.-K. (2009), Sulfide selective chemo signaling by a Cu^{2+} complex of dipicolylamine appended fluorescein, Chem. Commun., 2009, 7390-7392 (DOI: 10.1039/B916476F)

[76] Xu Y.-L., Li C.-T., Cao Q.-Y., Wang B.-Y., Xie Y. (2017), A pyrenylappended organogel for fluorescence sensing of anions, Dyes Pigm., 139, 681-687 (DOI: 10.1016/j.dyepig.2016.12.068)

[77] Howe R. C. T., Smalley A. P., Guttenplan A. P. M., Doggett, M. W. R., Eddleston M. D., Tan J. C., Lloyd G. O. (2013), A family of simple benzene 1,3,5-tricarboxamide (BTA) aromatic carboxylic acid hydrogels, Chem. Commun., 49, 4268-4270 (DOI: 10.1039/C2CC37428E)

[78] Gou F., Cheng J., Zhang X., Shen G., Zhou X., Xiang H. (2016), Unusual aggregation/gelation-induced phosphorescence of propeller-type binuclear platinum(II) enantiomers, Eur. J. Inorg. Chem., 4862-4866 (DOI:10.1002/ejic.201600839)

[79] Yang C., Gu B., Zhang D., Ge C., Tao H. (2016), Coaxial carbon fiber/ZnO nanorods as electrodes for the electrochemical determination of dopamine, Anal. Methods, 8, 650-655 (DOI: 10.1039/C5AY02928G)

[80] Liang C. L., Zhong K., Liu M., Jiang L., Liu S. K., Xing D. D., Li H. Y., Na Y. Zhao W. X., Tong Y. X., Liu P. (2010), Synthesis of morphology-controlled silver nanostructures by electrodeposition, Nano-Micro Lett., 2, 6-10. (DOI: 10.5101/nml.v2i1.p6-10)

[81] Zhao J., Sun M., Liu Z., Quan B., Gu C., Li J. (2015), Three dimensional hybrids of vertical graphene-nanosheet sandwiched by Ag-nanoparticles for enhanced surface selectively catalytic reactions, Sci. Rep., 5, 16019 (DOI: 10.1038/srep16019)

[82] Jana A., Aliaga-Alcalde N., Ruiz E., Mohanta S. (2013), Structures, magnetochemistry, spectroscopy, theoretical study, and catechol oxidase activity of dinuclear and dimer-of-dinuclear mixed-valence Mn(III)/Mn(II) complexes derived from a macrocyclic ligand, Inorg. Chem., 52, 7732-7746 (DOI: 10.1021/ic400916h)

Chapter 4

Cobalt Metallogel Interface for Selectively Sensing L-Tryptophan among Essential Amino Acids

Chapter 4

Cobalt Metallogel Interface for Selectively Sensing L-Tryptophan among Essential Amino Acids

4.1 Introduction

The world of gel materials is getting more attention in the last few years as it has been explored to be utilized in various facets of life.[1-3] In recent years, π-conjugated fluorescent molecules are widely synthesized, and their self-assembling behavior was used in optoelectronics for sensing applications. However, synthesis of such class of π-conjugated molecules is challenging, tedious, and perilous to the environment. To overcome these challenges, supramolecular chemistry has gained extensive attention as an alternative approach for designing highly fluorescent materials.[4] The self-assembling tendency of these compounds leads to the aggregation-induced enhanced emission (AIEE) effect, which is used for the development of various devices like light-emitting diodes, sensors, and light-emitting liquid crystals.[5] The self-assembled soft materials could be classified on the basis of presence and absence of metal centers. The materials incorporate with metal complex or ion are called metallogels, whereas the self-assembled materials of organic compounds are called organogels or hydrogels depending upon their major (solvent) components. The design and fabrication of selected metal ions with various organic compounds and ligands are particularly appealing owing to their broader range of applications.[6-10] The self-assembled materials show several kinds of non-covalent interactions (π-π stacking, C-H-π interactions, dipole-dipole interactions, van der Waals interactions, and hydrogen-bonding), which contribute a significant role during self-assembly.[11-13]

In search of novel self-assembled materials, a large number of C_3 symmetric derivative of 1,3,5-tricarboxamide (BTA) based gelator molecules have been synthesized. Such molecules form a columnar packing owing to the intramolecular hydrogen bonding within

the consecutive amide groups which results in the formation of supramolecular assemblies of gelators. The advantage of derivatives of BTA in supramolecular chemistry is, it could be fabricated with various metals, and the chemical structure could be easily varied due to the greater number of functional groups available in it. It is worth mentioning that, nitrile derivatives of BTA are important class of gelators because of the electron-withdrawing tendency of nitrile groups which endow strong non-covalent interactions between aromatic rings.[5, 14] The introduction of the metal ion into a nitrile substituted gelator molecule reorganizes the structure significantly through coordination interaction between the donor (ligand) and acceptor (metal).

In general, metallogels have been proved to be quite effective in sensing certain anions when assembled with different gelators.[15-19] There were also certain reports when metallogel acted as a sensor material for ammonia, hydrogen sulfide, triethylamine, pyridine, and picric acid through different spectroscopic methodology.[20-23] Visual chiral detection of (R) and (S)-binap has also been achieved through the collapse of a platinum-based metallogel.[24] However, there is no such report available so far where metallogels have been utilized to discriminate between biomolecules of the same family. The sensing and recognition of important biological substrates, for example, an amino acid is very promising for the amino acid pool which is responsible for accomplishing a balanced metabolism.[25] Amino acids act as potential biomarkers and precursor for various key biological substances.[26] Though the interaction of metal ions with different amino acids have been explored extensively,[27-29] however, metallogel getting utilized as sensor come up as a new approach to discrimination of amino acid. Among the various amino acids, L-tryptophan is an important one because it is essential for neuronal balancing mechanisms.[30] The inadequacy of any amino acid may lead to a weakening of protein metabolism. Therefore, sensing of amino acid in solution is one of the best methodologies for proper treatment. Sensing of tryptophan in solution state has been performed by various methodologies so far, which include liquid chromatography, capillary electrophoresis, and spectroscopic detection.[31, 32]

In present work, we design a cobalt-based metallogel synthesized utilizing the gelator *N1*, *N3*, *N5*-tris(4-cyanomethyl-phenyl)benzene-1,3,5-tricarboxamide **G4.** We have successfully crystallized **G4** gelator, and their columnar stacking because of various non-covalent interactions present in it has been explored. We report the application of cobalt metallogel interface which senses L-tryptophan selectively in a gel state by drastic quenching of AIEE. Interestingly, our cobalt-based metallogel also sense tryptophan amino acid residue present in a complex structure like BSA protein even by naked eyes. This work also reports the role of water as a solvent in sol-gel transformation and the solid-state structure of the gelator molecule **G4**. These experimental findings would become a facile, robust, and cost-effective approach for tryptophan sensing in the various area of material chemistry to biology.

4.2 Experimental section

4.2.1 Material and method

All the required chemicals were purchased from Sigma and used without further purification. The specifications of all the instruments used for analysis purpose were the same as described in section 2.2.1 of chapter 2.

4.2.2 Synthesis of gelator G4 [*N1, N3, N5*-tris(4-cyanomethyl-phenyl)benzene-1,3,5-tricarboxamide]

1 g (4.75 mmol) of trimesoyl chloride was ice-cooled in the presence of dry DMF (8 mL). 2.18 g (16.5 mmol, 3.5 molar equivalent) of 4-aminobenzyl cyanide were slowly added to trimesoyl chloride solution which contains triethylamine (2.35 mL, 16.8 mmol) for the synthesis of gelator **G4** followed by stirring of the reaction mixture for overnight at ambient conditions. The resultant solution worked up by the addition of 100 mL of ethyl acetate and the dil. HCl (1 N, 100 mL). The combined organic layer further washed with the saturated Na_2CO_3 (100 mL) aqueous solution, and brine (100 mL). The resultant organic layer dried over anhydrous sodium sulfate and white colored powder was

obtained by evaporation of whole solvent under reduced pressure. The obtained gelator **G4** has been dried at 28 °C under moderate vacuum. Yield: 80% (for **G4**). ^{1}H NMR (400 MHz, 298 K, DMSO-d_6): δ = 10.86 (3H, amide, s), 8.81 (3H, aromatic, s), 7.94 (6H, aromatic, d), 7.44 (6H, aromatic, s), 4.10 (6H, aliphatic CH2, s). ^{13}C NMR (100 MHz, 293 K, DMSO-d_6): δ = 164 (amide), 138 (aromatic), 135 (aromatic), 130 (aromatic), 128 (aromatic), 127 (aromatic), 121 (aromatic), 119 (nitrile), 22 (aliphatic CH2). FT-IR of **G4** (KBr): ν = 3223, 3139, 2272, 1696, 1631, 1564, 1482 cm^{-1}. MS (ESI) of **G4**: *m/z* = 551.20 (in negative mode).

4.2.3 Preparation of gels

0.03 millimole of **G4** gelator was solubilised in a 1.5 mL of dimethyl sulfoxide (DMSO) or dimethylformamide (DMF) after which addition of 0.5 mL of Milli-Q water in the glass vial has been taken up. Spontaneous formation of organogel has been observed when solution was left undisturbed for a few minutes. However, metallogels has been obtained via the same methodology as described in the section 2.2.3 of chapter 2.

4.2.4 Gel to Crystal transition

The solution (obtained from the heating of **G4** gel) left undisturbed at room temperature. We observed the formation of crystal by the gradual cooling of this solution. However, the solution, when left undisturbed after the addition of 0.5 mL of Milli-Q water forms a stable gel.

4.2.5 Gel melting temperature

Gel melting temperature (Tgel) of **G4** has been measured in the same procedure described in the section 2.2.4 of chapter 2.

4.2.6 Characterizations

Characterizations techniques like UV-visible Spectroscopy, Fluorescence Spectroscopy, FT-IR Spectroscopy, powder X-ray Diffraction (PXRD) and morphological Study, Rheological Properties of **G4** and their metallogels have been same as described in the section 2.2.5 of chapter 2.

Circular Dichroism (CD) Spectroscopy. The circular dichroism (CD) experiment was performed by JASCO J-815 spectropolarimeter at 25 °C using a quartz cell (path length: 1 mm). The concentration-dependent UV/vis CD spectra were recorded for only BSA protein and the BSA with varying the concentration (from 0 to 24 μM) of **Co(II)G4** metallogel. The solution was scanned at 1 nm bandwidth, 20 nm min-1 scanning speed, and 1 s response time. All the spectra were recorded within the range of 190-260 nm with a data pitch of 0.1 nm. Experimental data were recorded in an accumulation of three scans, and the average data are collected.

Single Crystal X-ray Diffraction (SXRD). For X-ray crystallographic analysis, yellow needle-like crystal of **G4** has been taken with approximate 0.020 mm × 0.060 mm × 0.080 dimensions. The quartz fibers were used to mount the crystals, and the X-ray diffraction intensity data have been measured by Bruker APEX II diffractometer equipped with a CCD detector at 153 K temperature. Employing Mo Kα radiation (λ = 0.71073 Å), with the SMART suite of programs.[34] The data were processed and corrected for Lorentz and polarization effects with SAINT and absorption effects with SADABS.[35] The SHELXTL suite of programs were used for structure solution and refinement.[36] Multi-scan method (SADABS) has been used to correct the data for absorption effects. The structures were solved by Patterson maps to locate the heavy atoms, followed by the difference in maps for the light, non-hydrogen atoms. All non-hydrogen atoms were refined with anisotropic thermal parameters. All the data (crystal data, refinement and collection parameters) for **G4** have been calculated. SQUEEZE has been applied to remove the disorder in a solvent of crystallization

4.2.7 L-Tryptophan Sensing by Co(II)G4 Metallogel

Fluorescence spectroscopic experiment was performed to study the interaction of metallogels with different amino acids. Appropriate amount of stocks of metallogels [**Fe(II)G4**, **Fe(III)G4**, **Co(II)G4**, **Ni(II)G4**, **Cu(II)G4**, **Zn(II)G4**, **Ag(I)G4**, **Cd(II)G4**] of **G4** gelator were prepared. All the metallogels treated with the different amino acids (Try, Leu, Lys, Phe, Trp, Ala, Glu, Asp, Ser, His) in a molar ratio of 1:0.5. The fluorescence spectra of amino acids treated gels have been recorded using (10×10 mm^2) standard quartz cuvette. The gels were excited at 356 nm, and the emission signal at 464 nm was monitored. Both excitation and emission slit widths with 1 nm data pitch were set to be 2 nm.

4.2.8 Supplementary materials

CCDC 1551439 contain the supplementary crystallographic data for **G4**, respectively. These data can be obtained free of charge via http://www.ccdc.cam.ac.uk/conts/retrieving.html, or from the Cambridge Crystallographic Data Centre, 12 Union Road, Cambridge CB2 1EZ, UK; fax: (+44) 1223-336-033; or e-mail: deposit@ccdc.cam.ac.uk.

4.3 Results and discussion

In a strategic approach to design a self-assembling gelator, chosen a nitrile derivative of BTA molecule because of self-assembling ability gets enhanced by nitrile group through the participation of various non-covalent interactions. It is widely accepted that the higher charge density and nucleophilicity of nitrile group offer suitable metal-ligand interactions.[19,37] The gelator molecule **G4** was successfully synthesized by the treatment of trimesoyl chloride with an excess of 4-amino benzyl cyanide (3.5 eqv) in the presence of triethylamine (scheme 4.1). The gelator from the resultant reaction mixture has been extracted by ethyl acetate. Further, the obtained gelator was well characterized by various spectroscopic techniques [electrospray ionization mass spectrometry (ESI-MS), IR, ^{1}H, ^{13}C NMR spectroscopy, and SXRD].

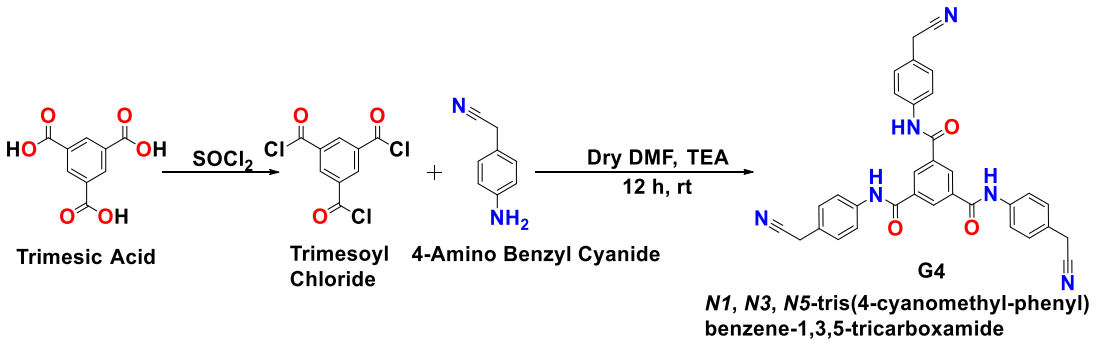

Scheme 4.1. *Systematic scheme for the synthesis of gelator* ***G4****.*

The IR spectrum analysis of the gelator **G4** reveals that the characteristic band for carboxamide N-H at 3139 cm^{-1}, for C=O at 1695 cm^{-1} and for -C≡N at 2272 cm^{-1} (Figure 4.1).[19, 38]

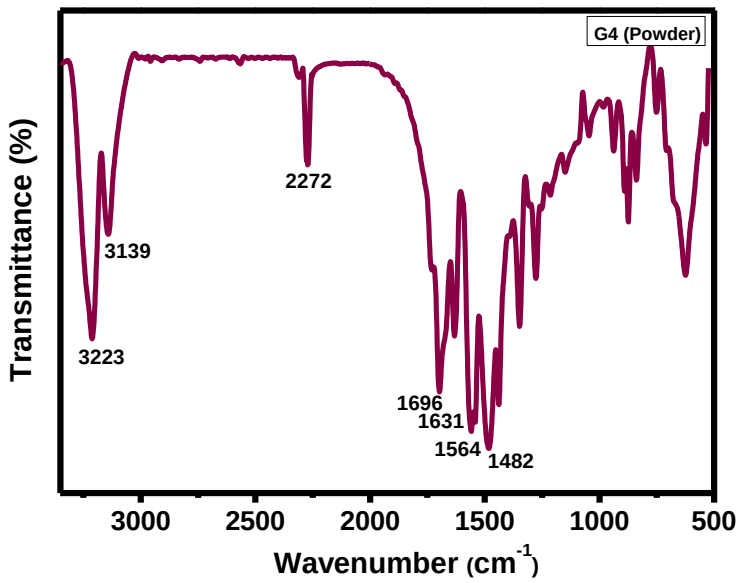

Figure 4.1. *FT-IR spectrum of gelator* ***G4.***

The molecular ion peak at 551.20 (negative mode) in ESI-MS spectrum confirms the formation of the **G4** gelator (Figure 4.2).

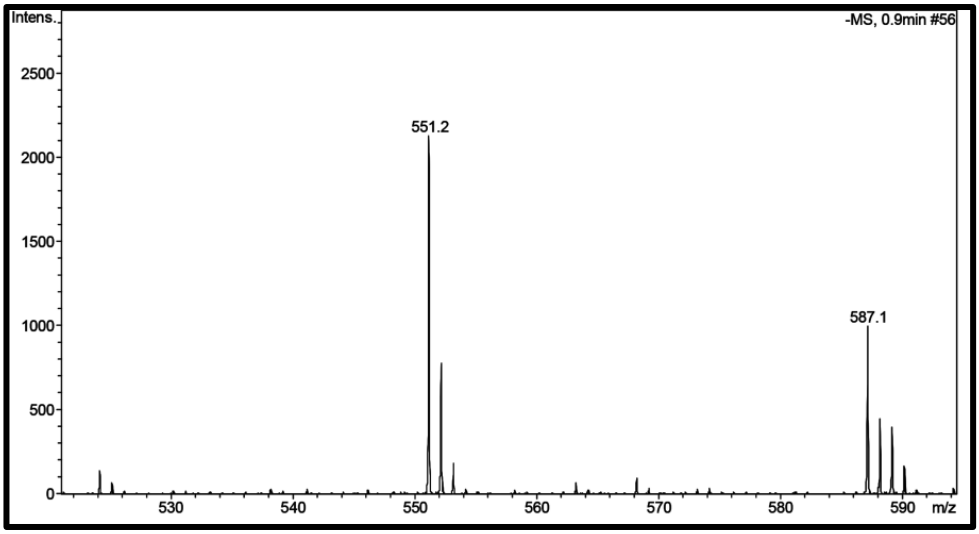

Figure 4.2. *ESI- Mass spectrum of gelator* ***G4.***

^{1}H NMR spectrum of **G4** indicates the aromatic ring protons in region of 8.81-7.44 ppm, the aliphatic proton of benzyl nitrile at 4.10 ppm and carboxamide protons at 10.86 ppm. (Figure 4.3).[39]

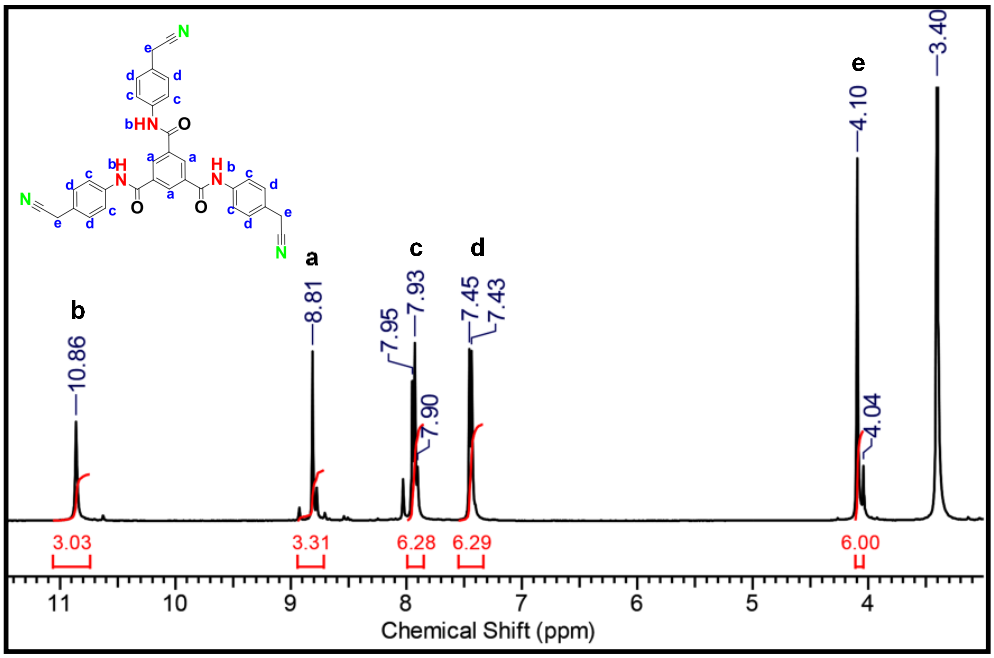

Figure 4.3. *^{1}H NMR spectrum of gelator* ***G4.***

^{13}C NMR, displays the peak at 164.92 ppm, and 119.74 ppm for the carboxamide and the nitrile carbons (Figure 4.4) apart from signature peaks of aromatic and benzyl carbon.[40]

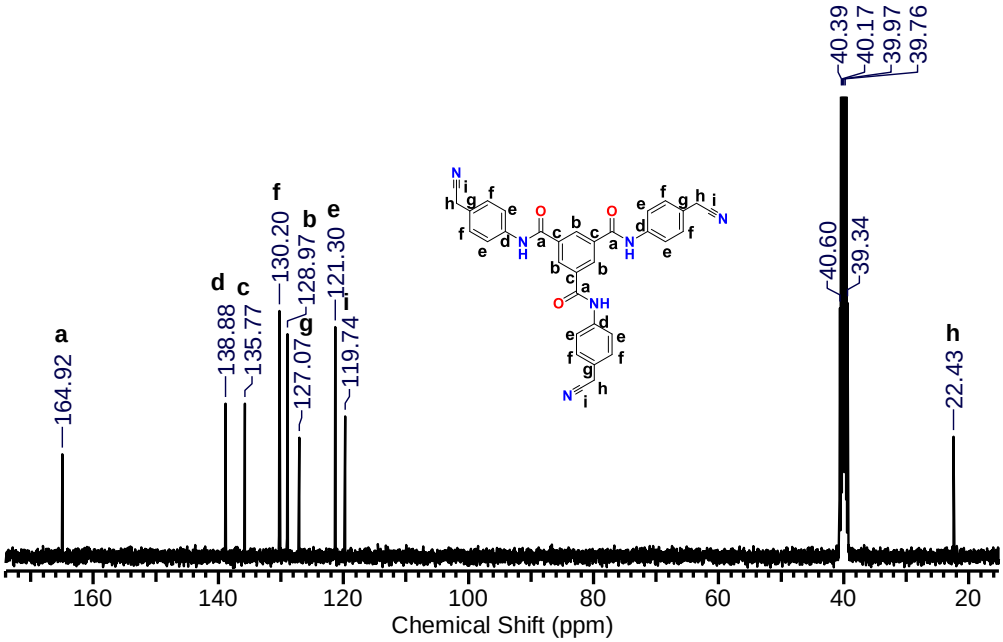

Figure 4.4. *^{13}C NMR spectrum of gelator **G4**.*

The gelation nature of gelator **G4** was further determined by "test tube inversion" method (Figure 4.5). Solubility of **G4** gelator is good in DMF/DMSO solvent but not in any other solvents even under heating. However, gelation is initiated by the addition of water in DMF/DMSO solution. In this process, water molecule assists unidirectional non-covalent interactions (hydrogen bonding, π-π stacking, van der Waals interactions). These needle-like aggregate entangle into the 3D network and encapsulate the solvent molecules by capillary action.[41,42] Influence of certain quantity of water in gel formation has been studied utilizing different ratio of DMSO/water and monitoring the AIEE, SEM, rheology. The critical gel concentration (CGC) of the gelator **G4** is found to be 15 mM in DMSO/water. The standard heating-and-cooling technique and temperature-dependent fluorescence spectroscopic experiments were used to investigate the propensity of the gelator to exhibit AIEE. Gelator **G4** was non-emissive when in a solution state, whereas gel state showed intense emission because of AIEE which might be due to curbing of free

rotations of molecules which results in blockage of non-radiative emission pathways of the excited state and consequently unlocks the radiative decay in the aggregate state.[43,44] During gradual heating of the gel from 25 to 95 °C, emission maxima was moved because of disturbance in self-assembly on heating. At 85 °C the gel converts into a sol state which is known as phase transition temperature (T_{gel}). However, it shows significant shifting in the emission maxima from 412 nm to 464 nm during gelation. In the gel phase, **G4** gelator has shown red-shifts probably due to *J*- aggregation, which specifies π-π stacking among aromatic moiety (Figure 4.6).[45] Astonishingly, a heated DMF solution of **G4** upon gradual cooling in the absence of water deposits yellow-colored crystals (Figure 4.5). In the absence of water, gelator molecules slowly self-assemble in a multidirectional way, which may lead to crystallization of gelator.[41]

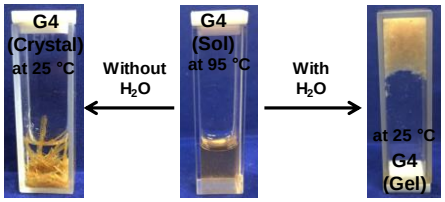

Figure 4.5. *Role of water in phase transitions between Sol to Gel and Sol to Crystal.*

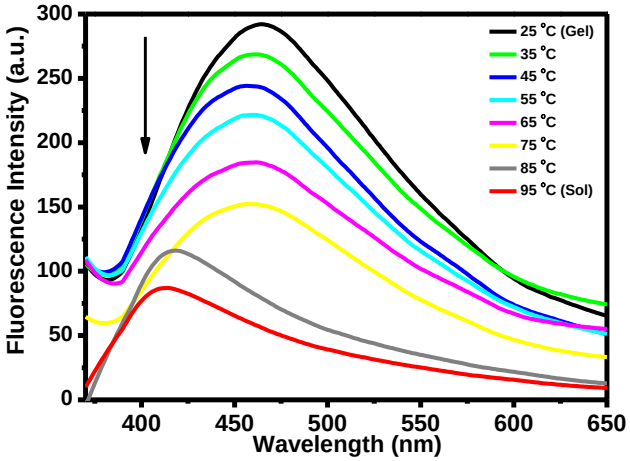

Figure 4.6. *Temperature-dependent fluorescence spectra for **G4** (in DMSO) during the gelation process (λ_{ex} = 356 nm).*

A detailed crystallographic study of **G4** gelator signifies that the gelator gets crystallized with one molecule of DMF as a solvent of crystallization (Figure 4.7a). Interpretation of the single crystal structure of gelator reveals the required information of non-covalent interactions which might be responsible for the establishment of supramolecular gel assembly. The molecular packing of the **G4** designates the varied molecular recognition pattern. Amide group present in middle of the columnar arrangements utilizes its hydrogen bond as a donor and acceptor in molecular recognition with its neighboring molecules. The hydrogen bonding sites between the solvent of crystallization and gelator have been revealed by the crystallographic data of **G4** gelator. The DMF solvent, C=O and NH group of **G4** gelator has played a critical role during intermolecular hydrogen bonding. Hirshfeld surface analysis was used to determine the hydrogen bonding interactions and close contacts in the crystal structure.[46] The dark red spots of hydrogen bond acceptors of types N-H···O, C-H···O, and C-H···N were visualized through the hirshfeld surface of **G4** (Figure 4.7b).

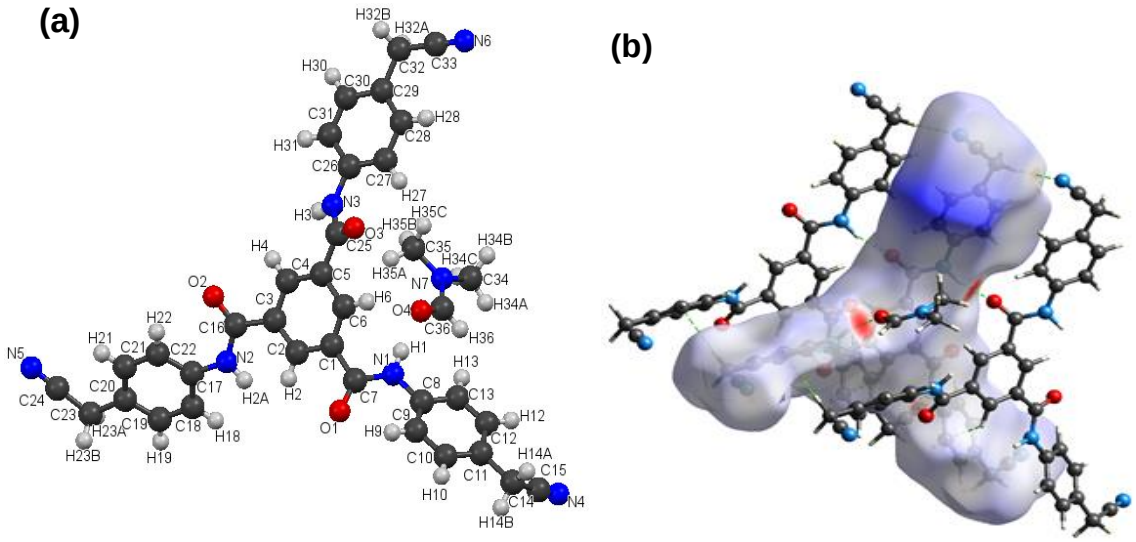

Figure 4.7 (a). *Single-crystal X-ray diffraction studies for* ***G4****;* ***(b).*** *Columnar aggregation of* ***G4*** *gelator showed the molecular recognition between molecules through N−H···O hydrogen bonds.*

Hydrogen bonds are exhibited along *a*-axis through N3-H3···O3 while the solvent molecule, DMF, forms discrete hydrogen bonds through N1-H1···O4 (Figure 4.8, Table

4.1). The supramolecular assembly of the crystal structure of gelator **G4** indicates *π-π* stacking and intercolumnar stacking between the benzene ring during the gelation. Each column of gelator molecule contains two N−H···O intracolumnar hydrogen bonds and 4.885 Å distance was found in between the central phenyl ring of successive molecules. (Figure 4.8). The **G4** gelator yielded one-dimensional molecular assembly via *π-π* stacking and hydrogen bonding. Furthermore, bond distance and bond angles between atoms of **G4** gelator are comparable with the similar molecules as in previous reports.[47]

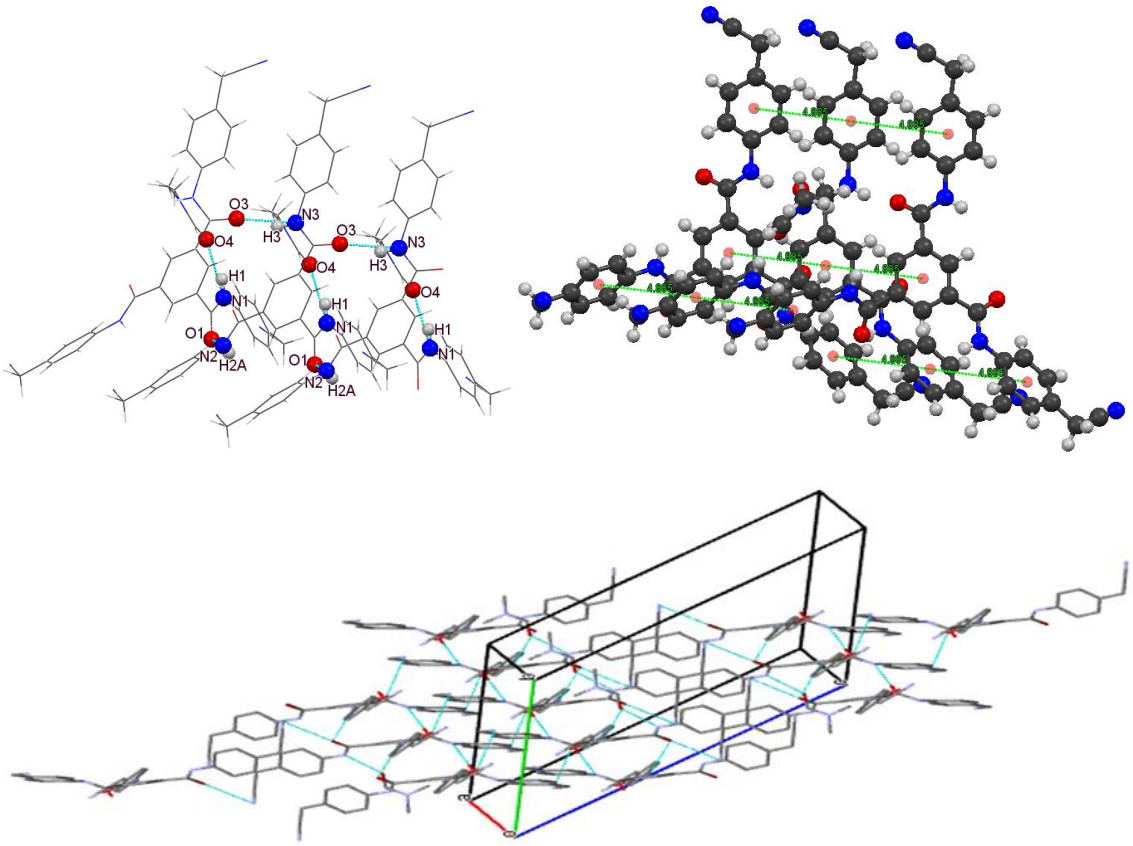

Figure 4.8. *Crystal structure of gelator **G4** showing N−H···O Hydrogen Bonding with consecutive gelator molecule and π-π stacking and intercolumnar stacking between the benzene ring with consecutive gelator molecule.*

Table 4.1. *Hydrogen bonds and the bond angle of Donor--H... Acceptor atoms of gelator* ***G4****.*

S. N.	Donor--H... Acceptor	Bond Distance			Bond Angle D-H..A	Symmetry Code
		D--H	H... A	D... A		
1	N (1) --H (1) ...O (4)	0.87 Å	2.00 Å	2.831(5) Å	160°	x, y, z
2	N (2) --H(2A) ...O (1)	0.87 Å	2.41 Å	3.013(4) Å	126°	1+x, y, z
3	N (3) –H (3) ...O (3)	0.87 Å	1.93 Å	2.738(4) Å	154°	1+x, y, z
4	C (9) -- H (9) ...O (1)	0.94 Å	2.41 Å	2.912(5) Å	113°	x, y, z
5	C (22) – H (22) ...O (2)	0.94 Å	2.33 Å	2.860(5) Å	115°	x, y, z
6	C (27) – H (27) ...O (3)	0.94 Å	2.45 Å	2.908(5) Å	110°	x, y, z
7	C (32) – H (32A) ...N (6)	0.98 Å	2.57 Å	3.548(7) Å	174°	1+x, y, z
8	C (32) – H (32B) ...O (2)	0.98 Å	2.59 Å	3.204(5) Å	120°	2-x,1-y, -z

Absolute fluorescence quantum yield experiment was performed to get a deeper insight into the emissive nature of the gel. Gelator **G4** did not show fluorescence emission in DMSO solution state. However, the fluorescence intensity got increased after the addition of 0.5 mL of water in the above solution of **G4**. Fluorescence quantum yield reaches around $\phi = 0.015$ after gelation.

The presence of non-covalent interactions (π-π stacking, weak supramolecular interactions, and hydrogen bonding) indicatesa specific role during gelation.[48,49] It was expected that the self-assembled gel structure established not only by the extensive hydrogen bonding between carboxamide and nitrile but also owing to the presence of intercolumnar stacking, π-π stacking, and van der Waals interactions.[49,50] A closer concentration-dependent study of self-assembly through ^{1}H NMR spectroscopy indicates that upon an increment of the concentration from 10 to 150 mM, aromatic and carboxamide protons have shifted downfield revealing the role of hydrogen bonding (Figure 4.9) in concentrated solution.[51,52]

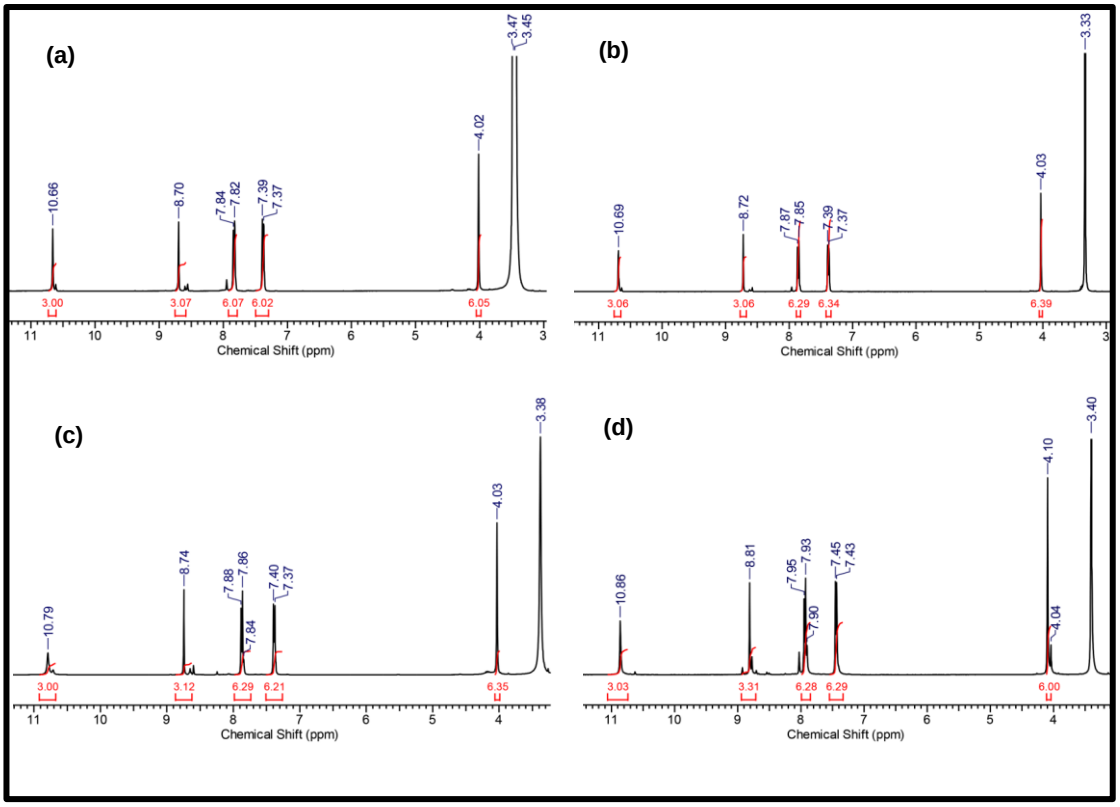

Figure 4.9. *^{1}H NMR spectra of **G4** in DMSO d_6 at different concentrations: (a) 10 mM (b) 50 mM (c) 100 mM (d) 150 mM.*

In the IR spectra of powder and xerogel, almost all the important vibrations shift towards lower wavenumber after gelation showing hydrogen bond network formation (Figure 4.10).[53]

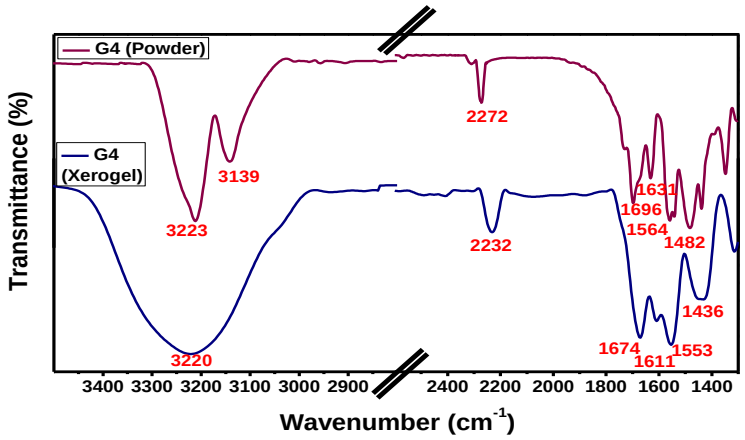

Figure 4.10. *FT-IR spectra of powder and gel state of **G4**.*

The powder X-ray diffraction of xerogel of **G4** has an intense peak around 2θ = 20.8° with 4.20 Å *d*-spacing value, which represented intercolumnar stacking.[54] The peaks at 2θ = 24.49° and 25.71° equivalent to 3.63 and 3.43 Å *d*-spacing value confirmed the *π*-*π* stacking between aromatic rings.[55,56] The peak at 2θ = 34.16° equivalent to 2.62 Å *d*-spacing value indicates the hydrogen bonding between nitrile group and amide NH proton (Figure 4.11).[57]

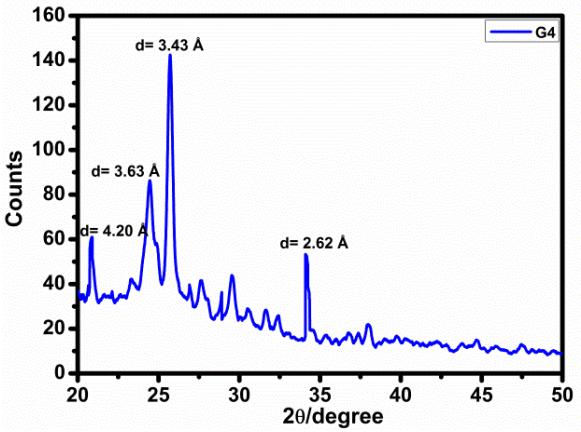

Figure 4.11. *Powder XRD patterns of xerogel of* ***G4****.*

Induction of aggregate morphology of **G4** organogel was further examined with the help of FE-SEM technique.[58,59] The morphology of the gel also influenced with the different amount of water during formation of **G4** organogel. The SEM image of **G4** organogel has shown 1 µm approximate length of dense needle-like morphology which indicates the aggregation of the material (Figure 4.12).

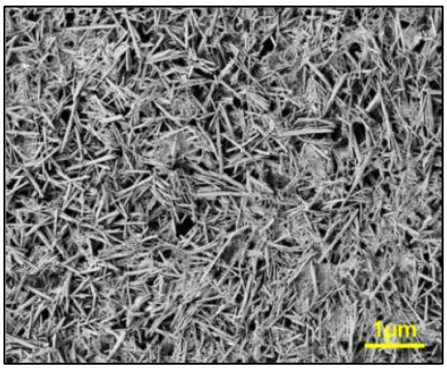

Figure 4.12. *FE-SEM images of* ***G4*** *organogel.*

The rheological experiment conclusively proves the elastic nature of gel, as average storage modulus (G') obtained around 8×10^3 Pa, which is more than loss modulus (G''). There is no crossover point found for **G4**. The shear stress has been found around 8.3×10^3 Pa during frequency sweep (Figure 4.13). To understand the effect of different amount of water in the gel strength, the rheological experiments were performed at different DMSO: H_2O ratio. The data from rheology reveals that certain quantity (DMSO: H_2O = 1500:500 μL) of water is essential for the gel formation.

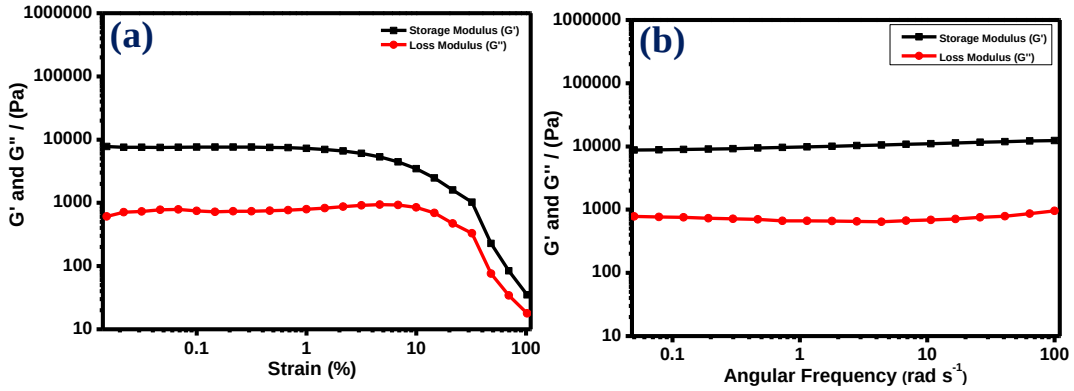

Figure 4.13. *(a) Linear viscoelastic (LVE) and (b) Dynamic frequency sweep for organogel of* ***G4****.*

The organogel upon addition of different transition metal salts maintained its gel structure. As a result, metallogel formed and its fluorescence responses have been explored and found to be comparable to previous chapters.[18, 19] The complete quenching of fluorescence occurred in case of Fe^{2+}/Fe^{3+} among various metal perchlorate salts (Fe^{2+}, Fe^{3+}, Ni^{2+}, Co^{2+}, Cu^{2+}, Zn^{2+}, Cd^{2+}, Ag^{+}) (Figure 4.14) when taken as 2:1 molar ratio of DMSO/H_2O mixture. We have tried to crystallize the metal complexes formed from solution, but we did not get success. It could be due to a lack of potent donor sites surrounding the metal ions. Further to this, the additions of different unidentate heterocyclic moieties to fulfill the coordination geometry surrounding the metal center lead to an interesting observation. Upon treatment with indole ligand, the cobalt-metallogel showed drastic quenching of the fluorescence. This observation provided a unique opportunity to extend the sensing ability of the cobalt metallogel for

discrimination of L-tryptophan with an indole side chain among other essential amino acids. We treated all metallogels [**Ag(I)G4**, **Cd(II)G4**, **Zn(II)G4**, **Cu(II)G4**, **Ni(II)G4**, **Fe(II)G4**] with the different amino acids in a molar ratio of 1:0.5 (Tyr, Leu, Lys, Phe, Trp, Ala, Glu, Asp, Ser, His). Remarkably, **Co(II)G4** metallogel selectively sensed L-tryptophan by significant quenching the fluorescent emissive band (Figure 4.14, 4.15).

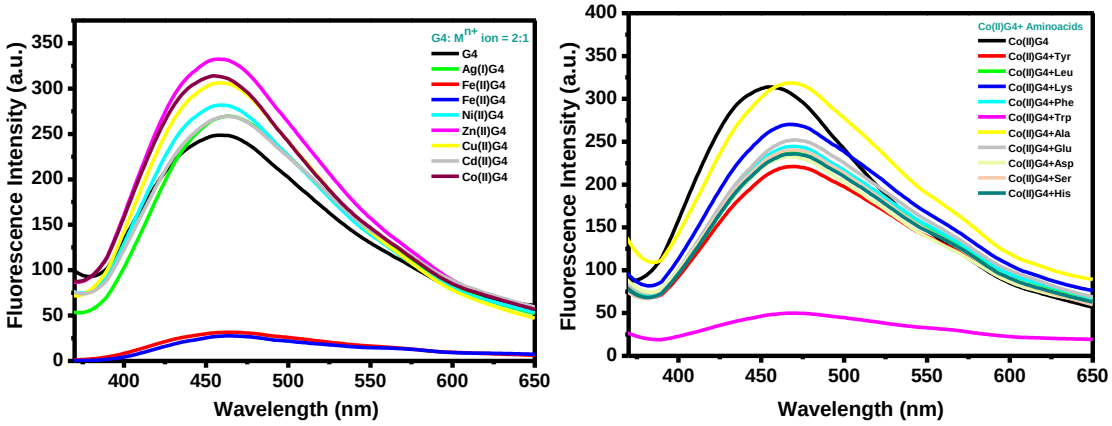

Figure 4.14. *Fluorescence spectra of organogel **G4** in the presence of several metal ions (in DMSO) (with sources of their perchloric salts) when added in 2:1 molar ratio of **G4** and metal precursor (λ_{ex} = 356 nm); Fluorescence spectra for **Co(II)G4** metallogel in the presence of 100 μM of various amino acids (in DMSO) (λ_{ex} = 356 nm).*

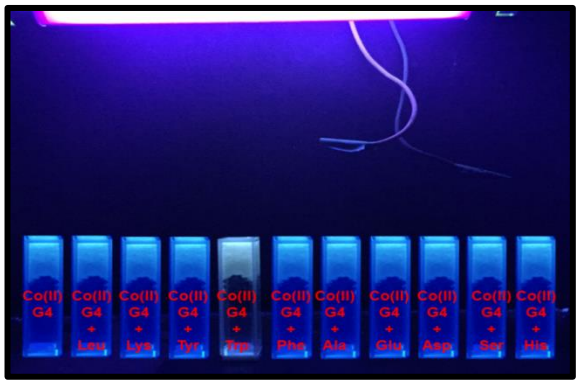

Figure 4.15. *Images of **Co(II)G4** metallogel with tryptophan under UV light.*

Interestingly, color change of the metallogel can get noticed even by the naked eye. **Co(II)G4** showed a green colored solution in DMSO, and upon addition of small quantity

of water, it turned into a pinkish gel. It is noteworthy here to mention that upon addition of L-tryptophan (aqueous solution), the visible color of the gel turned yellow, which was easily observable (Figure 4.16). The tryptophan binding with **Co(II)G4** changes the coordination environment around the metal center, which might be the factor for such a drastic color change, which can be observed in the naked eye. Furthermore, the efficacy of metallogels towards sensing of amino acid was determined through analyzing the effect on the change of fluorescence peaks intensity by increasing the concentration of L-tryptophan. The sensing experiment was done in a multi-analytical condition to determine the efficiency of metallogel system towards specific amino acid. The outcome of the treatment of **Co(II)G4** metallogel with a mixture of amino acids reveals selective sensing of L-tryptophan.

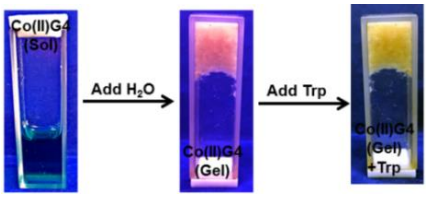

Figure 4.16. *Colorimetrically changes during formation* ***Co(II)G4*** *metallogel 15 mM gelator and 7.5 mM metal salt (2:1 molar equivalent) and sensing of tryptophan 100 μM, respectively.*

The mechanistic aspect of sensing behavior was investigated by fluorescence, IR spectroscopy, and mass spectrometry. These experiments show electron transfer from tryptophan (donor) to cobalt (acceptor) would be the driving force behind selective tryptophan sensing by quenching in fluorescence.[60,61] We have carried out concentration-dependent fluorescence study for cobalt metallogel with each amino acid (Trp, Tyr, Leu, Lys, Phe, Ala, Glu, Asp, Ser, His) . The concentration-dependent fluorescence study demonstrates a gradual decrease with red-shift in fluorescence intensity of cobalt metallogel only after addition of tryptophan (0.1 to 1000 μM) (Figure 4.17). Such an effect is not observed in the case of other aromatic amino acids like tyrosine and histidine.

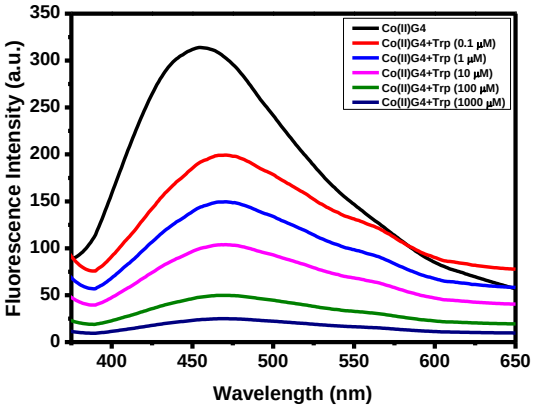

Figure 4.17. *Concentration-dependent fluorescence spectra of* ***Co(II)G4*** *with increasing concentration of* ***tryptophan amino acid*** *(λ_{ex} = 356 nm).*

Detection limit of particular amino acid using equation, "**detection limit = 3S/k**" (S represent the standard deviation of the blank solution, k means the slope between the emission intensity with respect to amino acid) was calculated to find out the metallogel sensing capability.[62,63] The detection limit for each amino acids in **[Co(II)G4]** has been calculated. The detection limit value for an L-tryptophan amino acid in **[Co(II)G4]** has been found to be 2.4×10^{-8} M. To further confirm whether it can sense L-tryptophan residues in proteins or not, we have tested the sensing property of cobalt metallogel for Bovine Serum Albumin (BSA) which also responded similarly with the detection limit of protein 8.7×10^{-9} M (Figure 4.18). Alike, the identification of BSA protein is also observable through significant color change as in the case of L-tryptophan with the naked eye.

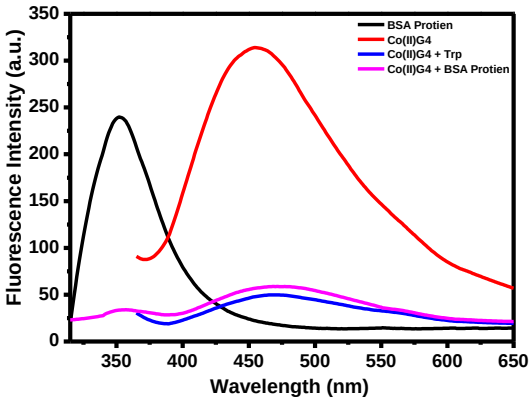

Figure 4.18. *Fluorescence spectra and optical image of* ***Co(II)G4****+100 μM BSA (DMSO, λ_{ex} = 356 nm).*

To further explore the effect of cobalt metallogel on protein structure, we have taken fluorescence (λ_{ex} = 295 nm) by altering the ratio of BSA and **Co(II)G4** metallogel. Upon addition of **Co(II)G4** metallogel (from 0 to 24 μM) in BSA protein (2 μM) shifting of λ_{max} results from 352 to 344 nm with quenching in fluorescence intensity (Figure 4.19). The quenching in fluorescence intensity occurs due to the interactions between tryptophan (Trp-134) and cobalt metallogel. Increment in the concentration of cobalt metallogel results in the complete quenching in the fluorescence intensity. These data suggest binding of cobalt metallogel with Trp-231 residue buried in the hydrophobic environment. The whole result indicates that the cobalt metallogel behave like SDS anionic surfactant, which used previously for the denaturation of the protein.[64]

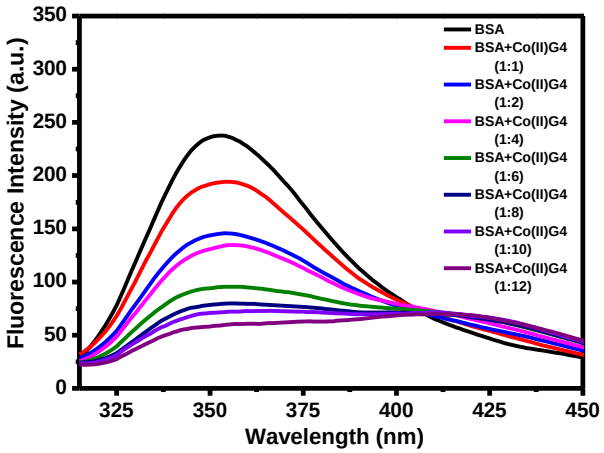

Figure 4.19. *Fluorescence spectra of 2 μM BSA and BSA (2 μM) with increasing concentration (from 0 to 24 μM) of* ***Co(II)G4*** *(λ_{ex} = 295 nm).*

Further the protein structure was validated by circular dichroism spectroscopy. The CD spectrum of BSA protein shows one positive signal at 196 nm and two negative signals around 208 and 223 nm. The different concentrations of **Co(II)G4** metallogel with BSA protein leads to the denaturation of protein. The CD signal can no longer be seen at 1:10 molar equivalent of BSA: **Co(II)G4** metallogel (Figure 4.20).

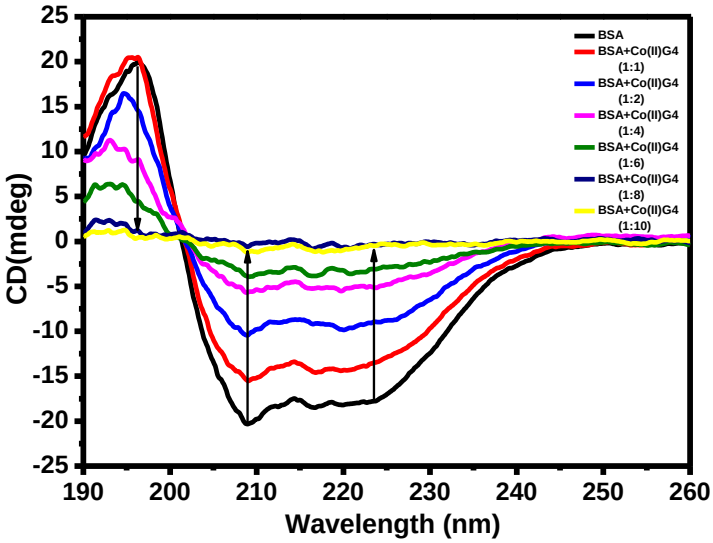

Figure 4.20*. CD spectra of 2 μM BSA and BSA (2 μM) with increasing concentration (from 0 to 24 μM) of* ***Co(II)G4*** *metallogel.*

Stern-Volmer plot has been used to understand quenching in AIEE caused by tryptophan amino acid. The data from Stern-Volmer plot suggests linear sensing of tryptophan by **Co(II)G4**.[65] To investigate the type of interaction during self-assembly, various experiments have been carried out. Job plot has been taken to find out the possible ligand to the metal ratio in cobalt metallogel formation, and this has been found to be in 1:1 stoichiometric ratio. Additionally, the mass spectrometry and IR spectroscopy data also reveal the binding of tryptophan with cobalt complex. The IR spectra of the metallogels **Fe(II)G4**, **Co(II)G4**, **Trp** and **Co(II)G4+Trp** have been recorded, and a significant shift of stretching frequencies of C=O, amide 1, amide 2 and nitrile group have been observed. In case of **Fe(II)G4**, the nitrile stretching frequency shifts were much more pronounced and observed at 2125 cm^{-1} indicating that the nitrile gets attached to Fe^{2+} centers through π-coordination which might cause the disordered aggregated structure and consequent quenching in AIEE.[18,66] However, **Co(II)G4** metallogel shows stretching frequency of C=O group shifts towards lower wavenumber 1668 cm^{-1} indicating the coordination of C=O of amide group to a metal center (Figure 4.21). It has been observed a shift in nitrile group stretching frequency is insignificant in the case of cobalt metallogel, but upon treatment with L-tryptophan, the nitrile stretching frequency splits into two closely spaced

bands (2243 cm^{-1} and 2200 cm^{-1}) indicating "nitrile-metal σ bond" and "a nitrile-metal π-interaction" respectively (Figure 4.21).[18, 19] The carboxylic stretching frequency of amino acid gets shifted from 1670 cm^{-1} to 1710 cm^{-1} confirming possible interaction between carboxylate and a metal ion suggesting electron transfer from tryptophan to metal in the gel state. These interactions between tryptophan and cobalt metallogel may be responsible for selective sensing of tryptophan among other amino acids. However, such strong shifting is not observed in the case of other amino acids.

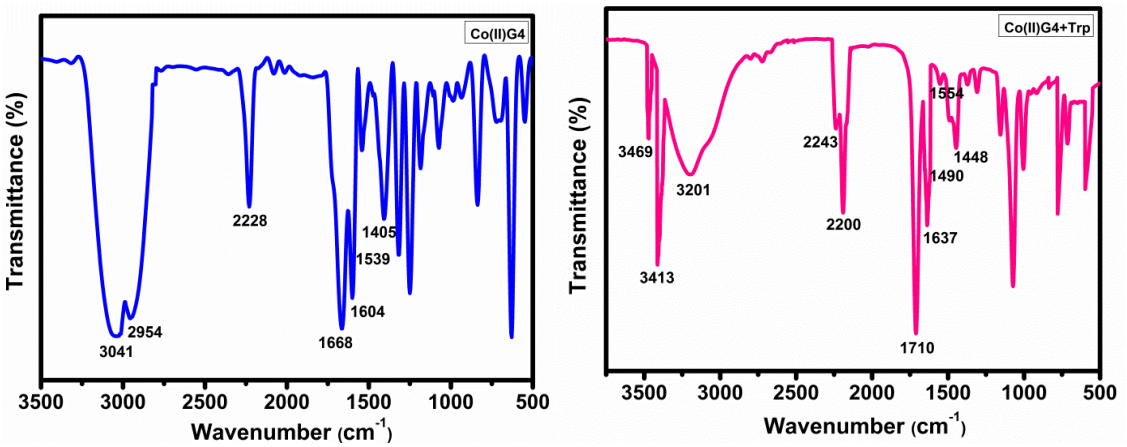

Figure 4.21 *FT-IR spectra of* ***Co(II)G4*** *and* ***Co(II)G4+Trp.***

The probable composition of cobalt metallogel in the presence of L-tryptophan by ESI-MS has been also investigated. A peak around 892.50 indicates a possible composition like $[CoG4(2\text{-amino-3-(1H-indol-3-yl)propanoate})(DMSO)]^+$ where the cobalt center most probably has coordinated through carboxylate/ indole. The PXRD spectrum of **Fe(II)G4** showed disappearance of peak around $2\theta = 25.71°$ indicating disruption of π-π stacking. The **Co(II)G4** spectrum features a similar pattern like original organogel (Figure 4.22). After incorporation of tryptophan with **Co(II)G4** metallogel, significant shifts with decrease in peak intensity centered at $2\theta = 24.56°$ and 25.54° with 3.62 and 3.48 Å *d*-spacing values were observed which indicates disruption of π-π stacking (Figure 4.22).[55,56] The shifting of the peak centered at 35.43 and 44.06 corresponding to 2.54

and 2.05 Å reveals the probable disruption of hydrogen bonding which might lead to the fluorescence quenching.[67,68]

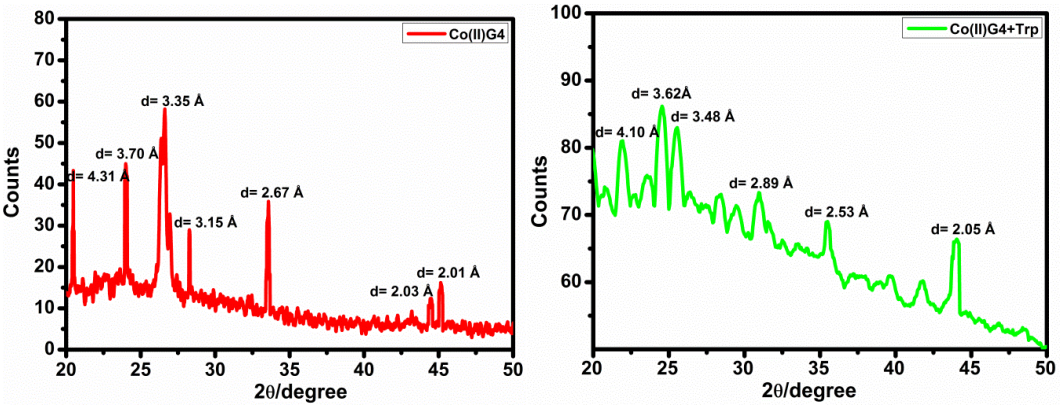

Figure 4.22 *Powder XRD patterns for* ***Co(II)G4*** *and* ***Co(II)G4+Trp****.*

Additionally, FE-SEM technique plays a central role to identify morphological features in metallogel of **G4**. SEM of both **Fe(II)G4** and **Co(II)G4** metallogels reveal cylindrical rod-like morphology with almost 1 μm length (Figure 4.23). These results indicate that metallogels show significant changes in morphology due to interaction between gelator molecule and a metal ion. Interestingly, **Co(II)G4** selectively bind with tryptophan, which is manifested by the alteration in morphological features (Figure 4.23). The **Co(II)G4+Trp** showed 3D micro flower leaf-like microstructure with dimension around 1-2 μm. The FE-SEM images of other metallogels are also recorded to investigate the structural morphology in the aggregate state. The changes in self-assembly behavior would be the reason for different morphology of materials.[69]

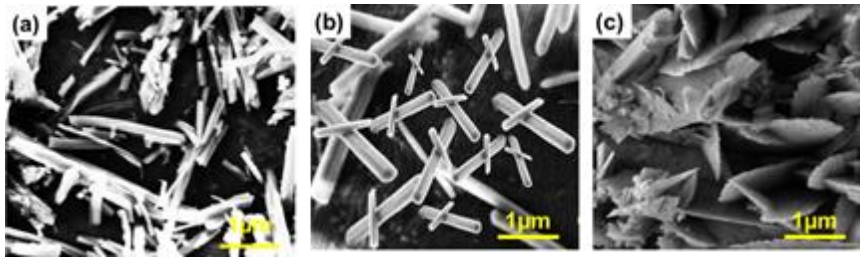

Figure 4.23 *SEM images of metallogel (a)* ***Fe(II)G4****, (b)* ***Co(II)G4****, (c)* ***Co(II)G4+Trp****.*

Strength and stiffness of metallogel were determined by the rheological study.[70] The **G4** incorporated with Fe^{2+} metal ion showed a dramatic increase in the value of the average storage modulus indicating an increase in the stiffness which might be due to the formation of the efficient metal-organic framework (MOF) disrupting the self-assembled organogel aggregate. Further, in the case of **Co(II)G4**, average storage modulus value has been found at 2×10^3 Pa, indicating the formation of metallogel with a decrease in stiffness. Whereas, on the addition of tryptophan in **Co(II)G4,** the value of average storage modulus has been decreasing and found at 219 Pa. The crossover points for **Fe(II)G4**, **Co(II)G4**, **Co(II)G4+Trp** have been observed around 1200, 30 and 4 Pa. The shear stress has been calculated with the help of frequency sweep which was found to be 2×10^4 Pa for **Fe(II)G4**, 500 Pa for **Co(II)G4** and 176 Pa for **Co(II)G4+Trp**. The positive entire sweep range for all samples and higher value of G′ has shown the viscoelastic nature of the gels.

4.4 Conclusions

A nitrile derivative of BTA molecule has been synthesized and well characterized through spectroscopic tools and X-ray crystallography. The compound tends to show gelation behavior in DMSO/water mixture with subsequent enhancement of emission property because of self-assembly and AIEE. A closer look into the possible interaction between the molecules reveals the formation of extensive hydrogen bonding, π-π stacking and intercolumnar stacking as the reason behind the molecular aggregation which enhances the emission by blocking the non-radiative emission pathways of the excited state. Though the incorporation of various metal ions in gel affects the morphology of the gel to some extent, still the integrity of the gels remains intact, and it recognizes the ferrous ion through turning off the AIEE as the nitrile group tends to form π-bonding with the metal center. Surprisingly, the cobalt metallogel can selectively sense L-tryptophan among the various amino acids by quenching off the AIEE and visual color change. Proteins like BSA with L-tryptophan residue also respond similarly, and a load of detection is found to be in the range of 10^{-8}-10^{-9} M, making the system very much

efficient. The interaction between the indole center with the metallogel has been found to be the key behind the molecular recognition pattern. A thorough search of the relevant literature revealed novelty of work as the metallogel has not been utilized to discriminate and selectively sense L-tryptophan and protein containing L-tryptophan residue. Moreover, the notable point is that the presence of water in the gel has played a crucial role in gelation, whereas the gelator molecule can crystallizing from the sol state only inthe absence of the water molecule. It seems the designed material would be the feasible and new tool for selective detection of L-tryptophan containing proteins and peptides such as BSA, HSA, and lysozyme. Additionally, the crystal and gel data would encourage the researchers for designing and understanding the supramolecular arrangement of gelator in different environments.

4.5 References

[1] Piepenbrock M. O. M., Lloyd G. O., Clarke N., Steed J. W. (2009), Metal and anion-binding supramolecular gels, Chem. Rev., 110, 1960-200 (DOI:10.1021/cr9003067)

[2] Ren J., Wang L., Han X., Cheng J., Lv H., Wang J., Jian X., Zhao M., Jia L. (2012), Organic silicone sol-gel polymer as a noncovalent carrier of receptor proteins for label-free optical biosensor application, ACS Appl. Mater. Interfaces, 5, 386-394 (DOI: 10.1021/am3024355)

[3] Li Z., Lou X., Li Z., Qin J. (2009), A new approach to fluorescence "turn-on" sensing of α-amino acids, ACS Appl. Mater. Interfaces, 1, 232-234 (DOI: 10.1021/am800093d)

[4] Reinhoudt D. N., Crego-Calama M. (2002), Synthesis beyond the molecule, Science, 295, 2403-2407 (DOI: 10.1126/science.1069197)

[5] Babu S. S., Praveen V. K., Ajayaghosh A. (2014), Functional π-gelators and their applications, Chem. Rev., 114, 1973-2129 (DOI: 10.1021/cr400195e)

[6] Fang W., Zhang Y., Wu J., Liu C., Zhu H., Tu T. (2018), Recent advances in supramolecular gels and catalysis, Chem. Asian J., 13, 712-729 (DOI: 10.1002/asia.201800017)

[7] Miao W., Zhang L., Wang X., Cao H., Jin Q., Liu M. (2013), A dual-functional metallogel of amphiphilic copper (II) quinolinol: Redox responsiveness and enantioselectivity, Chem. Eur. J., 19, 3029-3036 (DOI: 10.1002/chem.201203401)

[8] Biswas A., Dubey M., Mukhopadhyay S., Kumar A., Pandey D. S. (2016), Anion triggered metallogels: Demetalation and crystal growth inside the gel matrix and improvement in viscoelastic properties using Au-NPs, Soft Matter, 12, 2997-3003 (DOI: 10.1039/C5SM02464A)

[9] Ganta S., Chand D. K. (2017), Multi-stimuli-responsive metallogel molded from a Pd_2L_4-type coordination cage: Selective removal of anionic dyes, Inorg. Chem., 57, 3634-3645 (DOI: 10.1021/acs.inorgchem.7b02239)

[10] Feldner T., Häring M., Saha S., Esquena J., Banerjee R., Díaz D. D. (2016), Supramolecular metallogel that imparts self-healing properties to other gel networks, Chem. Mater., 28, 3210-3217 (DOI: 10.1021/acs.chemmater.6b01144)

[11] Pang X., Yu X., Lan H., Ge X., Li Y., Zhen X., Yi T. (2015), Visual recognition of aliphatic and aromatic amines using a fluorescent gel: application of a sonication-triggered organogel, ACS Appl. Mater. Interfaces, 7, 13569-13577 (DOI: 10.1021/acsami.5b03000)

[12] Datta S., Bhattacharya S. (2015), Multifarious facets of sugar-derived molecular gels: Molecular features, mechanisms of self-assembly and emerging applications, Chem. Soc. Rev., 44, 5596-5637 (DOI: 10.1039/C5CS00093A)

[13] Cui Y., Chen B., Qian G. (2014), Lanthanide metal-organic frameworks for luminescent sensing and light-emitting applications, Coord. Chem. Rev., 273, 76-86 (DOI: 10.1016/j.ccr.2013.10.023)

[14] Cantekin S., de Greef T. F., Palmans A. R. (2012), Benzene 1,3,5-tricarboxamide: A versatile ordering moiety for supramolecular chemistry, Chem. Soc. Rev., 41, 6125-6137 (DOI: 10.1039/C2CS35156K)

[15] Sun J., Liu Y., Jin L., Chen T., Yin B. (2016), Coordination-induced gelation of an L-glutamic acid Schiff base derivative: The anion effect and cyanide-specific selectivity, Chem. Commun., 52, 768-771 (DOI: 10.1039/C5CC07903A)

[16] Offiler C. A., Jones C. D., Steed J. W. (2017), Metal 'turn-off', anion 'turn-on' gelation cascade in pyridinyl methyl urea's, Chem. Commun., 53, 2024-2027 (DOI: 10.1039/C6CC09126A)

[17] Chen H., Feng Y., Deng G. J., Liu Z. X., He Y. M., Fan Q. H. (2015), Fluorescent dendritic organogels based on 2-(2′-Hydroxyphenyl)benzoxazole: emission enhancement and multiple stimuli-responsive properties, Chem.-Eur. J., 21, 11018-11028 (DOI: 10.1002/chem.201500849)

[18] Malviya N., Sonkar C., Kundu B. K., Mukhopadhyay S. (2018), Discotic organic gelators in ion sensing, metallogel formation and bioinspired catalysis, Langmuir, 34, 11575-11585 (DOI: 10.1021/acs.langmuir.8b02352)

[19] Malviya N., Das M., Mandal P., Mukhopadhyay S. (2017), A smart organic gel template as metal cation and inorganic anion sensor, Soft Matter, 13, 6243-6249 (DOI: 10.1039/C7SM01199G)

[20] Xue P., Ding J., Shen Y., Gao H., Zhao J., Sun J., Lu R. (2017), Aggregation-induced emission nanofiber as dual sensor for aromatic amine and acid vapor, J. Mater. Chem. C., 5, 11532-11541 (DOI: 10.1039/C7TC03192K)

[21] Lee J. H., Baek Y. E., Kim K. Y., Choi H., Jung J. H. (2016), Metallogel of bis(tetrazole)-appended pyridine derivative with $CoBr_2$ as a chemoprobe for volatile gases containing chloride atom, Supramol. Chem., 28, 870-873 (DOI: 10.1080/10610278.2016.1142088)

[22] Bhuniya S., Kim B. H. (2006), An insulin-sensing sugar-based fluorescent hydrogel, Chem. Commun., 1842-1844 (DOI: 10.1039/B516632B)

[23] Biswas P., Ganguly S., Dastidar P. (2018), Stimuli-responsive metallogels for synthesizing Ag nanoparticles and sensing hazardous gases, Chem. Asian J., 13, 1941-1949 (DOI: 10.1002/asia.201800743)

[24] Tu T., Fang W., Bao X., Li X., Dötz K. H. (2011), Visual chiral recognition through enantioselective metallogel collapsing: synthesis, characterization, and application of platinum-steroid low-molecular-mass gelators, Angew. Chem. Int. Ed., 50, 6601-6605 (DOI: 10.1002/anie.201100620)

[25] Wu G. (2009), Amino acids: metabolism, functions, and nutrition, Amino Acids., 37, 1-17 (DOI: 10.1007/s00726-009-0269-0)

[26] Borghei Y. S., Hosseini M., Khoobi M., Ganjali M. R. (2017), Copper nanocluster-enhanced luminol chemiluminescence for high-selectivity sensing of tryptophan and phenylalanine, Luminescence., 32, 1045-1050 (DOI: 10.1002/bio.3289)

[27] Wei Y., Li H., Hao H., Chen Y., Dong C., Wang G. (2015), β-Cyclodextrin functionalized Mn-doped ZnS quantum dots for the chiral sensing of tryptophan enantiomers, Polym. Chem., 6, 591-598 (DOI: 10.1039/C4PY00618F)

[28] Neupane L. N., Park J. Y., Park J. H., Lee K. H. (2013), Turn-on fluorescent chemosensor based on an amino acid for Pb (II) and Hg (II) ions in aqueous solutions and role of tryptophan for sensing, Org. Lett., 15, 254-257 (DOI: 10.1021/ol3029516)

[29] Wu D., Yu Y., Zhang J., Guo L., Kong Y. (2018), Chiral poly(ionic liquid) with nonconjugated backbone as a fluorescent enantioselective sensor for phenylalaninol and tryptophan, ACS Appl. Mater. Interfaces, 10, 23362-23368 (DOI: 10.1021/acsami.8b04869)

[30] Ruddick J. P., Evans A. K., Nutt D. J., Lightman S. L., Rook G. A., Lowry C. A. (2006), Tryptophan metabolism in the central nervous system: medical implications, Expert Rev. Mol. Med., 8, 1-27 (DOI: 10.1017/S1462399406000068)

[31] Delgado-Andrade C., Rufián-Hanares J. A., Jiménez-Pérez S., Morales F. J. (2006), Tryptophan determination in milk-based ingredients and dried sport supplements by liquid chromatography with fluorescence detection, Food Chem., 98, 580-585 (DOI: 10.1016/j.foodchem.2005.07.036)

[32] Qin M., Li F., Huang Y., Ran W., Han D., Song Y. (2014), Twenty natural amino acids identification by a photochromic sensor chip, Anal. Chem., 87, 837-842 (DOI: 10.1021/ac504121d)

[33] Zhang Y., Liang C., Shang H., Ma Y., Jiang S. (2013), Supramolecular organogels and nanowires based on a V-shaped cyanostilbene amide derivative with

aggregation-induced emission (AIE) properties, J. Mater. Chem. C., 1, 4472-4480 (DOI: 10.1039/C3TC30545G)

[34] SAINT V8.34A; Bruker AXS Inc., Madison, WI, USA, 2013.

[35] Sheldrick, G. M. SADABS; University of Göttingen, Göttingen, Germany, 1996.

[36] SHELXTL -2014/7; Bruker AXS Inc., Madison, WI, USA, 2014.

[37] Mehdi H., Pang H., Gong W., Dhinakaran M. K., Wajahat A., Kuang X., Ning G. (2016), A novel smart supramolecular organic gelator exhibiting dual-channel responsive sensing behaviors towards fluoride ion *via* gel-gel states, Org. Biomol. Chem., 14, 5956-5964 (DOI: 10.1039/C6OB00600K)

[38] Sun Y., Wang Y. X., Wu M., Yuan W., Chen Y. (2017), p-Quaterphenylene as an aggregation-induced emission fluorogen in supramolecular organogels and fluorescent sensors, Chem.-Asian. J., 12, 52-59 (DOI: 10.1002/asia.201601388)

[39] Lin Q., Sun B., Yang Q. P., Fu Y. P., Zhu X., Wei T. B., Zhang Y. M. (2014), Double metal ions competitively control the guest-sensing process: A facile approach to stimuli-responsive supramolecular gels, Chem.-Eur. J., 20, 11457-11462 (DOI: 10.1002/chem.201403327)

[40] Adams D. J., Morris K., Chen L., Serpell L. C., Bacsa J., Day G. M. (2010), The delicate balance between gelation and crystallisation: Structural and computational investigations, Soft Matter, 6, 4144-4156 (DOI: 10.1039/C0SM00409J)

[41] Vidyasagar A., Sureshan K. M. (2015), Stoichiometric sensing to opt between gelation and crystallization, Angew. Chem. Int. Ed., 127, 12246-12250 (DOI: 10.1002/anie.201506544)

[42] Castilla A. M., Dietrich B., Adams D. J. (2018), Using aggregation-induced emission to understand dipeptide gels, Gels., 4, 17 (DOI: 10.3390/gels4010017)

[43] Mei J., Leung N. L., Kwok R. T., Lam J. W., Tang B. Z. (2015), Aggregation-induced emission: Together we shine, united we soar!, Chem. Rev., 115, 11718-11940 (DOI: 10.1021/acs.chemrev.5b00263)

[44] Yan X., Zhu P., Li J. (2010), Self-assembly and application of diphenylalanine-based nanostructures, Chem. Soc. Rev., 39, 1877-1890 (DOI: 10.1039/B915765B)

[45] Spackman M. A., Jayatilaka D. (2009), Hirshfeld surface analysis, Cryst. Eng. Comm., 11, 19-32 (DOI: 10.1039/B818330A)

[46] Nagarajan V., Pedireddi V. R. (2014), Gelation and structural transformation study of some 1,3,5-benzenetricarboxamide derivatives, Cryst. Growth Des., 14, 1895-1901 (DOI: 10.1021/cg500026t)

[47] Chan M. H. Y., Ng M., Leung S. Y. L., Lam W. H., Yam V. W. W. (2017), Synthesis of luminescent platinum(II) 2,6-bis(N-dodecylbenzimidazol-2′-yl)pyridine foldamers and their supramolecular assembly and metallogel formation, J. Am. Chem. Soc., 139, 8639-8645 (DOI: 10.1021/jacs.7b03635)

[48] Zhang F., Xu Z., Dong S., Feng L., Song A., Tung C. H., Hao J. (2014), Hydrogels formed by enantioselective self-assembly of histidine-derived amphiphiles with tartaric acid, Soft Matter, 10, 4855-4862 (DOI: 10.1039/C4SM00479E)

[49] Yang X., Fleming F. F. (2017), C- and N-metalated nitriles: the relationship between structure and selectivity, Acc. Chem. Res., 50, 2556-2568 (DOI: 10.1021/acs.accounts.7b00329)

[50] Ma X., Liu S., Zhang Z., Niu Y., Wu J. (2017), A novel thermo-responsive supramolecular organogel based on dual acylhydrazone: fluorescent detection for Al^{3+} ions, Soft Matter, 13, 8882-8885 (DOI: 10.1039/C7SM02141K)

[51] Arnedo-Sánchez L., Bhowmik S., Hietala S., Puttreddy R., Lahtinen M., De Cola L., Rissanen K. (2017), Rapid self-healing and anion selectivity in metallosupramolecular gels assisted by fluorine-fluorine interactions, Dalton Trans, 46, 7309-7316 (DOI: 10.1039/C7DT00983F)

[52] Dautel O. J., Robitzer M., Lère-Porte J. P., Serein-Spirau F., Moreau J. J. (2006), Self-organized ureido substituted diacetylenic organogel. photopolymerization of one-dimensional supramolecular assemblies to give conjugated nanofibers, J. Am. Chem. Soc., 128, 16213-16223 (DOI: 10.1021/ja065434u)

[53] Beltrán E., Garzoni M., Feringán B., Vancheri A., Barberá J., Serrano J. L., Pavan G. M., Giménez R., Sierra T. (2015), Self-organization of star-shaped columnar liquid crystals with coaxial nanophase segregation revealed by a combined experimental and simulation approach, Chem. Commun., 51, 1811-1814 (DOI: 10.1039/C4CC08602C).

[54] Kartha K. K., Babu S. S., Srinivasan S., Ajayaghosh A. (2012), Attogram sensing of trinitrotoluene with self-assembled molecular gelator, J. Am. Chem. Soc., 134, 4834-4841 (DOI: 10.1021/ja210728c)

[55] Ma Y., Ma H., Yang Z., Ma J., Su Y., Li W., Lei Z. (2015), Methyl cinnamate-derived fluorescent rigid organogels based on cooperative π-π stacking and C=O$\cdots\pi$ interactions instead of H-bonding and alkyl chains, Langmuir, 31, 4916-4923 (DOI: 10.1021/acs.langmuir.5b00275)

[56] Mitsumoto K., Cameron J. M., Wei R. J., Nishikawa H., Shiga T., Nihei M., Newton G. N., Oshio H. (2017), A multi-redox responsive cyanometalate-based metallogel, Chem.-Eur. J., 23, 1502-1506 (DOI: 10.1002/chem.201605542)

[57] Mears L. L., Draper E. R., Castilla A. M., Su H., Zhuola, Dietrich B., Nolan M. C., Smith G. N., Doutch J., Rogers S., Akhtar R., Cui H., Adams D. J. (2017), Drying affects the fiber network in low molecular weight hydrogels, Biomacromolecules., 18, 3531-3540 (DOI: 10.1021/acs.biomac.7b00823)

[58] Adams D. J. (2018), Does drying affect gel networks?, Gels., 4, 32 (DOI: 10.3390/gels4020032)

[59] Adams P. D., Chen Y., Ma K., Zagorski M. G., Sonnichsen F. D., McLaughlin M. L., Barkley M. D. (2002), Intramolecular quenching of tryptophan fluorescence by the peptide bond in cyclic hexapeptides, J. Am. Chem. Soc., 124, 9278-9286 (DOI: 10.1021/ja0167710)

[60] Lakowicz J. R. (2006), Principles of fluorescence spectroscopy, Springer US (DOI: 10.1007/978-0-387-46312-4)

[61] Yu C., Li X., Zeng F., Zheng F., Wu S. (2013), Carbon-dot-based ratiometric fluorescent sensor for detecting hydrogen sulfide in aqueous media and inside live cells, Chem. Commun., 49, 403-405 (DOI: 10.1039/C2CC37329G)

[62] Masih D., Aly S. M., Alarousu E., Mohammed O. F. (2015), Photoinduced triplet-state electron transfer of platinum porphyrin: a one-step direct method for sensing iodide with an unprecedented detection limit, J. Mater. Chem. A., 3, 6733-6738 (DOI: 10.1039/C4TA07033J)

[63] Deep S., Ahluwalia J. C. (2001), Interaction of bovine serum albumin with anionic surfactants, Phys. Chem. Chem. Phys., 3, 4583-4591 (DOI: 10.1039/B105779K)

[64] Chen H., Ahsan S. S., Santiago-Berrios M. E. B., Abruña H. D., Webb W. W. (2010), Mechanisms of quenching of alexa fluorophores by natural amino acids, J. Am. Chem. Soc., 132, 7244-7245 (DOI: 10.1021/ja100500k)

[65] Mei J., Hong Y., Lam J. W., Qin A., Tang Y., Tang B. Z. (2014), Aggregation-induced emission: the whole is more brilliant than the parts, Adv. Mater., 26, 5429-5479 (DOI: 10.1002/adma.201401356)

[66] Howe R. C., Smalley A. P., Guttenplan A. P., Doggett M. W., Eddleston M. D., Tan J. C., Lloyd G. O. (2013), A family of simple benzene 1,3,5-tricarboxamide (BTA) aromatic carboxylic acid hydrogels, Chem. Commun., 49, 4268-4270 (DOI: 10.1039/C2CC37428E)

[67] Gou F., Cheng J., Zhang X., Shen G., Zhou X., Xiang H. (2016), Unusual aggregation/gelation-induced phosphorescence of propeller-type binuclear platinum(II) enantiomers, Eur. J. Inorg. Chem., 2016, 4862-4866 (DOI: 10.1002/ejic.201600839).

[68] Zhang Y., Zhou Q. F., Huo G. F., Yin G. Q., Zhao X. L., Jiang B., Tan H., Li X., Yang H. B. (2017), Hierarchical self-assembly of an alkynylplatinum(ll) bzimpy-functionalized metallacage via Pt⋯ Pt and π-π Interactions, Inorg. Chem., 57, 3516-3520 (DOI: 10.1021/acs.inorgchem.7b02777)

[69] Xue M., Lü Y., Sun Q., Liu K., Liu Z., Sun P. (2015), Ag(I)-coordinated supramolecular metallogels based on schiff base ligands: Structural characterization and reversible thixotropic property, Cryst. Growth Des., 15, 5360-5367 (DOI: 10.1021/acs.cgd.5b00952)

Chapter 5

Novel Approach to Generate Self-Deliverable Anticancer Ru(II) agent in the Self-Reacting Confined Gel Space

Chapter 5

Novel Approach to Generate Self-Deliverable Anticancer Ru(II) agent in the Self-Reacting Confined Gel Space

5.1 Introduction

Extensive research in various fields of science and rapid growth of related information in various spheres propelled the idea of bringing up smart materials and molecules with lot of versatility combining the knowledge gathered all together. Research in the borderline of diverse fields empowered us to develop many advanced materials and molecules which can remarkably successful to tackle various aspects related to a particular problem.[1-3] Extensive studies on the properties of gel materials, particularly in the last two decades open up the possibility to utilize them as smart materials in various fields.[4,5] However, introduction of metal ions with gelator molecules[6] often opens up the possibility to utilize them as catalysts,[7] magnetic materials,[8] in adsorption,[9] self-healing material,[10] sensing,[11,12] tunable emissive material,[13] drug-delivery[14] and others.[15-17] With the development of the possibility of introduction of metal ions with different ligands in gels, the idea of utilizing a metal-based biologically active compound acting as pro-drug or drug which itself can get delivered as gel material is a logical development. Drug delivery is an important phenomenon as it can affect the duration of delivery, rate of release, pharmacokinetic, and side effect profile. Cancer being a dynamic and heterogeneous disease with high mortality and morbidity and its treatment being largely dependent upon chemotherapy, delivering therapeutic agent is a major hurdle. Among various methodologies liposomes,[18]antibody-drug conjugates,[19] nanoparticles,[20] polymer implants,[21] targeted radionuclide,[22] polymer-drug conjugates,[23] polymer micelles[24] and hydrogels[25] are important. Various drug delivery systems are getting utilized clinically to deliver a wide variety of chemotherapeutic drugs. From the

perspective of inorganic and coordination chemists, with the invention of the anticancer property of *cis*-platin, many platinum complexes have been screened for possible application as an anticancer agent and due to extreme toxicity and henceforth side effects of the platinum complexes, many drug delivery systems have been tested for more efficient delivery with fewer complications.[26-28] However, in search of alternative metal-based anticancer agents, it has been found that some of the ruthenium-based complexes can work effectively against various cancerous growths. Among the, NAMI-A and KP1019 has been found to be effective against the metastatic and primary tumor, respectively.[29] Though the first compound completed the clinical trial without much success, the second compound is in an advanced stage of clinical trial and performing good results. Another group of organometallic ruthenium complex *viz*. ruthenium arene complexes have shown high activities towards diverse cancer cells with low *in vivo* toxicity. The mechanistic pathways of the ruthenium complexes have been explored extensivel, and it has been found many of them undergoes solvation process in the solution state, and solvated ruthenium ion can bind different biomolecules like enzymes, cell walls, proteins like histone, midkine or pleiotrophin.[30-32] Interestingly, among ruthenium-arene complexes which showing substantial anticancer activities, there are few compounds reported where carboxylate group act as a chelating ligand to fulfill the coordination geometry surrounding the ruthenium ion along with chloride or other co-ligands.[33] In the present thesis, it is already presented that some tricarboxamide based nitrile molecules which can act as a gelator in DMF/H_2O mixture can also form metallogels with diverse metal ions.[34,35] The self-assembled structure has also shown typical aggregation induced enhanced emission (AIEE) and can sense various cations, anions (in metallogel) and bioinspired catalytic reaction (in metallogel). As continuation of that project, it is conceived to develop a dicarboxamide gelator molecule keeping one carboxylic acid of precursor trimesic acid intact which can be utilized for coordinating ruthenium center in the presence of arene ring. Accordingly, the synthesis of a new gelator molecule 3,5-bis((4-(cyanomethyl)phenyl)carbamoyl)benzoic acid **G5** and the gel formation ability is presented herewith. Supramolecular self-assembly formed by non-covalent bond play a promising role for the formation of molecular building blocks.[36,37]

However, in recent years, confined space strategy for specific metal-ligand coordination-driven self-assembly has been taken up as a promising approach for the synthesis of new molecules and chemical transformations.[38-40] In this report, the formation of ruthenium-based metallogel with **G5**, conversion of ruthenium [Ru_2(*p*-cymene)$_2Cl_4$] complex into [Ru(G5')(*p*-cymene)Cl] [**Ru(II)G5**] in confined gel space and delivery of the ruthenium ion in cancerous cell through gel collapse in presence of lactic acid have been also explored. As per Warburg mechanism the cancerous cell produces extra energy by extensive glycolysis which tends to generate excess lactic acid.[41] The accumulation of lactate is regulated by monocarboxylate transporter as it transports lactate from peripheral tissues to liver to undergo Cori cycle to regenerate pyruvate.[42] It is assumed that gelator **G5** once out of coordination sphere of ruthenium under acidic condition upon treatment with lactic acid may interact with monocarboxylate transporter to disrupt the lactate transportation chain and can induce apoptosis by accumulation of lactate or hyper-acidification therapy[43] along with the anticancer effect of ruthenium(II) metal ion upon interactions with biomolecules.

5.2 Experimental section

5.2.1 Material and method

All the required chemicals were purchased from Sigma and used without further purification. The specifications of all the instruments used for analysis purpose were the same as described in section 2.2.1 of chapter 2.

5.2.2 Synthesis of gelator G5 [3,5-bis{(4-(cyanomethyl)phenyl) carbamoyl} benzoic acid]

For the synthesis of gelator **G5**, trimesic acid (2 g, 9.5 mmol) and two molar equivalent of reagent 1-Ethyl-3-(3′-dimethylaminopropyl) carbodiimide Hydrochloride (3.64 g, 19 mmol) have been mixed in DMF and kept 30 minutes for stirring. The reaction mixture then ice-cooled for 30 minutes and 2 molar equivalents of 4-aminobenzyl cyanide (2.5

g, 19 mmol) has been added in ice-cooled condition over 1 h. The ice-cold condition of the reaction medium has been maintained for 3 hours, and then it was kept stirring for 12 h in room temperature. Then 100 mL of ethyl acetate was added in the solution mixture. The combined organic layer was washed with dil. HCl (1 N, 100 mL) and subsequently with saturated Na_2CO_3 (100 mL) aqueous solution, and brine (100 mL). The organic layer was then dried over anhydrous sodium sulfate and evaporated under reduced pressure to obtain a resultant white colored powder. The isolated compound was then dried at room temperature under vacuum. Yield: 90% (for **G5**). ^{1}H NMR (400 MHz, 298 K, DMSO-d_6): δ = 13.58 (1H, acid, s), 10.76 (2H, amide, s), 8.81 (2H, aromatic, d), 8.71 (1H, aromatic, s), 7.89, 7.87 (4H, aromatic, d), 7.43, 7.41 (4H, aromatic, d), 4.08 (4H, aliphatic CH_2, s). ^{13}C NMR (100 MHz, 293 K, DMSO-d_6): δ = 166 (acid), 165 (amide), 139 (aromatic), 135 (aromatic), 134 (aromatic), 131 (aromatic), 130 (aromatic), 128 (aromatic), 126 (aromatic), 121 (aromatic), 119 (nitrile), 22 (aliphatic CH_2). FT-IR of **G5** (KBr): ν = 3467, 3394, 3216, 2291, 1728, 1672, 1599, 1449 cm^{-1}. MS (ESI) of **G5**: *m/z* = 437.20 (in negative mode).

5.2.3 Synthesis of Me-G5' [methyl-3,5-bis{(4-(cyanomethyl)phenyl}carbamoyl benzoate]

0.05 millimole of **G5** was dissolved in 1 mL of DMF solvent and layered by 1 mL of methanol. Needle-shaped red colored fine crystals of **Me-G5'** were obtained within 6 hrs. Yield: 99% (for **Me-G5'**). ^{1}H NMR (400 MHz, 298 K, DMSO-d_6): δ = 10.70 (2H, amide, s), 8.81 (2H, aromatic, s), 8.71 (1H, aromatic, s), 7.83 (4H, aromatic, d), 7.38 (6H, aromatic, d), 4.03 (4H, aliphatic CH_2, d), 3.98 (3H, aliphatic CH_3 of ester, s). ^{13}C NMR (100 MHz, 293 K, DMSO-d_6): δ = 165 (ester), 164 (amide), 138 (aromatic), 136 (aromatic), 132 (aromatic), 131 (aromatic), 130 (aromatic), 128 (aromatic), 127 (aromatic), 121 (aromatic), 119 (nitrile), 53 (aliphatic CH_3 of ester), 22 (aliphatic CH2). FT-IR of **Me-G5'** (KBr): ν = 3441, 3259, 3128, 3065, 2962, 2245, 1730, 1651, 1609, 1542, 1524 cm^{-1}. MS (ESI) of **Me-G5'**: *m/z* = 451.20 (in negative mode).

5.2.4 Preparation of gels

0.05 millimole of **G5** gelator was dissolved in 2 mL of solvent (1 mL of DMSO and 1 mL of Milli-Q water) in a glass vial. The solution was left undisturbed for a couple of minutes, and a stable organogel formed spontaneously. On the other hand, 0.05 millimole **G5** gelator was dissolved with 0.0023 millimoles of **$[RuCl_2(\eta^6$-*p*-cymene)$]_2$** in molar ratio **G5:$[RuCl_2(\eta^6$-*p*-cymene)$]_2$ = 1:0.05** and it dissolves in 2 mL of solvent (0.5 mL DMSO and 1.5 mL of Milli-Q water). Upon standing the solution furnished **Ru(II)G5** metallogel.

5.2.5 Analysis of Ru(II)G5 Xerogel

^{1}H NMR (400 MHz, 298 K, DMSO-d_6): δ = 8.84 (2H, -NH of amide group of G5, s), 8.65, 8.64 (2H, -CH of aromatic ring of **G5**, d), 8.54 (1H, -CH of aromatic ring of **G5**, s), 7.73, 7.69 (4H, -CH of aromatic ring of G5, dd), 7.59, 7.46 (4H, -CH of aromatic ring of G5, dd), 7.25, 7.23 (1H, -CH of aromatic ring of *p*-cymene, d), 7.06, 7.04 (1H, -CH of aromatic ring of *p*-cymene, d), 6.08 (1H, -CH of aromatic ring of *p*-cymene, d), 5.68 (1H, -CH of aromatic ring of *p*-cymene, d), 3.64, 3.58 (4H, aliphatic 2×CH_2 of G5, d), 3.26 (1H, aliphatic CH of *p*-cymene, m), 2.80 (3H, aliphatic CH_3 of *p*-cymene, s), 1.35 (6H, aliphatic 2×CH_3 of *p*-cymene). ^{13}C NMR (100 MHz, 293 K, DMSO-d_6): δ = 167 (acid of G5), 164 (amide of G5), 139 (aromatic carbon of G5), 135 (aromatic carbon of G5), 134 (aromatic carbon of G5), 132 (aromatic carbon of G5), 131 (aromatic carbon of G5), 129 (aromatic carbon of G5), 125 (aromatic carbon of G5), 121 (aromatic carbon of G5), 118 (nitrile of G5), 101 (aromatic carbon of *p*-cymene), 96 (aromatic carbon of *p*-cymene), 94 (aromatic carbon of *p*-cymene), 80 (aromatic carbon of *p*-cymene), 30 (aliphatic CH of *p*-cymene), 22 (aliphatic CH_2 of G5), 21 (aliphatic 2×CH_3 of *p*-cymene), 18 (aliphatic CH_3 of p-cymene). FT-IR of **Ru(II)G5** (KBr): ν = 3385, 3197, 3010, 2824, 2245, 1706, 1649, 1506, 1469, 1425 cm^{-1}. MS (ESI) of **Ru(II)G5**: *m/z* = 673.13 [Ru(**G5'**)(*p*-cymene)]$^+$ (in positive mode).

5.2.6 Analysis of [Ru(II)(lactyl-lactato)$_n$(DMSO)$_m$]$_x$.yDMSO = [Ru(II)L]

^{1}H NMR (400 MHz, 298 K, DMSO-d_6): δ = 4.14 (2H, 2×CH of lactic acid, s), 1.32 (6H, 2×CH_3 of lactic acid, dd), 2.57 (6H, 2×CH_3 of DMSO, s). ^{13}C NMR (100 MHz, 293 K, DMSO-d_6): δ = 177 (acid), 172 (acid), 68 (CH of lactic acid), 66 (CH of lactic acid), 20 (CH_3 of lactic acid), 16 (CH_3 of lactic acid), 39 (CH_3 of DMSO). MS (ESI) of **Ru(II)L**: *m/z* = 339.1395 [Ru{OC(O)C(Me)OC(O)C(Me)OH}(DMSO)]$^+$ (in positive mode).

5.2.7 Gel to Crystal transition

G5 gel placed in a glass vial and heated up to the formation of sol. The solution without adding water left undisturbed at room temperature. Formation of the crystals can be observed with the gradual cooling of the sol.

5.2.8 Gel melting temperature

Gel melting temperature (Tgel) of **G5** has been finding out same as described in the section 2.2.4 of chapter 2.

5.2.9 Characterizations

Characterizations techniques like UV-visible Spectroscopy, Fluorescence Spectroscopy, FT-IR Spectroscopy, powder X-ray Diffraction (PXRD) and morphological Study, Rheological Properties of **G5** and their metallogels have been same as described in the section 2.2.5 of chapter 2. The details about the method for single crystal X-ray diffraction (SXRD) analysis of **G5** and **Me-G5'** has been the same as described in section 4.2.6 of chapter 4.

5.2.10 Biological Experiments

Cell Culture. Human NSCLC cells (A549), breast carcinoma cells (MCF7), were purchased from (National centre or cell science) NCCS, Pune. Roswxell Park Memorial Institute (RPMI)-1640 was used to culture A549, MCF-7 cells. This medium were supplemented with 10 % foetal bovine serum (FBS), and 1% penicillin-streptomycin and cells were grown at 37 °C in 5% CO_2 incubator. Cells were grown to 70-80% confluency and centrifuged at 200 g for A549, 130 g for MCF-7 cells and 1500 rpm for HEK cells which were reseeded in T25 cm^2 and then were cryopreserved after second and third passages. These preserved cells were revived and used for further experiment. For positive control, 5-fluorouracil was purchased from chempura enterprises, (Indore, India). Hoechst 33258 were purchased from Hi-Media chemical, India.

Invitro Cytotoxicity Assay. All the cell lines were grown till 70-80% confluency. After trypsinization, the cell lines were resuspended in media such that 5×10^3 cells were seeded in each well of 96 well flat-bottomed microtiter plate (Nest; USA) in 100 µL cell suspension. The cells were kept for overnight for attachment of the cells at 37 °C in 5% CO_2 incubator. 25 mM **G5** organogel, 2.3 mM **Ru(II)G5** and **Ru(II)L** with respect to ruthenium was taken as stock for the cell treatment. It is further diluted by DMEM media for A549 cell line and by RPMI media for MCF-7 cell line up to various concentrations and treated with cell lines. A549 cell line in DMEM media and MCF-7 cell line in RPMI media were utilized as control experiment. After 24 h treatment the 10 µL of MTT [3-(4,5-Dimethylthiazol-2-yl)-2,5- diphenyltetrazolium bromide] solution was added in the media, and after 4 h incubation the media was removed, and formazan salts were dissolved in 100 µL of 100% DMSO. The reading was taken after 5 min incubation in SYNERGY H1 microplate reader at absorbance 570 nm wavelength. The IC_{50} values are the concentration of the reagent, which decreases the cell viability to 50% in treated cell population to non-treated cell population, and these values were determined by cell viability graphs. The experiment was repeated at least three times.

Hoechst Staining. Cell morphology was determined using Hoechst stain 33258. The 5×10^4 A549 cells were seeded in 6 well plate with coverslips in each well and kept for

overnight in CO_2 incubator for adherence. These cells were treated with IC_{50} concentration of **Ru(II)G5** metallogel and **Ru(II)L** with positive control being 5-fluorouracil and control with untreated cells. Kept the cells treated with **Ru(II)G5** metallogel and **Ru(II)L** and 5-fluorouracil for incubation for 24 hrs. For positive control 5 mM Stock solution of 5-fluorouracil was prepared in DMSO and 20 μL solution was added a well containing 2 mL DMEM media. These cells were then fixed with 4% paraformaldehyde followed by permeabilization with 0.1% triton x 100. These cells were now stained with 5 μg/mL Hoechst 33258 for 30 min at room temperature followed by washing with PBS buffer. Then the coverslips were mounted on glass slides and the fluorescence were viewed under OLYMPUS confocal microscope.

5.2.11 Release of Ru-drug from metallogel

Release studies of the anticancer drug from the **G5** organogel triggered from **Ru(II)G5´** metallogel was monitor by UV-visible Spectroscopic. Drug delivery experiment carried in two steps in PBS buffer. In the first step, **G5** organogel was prepared, which is used for the loading of **$[RuCl_2(\eta^6$-*p*-cymene)$]_2$** drug. The resultant compound is known as **Ru(II)G5** metallogel. In the second step, addition of lactic acid in a controlled way in the **Ru(II)G5** metallogel and at pH 5.67 leads to collapsing of the gel. The lactic acid containing **Ru(II)G5** sample kept at room temperature. UV-Vis spectra of the sample were recorded at definite time intervals.

pH Determination. The pH values of lactic acid containing **Ru(II)G5** metallogel samples were monitored using digital pH meter. Practically, the pH of the hydrogels was scrutinized by allowing the probe of the pH meter to be in contact with the samples via direct immersion of the probe of pH meter in a beaker containing a suitable amount of the gel.

5.2.12 Optimization for molecular docking

All calculations were performed using Gaussian09 suite of quantum chemical program. The hybrid Becke 3-Lee-Yang-Parr (B3LYP) exchange-correlation function was applied for DFT calculations. Geometries were fully optimized in the gas phase at B3LYP level of theory using the 6-31++G (d, p) basis sets. Energy minimizations of all the ligands have been performed by this same setting, and finally, optimized structures were taken for docking study.

5.2.13 Supplementary materials

CCDC 1855703 and 1551443 contain the supplementary crystallographic data for **G5** and **Me-G5'** respectively. These data can be obtained free of charge via http://www.ccdc.cam.ac.uk/conts/retrieving.html, or from the Cambridge Crystallographic Data Centre, 12 Union Road, Cambridge CB2 1EZ, UK; fax: (+44) 1223-336-033; or e-mail: deposit@ccdc.cam.ac.uk.

5.3 Results and discussion

Certain trimesic acid-based molecules have already shown typical gelation behavior in a various solvent or solvent pairs. Some of them have shown unique properties of selective recognition of certain metal cations and transformation into metallogels.[34,35] These metallogels also tend to show some specificity to bind certain anions and catalytic properties.[34,35] This opportunity has been taken to derivatize two arms of trimesic acid with 4-amino benzyl cyanide leaving one of the carboxylic acid group intact. Synthesis of the gelator molecule **G5** has been carried out by treatment of trimesic acid with 2 equivalent of 4-amino benzyl cyanide in the presence of coupling agent 1-Ethyl-3-(3′-dimethylaminopropyl) carbodiimide Hydrochloride (EDC) (2 equivalent) at ice-cooled temperature (Scheme 5.1). The isolated compound has been characterized by ^{1}H and ^{13}C NMR and IR spectroscopy and ESI-MS spectrometry. The solid-state structure of **G5** has been further confirmed by single crystal X-ray crystallography.

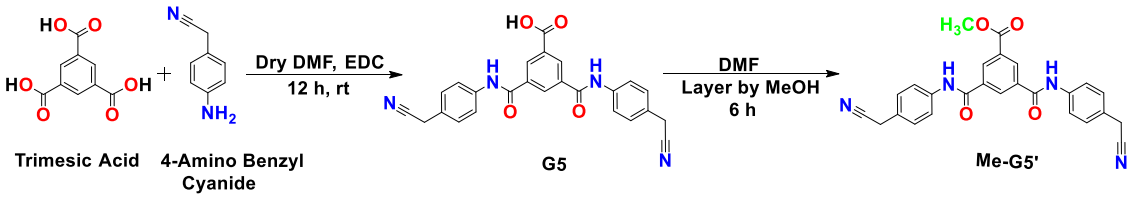

Scheme 5.1. *Systematic scheme for the synthesis of gelator* ***G5*** *and* ***Me-G5'****.*

The IR spectrum of **G5** reveals strong peak at 1672 cm^{-1} indicative of amide bond (Figure 5.1).[35] The asymmetric stretch for the carboxylic acid group has been found at 1599 cm^{-1} and symmetric stretch at 1449 cm^{-1}, respectively (Figure 5.1).[44] The characteristic nitrile stretch has been found at 2291 cm^{-1} (Figure 5.1).[35]

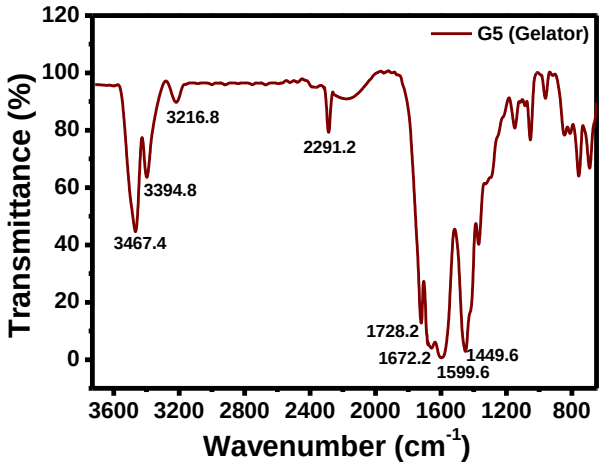

Figure 5.1. *FT-IR spectrum of gelator* ***G5****.*

The ^{1}H and ^{13}C spectra of gelator **G5** reveals the characteristic peaks for different electronic environments. While the carboxylic acid proton has been found at 13.58 ppm, the amide proton peak is observed at 10.76 ppm (Figure 5.2).[35,44]

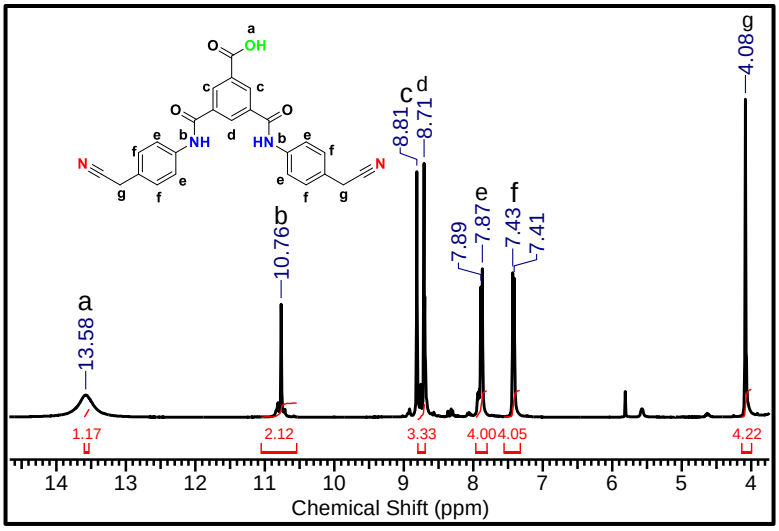

Figure 5.2. *^{1}H NMR spectrum of gelator* ***G5.***

The ^{13}C NMR spectrum shows the peak for -*C*OOH at 166 ppm, -*C*ONH- at 165 and -*C*N at 119 ppm (Figure 5.3).[35] The ESI-MS of gelator **G5** furnished molecular ion peak at 437.2 $[M\text{-}H^{+}]^{-}$ in negative mode (Figure 5.4).

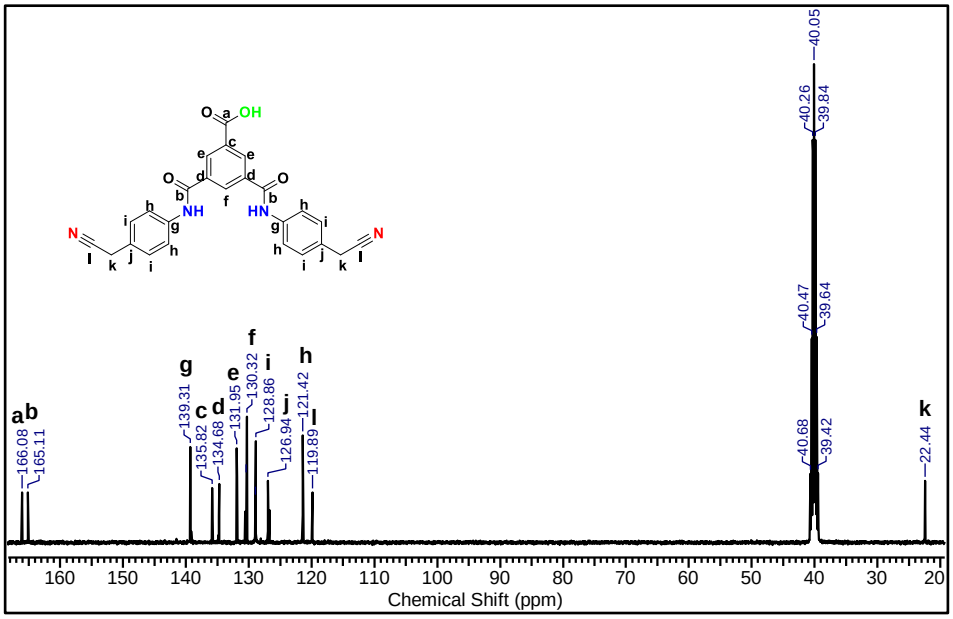

Figure 5.3. *^{13}C NMR spectrum of gelator* ***G5****.*

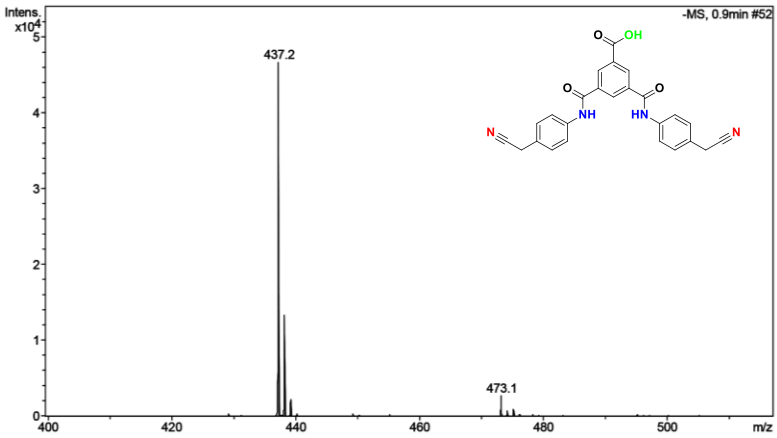

Figure 5.4. *ESI- Mass spectrum of gelator* ***G5.***

The solubility pattern of **G5** reveals it is only soluble in DMF/DMSO and insoluble to other organic solvents even under heating. Interestingly upon addition of a certain quantity of water in DMSO solution induce gelation, and critical gel concentration (CGC) of the gelator **G5** is found to be 25 mM in DMSO/water. Formation of the gel has been ascertained by "test-tube inversion" experiment (Figure 5.5). Addition of excess water in the solution leads to the precipitation of the gelator molecule. Interestingly in the absence of water, heated DMSO solution of **G5** gelator deposits the yellow plate-like crystals on gradual cooling (Figure 5.5). In the absence of water, gelator molecules slowly self-assemble in a multidirectional way, which may lead to crystallization of gelator.[45, 46]

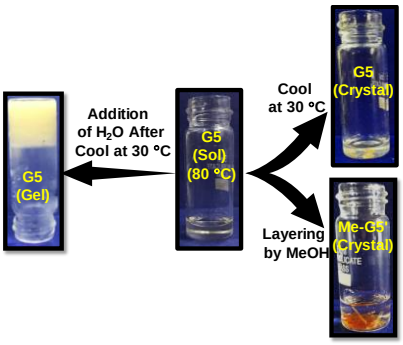

Figure 5.5. *Sol-Gel-Crystal conversion of Gelator* ***G5*** *and* ***Me-G5'****.*

Gelator **G5** crystallize in monoclinic space group P21/C (Figure 5.6a). Three aromatic rings are interestingly not found in the same plane. The dihedral angle between aromatic ring of trimesic moiety and one aromatic ring of benzylaromatic ring has been found to

be 34.75° whereas with other benzylnitrile ring is 56.0°. The benzylnitrile group has been found to be disordered to a certain extent. H-bonding plays an important role in the packing of the molecules. Each molecule is attached with two neighboring molecules through O(1)-H(1)...O(5), N(6)-H(6A)...O(3) and N(4)-H(4A)...O(2). The hydrogen bond interactions and close contacts in the crystal structure were further visualized by carrying out the hirshfeld surface analysis.[42] The hydrogen bond interactions were visualized through dark red spots obtained as a result of hydrogen bond acceptors of types N-H···O, C-H···O and C-H···N (Figure 5.7a), green dotted lines show the H-bond) on the hirshfeld surface of **G5**. Intra- as well inter-molecular hydrogen bond is exhibited by the molecule. O1-H1...O5 forms a strong intermolecular hydrogen bond while N4-H4A..O2 also forms rather strong intermolecular hydrogen bonds along *a*-axis (Figure 5.7b, Table 5.1).

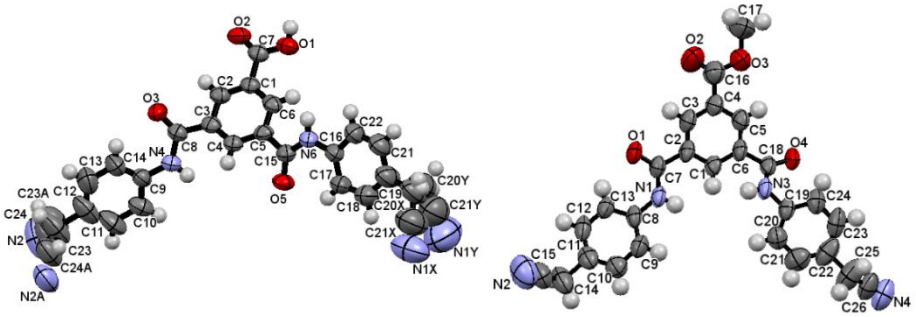

Figure 5.6. *Single-crystal X-ray diffraction studies for (a)* ***G5*** *and (b)* ***Me-G5'****.*

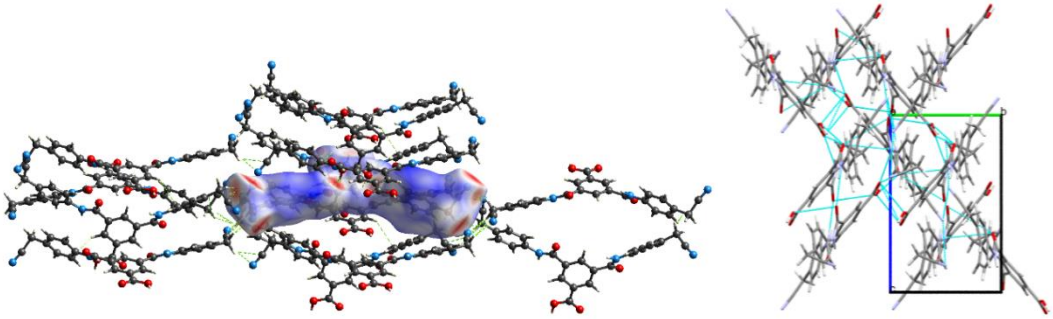

Figure 5.7. (a) *Columnar aggregation of* ***G5*** *gelator showed the molecular recognition between molecules through N−H···O hydrogen bonds and* ***(b)*** *N−H···O Hydrogen bonding with consecutive gelator molecule.*

Table 5.1. *Hydrogen bonds and bond angles of Donor—H... Acceptor atoms of* ***G5****.*

Donor--H....Acceptor	D--H(Å)	H...A(Å)	D...A(Å)	D--H...A(Å)	Symmetry Code
O1 -- H…. O5	0.82	1.79	2.536	151	x, -1/2-y, -1/2+z
N4 -- H4A.... O2	0.86	2.12	2.960	165	x, -1/2-y,1/2+z
N6 -- H6A.... O3	0.86	2.23	3.074	168	-x, -y, -z
C14 -- H14.... O3	0.93	2.38	2.920	116	Intra
C17 -- H17.... O5	0.93	2.22	2.825	122	Intra
C20X -- H20B.... N1X	0.97	2.13	2.90	134	1-x,1-y,1-z

Interestingly when a DMSO solution of **G5** has been layered with methanol, spontaneous esterification of the carboxylic acid is observed, and methyl 3,5-bis((4-(cyanomethyl)phenyl)carbamoyl benzoate **Me-G5'** (G5' = G5-H) has been obtained and well characterized by spectroscopic tools (Scheme 5.1, Figure 5.8-5.11).

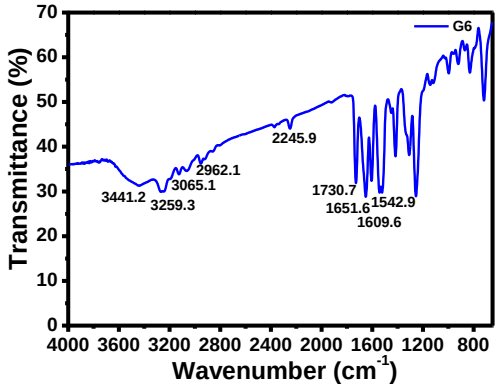

Figure 5.8. *FT-IR spectrum of gelator* ***Me-G5'****.*

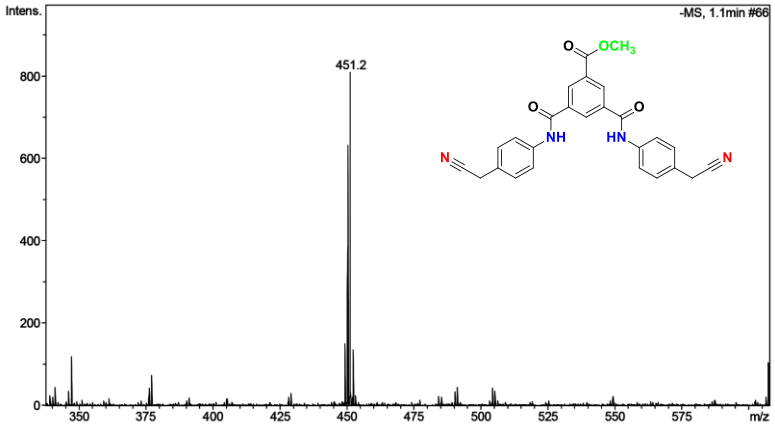

Figure 5.9. *ESI- Mass spectrum of gelator* ***Me-G5'.***

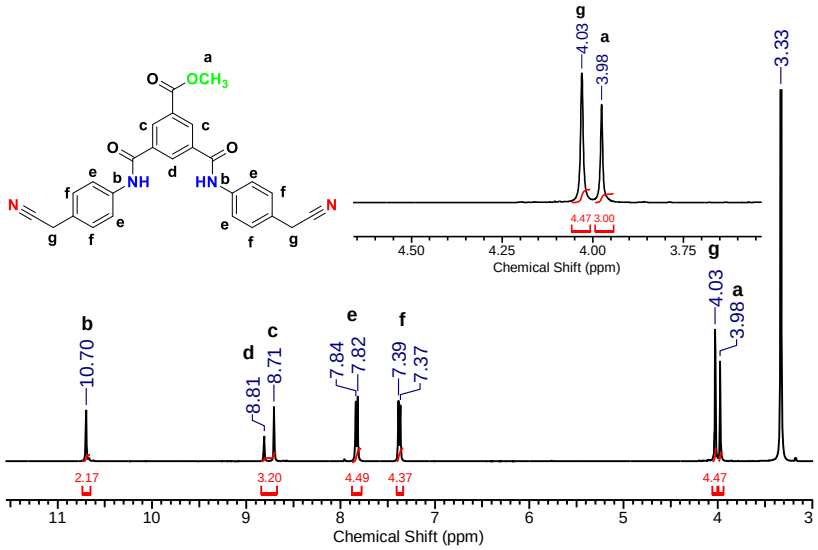

Figure 5.10. *^{1}H NMR spectrum of gelator* ***Me-G5'.***

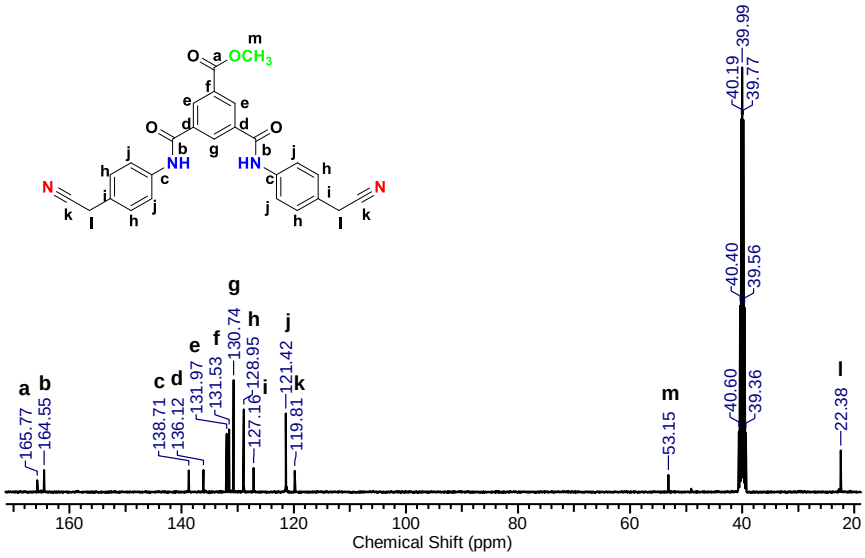

Figure 5.11. *^{13}C NMR spectrum of gelator* ***Me-G5'****.*

The subtle change in the carboxylic acid through methylation bring out the coplanarity in all the benzene rings involved as the dihedral angle for one of the phenyl ring comes out as 3.18°, and the other ring remains parallel to trimesic benzene ring. In this case, also the molecule is hydrogen bonded to two nearby molecules. The hydrogen bond interactions and close contacts in the crystal structure were visualized by carrying out the Hirsfeld surface analysis.[47] The hydrogen bond interactions were visualized through

dark red spots obtained as a result of hydrogen bond acceptors of types N-H···O, C-H···O and C-H···N (Figure 5.6b, 5.12a, green dotted lines show the H-bond) on the Hirshfeld surface of **Me-G5'**. Intra- as well inter-molecular hydrogen bond is exhibited by the molecule. N1-H1N..O4 and N3-H2N..O1 form rather strong intermolecular hydrogen bonds along *a*-axis (Figure 5.12b, Table 5.2). However, it has been observed that **Me-G5'** does not form any gel in any solvent combination. Therefore, the hydrogen-bonded 2D structure of **G5** is very much important for entrapment of the solvent molecules to furnish a gel in the proper medium.

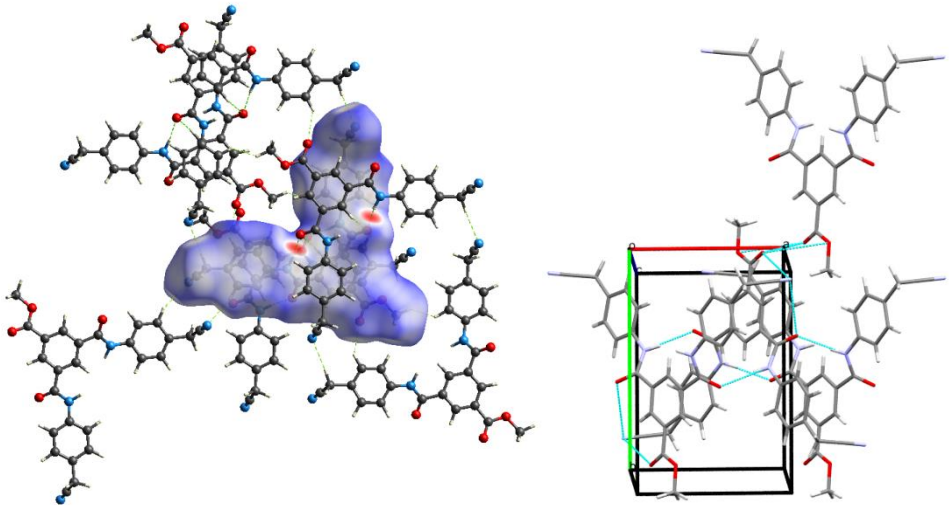

Figure 5.12. ***(a)*** *Columnar aggregation of* ***Me-G5'*** *gelator showed the molecular recognition between molecules through N−H···O hydrogen bonds and* ***(b)*** *N−H···O Hydrogen bonding with consecutive gelator molecule.*

Table 5.2. *Hydrogen bonds and bond angles of Donor--H... Acceptor atoms of* ***Me-G5'.***

Donor--- H...Acceptor	**D–H(Å)**	**H... A(Å)**	**D... A(Å)**	**D--H... A(Å)**	**Symmetry Code**
N1 -- H1N.... O4	0.84	2.10	2.925	169	1-x,1-y, -z
N3 -- H2N.... O1	0.82	2.05	2.868	173	2-x,1-y, -z
C10 -- H10.... O2	0.93	2.60	3.380	142	x,1+y, z
C13 -- H13.... O1	0.93	2.42	2.905	113	Intra
C14 -- H14B.... N4	0.97	2.60	3.565	175	1-x,2-y, -z
C24 -- H24.... O4	0.93	2.50	2.955	110	Intra

The propensity of **G5** to form gel has been monitored through heating-cooling technique and temperature-dependent fluorescence spectroscopic experiments as the gels tend to exhibit aggregation induced enhance emission (AIEE) (Figure 5.13). The gel at room temperature has been found highly fluorescent in nature showing peak position around 503 nm. However, with increasing temperature, the gel starts to convert into sol, and the emission intensity decreases to almost nil at 80 °C. Red shift in the emission intensity has been also observed as the maximum gradually shifts to 485 nm may be due to formation of *J*-aggregate.[48] The phase transition temperature (T_{gel}) from gel to sol has been found to be 70 °C. Enhanced emission due to aggregation has been observed because of the blocking of the non-radiative emission pathways of the excited state by restricting the free rotations of the molecule. The quantum yield for the fluorescent gel has been found to be reaching around $\phi = 0.06$.

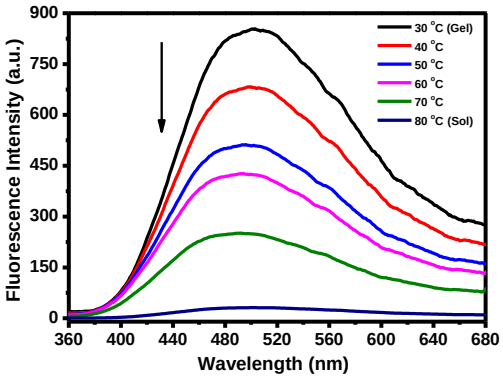

Figure 5.13. *Temperature-dependent fluorescence spectra for* ***G5*** *(in DMSO) during the gelation process (λ_{ex} = 345 nm).*

To explore the self-assembly process in gel structure, several other studies have been taken up for further insight. The IR spectrum of xerogel of **G5** reveals vibrational stretching frequencies of all key functional groups shift towards lower wave number indicating the involvement of extensive H-bonding.[34,35] The amide band stretching shifts to 1626 cm^{-1} (from 1672 cm^{-1}), carboxylate asymmetric stretch and symmetric stretch shifts to 1537 and 1398 cm^{-1} (from 1599 and 1449 cm^{-1}). The nitrile stretching frequency also shifts to 2251 cm^{-1} (from 2291 cm^{-1}) (Figure 5.14).

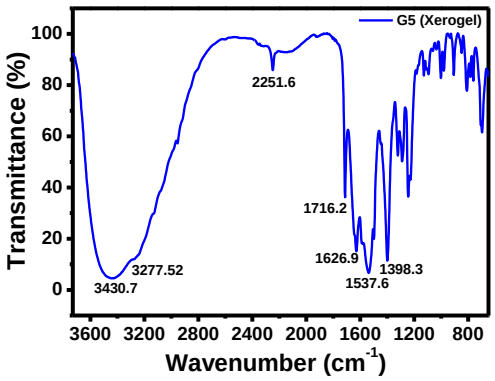

Figure 5.14. *FT-IR spectrum of* ***G5*** *xerogel.*

A concentration-dependent ^{1}H NMR experiment also reveals aromatic and carboxamide protons shifts towards downfield on raise of the concentration from 15 to 45 mM, indicating extensive H-bonding. Interestingly treatment of **G5** gel in 20:1 ratio with a dimeric ruthenium arene precursor $[RuCl_2(\eta^6\text{-}p\text{-cymene})]_2$ maintains the gel structure intact (Scheme 5.2, Figure 5.15).

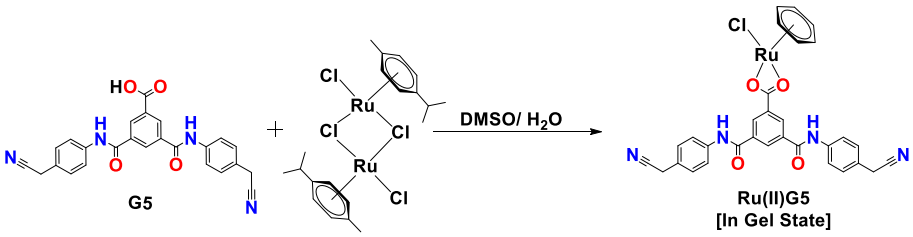

Scheme 5.2. *Systematic scheme for the preparation of* ***Ru(II)G5*** *metallogel.*

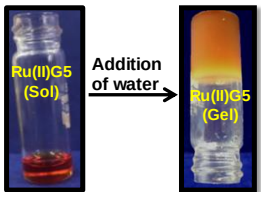

Figure 5.15. *Optical images to indicates the conversion* $[RuCl_2(\eta^6\text{-}p\text{-cymene})]_2$ *into anticancer drug [****Ru(II)G5****] in confined gel space.*

Spectroscopic tools are employed to understand if there is any chemical transformation happens to the ruthenium dimeric compound. The metallogel has been left undisturbed for twenty-four hours, and then it was subjected to various analytical experiments. The

IR spectrum of xerogel reveals the shift of the carboxylate asymmetric and symmetric stretch to 1649 and 1506 cm^{-1}, indicating possible coordination of the gelator molecule to ruthenium center through chelating carboxylate. There is not much change observed in the nitrile stretching frequency, which corroborates the fact that there is no coordination by nitrile molecules to ruthenium center. To investigate the probable composition of ruthenium complex after incorporation, the xerogel has been treated with chloroform to extract the ruthenium complex, as the **G5** molecule is insoluble in chloroform. The filtered solution has been subjected to ESI-MS spectrometry and ^{1}H and ^{13}C NMR. The ESI-MS have shown a peak at 673.13, indicating the presence of [Ru(**G5'**)(*p*-cymene)]$^{+}$ (Figure 5.16).

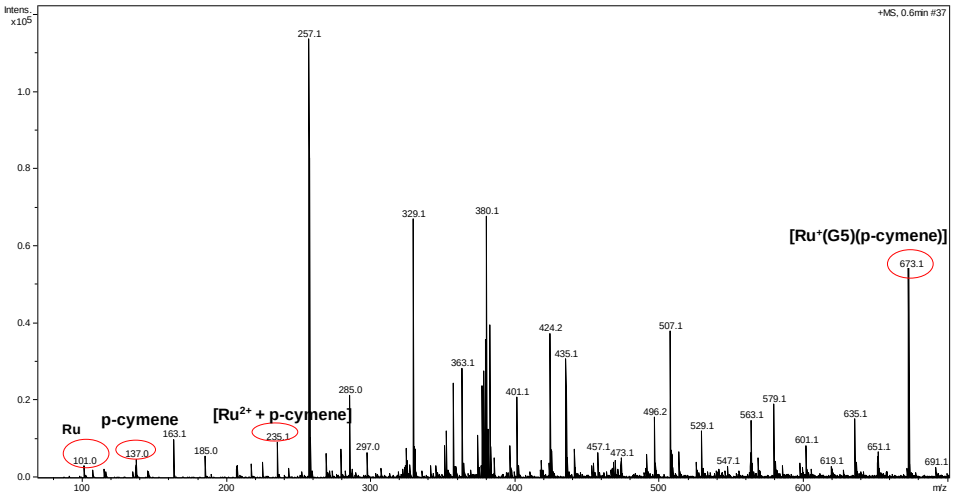

Figure 5.16. *ESI- Mass spectrum of gelator* ***Ru(II)G5.***

It is further corroborated with NMR spectra as it furnished the presence of both *p*-cymene moiety and **G5'** and absence of any proton peak for carboxylic acid indicates chelating coordination through carboxylate (Figure 5.17 and 5.18). Therefore based on the above analysis, it can be inferred that the ruthenium dimer $[RuCl_2(\eta^6\text{-}p\text{-cymene})]_2$ in an organogel environment of **G5** converts into [Ru(G5')(*p*-cymene)Cl] [**Ru(II)G5**]. More interestingly, every effort to synthesize the same compound in solution remains futile. Upon refluxing **G5** with $[RuCl_2(\eta^6\text{-}p\text{-cymene})]_2$ in DMF an insoluble polymeric species gets precipitated out which is difficult to characterize. However, treatment of the same

dimer with **G5** in room temperature does not furnish any solid and the profile of ESI-MS of the reaction mixture found to be completely different than what was obtained in the gel. Therefore, it is evident that the organogel itself works as a unique reaction vessel for selective formation of [**Ru(G5')(*p*-cymene)Cl**] in the gel state.

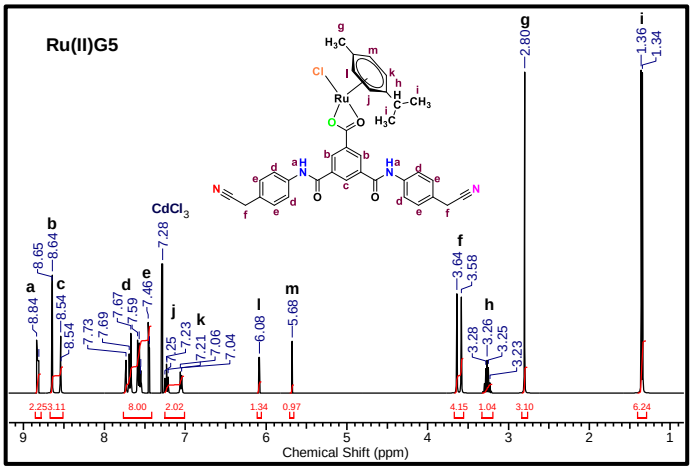

Figure 5.17. *^{1}H NMR spectrum of gelator* ***Ru(II)G5****.*

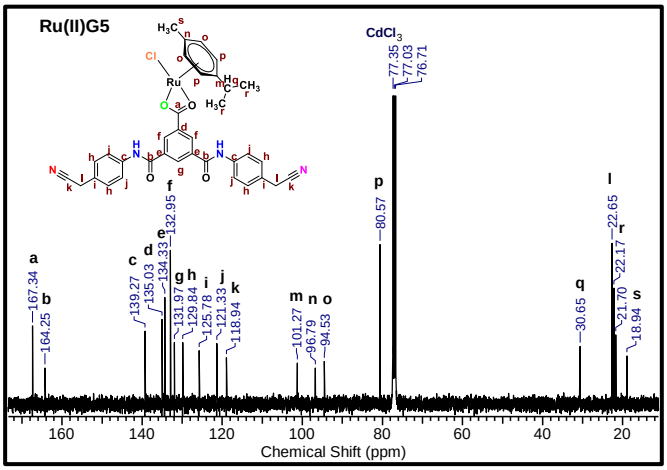

Figure 5.18. *^{13}C NMR spectrum of gelator* ***Ru(II)G5****.*

The structure of the xerogel has been further investigated with powder X-ray diffraction experiments. In the case of **G5** intense peak has been observed at 2θ = 20.7° and 21.6° with a *d*-spacing value of 4.29 Å and 4.19 Å representing intercolumnar stacking (Figure 5.19).[35] The peak at 2θ = 25.72° corresponds to *d*-spacing value of 3.46 Å revealing *π*-

π stacking between aromatic moieties[49,50] while peak at 2θ = 33.44° corresponds to *d*-spacing value of 2.68 Å suggest hydrogen bonding between NH proton of amide and nitrile group.[35] However, in the ruthenium-based gel, the peaks are found in the range 4.22 Å, 3.40 and 2.63 Å, respectively (Figure 5.19).

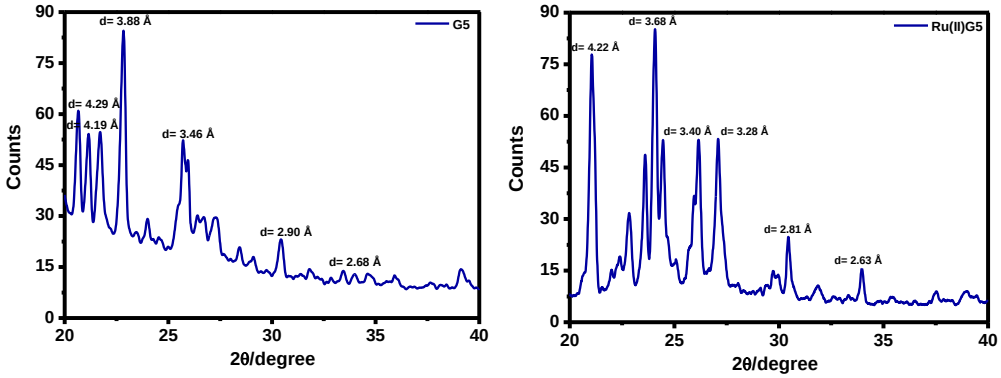

Figure 5.19. *Powder XRD patterns of xerogel of* ***G5*** *and* ***Ru(II)G5****.*

To look further down the morphological features of the aggregates was explored through FE-SEM.[51,52] The **G5** organogel has shown a clover leaf-like morphology with an approximate diameter of 10 μm (Figure 5.20). On interaction of ruthenium ion with **G5** the product **Ru(II)G5** shown aggregation of the material with dense lumps of needle close to 3 μm in diameter (Figure 5.20). These results show significant changes in morphology after formation of metallogel.

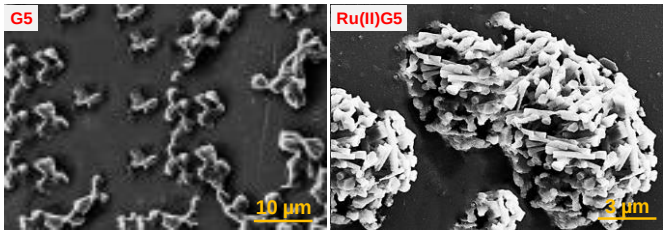

Figure 5.20*. FE-SEM images of* ***G5*** *organogel and* ***Ru(II)G5*** *metallogel.*

A rheological experiment has been carried out to determine the mechanical strength as it is very crucial for understanding the stiffness of the material for probable applications. The average storage modulus (G') for **G5** organogel was found to be around 1435 Pa, which is higher than loss modulus (G") (Figure 5.21). There is no crossover point found

for **G5**. The shear stress has been found around 250 Pa during frequency sweep. Upon incorporation of ruthenium(II) along with *p*-cymene ring, there is a decrement in average storage modulus to 925 Pa indicating less stiffness in the gel. The crossover points with increasing strain for **RuG5** have been observed around 100 Pa. The shear stress has been calculated with the help of dynamic frequency sweep experiment, which was found near 1425 Pa for **Ru(II)G5** (Figure 5.21). The dynamic frequency sweep measurement for organogel and metallogel showed higher storage modulus (G') compare to the loss modulus (G") during the experiment indicated its viscoelastic nature. The rigidity of the metallogel was observable from G' - G" values which remained positive in the entire sweep range.

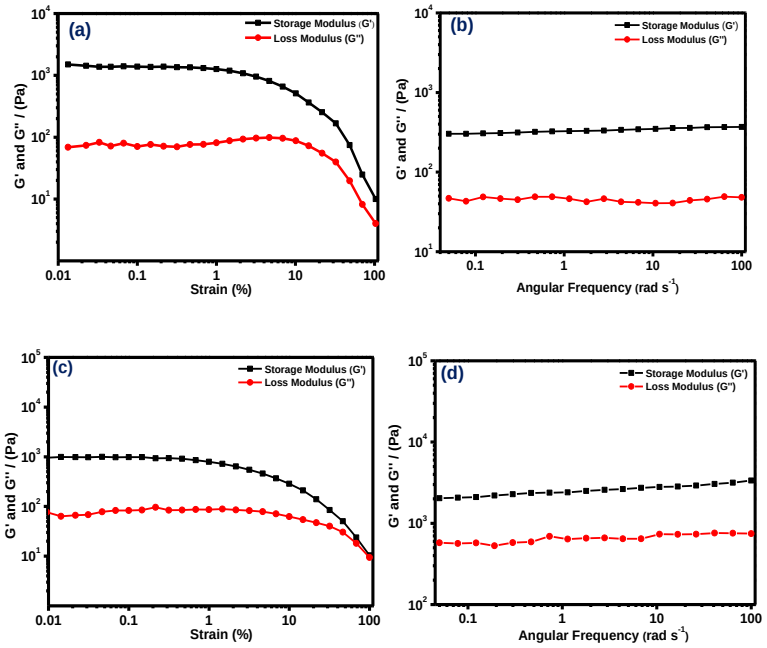

Figure 5.21. *(a) and (c) Linear viscoelastic (LVE) for* ***G5*** *organogel and* ***Ru(II)G5*** *metallogel; (b) and (d) Dynamic frequency sweep for* ***G5*** *organogel and* ***Ru(II)G5*** *metallogel.*

As there are various reports where ruthenium(II)-arene complexes can act as a potential anticancer agent,[53,54] therefore, it has been perceived to check the efficacy of the metallogel itself as a potential anticancer agent against various cancerous cell lines. It has been known that gel can form a 3D crosslinked network that swells in solution and can

act as a good carrier for drug delivery.[55] Low molecular weight-based gel can offer the possibility of slow release or sudden burst of metallodrugs from pH-triggered gel-sol transition. Production of lactic acid is a natural phenomenon in our body due to glycolysis. However, cancer cells undergo faster glycolysis and produce more lactate as compared to normal cells due to increase in energy demand.[56] Conversion of pyruvate into lactate becomes essential to regenerate NAD^+ from NADH, making the solid tumor more acidic in nature.[41] Therefore it was also interesting to explore the response of the ruthenium-gel in different pH, particularly in acidic condition. To find out a correlation with actual cell environment, lactic acid has been utilized to render the pH in the acidic region. Gradual addition lactic acid in ruthenium gel makes the whole system further acidic in nature and around pH 5.6 the gel gets collapsed, forming a brown solution and white colored solid (Figure 5.22).

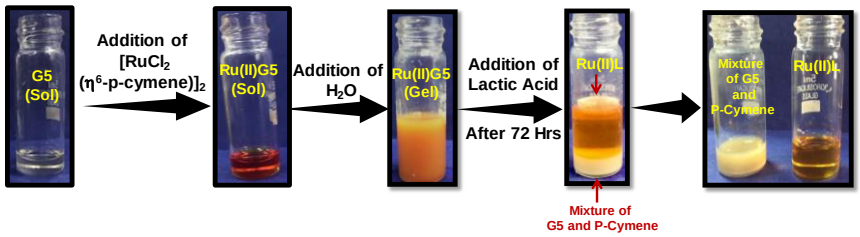

Figure 5.22. *Optical images to indicates self-delivery of anticancer drug through pH variation.*

The supernatant brown colored liquid obtained has been filtered and subjected to analytical experiments like ESI-MS and ^1H and ^{13}C NMR spectroscopy. The NMR spectroscopy indicates the absence of *p*-cymene ring or **G5** in solution. It only indicates the presence of the dimeric form of lactic acid likely coordinated through carboxylate to ruthenium center and the brown color of the solution is indicative of ruthenium(II) in solution. The ^1H NMR peak observed at 2.57 ppm indicates the presence of free DMSO or *O*-bonded DMSO to the ruthenium center (Figure 5.23). The ^{13}C NMR reveals the carboxylate carbon shifts towards more downfield as it is observed around 177.3 ppm in $CDCl_3$ (Figure 5.24). The profile of the ^1H and ^{13}C NMR has been found to be similar to that of coordinated carboxylato (lactyl-lactato) ligand.[57] The ESI-MS spectrum of

supernatant liquid also reveals the signature peak like [Ru (OC(O)C(Me)OC(O)C(Me)OH)]$^{+}$ at 261.05 and [Ru (OC(O)C(Me)OC(O)C(Me)OH)(DMSO)]$^{+}$ at 339.1 indicating coordination by (lactyl-lactato) ligand (Figure 5.25). However, the exact composition of the ruthenium complex could not be ascertained with exact precision as no solid has been isolated with sufficient purity, however, based on the information available it can be assigned with a tentative molecular formula [Ru(II)(lactyl-lactato)n(DMSO)m]^{x}·yDMSO [**Ru(II)L**].

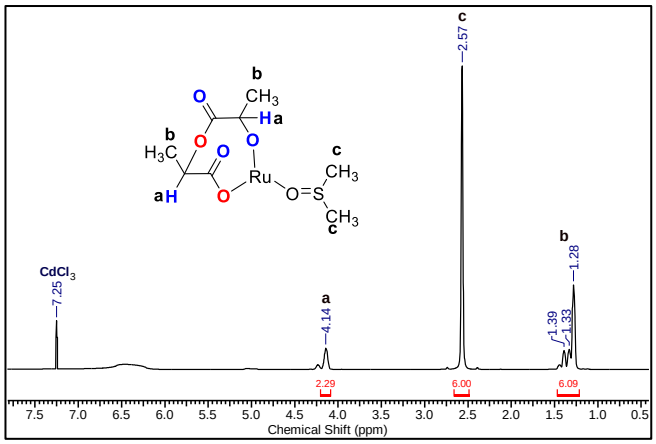

Figure 5.23. *^{1}H spectrum of* ***Ru(II)L****.*

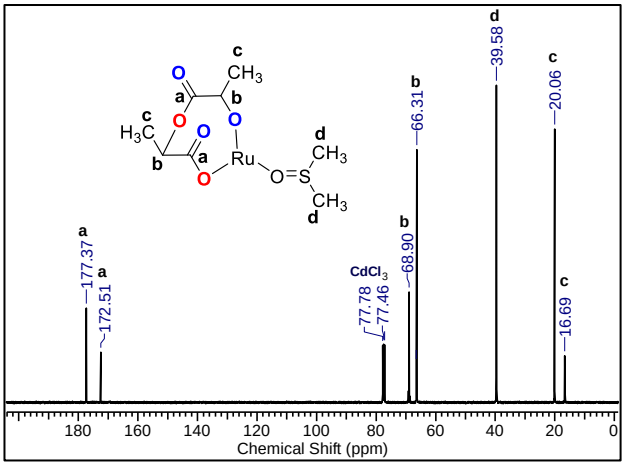

Figure 5.24. *^{13}C NMR spectrum of* ***Ru(II)L****.*

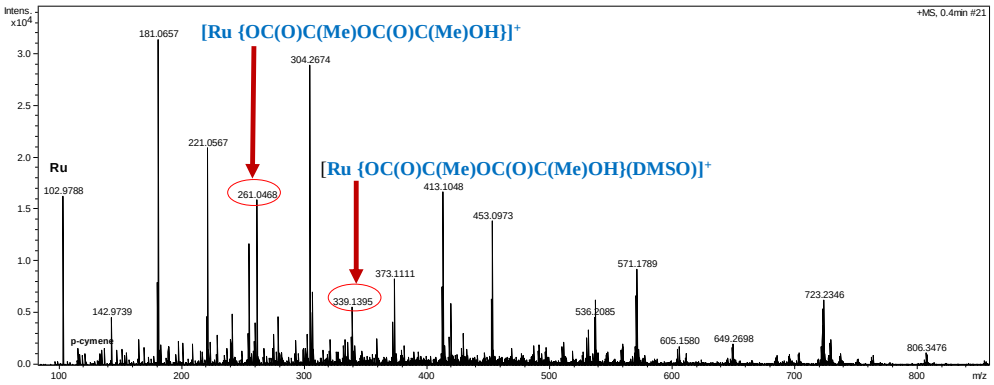

Figure 5.25. *ESI- Mass spectrum of gelator* ***Ru(II)L****.*

Though the composition is not known with certainty, the release of the ruthenium moiety from the gel structure has been monitored through UV-Vis spectroscopy (Figure 5.26, Figure 5.27). While **G5** used to show a characteristic π-π* peak around 345 nm in PBS buffer, the ruthenium dimer used to show peaks at 375 nm ($^1A_1 \rightarrow B_2$), 400 nm ($^1A_1 \rightarrow B_1$) and 470nm ($^1A_1 \rightarrow {}^1A_2$).[58] A closer look of ruthenium gel indicates subtle change in the peak position to 360, 410, and 460 nm. However, addition of lactic acid leads to collapsing of the gel and transformation of the ruthenium complex has been monitored spectroscopically. A drastic decrease in peak intensity around 340 nm has been observed along with arising of a new peak around 440 nm. The transformation occurs through an isobestic point around 370 nm. The change in the spectral pattern could be observable up to 72 h, indicating gradual transformation of the ruthenium moiety with release of ruthenium ion at pH 5.7 (pH observable in tumor issue is around 6).

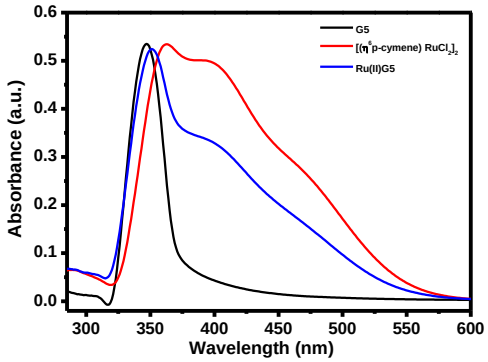

Figure 5.26. *UV-visible spectra of* ***G5****,* ***[(η^6-p-cymene) RuCl$_2$]$_2$*** *and* ***Ru(II)G5****.*

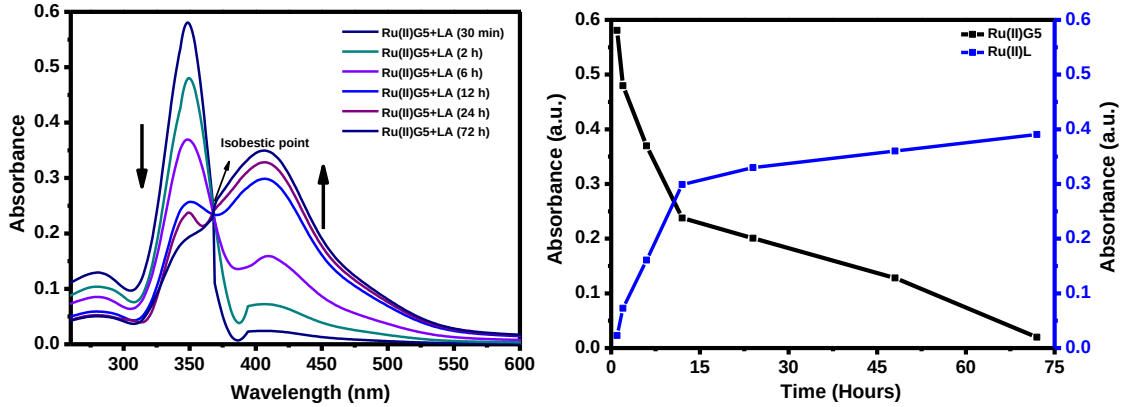

Figure 5.27. *Release of Ru-drug [**Ru(II)L**] from **Ru(II)G5** metallogel monitor by UV-visible spectroscopy.*

The **G5** organogel, **Ru(II)G5** metallogel and the [Ru(II)(lactyl-lactato)n(DMSO)m]^{x} [**Ru(II)L**] solution have been further used for the cytotoxicity study toward human NSCLC cells (A549) and breast carcinoma cells (MCF7) (Figure 5.28). The cell lines were treated with compounds for twenty-four hours with increasing concentration of the compounds, and cytotoxicity was calculated as inhibitory concentration (IC_{50}) of the compounds. The IC_{50} values of **G5** organogel indicated the non-cytotoxic nature toward the cancers cell. However, the **Ru(II)G5** metallogel has been found to be moderately cytotoxic towards the A549 and MCF7 cell lines with IC_{50} values 10.53 μM and 23.16 μM. An MTT assay of [**Ru(II)(lactyl-lactato)n(DMSO)m]^{x}** towards the same cell lines indicates moderate cytotoxicity. However, as the actual composition of the ruthenium complex is unknown calculation based on only ruthenium ion furnished IC_{50} values of 17.72 μM and 29.76 μM for A549 and MCF7. It is noteworthy to mention that the ruthenium(II) precursor complex dichloro(p-cymene)ruthenium(II) dimer has been found non-cytotoxic towards both the cell lines.

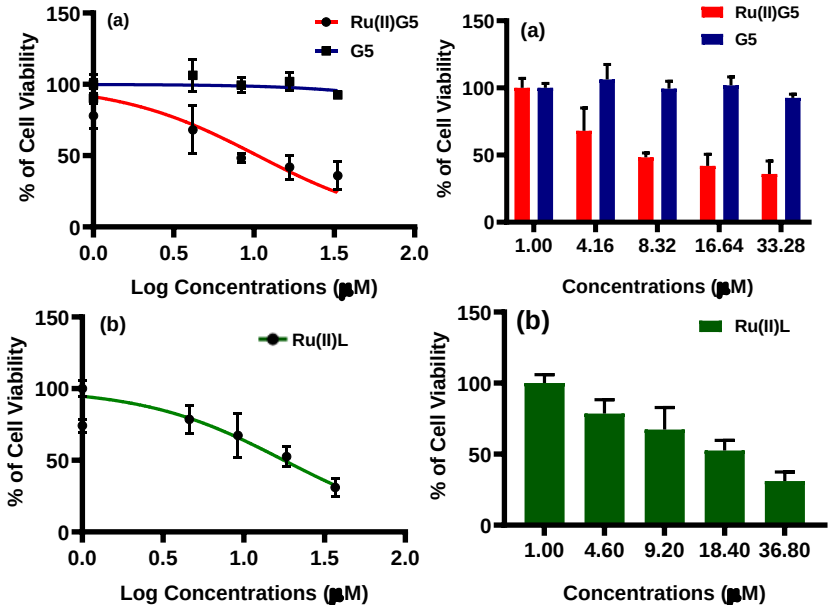

Figure 5.28. *Cytotoxicity study in A549 cell by MTT assay after 24 h incubation at 37 °C of (a)* ***G5*** *organogel and* ***Ru(II)G5*** *metallogel at concentrations 33.28 μM, 16.64 μM, 8.32 μM, 4.16 μM; (b) Ru-drug [**Ru(II)L**] at concentrations 4.6 μM, 9.2 μM, 18.4 μM, 36.8 μM with respect to ruthenium.*

The major factor for the cell death by the treatment of ruthenium gel is apoptosis which is indicated by the significant morphological changes of nuclei, chromatin fragmentation, multinucleation, nuclear swelling, cytoplasmic blebbing, and chromatin condensation.[59,60] These morphological changes can be determined by Hoechst staining.[61] Induction of apoptosis by **Ru(II)G5** metallogel and [**Ru(II)(lactyl-lactato)n(DMSO)m]^{x}** was assessed by evaluation of nuclear morphology after a Hoechst staining assay. Hoechst staining was done in A549 cells with an appropriate concentration of the ruthenium complex, and morphological changes were clearly seen in the images done through confocal microscopy (Figure 5.29). The normal cells are uniformly and lightly stained, whereas the cells treated with metallogel and gel collapsed product and positive control can be seen as brightly stained along with condensed nuclei.

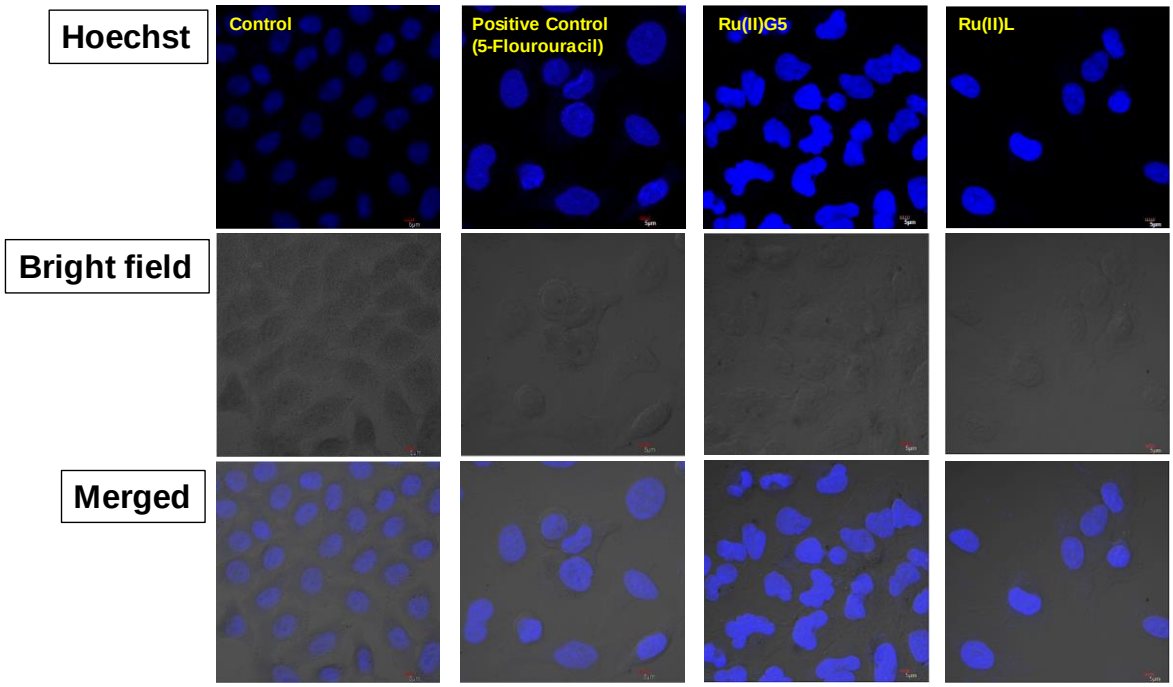

Figure 5.29. *Morphological analysis of nucleus by Hoechst stain in A549 cell line.*

Molecular docking results for MCT-1 Binding. MCT-1 (Monocarboxylate transporter-1) is widely distributed member of the MCT family identified as the lactate transporter present in the red blood cells. MCT transporters are the trans-membrane protein (TM) which activates and shows catalytic activities in presence of other TM-like proteins such as, Besigin and Emigin. Presently,the crystallographic structure of MCT-1 and other sub-family are not available. Therefore, a homology modeled MCT-1 has been utilized for docking study as reported by Wilson MC, *et al*, 2009; for the preliminary screening of compound.[62] The model suggests some important lysine residues which was found in exofacial site of the MCT-1, might be important for their irreversible inhibition. The major residues are **Lys 38, Lys 45, Lys 282, Lys 284, Lys 290,** and **Lys 413**. MCT-1 has a substrate binding site, which was hypothesized as an 'open' conformation to the extracellular site. It first accepts, proton followed by the lactate anion. The protein then undergoes a major conformational change to a new ‘closed’ conformation that exposes both the proton and lactate to the opposite surface of the membrane. Finally, it releases the lactate anion and then the proton from the exofacial surface.[63] In the present study,

the newly synthesized compound **G5** was studied for its interaction with MCT-1 and compared to that of lactic acid (LA) as well as DIDS as positive controls (Figure 5.30). All the compounds have shown promising interaction with several Lysine residues in both 'open' as well as Besigin attached MCT-1 homology modeled protein. The interaction parameters are shown in Table 5.3, and interaction poses are shown in Figure 5.31.

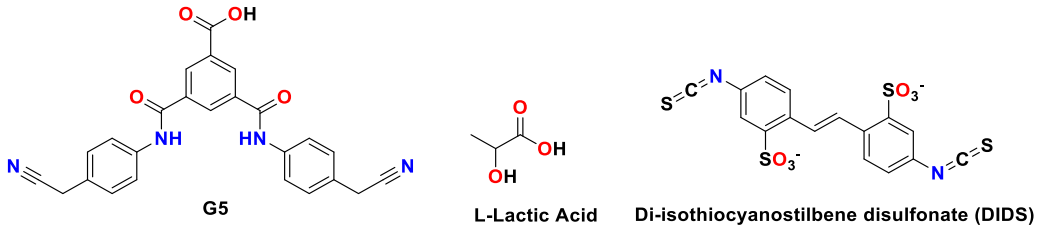

Figure 5.30. *Chemical structures of ligands used here for their binding with MCT-1.*

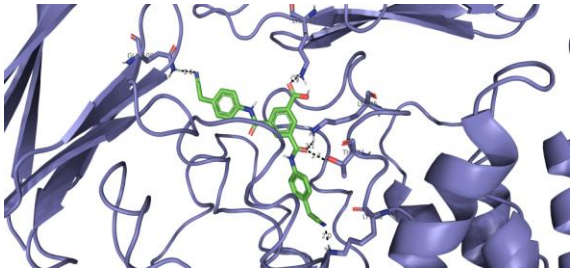

G5- Basigin-MCT-1 complex

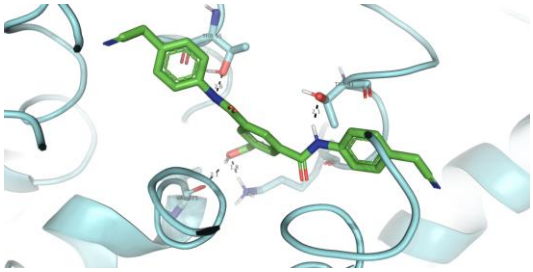

G5- MCT-1 complex

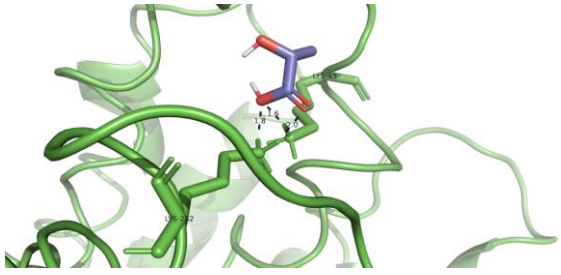

LA-Open-MCT-1 complex

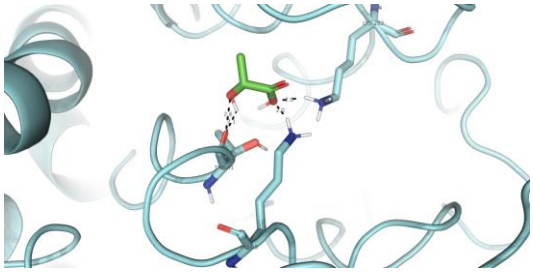

LA- Basigin-MCT-1 complex

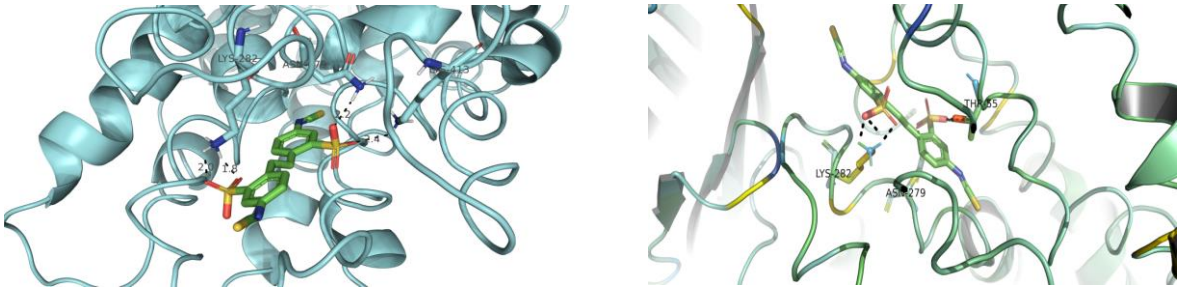

DIDS-Open-MCT-1 complex DIDS-Basigin-MCT-1 complex

Figure 5.31. *Binding interaction with* ***MCT-1*** *and* ***Basigin-MCT-1****.*

Table 5.3. *Interaction parameters for the binding of* ***G5****, Lactic acid, and DIDS with MCT-1.*

S. N.	Protein	Ligand	Energy (Kcal/mol)	Interaction	Hydrogen Bonding
1	MCT-1 Open	**LA**	-4.72	Lys 45, Lys 242	3
		G5	-9.92	Thr 55, Val 275, Thr 41	4
		DIDS	-11.70	Lys 282, Asn 279, Lys 413	4
2	MCT-1 - Besigin	**LA**	-5.03		
		G5	-9.19	Gln 100, Lys 127, Thr 41, Lys 45, Lys 38	5
		DIDS	-12.34	Lys 282, Asn 279, Thr 55	5

5.4 Conclusions

A monocarboxylate gelator molecule [3,5-bis{(4-(cyanomethyl)phenyl) carbamoyl} benzoic acid] **G5** has been synthesized purposefully to stabilize the ruthenium(II)-arene moiety in gel state via coordination through carboxylate donor site. The gelator **G5** has shown similar propensity like other TBA derivatives for gel formation. Treatment of the **G5** gel with $[RuCl_2(\eta^6\text{-}p\text{-cymene})]_2$ leads to the formation of a ruthenium-based metallogel. ESI-MS and NMR spectroscopy reveals the fate of ruthenium center as the formation of $[Ru(\mathbf{G5'})(p\text{-cymene})]^{+\cdot}$ Interestingly, this transformation has been only observed in a gel state, and any effort to synthesize the same molecules in a solution state proves futile. The ruthenium(II) metallogel [**Ru(II)G5**] has been found to be pH sensitive, and treatment of the gel with lactic acid leads to collapse of the gel, and the

ruthenium(II) ion has been found to be released as lactyl-lactato complex which to be cytotoxic against different cancer cell lines. The ruthenium gel [Ru(**G5'**)(*p*-cymene)]$^{+}$ has also shown moderate cytotoxicity. **G5** molecule has shown immense potential to disturb the MCT transport chain in cell division progression through molecular docking study. This could be one of the reason for the ruthenium(II) metallogel [**Ru(II)G5**] being cytotoxic. Derivatization of the carboxylic acid group into ester of **G5** takes away the gel-forming ability of the molecule indicating the role of carboxylic acid proton in solvent entrapment and gel formation capability.

5.5 References

[1] Kalmutzki M. J., Diercks C. S., Yaghi O. M. (2018), Metal–organic frameworks for water harvesting from air, Adv. Mater., 30, 1704304 (DOI: 10.1002/adma.201704304)

[2] Zhao J., Gao J., Xue W., Di Z., Xing H., Lu Y., Li L. (2018), Upconversion luminescence-activated DNA nanodevice for ATP sensing in living Cells, J. Am. Chem. Soc., 140, 578-581 (DOI: 10.1021/jacs.7b11161)

[3] Xiang Q., Cheng B., Yu J. (2015), Graphene-based photocatalysts for solar-fuel generation, Angew. Chem. Int. Ed., 54, 11350-11366 (DOI: 10.1002/anie.201411096)

[4] Okesola B. O., Smith D. K. (2016), Applying low-molecular weight supramolecular gelators in an environmental setting-self-assembled gels as smart materials for pollutant removal, Chem. Soc. Rev., 45, 4226-4251 (DOI: 10.1039/C6CS00124F)

[5] Du X., Zhou J., Shi J., Xu B. (2015), Supramolecular hydrogelators and hydrogels: rom soft matter to molecular biomaterials, Chem. Rev., 115, 13165-13307 (DOI: 10.1021/acs.chemrev.5b00299)

[6] Piepenbrock, M. O. M., Lloyd G. O., Clarke N., Steed, J. W. (2009), Metal-and anion-binding supramolecular gels, Chem. Rev., 110, 1960-2004 (DOI: 10.1021/cr9003067)

[7] Fang W., Zhang Y., Wu J., Liu C., Zhu H., Tu T. (2018), Recent advances in supramolecular gels and catalysis, Chem. Asian J., 13, 712-729 (DOI: 10.1002/asia.201800017)

[8] Tam A. Y. Y., Yam V. W. W. (2013), Recent advances in metallogels, Chem. Soc. Rev., 42, 1540-1567 (DOI: 10.1039/C2CS35354G)

[9] Ganta S., Chand D. K. (2017), Multi-stimuli-responsive metallogel molded from a Pd_2L_4-type oordination cage: selective removal of anionic dyes, Inorg. Chem., 57, 3634-3645 (DOI: 10.1021/acs.inorgchem.7b02239)

[10] Feldner T., Häring M., Saha S., Esquena J., Banerjee R., Díaz D. D. (2016), Supramolecular metallogel that imparts self-healing properties to other gel networks, Chem. Mater., 28, 3210-3217 (DOI: 10.1021/acs.chemmater.6b01144)

[11] Biswas P., Ganguly S., Dastidar P. (2018), Stimuli-responsive metallogels for synthesizing Ag nanoparticles and sensing hazardous gases, Chem. Asian J., 13, 1941-1949 (DOI: 10.1002/asia.201800743)

[12] Lin Q., Sun B., Yang Q. P., Fu Y. P., Zhu X., Wei T. B., Zhang Y. M. (2014), Double metal ions competitively control the guest-sensing process: a facile approach to stimuli-responsive supramolecular gels, Chem.-Eur. J., 20, 11457-11462 (DOI: 10.1002/chem.201403327)

[13] Chen P., Li Q., Grindy S., Holten-Andersen N. (2015), White-light-emitting lanthanide metallogels with tunable luminescence and reversible stimuli-responsive properties, J. Am. Chem. Soc., 137, 11590-11593 (DOI: 10.1021/jacs.5b07394)

[14] Sheikhi A., van de Ven T. G. (2016), Trapping it softly: ultrasoft zirconium metallogels for macromolecule entrapment and reconfiguration, ACS Macro Lett., 5, 904-908 (DOI: 10.1021/acsmacrolett.6b00447)

[15] Miao W., Zhang L., Wang X., Cao H., Jin Q., Liu M. (2013), A dual-functional metallogel of amphiphilic copper (II) quinolinol: redox responsiveness and enantioselectivity, Chem. Eur. J., 19, 3029-3036 (DOI: 10.1002/chem.201203401)

[16] Biswas A., Dubey M., Mukhopadhyay S., Kumar A., Pandey D. S. (2016), Anion triggered metallogels: demetalation and crystal growth inside the gel matrix and improvement in viscoelastic properties using Au-NPs. Soft matter., 12, 2997-3003 (DOI: 10.1039/C5SM02464A)

[17] Tu T., Fang W., Bao X., Li X., Dötz K. H. (2011), Visual chiral recognition through enantioselective metallogel collapsing: synthesis, characterization, and application of platinum–steroid low-molecular-mass gelators, Angew. Chem. Int. Ed., 50, 6601-6605 (DOI: 10.1002/anie.201100620)

[18] Bulbake U., Doppalapudi S., Kommineni N., Khan W. (2017), Liposomal formulations in clinical use: an updated review, Pharmaceutics., 9, 12 (DOI: 10.3390/pharmaceutics9020012)

[19] Sau S., Alsaab H. O., Kashaw S. K., Tatiparti K., Iyer A. K. (2017), Advances in antibody-drug conjugates: a new era of targeted cancer therapy, Drug Discov. Today, 22, 1547-1556 (DOI: 10.1016/j.drudis.2017.05.011)

[20] Anselmo A. C., Mitragotri S. (2016), Nanoparticles in the clinic, Bioeng. Transl. Med., 1, 10-29 (DOI: 10.1002/btm2.10003)

[21] Han Z., Li Y., Roelle S., Zhou Z., Liu Y., Sabatelle R., DeSanto A., Yu X., Zhu H., Magi-Galluzzi C., Lu Z.-R. (2017), Targeted contrast agent specific to an oncoprotein in tumor microenvironment with the potential for detection and risk stratification of prostate cancer with MRI, Bioconjugate Chem., 28, 1031-1040 (DOI: 10.1021/acs.bioconjchem.6b00719)

[22] Gill M. R., Falzone N., Du Y., Vallis K. A. (2017), Targeted radionuclide therapy in combined-modality regimens, Lancet. Oncol., 18, 414-423 (DOI: 10.1016/S1470-2045(17)30379-0)

[23] Li C., Wallace S. (2008), Polymer-drug conjugates: recent development in clinical oncology, Adv. Drug Delivery Rev., 60, 886-98 (DOI: 10.1016/j.addr.2007.11.009)

[24] Houdaihed L., Evans J. C., Allen C. (2017), Overcoming the road blocks: advancement of block copolymer micelles for cancer therapy in the clinic, Mol. Pharmaceutics, 14, 2503-2517 (DOI: 10.1021/acs.molpharmaceut.7b00188)

[25] Tibbitt M. W., Dahlman J. E., Langer R. (2016), Emerging frontiers in drug delivery, J. Am. Chem. Soc., 138, 704-717 (DOI: 10.1021/jacs.5b09974)

[26] Chen Q., Yang Y., Lin X., Ma W., Chen G., Li W., Wang X., Yu Z. (2018), Platinum (IV) prodrugs with long lipid chains for drug delivery and overcoming cisplatin resistance, Chem. Commun., 54, 5369-5372 (DOI: 10.1039/C8CC02791A)

[27] Cheng C., Zhang X., Meng Y., Chen L., Zhang Q. (2017), Development of a dual drug-loaded hydrogel delivery system for enhanced cancer therapy: in Situ formation, degradation and synergistic antitumor efficiency, J. Mater. Chem. B., 5, 8487-8497 (DOI: 10.1039/C7TB02173A)

[28] Pontillo N., Pane F., Messori L., Amoresano A., Merlino A. (2016), Cisplatin encapsulation within a ferritin nanocage: a high-resolution crystallographic study, Chem. Commun., 52, 136-4139 (DOI: 10.1039/C5CC10365G)

[29] Dyson, P. J., Sava, G. (2006), Metal-based antitumour drugs in the post genomic era, Dalton Trans., 1929-1933 (DOI: 10.1039/b601840h)

[30] Babak M. V., Meier S. M., Huber, K. V., Reynisson J., Legin A. A., Jakupec M. A., Roller A., Stukalov A., Gridling M., Bennett K. L., Colinge J. (2015), Target profiling of an antimetastatic RAPTA agent by chemical proteomics: relevance to the mode of action, Chem. Sci., 6, 2449-2456 (DOI: 10.1039/C4SC03905J)

[31] Alessio E. (2017), Thirty years of the drug candidate NAMI-A and the myths in the field of Ruthenium anticancer compounds: A personal perspective, Eur. J. Inorg. Chem., 12, 1549-1560 (DOI: 10.1002/ejic.201600986)

[32] Trondl R., Heffeter P., Kowol C. R., Jakupec M. A., Berger W., Keppler B. K. (2014), NKP-1339, the first ruthenium-based anticancer drug on the edge to clinical application, Chem. Sci., 5, 2925-2932 (DOI: 10.1039/C3SC53243G)

[33] Paunescu E., McArthur S., Soudani M., Scopelliti R., Dyson P. J. (2016) Nonsteroidal anti-inflammatory-organometallic anticancer compounds, Inorg. Chem., 55, 1788-1808 (DOI: 10.1021/acs.inorgchem.5b02690)

[34] Malviya N., Sonkar C., Kundu B. K., Mukhopadhyay, S. (2018), Discotic organic gelators in ion sensing, metallogel formation and bioinspired catalysis, Langmuir, 34, 11575-11585 (DOI: 10.1021/acs.langmuir.8b02352)

[35] Malviya N., Das M., Mandal P., Mukhopadhyay S., (2017), A smart organic gel template as metal cation and inorganic anion sensor, Soft Matter, 13, 6243-6249 (DOI: 10.1039/C7SM01199G)

[36] Steed J. W., Atwood J. L. (2009), Supramolecular chemistry; John Wiley& Sons, Ltd: Chichester, U.K.

[37] Northrop B. H., Zheng Y.-R., Chi K.-W., Stang P. J. (2009), Self-organization in coordination-driven self-assembly, Acc. Chem. Res., 42, 1554-1563 (DOI: 10.1021/ar900077c)

[38] Sinha I., Mukherjee, P. S. (2018), Chemical transformations in confined space of coordination architectures, Inorg. Chem., 57, 4205-4221 (DOI: 10.1021/acs.inorgchem.7b03067)

[39] Wei Q., James S. L. (2005), A metal–organic gel used as a template for a porous organic polymer, Chem. Commun., 12, 1555-1556 (DOI: 10.1039/B418554D)

[40] Wang W., Wang Y.-X., Yang H.-B. (2016), Supramolecular transformations within discrete coordination-driven supramolecular architectures, Chem. Soc. Rev., 45, 2656-2693 (DOI: 10.1039/C5CS00301F)

[41] Corbet C., Feron O. (2017), Tumour acidosis: from the passenger to the driver's seat, Nat. Rev. Cancer, 17, 577 (DOI: 10.1038/nrc.2017.77)

[42] Martínez-Reyes I., Chandel N. S. (2017), Waste not, want Not: lactate oxidation fuels the TCA cycle, Cell Metab., 26, 803-804 (DOI: 10.1016/j.cmet.2017.11.005)

[43] Lee Z. W., Teo X. Y., Song Z. J., Nin D. S., Novera W., Choo B. A., Dymock B. W., Moore P. K., Huang R. Y. J., Deng L. W. (2017), Intracellular hyper-acidification potentiated by hydrogen sulfide mediates invasive and therapy resistant cancer cell death, Front. Pharmacol., 8, 763 (DOI: 10.3389/fphar.2017.00763)

[44] Howe R. C., Smalley A. P., Guttenplan A. P., Doggett M. W., Eddleston M. D., Tan J. C., Lloyd G. O. (2013), A family of simple benzene 1,3,5-tricarboxamide (BTA) aromatic carboxylic acid hydrogels, Chem. Commun., 49, 4268-4270 (DOI: 10.1039/C2CC37428E)

[45] Adams D. J., Morris K., Chen L., Serpell L. C., Bacsa J., Day G. M. (2010), The delicate balance between gelation and crystallisation: structural and computational investigations, Soft Matter, 6, 4144-4156 (DOI: 10.1039/C0SM00409J)

[46] Vidyasagar A., Sureshan K. M. (2015), Stoichiometric sensing to opt between gelation and crystallization, Angew. Chem. Int. Ed., 127, 12246-12250 (DOI: 10.1002/anie.201506544)

[47] Spackman M. A., Jayatilaka, D. (2009), Hirshfeld surface analysis, Cryst. Eng. Comm., 11, 19-32 (DOI: 10.1039/B818330A)

[48] Yan X., Zhu P., Li J. (2010), Self-assembly and application of diphenylalanine-based nanostructures, Chem. Soc. Rev., 39, 1877-1890 (DOI: 10.1039/B915765B)

[49] Kartha K. K., Babu S. S., Srinivasan S., Ajayaghosh A. (2012), Attogram sensing of trinitrotoluene with self-assembled molecular gelator, J. Am. Chem. Soc., 134, 4834-4841 (DOI: 10.1021/ja210728c)

[50] Ma Y., Ma H., Yang Z., Ma J., Su Y., Li W., Lei Z. (2015), Methyl cinnamate-derived fluorescent rigid organogels based on cooperative π-π stacking and C=O$\cdots\pi$ interactions instead of H-bonding and alkyl chains, Langmuir, 31, 4916-4923 (DOI: 10.1021/acs.langmuir.5b00275)

[51] Mears L. L., Draper E. R., Castilla A. M., Su H., Dietrich B., Nolan M. C., Smith G. N., Doutch J., Rogers S., Akhtar R., Cui H. (2017), Drying affects the fiber network in low molecular weight hydrogels, Biomacromolecules, 18, 3531-3540 (DOI: 10.1021/acs.biomac.7b00823)

[52] Adams D. J. (2018), Does drying affect gel networks?, Gels, 4, 32 (DOI: 10.3390/gels4020032)

[53] Furrer J., Süss-Fink G. (2016), Thiolato-bridged dinuclear arene ruthenium complexes and their potential as anticancer drugs, Coord. Chem. Rev., 309, 36-50 (DOI: 10.1016/j.ccr.2015.10.007)

[54] Lam N. Y., Truong D., Burmeister H., Babak M. V., Holtkamp H. U., Movassaghi S., Ayine-Tora D. M., Zafar A., Kubanik M., Oehninger L., Söhnel T. (2018), From catalysis to cancer: toward structure–activity relationships for benzimidazol-2-ylidene-derived N-heterocyclic-carbene complexes as anticancer agents, Inorg. Chem., 57, 14427-14434 (DOI: 10.1021/acs.inorgchem.8b02634)

[55] Li J., Mooney D. J. (2016), Designing hydrogels for controlled drug delivery, Nat. Rev. Mater., 1, 16071 (DOI: 10.1038/natrevmats.2016.71)

[56] Martinez-Outschoorn U. E., Peiris-Pages M., Pestell R. G., Sotgia F., Lisanti M. P. (2017), Cancer metabolism: a therapeutic perspective, Nat. Rev. Clin. Oncol., 14, 11 (DOI: 10.1038/nrclinonc.2016.60)

[57] Cuesta L., Hevia E., Morales D., Pérez J., Riera L., Miguel D. (2006), Reactivity of molybdenum and rhenium hydroxo complexes toward organic electrophiles: reactions that afford carboxylato products, Organometallics, 25, 1717-1722 (DOI: 10.1021/om051081g)

[58] Małecki J. G. (2012), Half-sandwich ruthenium (II) complexes with N-and N,(N, O)-donor ligands: molecular, electronic structures, and computational study, Struct. Chem., 23, 461-472 (DOI: 10.1007/s11224-011-9890-0)

[59] Cloonan S. M., Elmes R. B., Erby M., Bright S. A., Poynton F. E., Nolan D. E., Quinn S. J., Gunnlaugsson T., Williams D. C. (2015), Detailed biological profiling of a photoactivated and apoptosis inducing Pdppz ruthenium (II) polypyridyl complex in cancer cells, J. Med. Chem., 58, 4494-4505 (DOI: 10.1021/acs.jmedchem.5b00451)

[60] Ichim G., Tait S. W. (2016), A fate worse than death: apoptosis as an oncogenic process, Nat. Rev. Cancer, 16, 539 (DOI: 10.1038/nrc.2016.58)

[61] Atale N., Gupta S., Yadav U. C. S., Rani V. (2014), Cell-death assessment by fluorescent and nonfluorescent cytosolic and nuclear staining techniques, J. Microsc., 255, 7-19 (DOI: 10.1111/jmi.12133)

[62] Wilson M.C., Meredith D., Bunnun C., Sessions R. B., Halestrap A. P. (2009), Studies on the DIDS-binding site of monocarboxylate transporter 1 suggest a homology model of the open conformation and a plausible translocation cycle, J. Biol. Chem., 284, 20011-20021 (DOI: 10.1074/jbc.M109.014217)

[63] Verlet L. Computer" experiments" on classical fluids. I. (1967), Thermodynamical properties of lennard-jones molecules, Phys. Rev., 159, 98 (DOI: 10.1103/PhysRev.159.98)

Chapter 6

Self-Healable Lanthanoid Based Photoluminescent Metallogel and Confined Gel Space Crystallization

Chapter 6

Self-Healable Lanthanoid Based Photoluminescent Metallogel and Confined Gel Space Crystallization

6.1 Introduction

Investigation of supramolecular metallogels based on low molecular weight gelators (LMWGs) has become a very interesting topic in the current scenario. LMWGs can play a significant role to form ordered self-assembly.[1,2,3] The supramolecular self-assembly of LMWGs is associated with the non-covalent interaction, which makes them more attractive.[4] Self-assembly generally gets initiated due to the aggregation of the molecules into different morphologies in suitable solvent systems by non-covalent interactions like π-π stacking, CH-π interactions, hydrogen-bonding, hydrophobic-hydrophobic interactions, van der Waals interactions, leading to the formation of three-dimensional networks.[5] Formation of supramolecular self-assembly by the interaction of metal ions and small molecules can invoke further versatility. The metal-ligand interaction is the main force behind the formation of metallogels.[6,7] The metallogels formed by LMWGs have found applications in various fields like sensors, drug delivery, catalysis, biomaterials, and so on.[8-13] Among various small molecules (LMWGs), tetrazoles derivatives have been found to be easy to prepare[14], and with multiple binding site, they can endorse gelation by the formation of cross-link supramolecular assemblies.[15] Coordination of metal with tetrazole based ligands offering attractive, dynamic properties has been proven to be a useful tool for the formation of ordered structures with more complexity.[16] The diversity in the coordination of metal with LMWG could be induced and control the self-assembled gelation and their properties. Compared with complexes with 3d transition metals, lanthanide metals can show unique features in terms of magnetic and spectroscopic properties.[17] The Ln^{3+} ions are the hard acid according to HSAB theory, which makes them interact with donor atom in following order O, N, S

and formed the lanthanide-based complexes.[18] Ln^{3+} ions complexes have specific electron configuration (the possibility of high coordination numbers), high flexibility in coordination mode (the possibility of easy changes of the ligands), and specific physicochemical properties.[19] As per previous reports, lanthanides-based complexes have applications in various fields, *e.g.*, as the luminescent material, magnetic materials, anticorrosion materials, gas separation, medicinal chemistry. They can also show biological applications like as anticancer and antibacterial agent, in bioimaging and magnetic resonance imaging (MRI) and also as *in vivo* luminescent imaging material.[20-24] On the other hand, the applications of lanthanoid based metallogels have found in white light emitting materials, luminescent materials, thermo-responsive materials, and stimuli-responsive materials. Lanthanoid based metallogels can also show self-healing ability in suitable conditions.[25-33]

The low molecular weight luminescent lanthanoid based metallogel is getting explored more and more in the last few years. The lanthanoid based metallogels have unique photophysical properties due presence of *f*-electrons. Lanthanoid ions have "Laporte forbidden *f-f* transition" with low extinction coefficient and the light absorbing capacity is very poor.[34] However, dynamic coordination between lanthanoids and fluorescent probe (LMWGs) involve the absorption of light by the fluorescent probe, the electronic excitation energy is transferred and make them photoluminescence in nature with intense emission.[35]

Another worth investigating property of LMWGs based lanthanoid metallogels is their self-healing ability. The self-healing materials have ability to repair itself after damage like tissues during wound healing.[36] Self-healing materials are mainly two type based on their nature, *i.e.* extrinsic self-healing material in which healing ability is due to some external healing components while intrinsic self-healing material not required any external component, it can inherently reform the bond after damage with reversibility.[37] The self-healing metallogels are formed *via in situ* gelations, and the cooperative effects of all components like ligand, metal and solvent molecules in suitable proportion and experimental situations play important roles.[38]

In this chapter, the synthesis of lanthanoid based LMW metallogels [**La(III)G6-Cl**, **Pr(III)G6-Cl**, **La(III)G6-NO$_3$** and **Gd(III)G6-NO$_3$**] by using Di(1*H*-tetrazol-5-yl) methane (**G6**) has been explored and reported. Interestingly, **La(III)G6-Cl** showed self-healing ability, which makes them more interesting. Furthermore, in the recent era, by the help of various methods, the formation of crystals from the metallogels become an outstanding chemical tool.[39] The crystals of metallogels are often helpful to understand the molecular-level structure of the gel. Particularly, crystallizations from the confined space have become fascinating in nature.[40] The gelation and crystallization processes are differed by the formation of self-assembly with different dimensionality.[41,42] Gelation is occurring due to formation self-assembly in one dimension where three-dimensional self-assembly favors the formation of the crystal. However, gels can play a significant role during the crystallization process. The viscoelastic property of gel favors the slow diffusion, which provides slow nucleation and helps to obtain crystal from gel state.[43] Another interesting feature is their reversible nature, which provides easy recovery of crystal and reutilization of gel.[44]

In this chapter, the confined metallogel space crystallization has been also explored. Beautiful colorless square shape crystals are obtained from the **Gd(III)G6-NO$_3$** metallogel with aging, which was further subjected for the elucidation of structure of the metallogels.

The photoluminescent property, self-healing ability, and the confined metallogels space crystallization of low molecular weight tetrazole based lanthanoid metallogels provide us novel class of gelators and has been found useful in a number of applications.

6.2 Experimental section

6.2.1 Material and methods

All the required chemicals were purchased from Sigma and used without further purification. A HORIBA Jobin Yvon picosecond time-correlated single-photon counting (TCSPC) spectrometer (model Fluorocube-01-NL) was used for recording PL decays.

Lifetime measurements were recorded using a photomultiplier (TBX-07C) and were analyzed using IBH DAS 6.0 software. Intensity decay profiles were fitted to the bi-exponential series:

$$\mathbf{F(t) = \sum_{i=1}^{2} a_i \exp(-t/\tau_i)}$$

where F(t) denotes normalized PL decay and a_1 and a_2 are the normalized amplitudes of decay components τ_1 and τ_2, respectively. The average lifetime was obtained from the equation

$$\mathbf{< \tau >= \sum_{i=1}^{2} a_i \tau_i}$$

The specifications of all the instruments used for analysis purpose were the same as described in section 2.2.1 of chapter 2.

6.2.2 Synthesis and preparation of metallogels [La(III)G6-Cl, Pr(III)G6-Cl, La(III)G6-NO_3, Gd(III)G6-NO_3

10 mg (0.07 mmol) of di(1*H*-tetrazol-5-yl) methane (**G6**) was dissolved in 3 mL of MeOH in presence of 0.14 μL (0.14 mmol) triethylamine base. The resultant solution was layered by equimolar (0.07 mmol) MeOH solution (3 mL) of Ln^{3+} salts [$LaCl_3.7H_2O$, $PrCl_3.6H_2O$, $La(NO_3)_3.6H_2O$, $Gd(NO_3)_3.6H_2O$] and left in undisturbed condition at room temperature. Gelation gets induced after some time and after 2 h metallogels (**La(III)G6-Cl**, **Pr(III)G6-Cl**, **La(III)G6-NO_3** and **Gd(III)G6-NO_3**) set-in.

6.2.3 Analysis of metallogels

La(III)G6-Cl. FT-IR of (KBr): ν = 3209, 2920, 2857, 2704, 2677, 1618, 1557, 1489, 1410, 1296, 1239, 1181, 1140, 1086 cm^{-1}. ^{1}H NMR (400 MHz, 298 K, DMSO-d_6): δ = 4.35 (2H, -CH_2, d). ^{13}C NMR (100 MHz, 293 K, DMSO-d_6): δ = 152.62 (CN_4), 19.18 (-CH_2). MS (ESI): *m/z* = 415.0051 $[La^{3+}(G6)(H_2O)_6Cl]+Na^+$ (in positive mode).

Pr(III)G6-Cl. FT-IR of (KBr): ν = 3188, 2992, 1610, 1498, 1447, 1366, 1262, 1203, 1105, 1065, 1018 cm^{-1}. MS (ESI): *m/z* = 304.2736 $[Pr^{3+}(G6)(H_2O)_6]$-Cl^- (in positive mode).

La(III)G6-NO_3. FT-IR of (KBr): ν = 3195, 1605, 1558, 1440, 1408, 1367, 1336, 1220, 1178, 1070, 1004 cm^{-1}. MS (ESI): *m/z* = 463.3028 $[La^{3+}(G6)(H_2O)_5NO_3]$+$Na^+$ (in positive mode). ^{1}H NMR (400 MHz, 298 K, DMSO-d_6): δ = 4.27 (2H, -CH_2, dd). ^{13}C NMR (100 MHz, 293 K, DMSO-d_6): δ = 152.19 (CN_4), 18.97 (-CH_2).

Gd(III)G6-NO_3. FT-IR of (KBr): ν = 3185, 2991, 2859, 2829, 2625, 2561, 1616, 1500, 1465, 1419, 1384, 1274, 1216, 1152, 1111, 1059, 1030 cm^{-1}. MS (ESI): *m/z* = 483.0589 $[Gd^{3+}(G6)(H_2O)_5NO_3]$ (in positive mode).

6.2.4 Confined metallogel space crystallization

The metallogel **Gd(III)G6-NO_3** was left at room temperature on undisturbed condition. After three days with aging, colorless square-shaped crystals were obtained inside the metallogel, which have been further characterized by single crystal X-ray diffraction (SXRD).

6.2.5 Characterizations

Characterizations techniques like UV-visible Spectroscopy, Fluorescence Spectroscopy, FT-IR Spectroscopy, powder X-ray Diffraction (PXRD) and morphological Study, Rheological Properties of **La(III)G6-Cl**, **Pr(III)G6-Cl**, **La(III)G6-NO_3**, **Gd(III)G6-NO_3** metallogels have been the same as described in the section 2.2.5 of chapter 2.

Single Crystal X-ray Diffraction (SXRD) Analysis of Gd(III)G6-NO_3. A colorless square-shaped crystal (molecular formula: $C_3H_{12}GdN_9O_8$) of **Gd(III)G6-NO_3** with approximate dimensions of 0.320x0.280x0.240 mm and were used for X-ray crystallographic analysis. Single crystal X-ray structural studies was performed on a CCD Agilent Technologies (Oxford Diffraction) SUPER NOVA diffractometer. Data were collected at 150(2) K using graphite-monochromatic Mo Kα radiation (λα = 0.71073 Å) and Cu Kα radiation (λα = 1.54184 Å) respectively. The strategy for the data collection

was evaluated using the CrysAlisPro CCD software. The data were collected by the standard phi-omega scan techniques and were scaled and reduced using the CrysAlisPro RED software. The structure was solved by direct methods using SHELXS-97 and refined by full matrix least-squares on F^2. The positions of all the atoms were obtained by direct methods. All non-hydrogen atoms were refined anisotropically. The remaining hydrogen atoms were placed in geometrically constrained positions and refined with isotropic temperature factors, generally 1.2 Ueq of their parent atoms. The contribution of solvent electron density was removed by the SQUEEZE routine in PLATON.51 Crystal data, data collection parameters, and refinement data for **Gd(III)G6-NO$_3$** are well explained.

6.2.6 Self-Healing Experiment

La(III)G6-Cl metallogel was cut in blocks of approximately same dimensions. The blocks were placed back in direct contact without giving any external stimuli. Recombination of all the block of metallogel after some time was observed.

6.2.7 Supplementary materials

CCDC 1872889 contains the supplementary crystallographic data for **Gd(III)G6-NO$_3$**, respectively. These data can be obtained free of charge via http://www.ccdc.cam.ac.uk/conts/retrieving.html, or from the Cambridge Crystallographic Data Centre, 12 Union Road, Cambridge CB2 1EZ, UK; fax: (+44) 1223-336-033; or e-mail: deposit@ccdc.cam.ac.uk.

6.3 Results and discussion

The design of the metallogels has been conceptualized based on some earlier reports.[45,46] It is well known that tetrazole is nitrogen-rich ligand and has multiple binding sites,[47,48] so it can stabilize the supramolecular self-assembled structure by participating in hydrogen bond formation.[49] Furthermore, ligand containing nitrogen donor atoms can form strong coordinate bonds with Ln^{3+} ions according to the HSAB principle. Moving forward with this strategical approach, four new lanthanoid based low molecular weight

metallogels by using N-donor chelating ligand *i.e.* Di(1*H*-tetrazol-5-yl) methane (**G6**) (Scheme 6.1). These four metallogels have been well characterized by various spectroscopic techniques. The ESI-MS spectra have displayed a molecular ion peak at 415.0051 for $[La^{3+}(G6)(H_2O)_6Cl]+Na^+$, 304.2736 for $[Pr^{3+}(G6)(H_2O)_6]-Cl^-$, 463.3028 for $[La^{3+}(G6)(H_2O)_5NO_3]+Na^+$ and 483.0589 for $[Gd^{3+}(G6)(H_2O)_5NO_3]$ in a positive mode, indicating the molecular composition of the gel (Figures 6.1, 6.2, 6.3, 6.4). For the preparation of metallogels (**La(III)G6-Cl**, **Pr(III)G6-Cl**, **La(III)G6-NO$_3$**, **Gd(III)G6-NO$_3$**), methanolic solution of ligand (**G6**) in presence of triethylamine (base used for the deprotonation of hydrogen from **G6**) has been layered by the methanolic solution of Ln^{3+} salts [$LaCl_3.7H_2O$, $PrCl_3.6H_2O$, $La(NO_3)_3.6H_2O$, $Gd(NO_3)_3.6H_2O$] and left it at undisturbed condition at room temperature (Scheme 6.1). Metallogels are obtained after 2 h, and the gelation has been confirmed by the test tube invertion method and heating and subsequent cooling. The heating cooling method indicated the reversible nature of all the metallogels. The critical gel concentration (CGC) for all metallogels are found around 25 mM in MeOH.

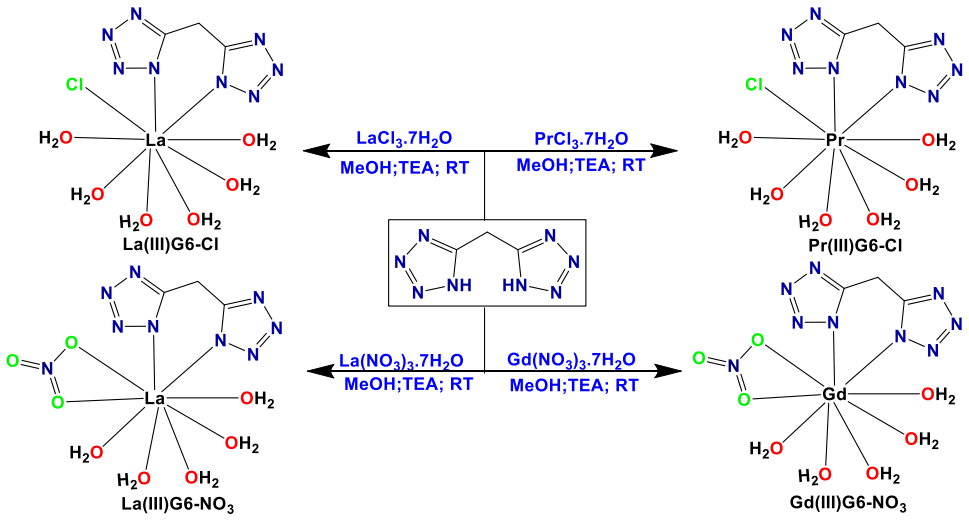

Scheme 6.1. *Systematic scheme for the synthesis of metal-based LMWGs forthe formation of metallogels (**La(III)G6-Cl**, **Pr(III)G6-Cl**, **La(III)G6-NO$_3$**, **Gd(III)G6-NO$_3$**).*

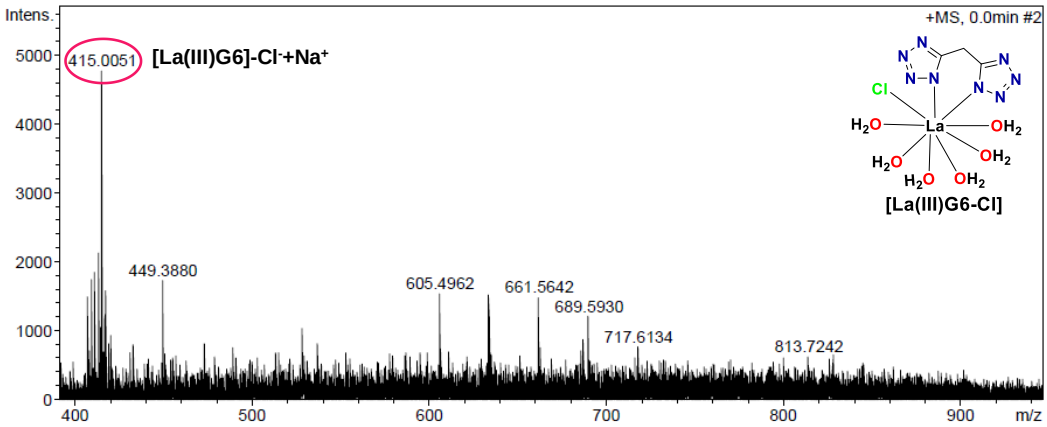

Figure 6.1. *ESI- Mass spectrum of gelator* ***La(III)G6-Cl.***

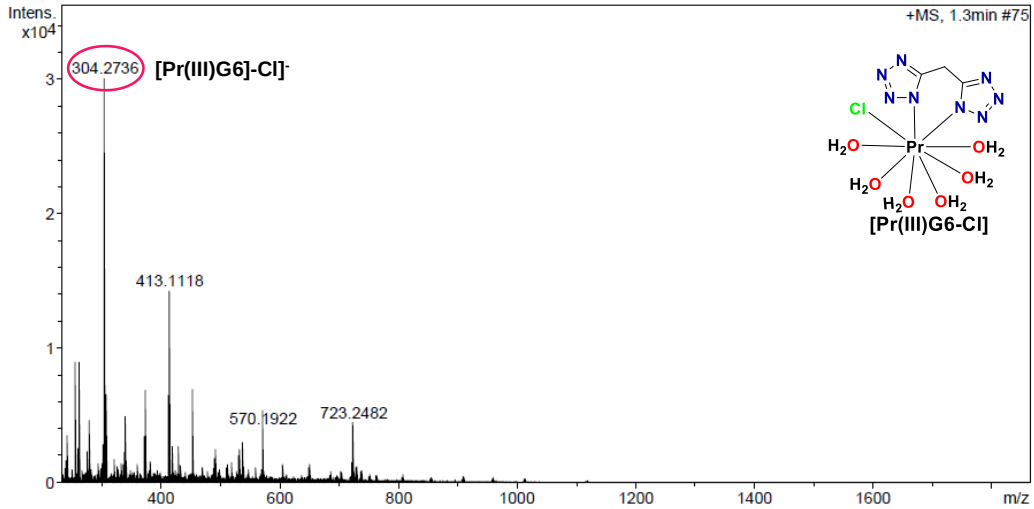

Figure 6.2. *ESI- Mass spectrum of gelator* ***Pr(III)G6-Cl.***

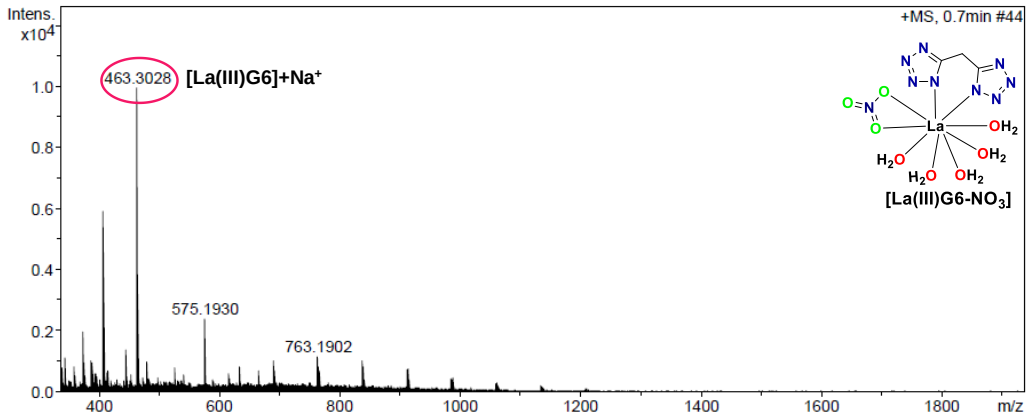

Figure 6.3. *ESI- Mass spectrum of gelator* ***La(III)G6-NO₃.***

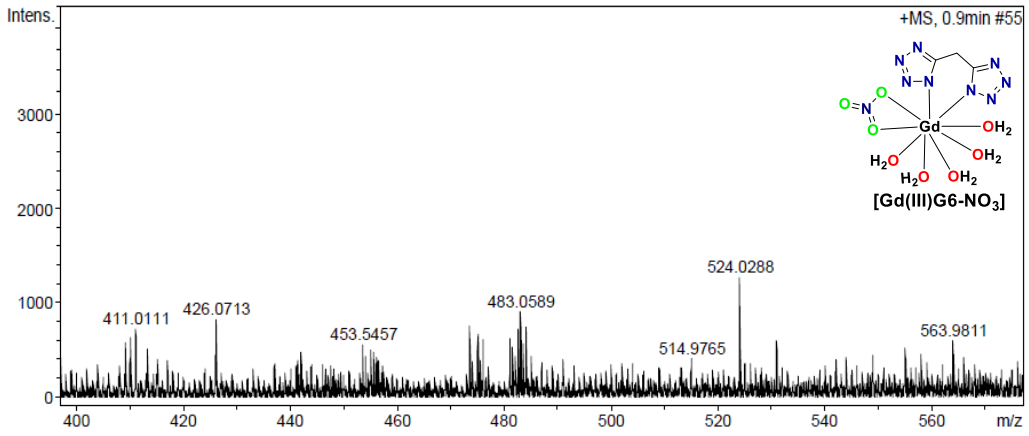

Figure 6.4. *ESI- Mass spectrum of gelator* ***Gd(III)G6-NO₃.***

This can be considered as a type of *in situ* gelations in which the cooperative effects of all components like ligand, solven, and metal in the solution mixture under suitable ratio play important roles. Further with the aging of metallogels, it has been noticed that the deposition of colorless square-shaped crystals takes place inside the **Gd(III)G6-NO₃** metallogel (Figure 6.5). The crystals were subjected to single crystal X-ray diffraction for the solid-state structure determination of **Gd(III)G6-NO₃**. It would deliver new insight toelucidate the type of non-covalent interaction involve for the formation of metallogel.

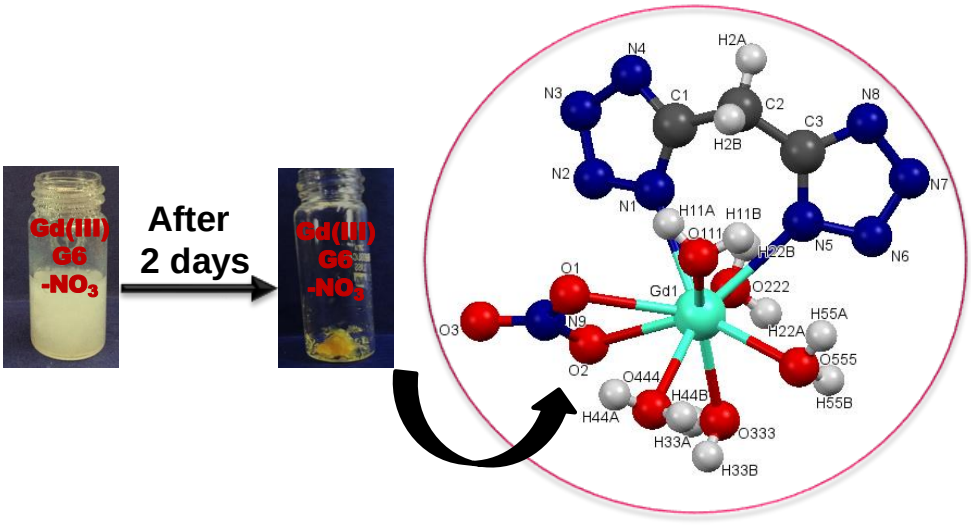

Figure 6.5. *Crystallization of* ***Gd(III)G6-NO₃*** *in confined gel state and Single-crystal X-ray diffraction.*

The crystal system for the **Gd(III)G6-NO$_3$** is found to be orthorhombic with Pbca space group. Gadolinium center is nine-coordinate by one chelating anionic bidentate ligand (**G6**), one anionic nitrate and five neutral water molecules. Coordination geometry for nine-coordinated **Gd(III)G6-NO$_3$** complex is tricapped trigonal prism (TTP). Single crystal structure determination indicates about the type of possible non-covalent interactions participated during the formation of metallogel self-assembly. The **Gd(III)G6-NO$_3$** molecular packing describes the varied molecular recognition pattern. Tetrazole rings and water molecules of the compound have participated in hydrogen bond formation as donor and acceptor in molecular recognition with its neighboring molecules. Hydrogen bonding interactions recognized through molecular packing in various planes and dimensions. The H_2O, NO_3, NH, and N atoms of tetrazole ring have been found to be involved in hydrogen bonding. The hydrogen bond acceptors of the types N-H···O, O-H···N were visualized in below structures (Figure 6.6, 6.7, Table 6.1). It indicates that extensive hydrogen bonding could be the main reason behind molecular self-assembly during metallogel formation.[50]

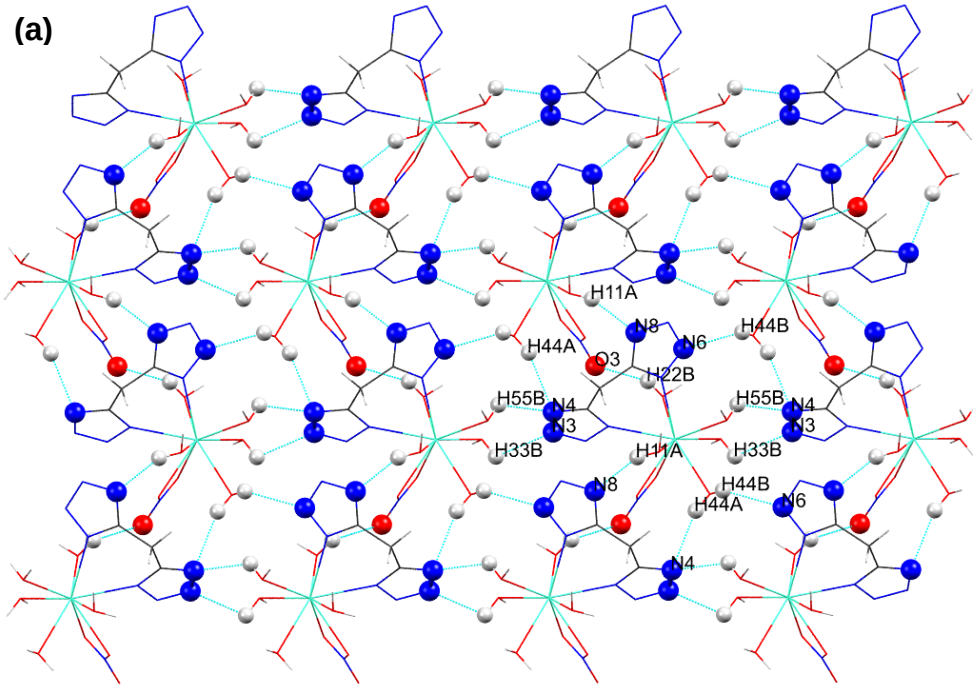

(b)

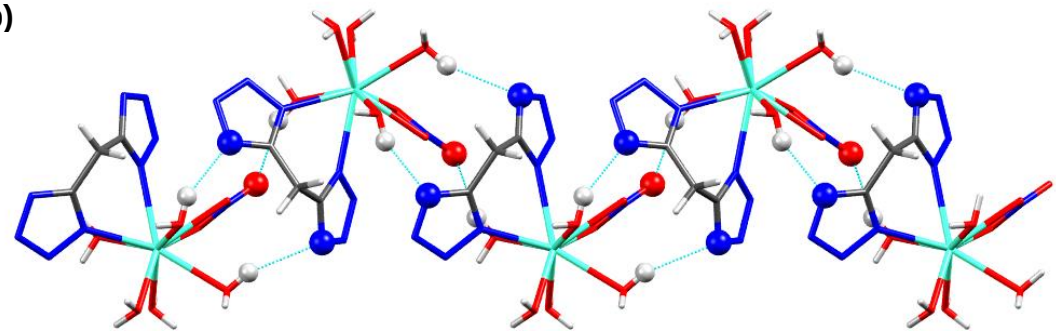

Figure 6.6. *Hydrogen bonding in between H_2O, NO_3, NH, and N atoms of tetrazole ring for* ***Gd(III)G6-NO$_3$*** *in (a) 2D layer, (b) 1D chain.*

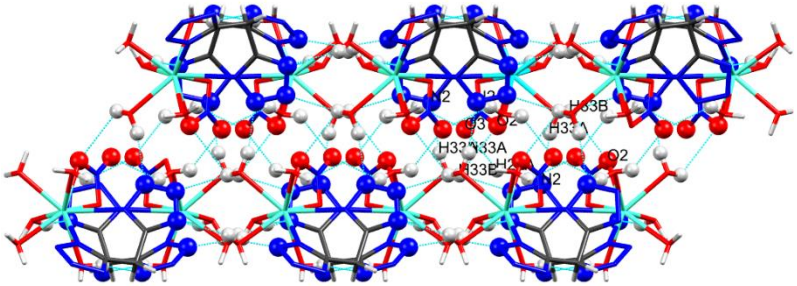

Figure 6.7. *Hydrogen bonding in between H_2O, NO_3, NH, and N atoms of tetrazole ring for* ***Gd(III)G6-NO$_3$*** *which represent interactions between forming a 2D layer and leading to 3D network.*

Table 6.1. *Hydrogen bonds and the bond angle between Donor--H... Acceptor atoms of* ***Gd(III)G6-NO$_3$***.

S. N.	Donor--H... Acceptor	Bond Distance (Å)			Bond Angle D--H... A
		D--H	H... A	D... A	
1	O222--H22B..O3	0.855	2.223	2.830	128.2°
2	O3--H22A..O222	2.225	0.850	2.830	137.3°
3	O333--H33B..O2	0.850	2.627	3.132	119.2°
4	O333--H33A..N2	0.850	2.095	2.930	167.0°
5	N6--H44B..O444	2.351	0.848	2.940	127.4°
6	O111--H11A..N8	0.550	2.090	2.876	153.4°
7	N4--H55B..O555	2.174	0.850	2.718	121.6°
8	O444--H44A..N4	0.850	2.393	3.196	157.7°

Further, the stochiometric ratios between **G6** and Ln^{3+} for metallogels formation were determined by Job plot. The obtained results indicate the stochiometric ratio is 1:1 between Ln^{3+} and **G6** for all the metallogels (**La(III)G6-Cl**, **Pr(III)G6-Cl**, **La(III)G6-NO_3**, **Gd(III)G6-NO_3**).

The photoluminescent property of lanthanoid based metallogel was explored by recording flourescence spectra. The emission spectra of **G6** and their metallogels (**La(III)G6-Cl**, **Pr(III)G6-Cl**, **La(III)G6-NO_3**, **Gd(III)G6-NO_3**) have been taken (Figure 6.8). Shifting in the emission maxima of **G6** from 404 to 397 nm was observed with enhancement in the flourescence intensity after the formation metallogels because of aggregation. This blue shift is probably due to effective hydrogen bonding in formation of the *H*-aggregate.[51]

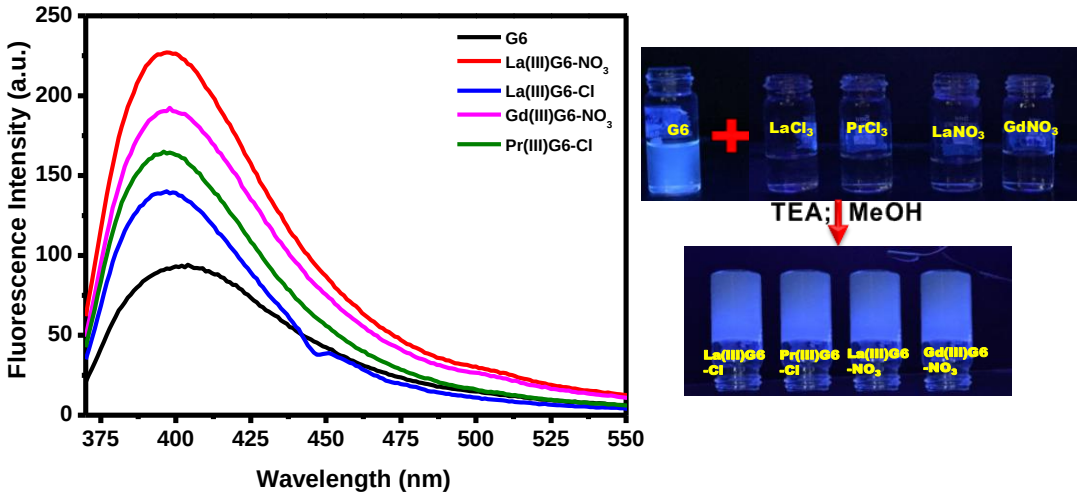

Figure 6.8. *Fluorescence spectra for ligand (**G**) and metallogels (**La(III)G6-Cl**, **Pr(III)G6-Cl**, **La(III)G6-NO_3**, **Gd(III)G6-NO_3**) (in MeOH) (λ_{ex} = 355 nm) and optical image of metallogels under UV lamp indicates their emissive nature.*

For the more deeper knowledge, absolute fluorescence quantum yield experiment was performed. The quantum yield for **G6** has been found to be around .04, and for the metallogels, the values of quantum yield are 0.075 for **La(III)G6-Cl**, 0.09 for **Pr(III)G6-Cl**, 0.12 for **La(III)G6-NO_3** and 0.11 for **Gd(III)G6-NO_3**. Increment in the value of quantum yield after formation metallogels from the solution of **G6** has been observed.

The enhancement in quantum yield might be due to the formation of ordered supramolecular self-assembly due to non-covalent interaction like hydrogen bonding between methanol and nitrogen-containing tetrazole. Further, the luminescent excited state lifetime for all the metallogels were also recorded by using TCSPC technique. The lifetimes and decay traces of metallogels have been predicted at λ_{ex} = 355 nm. The decay traces forall the metallogels was fitted with a Triexponential function (Figure 6.9). The average lifetime 0.369, 0.833, 0.631, 0.342 ns are observed for **Gd(III)G6-NO3**, **La(III)G6-NO3**, **La(III)G6-Cl**, **Pr(III)G6-Cl** metallogels (Table 6.2).

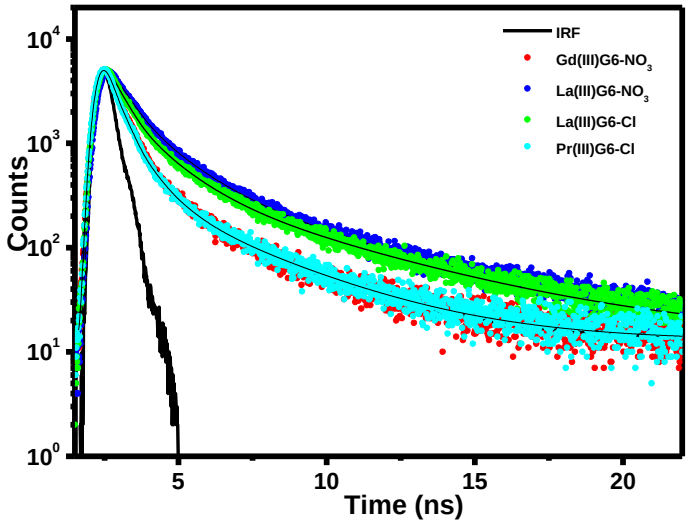

Figure 6.9. *Decay traces of* ***Gd(III)G6-NO3***, ***La(III)G6-NO3***, ***La(III)G6-Cl***, ***Pr(III)G6-Cl*** *metallogels at 25 mM concentration.*

Table 6.2. *Decay parameters for metallogel at 25 mM concentration (<**τ**>= Average lifetime,* ***a*** *= Normalized amplitude of each component)*

Metallogels	**τ_1 (ns)**	**a_1**	**τ_2 (ns)**	**a_2**	**τ_3 (ns)**	**a_3**	**<τ> (ns)**	**χ^2**
Gd(III)G6-NO_3	0.215	0.84	0.810	0.14	3.245	0.02	0.369	1.19
La(III)G6-NO_3	1.349	0.26	0.352	0.69	4.811	0.05	0.833	1.09
La(III)G6-Cl	1.249	0.19	4.903	0.04	0.284	0.78	0.631	1.12
Pr(III)G6-Cl	0.801	0.13	0.199	0.85	3.394	0.02	0.342	1.16

Various non-covalent interactions like H-bonding, π-π interactions, metal-ligand interactions play an important role for supramolecular self-assembly during metallogel formation.[52,53] To gain insight of formation of supramolecular self-assembly, various physicochemical experiments have been carried out by using various spectroscopic techniques like ^{1}H NMR, ^{13}C NMR, FT-IR and PXRD for the xerogel of **La(III)G6-Cl**, **Pr(III)G6-Cl**, **La(III)G6-NO$_3$** and **Gd(III)G6-NO$_3$**. Among the four metallogels, **La(III)G6-Cl** and **La(III)G6-NO$_3$** are diamagnetic in nature because of zero unpaired electrons and rest of them, *i.e.* **Pr(III)G6-Cl** and **Gd(III)G6-NO$_3$** are paramagnetic in nature. Therefore, only the NMR spectra of **La(III)G6-Cl** and **La(III)G6-NO$_3$** have been recorded for detailed study. ^{1}H NMR spectroscopy indicates that the chemical shift values of -CH_2 group around 4.74 ppm of **G6** get shifted towards upfield with splitting into double of doublet at 4.40, 4.35, 4.32, 4.27 ppm for **La(III)G6-Cl** (Figure 6.10) and 4.31, 4.27, 4.23, 4.19 ppm for **La(III)G6-NO$_3$** (Figure 6.11).

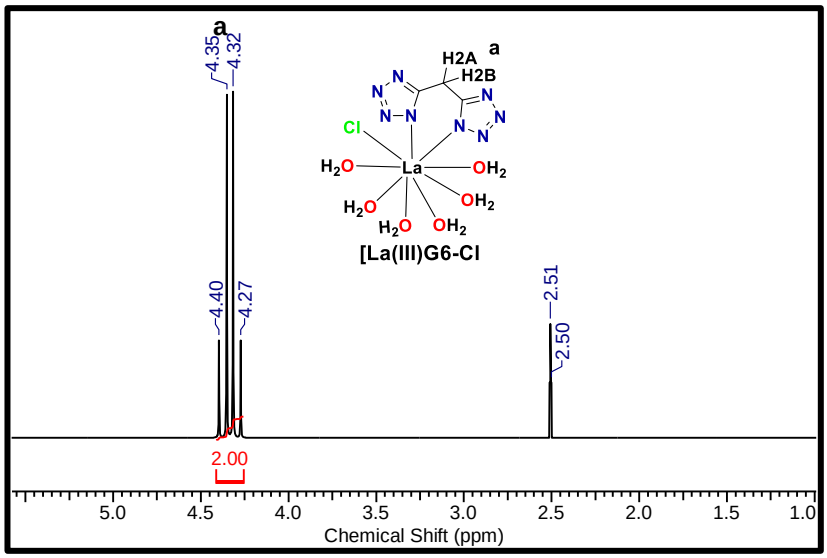

Figure 6.10. *^{1}H NMR spectrum of* ***La(III)G6-Cl*** *xerogel.*

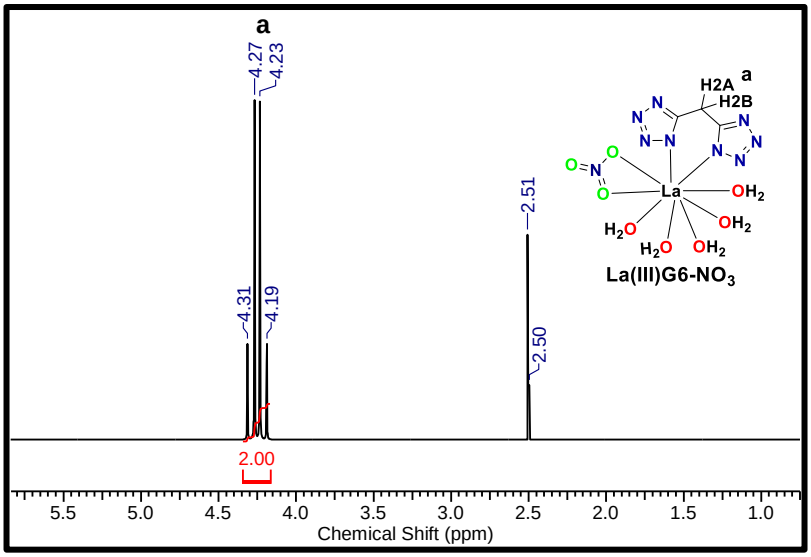

Figure 6.11. *^{1}H NMR spectrum of* ***La(III)G6-NO$_3$*** *xerogel.*

The splitting of peak from singlet to double doublet with shifting towards upfield may be due to different extent of involvement of CH_2 protons in intermolecular hydrogen bonding during gelation as well as different electronic environment around H2A and H2B proton of CH_2.[54] In case of ^{13}C NMR spectroscopic analysis, the carbon chemical shift values observed at 152.97 (-CN_4 group) and 19.45 ppm (-CH_2 group) of **G6** which have been shifted towards upfield region around 152.62 and 19.18 ppm for **La(III)G6-Cl (**Figure 6.12) and 152.19 and 18.97 ppm for **La(III)G6-NO$_3$** (Figure 6.13).

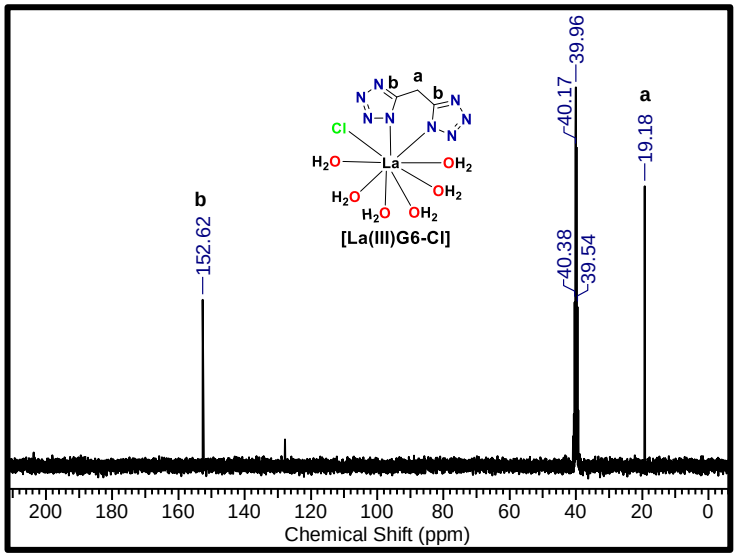

Figure 6.12. *^{13}C NMR spectrum of* ***La(III)G6-Cl*** *xerogel.*

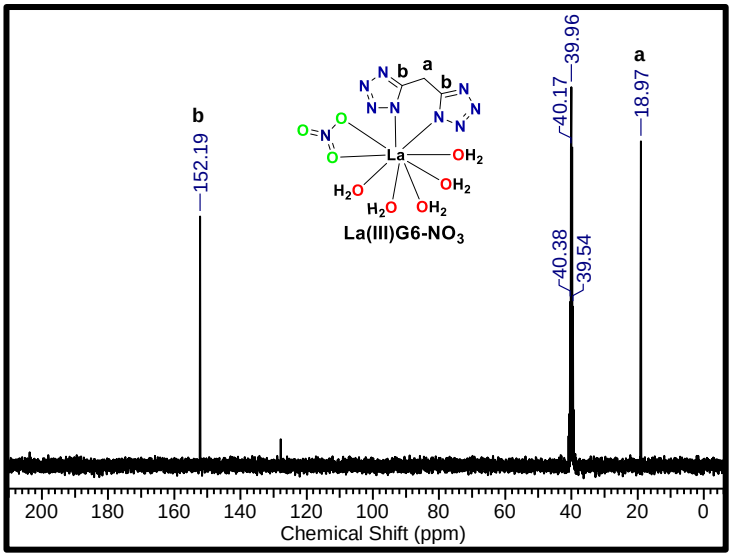

Figure 6.13. *^{13}C NMR spectrum of* ***La(III)G6-NO$_3$*** *xerogel.*

Further, FT–IR spectra of ligand **G6** and their metallogels (**La(III)G6-Cl**, **Pr(III)G6-Cl**, **La(III)G6-NO$_3$**, **Gd(III)G6-NO$_3$**) were recorded within the range of 3500–500 cm^{-1}. The C–H (CH_2 of Tetrazoles) stretching vibration at 3250 cm^{-1} for **G6** show characteristic downfield shifts in the region of 3212-3185 cm^{-1} after the formation of metallogels indicating hydrogen bond formation.[55] The IR band at 1638 cm^{-1} shifts towards the region of 1619-1610 cm^{-1} after the coordination of tetrazole N-atom to Ln^{3+} during metallogel formation.[56]

Further, the participation of non-covalent interaction has been predicted by recording the Powder XRD spectra for all the four metallogels (Figure 6.14). In PXRD spectra, peaks at 2θ = 35.14° corresponding to *d*-spacing value around 2.55 Å for **La(III)G6-Cl** , 2θ = 35.04° corresponding to *d*-spacing value at 2.56 Å for **Pr(III)G6-Cl** and **La(III)G6-NO$_3$** and 2θ = 35.42° corresponding to *d*-spacing value at 2.53 Å for **Gd(III)G6-NO$_3$** indicates participation of non-covalent interaction like hydrogen bonding between tetrazole NH proton and solvent molecules (H_2O and MeOH) which play the significant role during supramolecular self-assembly for formation of metallogels.[57]

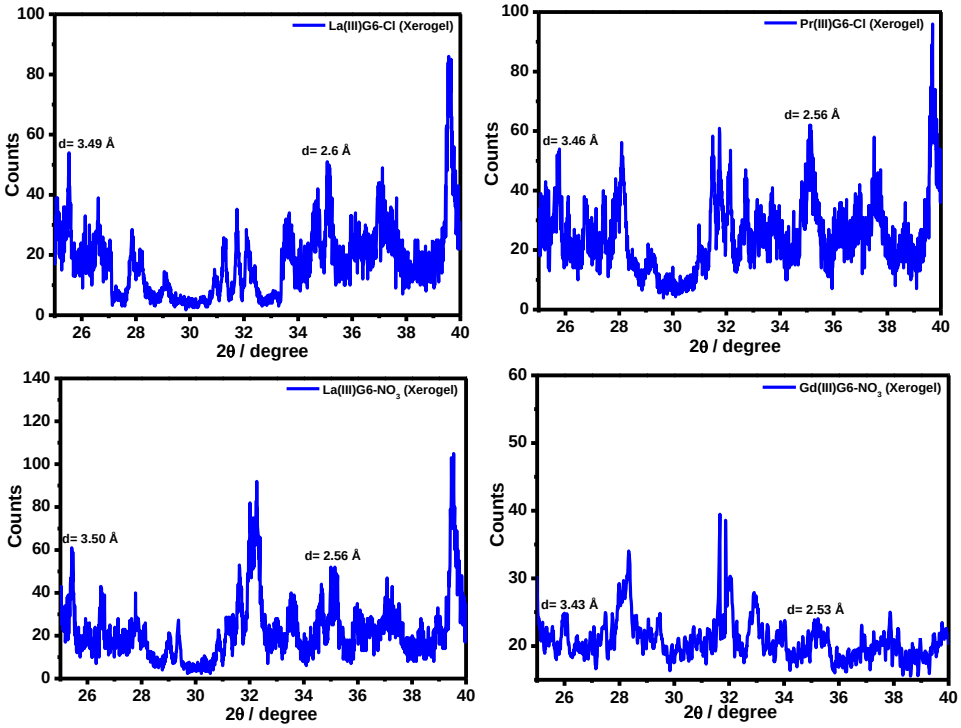

Figure 6.14. *Powder XRD spectra of xerogels of* ***La(III)G6-Cl***, ***Pr(III)G6-Cl***, ***La(III)G6-NO$_3$***, ***Gd(III)G6-NO$_3$***.

Furthermore, **La(III)G6-Cl** metallogel impressively show the ability to self-heal even after physical damage. For a clear understanding of self-healing nature, we cut the metallogel into blocks and place the fragmented part together in direct contact without giving any external stimuli. We observed the recombination of all the block of metallogel after some time (Figure 6.15).

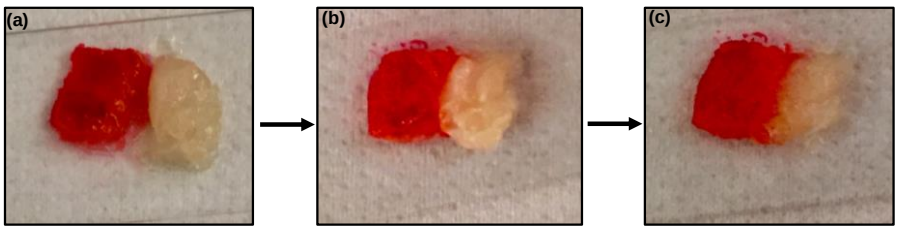

Figure 6.15a. *(a) Optical image dye-doped and dye undoped block of* ***La(III)G6-Cl*** *metallogel; (b) The block is put together; (c) optical image of* ***La(III)G6-Cl*** *metallogel indicates its self-healing ability.*

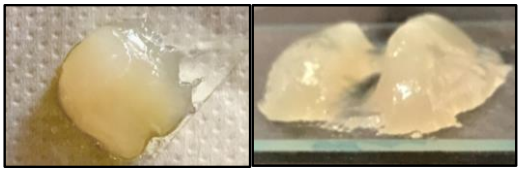

Figure 6.15b. *Self-healing property of* ***La(III)G6-Cl*** *metallogel.*

The mechanical strength and thixotropic properties of all the metallogels were estimated by rheological studies. It conclusively proves the elastic nature of gel, as average storage modulus (G') obtained around 3.5×10^4 Pa for **La(III)G6-Cl**, 1.3×10^5 Pa for **Pr(III)G6-Cl**, 5.3×10^4 Pa for **La(III)G6-NO$_3$**, 7.8×10^4 Pa for **Gd(III)G6-NO$_3$** is more than loss modulus (G''). The cross over point for the **Gd(III)G6-NO$_3$** at 46.7 Pa. However, there is no crossover point found for **La(III)G6-Cl**, **Pr(III)G6-Cl**, **La(III)G6-NO$_3$**. The shear stress for **La(III)G6-Cl**, **Pr(III)G6-Cl**, **La(III)G6-NO$_3$**, **Gd(III)G6-NO$_3$** have been found around 2.6×10^4, 1.2×10^5, 4.1×10^4 and 7.0×10^4 Pa during frequency sweep (Figure 6.16).

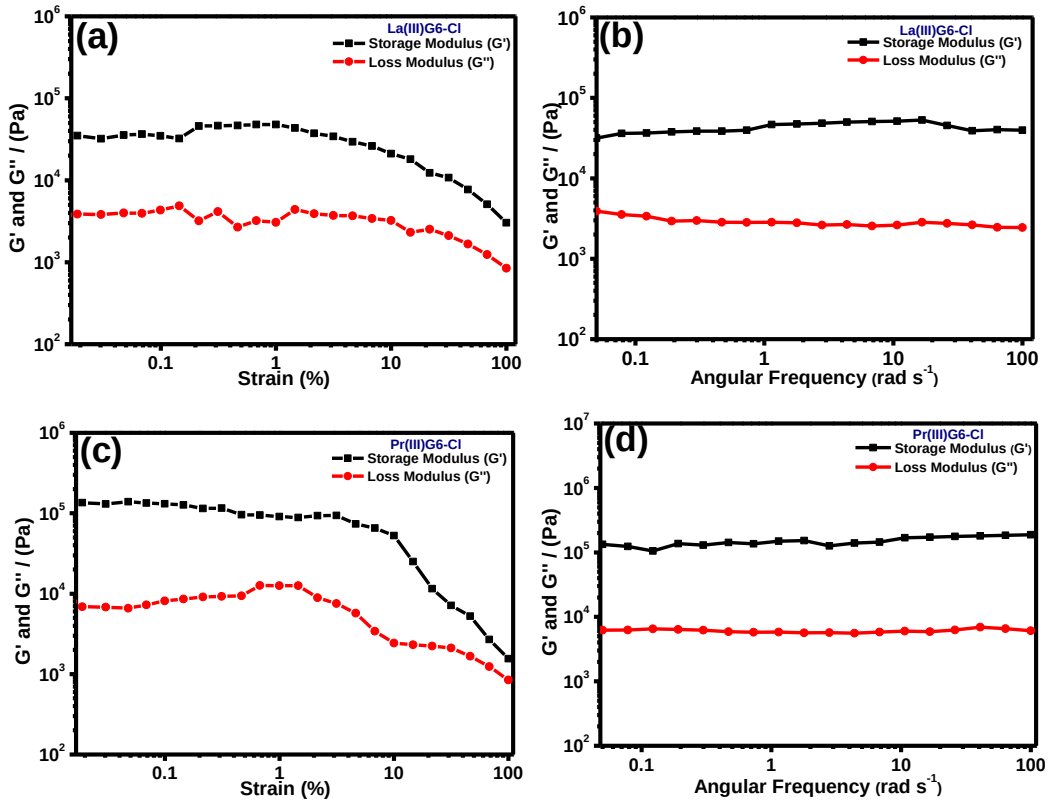

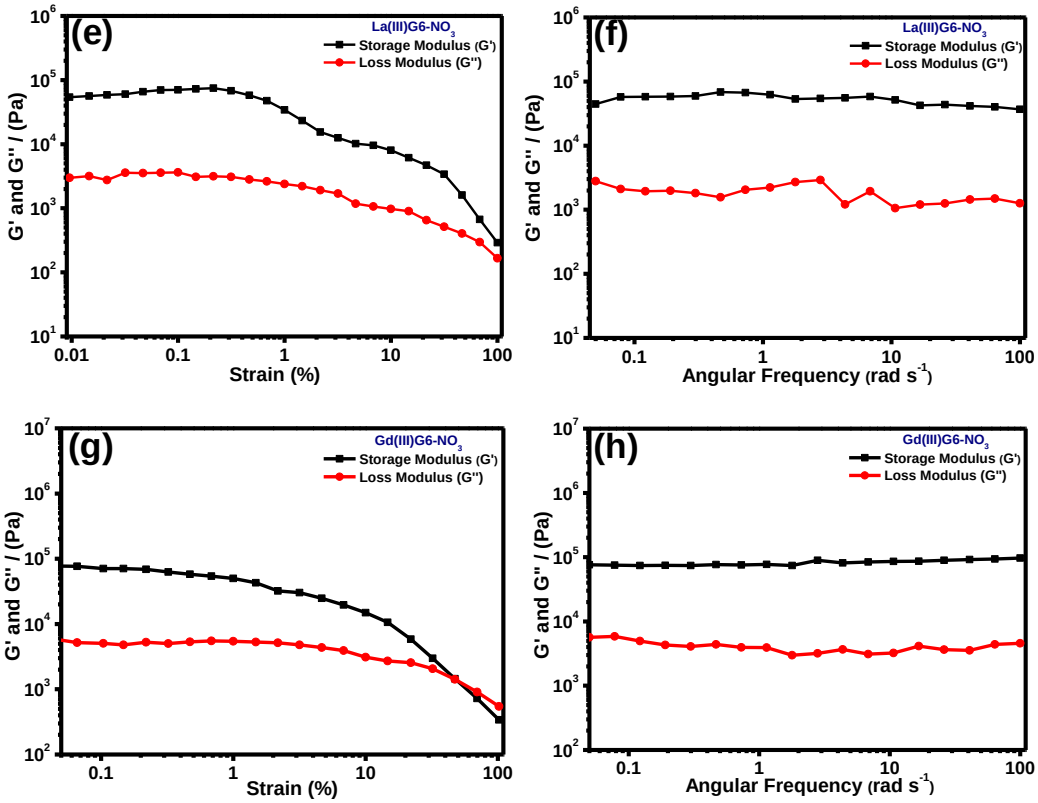

Figure 6.16. *(a), (c), (e), (g) are the Linear viscoelastic (LVE) of* ***La(III)G6-Cl***, ***Pr(III)G6-Cl***, ***La(III)G6-NO$_3$***, ***Gd(III)G6-NO$_3$*** *metallogels and (b), (d), (f), (h) are the Dynamic frequency sweep for* ***La(III)G6-Cl***, ***Pr(III)G6-Cl***, ***La(III)G6-NO$_3$***, ***Gd(III)G6-NO$_3$*** *metallogels.*

Rheological strain sweep experiments were done upon external strain at a constant angular frequency of 10 rad/sec to check the thixotropic nature of metallogels. **La(III)G6-Cl** metallogel only show self-healing ability (Figure 6.17). In step 1, **La(III)G6-Cl** metallogel were subjected below the deformation limit (at a low strain, γ = 0.5%). Storage moduli (G′) of **La(III)G6-Cl** metallogel are greater than their loss moduli (G″) indicating the cross-linked network in metallogel. In step 2, **La(III)G6-Cl** metallogel was subjected to a higher strain (γ = 50%), where the storage modulus (G′) decreased below the loss modulus (G″). These results indicate that the cross-linked networks of metallogel ruptured and turned into liquid-like sol state. In step 3, when a low strain (γ = 0.5% for **La(III)G6-Cl** metallogel) was applied for 120 sec, the

mechanical properties of the **La(III)G6-Cl** metallogel quickly recovered because of the reformation of 3D crosslinked networks. The periodic low/high strain was applied with an interval of 120 sec up to six cycles to ensure the self-healing nature of the **La(III)G6-Cl** metallogel. The recovery of the **La(III)G6-Cl** metallogel strength was apparently because of the formation of noncovalent interactions and metal-ligand interaction within the gelator molecules. The **La(III)G6-Cl** metallogel strength recovery time was short and recovered in 120 sec interval only.

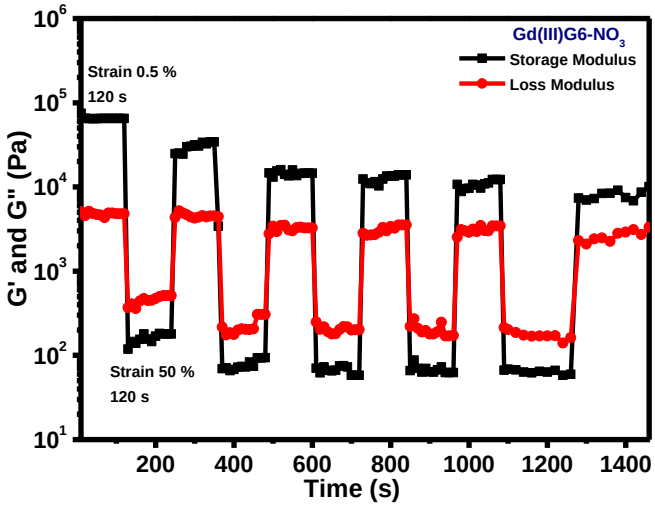

Figure 6.17. *Strain sweep experiments for* ***La(III)G6-Cl*** *metallogel.*

Further, the aggregate morphology of metallogels (**La(III)G6-Cl**, **Pr(III)G6-Cl**, **La(III)G6-NO3**, **Gd(III)G6-NO3**) have been confirmed by the FE-SEM technique (Figure 6.18).[58,59] The SEM image of metallogels have shown different morphologies *e.g.* thin needle-like morphology for **La(III)G6-Cl** metallogel, thick rod like morphology for **Pr(III)G6-Cl** metallogel, fiber-like morphology for **La(III)G6-NO3** metallogel and thick needle-like morphology for **Gd(III)G6-NO3** metallogel around 2 μm approximate length which indicates the aggregation after formation of metallogel.

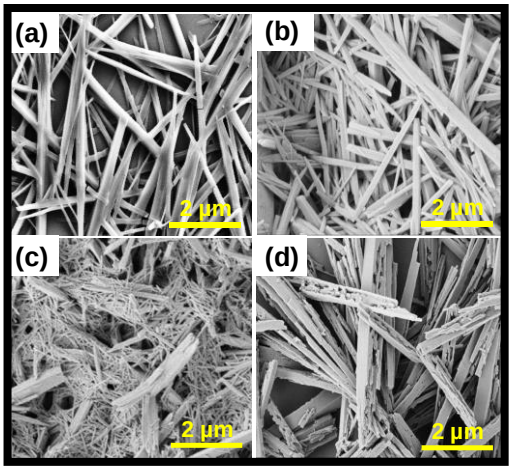

Figure 6.18. *FE-SEM images of metallogels (a)* ***La(III)G6-Cl****; (b)* ***Pr(III)G6-Cl****; (c)* ***La(III)G6-NO$_3$****; (d)* ***Gd(III)G6-NO$_3$****.*

6.4 Conclusions

The lanthanoids based metallogels *viz*. [**La(III)G6-Cl**, **La(III)G6-NO3**, **Pr(II)G6-Cl**, **Gd(III)G6-NO$_3$**] have been obtained by using di(1*H*-tetrazole-5-yl) methane (1,5-DTM) as gelator ligand (**G6**). All the metallogels have shown photoluminescence property due to AIEE during the formation of metallogels. Among all metallogels, **La(III)G6-Cl** metallogel has shown self-healing ability. Furthermore, beautiful crystals of **Gd(III)G6-NO$_3$** have been obtained from confined metallogel space, and its structure has been elucidated by SXRD.

6.5 References

[1] Draper E. R., Adams D. J. (2017), Low-molecular-weight gels: the state of the art, Chem., 3, 390-410 (DOI: 10.1016/j.chempr.2017.07.012)

[2] Sangeetha N.M., Maitra U. (2005), Supramolecular gels: Functions and uses. Chem. Soc. Rev., 34, 821-836 (DOI: 10.1039/B417081B)

[3] Estroff L. A., Hamilton A. D. (2004), Water gelation by small organic molecules, Chem. Rev., 104, 1201-1218 (DOI: 10.1021/cr0302049)

[4] Weiss R. G. (2014), The past, present, and future of molecular gels. What is the status of the field, and where is it going? J. Am. Chem. Soc., 136, 7519-7530 (DOI: 10.1021/ja503363v)

[5] Datta S., Bhattacharya S. (2015), Multifarious facets of sugar-derived molecular gels: Molecular features, mechanisms of self-assembly and emerging applications, Chem. Soc. Rev, 44, 5596-5637 (DOI: 10.1039/C5CS00093A)

[6] Zhang J., Su C.Y. (2013), Metal-organic gels: From discrete metallogelators to coordination polymers, Coord. Chem. Rev, 257, 1373-1408 (DOI: 10.1016/j.ccr.2013.01.005)

[7] Dastidar P., Ganguly S., Sarkar K. (2016), Metallogels from coordination complexes, organometallic, and coordination polymers, Chem. Asian J., 11, 2484-2498 (DOI:10.1002/asia.201600814)

[8] Tam A.Y.Y., Yam V.W.W. (2013), Recent advances in metallogels, Chem. Soc. Rev, 42, 1540-1567 (DOI: 10.1039/C2CS35354G)

[9] Miao W., Zhang L., Wang X., Cao H., Jin Q., Liu M. (2013), A dual functional metallogel of amphiphilic copper(II) quinolinol: Redox responsiveness and enantioselectivity, Chem. Eur. J, 19, 3029-3036 (DOI:10.1002/chem.201203401)

[10] Biswas A., Dubey M., Mukhopadhyay S., Kumar A., Pandey D. S. (2016), Anion triggered metallogels: demetalation and crystal growth inside the gel matrix and improvement in viscoelastic properties using Au-NPs, Soft Matter, 12, 2997-3003 (DOI: 10.1039/C5SM02464A)

[11] Ganta S., Chand D. K. (2017), Multi-stimuli-responsive metallogel molded from a Pd_2L_4-type coordination cage: selective removal of anionic dyes. Inorg. Chem., 57, 3634-3645 (DOI: 10.1021/acs.inorgchem.7b02239)

[12] Feldner T., Häring M., Saha S., Esquena J., Banerjee R., Díaz D. D. (2016), Supramolecular metallogel that imparts self-healing properties to other gel networks, Chem. Mater., 28, 3210-3217 (DOI: 10.1021/acs.chemmater.6b01144)

[13] Fang W., Zhang Y., Wu J., Liu C., Zhu H., Tu T. (2018), Recent advances in supramolecular gels and catalysis, Chem. Asian J., 13, 712-729 (DOI:10.1002/asia.201800017)

[14] Roh J., Vávrová K., Hrabálek A. (2012), Synthesis and functionalization of 5-substituted tetrazoles, Eur. J. Org. Chem, 31, 6101-6118 (DOI:10.1002/ejoc.201200469)

[15] Yan L., Gou S., Ye Z., Zhang S., Ma L. (2014), Self-healing and moldable material with the deformation recovery ability from self-assembled supramolecular metallogels, Chem. Commun., 50, 12847-12850 (DOI: 10.1039/C4CC06154C)

[16] Andrews P. C., Junk P. C., Massi M., Silberstein M. (2006), Gelation of La(III) cations promoted by 5-(2-pyridyl) tetrazole and water, Chem. Commun., 31, 3317-3319 (DOI: 10.1039/B605006A)

[17] Bünzli J. C. G., Andre N., Elhabiri M., Muller G., Piguet C. (2000), Trivalent lanthanide ions: versatile coordination centers with unique spectroscopic and magnetic properties, J. Alloys Compd., 303, 66-74 (DOI:10.1016/S0925-8388(00)00609-5)

[18] Kaczmarek M. T., Zabiszak M., Nowak M., Jastrzab R. (2018), Lanthanides: Schiff base complexes, applications in cancer diagnosis, therapy, and antibacterial activity, Coord. Chem. Rev., 370, 42-54 (DOI: 10.1016/j.ccr.2018.05.012)

[19] Bünzli J. C. G. (2006), Benefiting from the unique properties of lanthanide ions, Acc. chem. res, 39, 53-61 (DOI: 10.1021/ar0400894)

[20] Teo R. D., Termini J., Gray H.B. (2016), Lanthanides: applications in cancer diagnosis and therapy: Miniperspective, J. Med. Chem., 59, 6012-6024 (DOI: 10.1021/acs.jmedchem.5b01975)

[21] Aspinall H. C. (2002), Chiral lanthanide complexes: Coordination chemistry and applications, Chem. Rev., 102, 1807-1850 (DOI: 10.1021/cr010288q)

[22] Bethencourt M., Botana F. J., Calvino J. J., Marcos M., Rodriguez-Chacon M.A. (1998), Lanthanide compounds as environmentally-friendly corrosion inhibitors

of aluminium alloys: a review, Corros. Sci, 40, 1803-1819 (DOI:10.1016/S0010-938X(98)00077-8)

[23] Thompson K.H., Orvig C. (2006), Lanthanide compounds for therapeutic and diagnostic applications, Chem. Soc. Rev., 35, 499-499 (DOI: 10.1039/B606622B)

[24] Pagis C., Ferbinteanu M., Rothenberg G., Tanase S. (2016), Lanthanide-based metal organic frameworks: synthetic strategies and catalytic applications, ACS Catal., 6, 6063-6072 (DOI: 10.1021/acscatal.6b01935)

[25] Martínez-Calvo M., Kotova O., Möbius M. E., Bell A. P., McCabe T., Boland J. J., Gunnlaugsson T. (2015), Healable luminescent self-assembly supramolecular metallogels possessing lanthanide (Eu/Tb) dependent rheological and morphological properties, J. Am. Chem. Soc., 137, 1983-1992 (DOI: 10.1021/ja511799n)

[26] McCarney E. P., Byrne J. P., Twamley B., Martínez-Calvo M., Ryan G., Möbius M. E., Gunnlaugsson, T. (2015), Self-assembly formation of a healable lanthanide luminescent supramolecular metallogel from 2, 6-bis (1, 2, 3-triazol-4-yl) pyridine (btp) ligands, Chem. Commun., 51, 14123-14126 (DOI: 10.1039/C5CC03139G)

[27] Bradberry S. J., Savyasachi A. J., Peacock R. D., Gunnlaugsson T. (2015), Quantifying the formation of chiral luminescent lanthanide assemblies in an aqueous medium through chiroptical spectroscopy and generation of luminescent hydrogels, Faraday Discuss., 185, 413-431 (DOI: 10.1039/C5FD00105F)

[28] Chen P., Li Q., Grindy S., Holten-Andersen N. (2015), White-light-emitting lanthanide metallogels with tunable luminescence and reversible stimuli-responsive properties, J. Am. Chem. Soc., 137, 11590-11593 (DOI: 10.1021/jacs.5b07394)

[29] Wang T., Wang Z., Xie D., Wang C., Zhen X., Li Y., Yu X (2015), Ultrasound accelerated sugar-based gel for in situ construction of a Eu^{3+}-based metallogel

via energy transfer in a supramolecular scaffold, RSC Adv., 5, 107694-107699 (DOI: 10.1039/C5RA20661H)

[30] Yang H., Wang A., Zhang L., Zhou X., Yang G., Li Y., Zhang Y., Zhang B., Song J., Feng Y. (2017), Healable terpyridine-based supramolecular gels and the luminescent properties of the rare earth metal complex, New J. Chem., 41, 15173-15179 (DOI: 10.1039/C7NJ03175K)

[31] Ma X., Cui Y., Liu S., Wu J. (2017), A thermo-responsive supramolecular gel and its luminescence enhancement induced by rare earth Y^{3+}, Soft Matter, 13, 8027-8030 (DOI: 10.1039/C7SM01726J)

[32] Mahapatra T. S., Singh H., Maity A., Dey A., Pramanik S. K., Suresh E., Das A. (2018), White-light-emitting lanthanide and lanthanide-iridium doped supramolecular gels: modular luminescence and stimuli-responsive behavior, J. Mater. Chem C, 6, 9756-9766 (DOI: 10.1039/C8TC03487G)

[33] Guo M. Y., Zhang X., Zhao L., Li Y. K., Chen D. Y., Yang G. W., Li Q. Y (2018), Regulation of deprotonation of 3, 3-di (1H-tetrazol-5-yl) pentanedioic acid: Solvothermal synthesis of La(III) and heterometallic La(III)/Cu(II) compounds for ablation of A549 cells, J. Solid State Chem., 259,104-109 (DOI: 10.1016/j.jssc.2018.01.006)

[34] Zhan C. H., Wang F., Kang Y., Zhang J. (2011), Lanthanide-thiophene-2, 5-dicarboxylate frameworks: Ionothermal synthesis, helical structures, photoluminescent properties, and single-crystal-to-single-crystal guest exchange, Inorg. Chem., 51, 523-530 (DOI: 10.1021/ic201986m)

[35] Maas H., Currao A., Calzaferri G. (2002), Encapsulated lanthanides as luminescent materials, Angew. Chem. In. Ed., 41, 2495-2497 (DOI:10.1002/1521-3773(20020715)41)

[36] Feldner T., Häring M., Saha S., Esquena J., Banerjee R., Díaz D. D. (2016), Supramolecular metallogel that imparts self-healing properties to other gel networks, Chem. Mater, 28, 3210-3217 (DOI: 10.1021/acs.chemmater.6b01144)

[37] Hager M. D., Greil P., Leyens C., van der Zwaag, S., Schubert U. S. (2010), Self-healing materials, Adv. Mater., 22, 5424-5430 (DOI:10.1002/adma.201003036)

[38] Haering M., Díaz D. D. (2016), Supramolecular metallogels with bulk self-healing properties prepared by in situ metal complexation, Chem. Commun., 52, 13068-13081 (DOI: 10.1039/C6CC06533C)

[39] Foster J. A., Piepenbrock M. O. M., Lloyd G. O., Clarke N., Howard J. A., Steed J. W. (2010), Anion-switchable supramolecular gels for controlling pharmaceutical crystal growth, Nat. Chem., 2, 1037 (DOI:10.1038/nchem.859)

[40] Jiang Q., Ward M. D. (2014), Crystallization under nanoscale confinement, Chem. Soc. Rev, 43, 2066-2079 (DOI: 10.1039/C3CS60234F)

[41] Adams D. J., Morris K., Chen L., Serpell L. C., Bacsa J., Day G. M. (2010), The delicate balance between gelation and crystallisation: structural and computational investigations, Soft Matter, 6, 4144-4156 (DOI: 10.1039/C0SM00409J)

[42] Vidyasagar A., Sureshan K. M. (2015), Stoichiometric sensing to opt between gelation and crystallization, Angew. Chem. Int. Ed, 127, 12246-12250 (DOI:10.1002/anie.201506544)

[43] Fang W., Sun Z., Tu T. (2013), Novel supramolecular thixotropic metallohydrogels consisting of rare metal–organic nanoparticles: synthesis, characterization, and mechanism of aggregation, J. Phy. Chem. C, 117, 25185-25194 (DOI: 10.1021/jp409794a)

[44] Lloyd G. O., Steed J. W. (2011), Anion tuning of the rheology, morphology and gelation of a low molecular weight salt hydrogelator, Soft Matter, 7, 75-84 (DOI: 10.1039/C0SM00594K)

[45] Piepenbrock M. O. M., Clarke N., Steed J. W. (2009), Metal ion and anion-based "tuning" of a supramolecular metallogel, Langmuir, 25, 8451-8456 (DOI: 10.1021/la900145n)

[46] Wu H., Zheng J., Kjøniksen A. L., Wang W., Zhang Y., Ma J. (2019), Metallogels: availability, applicability, and advanceability, Adv. Mater., 1806204 (DOI:10.1002/adma.201806204)

[47] Aromí G., Barrios L. A., Roubeau O., Gamez P. (2011), Triazoles and tetrazoles: Prime ligands to generate remarkable coordination materials, Coord. Chem. Rev., 255, 485-546 (DOI: 10.1016/j.ccr.2010.10.038)

[48] Massi M., Stagni S., Ogden M. I. (2018), Lanthanoid tetrazole coordination complexes, Coord. Chem. Rev., 375, 164-172 (DOI: 10.1016/j.ccr.2017.11.017)

[49] Voitekhovich S. V., Wolf A., Guhrenz C., Lyakhov A. S., Ivashkevich L. S., Adam M., Gaponik N., Kaskel S., Eychmüller A. (2016), 5-(2-Mercaptoethyl)1H-tetrazole: Facile synthesis and application for the preparation of water soluble nanocrystals and their gels, Chem. Eur. J., 22, 14746-14752 (DOI:10.1002/chem.201602980)

[50] Meléndez R. E., Carr A. J., Linton B. R., Hamilton A. D. (2000), Controlling hydrogen bonding: From molecular recognition to organogelation, In molecular self-assembly organic versus inorganic approaches, Springer, Berlin, Heidelberg, 31-61.

[51] Yan X., Zhu P., Li J. (2010), Self-assembly and application of diphenylalanine-based nanostructures, Chem. Soc. Rev, 39, 1877-1890 (DOI: 10.1039/B915765B)

[52] Malviya N., Das M., Mandal P., Mukhopadhyay S. (2017), A smart organic gel template as metal cation and inorganic anion sensor, Soft Matter, 13, 6243-6249 (DOI:10.1039/C7SM01199G)

[53] Malviya N., Sonkar C., Kundu B. K., Mukhopadhyay S. (2018), Discotic organic gelators in ion sensing, metallogel formation and bioinspired catalysis, Langmuir, 34, 11575-11585 (DOI: 10.1021/acs.langmuir.8b02352)

[54] Liu D., Liu H., Song B., Chen M., Huang J., Wang J., Yang X., Sun W., Li X., Wang P. (2018), Terpyridine-based metallo-organic cages and supramolecular gelation by coordination-driven self-assembly and host-guest interaction, Dalton Trans., 47, 14227-14232 (DOI: 10.1039/C8DT01044G)

[55] Freis M., Klapötke T. M., Stierstorfer J., Szimhardt N. (2017), Di(1H-tetrazol-5-yl) methane as neutral ligand in energetic transition metal complexes, Inorg. Chem., 56, 7936-7947 (DOI: 10.1021/acs.inorgchem.7b00432)

[56] Mal S., Pietraszkiewicz M., Pietraszkiewicz O. (2018), Luminescent studies of binuclear ternary europium(III) pyridineoxide tetrazolate complexes containing bis-phosphine oxide as auxiliary co-ligands, Luminescence, 33, 370-375 (DOI:10.1002/bio.3423)

[57] Segarra-Maset M. D., Nebot V. J., Miravet J. F., Escuder B. (2013), Control of molecular gelation by chemical stimuli, Chem. Soc. Rev., 42, 7086-7098 (DOI: 10.1039/C2CS35436E)

[58] Mears L. L., Draper E. R., Castilla A. M., Su H., Dietrich B., Nolan M. C., Smith G. N., Doutch J., Rogers S., Akhtar R., Cui H. (2017), Drying affects the fiber network in low molecular weight hydrogels, Biomacromolecules, 18, 3531-3540 (DOI: 10.1021/acs.biomac.7b00823)

[59] Adams D. J. (2018), Does drying affect gel networks?, Gels, 4, 32 (DOI:10.3390/gels4020032)

Chapter 7

Nickel tetrazolato complexes synthesized by microwave irradiation: Catecholase like activity and interaction with biomolecules

Chapter 7

Nickel tetrazolato complexes synthesized by microwave irradiation: Catecholase like activity and interaction with biomolecules

7.1 Introduction

Metal-ligated azide ions provide an approach to synthesize tetrazole-based complexes by [2+3] cycloaddition of azide and organonitriles. [1-5] Synthesized complexes are obtained mostly via solvothermal methods [6-9] with little control over the reactivity and many times it generates insoluble metal-organic frameworks (MOFs) with possible applicability in gas absorption [10] and organic catalytic reactions [11-13] as the stability of the compounds provides an extra advantage. This chapter presents the synthesis and characterization of two new nickel–tetrazolato complexes *viz.* [NiL(5-phenyltetrazolato)] (**1**) and [NiL{5-(4-pyridyl)-tetrazolato}] (**2**) [HL = 3-(2-diethylamino-ethylimino)-1-phenyl-butan-1-one]. The synthesized compounds have interesting serum albumin protein binding and catechol oxidation ability.

7.2 Experimental section

7.2.1 Material and method

All the required chemicals were purchased from Sigma and SRL India and used without further purification. Elemental analyses were carried out with a Thermo Flash 2000 elemental analyzer.

The other specifications of all the instruments used for analysis purpose were same as described in the section 2.2.1 of the chapter 2 and section 6.2.1 of chapter 6. HL and [NiL(N_3)] were prepared according to reported methods. [14]

7.2.2 Synthesis of [NiL(5-phenyltetrazolato)] (1)

A solution of [NiL(N_3)] (0.11 g, 0.41 mmol) and benzonitrile (4 mL, 40 mmol) in DMF (5 mL) was added to a cylindrical Pyrex tube which was then placed in the focused microwave reactor. The system was left under irradiation for 2 h at 130 °C where upon the solution is filtered out. The filtrate was diffused with diethyl ether to obtain dark red crystalline compounds along with X-ray diffraction quality crystals. Yield 60%. ^{1}H NMR (400 MHz, 298 K, DMSO-d_6): δ = 8.16-7.42 (m, 10H), 5.72 (s, 1H), 3.24 (m, 8H), 2.08 (s, 2H), 1.24 (t, 6H). ^{13}C NMR (100 MHz, 293 K, DMSO-d_6): δ = 184.57, 164.86, 163.98, 133.83, 132.7, 129.97, 129.23, 128.61, 126.94, 119.32, 111.79, 79.94, 46.93, 33.45, 18.69, 12.22. Anal Calcd. for $C_{23}H_{28}N_6NiO$ (%): C, 59.64; H, 6.09; N, 18.14. Found: C, 59.04; H, 6.21; N 17.99%. FT-IR (KBr): ν = 2924, 1637 cm^{-1}; MS(ESI): *m/z* = 487.7 [NiL(5-phenyltetrazolato) + Na]$^+$ (in positive mode).

7.2.3 Synthesis of [NiL{5-(4-pyridyl)-tetrazolato}] (2)

About 0.11 g (0.41 mmol) of [NiL(N_3)] and 0.11 g (1.2 mmol) of 4-cyanopyridine was taken in 5 mL of DMF in a cylindrical Pyrex tube which was then placed in the focused microwave reactor. The system was irradiated in a microwave reactor for 2 h at 130 °C where upon the solution was filtered. The filtrate was diffused with diethyl ether to obtain dark red crystalline compounds along with some X-ray diffraction quality crystals. Yield 70%. ^{1}H NMR (400 MHz, 298 K, DMSO-d_6): δ = 8.75 (d, 2H), 7.99-7.33 (m, 7H), 5.73 (s, 1H), 4.37 (s, 2H), 3.10 (m, 6H), 2.07 (s, 1H), 1.15 (s, 2H), 1.07 (t, 6H). ^{13}C NMR (100.61 MHz, 293 K, DMSO-d_6): δ = 184.87, 164.18, 163.50, 151.56, 133.83, 132.70, 129.97, 126.94, 119.14, 111.65, 79.96, 46.93, 33.45, 18.52, 12.08. Anal Calcd for $C_{22}H_{29}N_7NiO$ (%): C, 56.92; H, 5.86; N, 21.12. Found: C, 56.34; H, 5.83; N, 21.43%. FT-IR (KBr): ν = 2925, 1627 cm^{-1}, MS(ESI): *m/z* = 464.5 [NiL(5-phenyltetrazolato) + H]$^+$ (in positive mode).

7.2.4 X-ray crystallography

A red block-like specimen $C_{23}H_{28}N_6NiO$ of **1** with approximate dimensions of 0.100mm×0.180mm×0.280 mm was used for X-ray crystallographic analysis. The crystallographic study have been same as described in the section 4.2.6 of chapter 4.The final cell constants of a = 13.6095(5) Å, b = 9.7612(3) Å, c = 16.9790(6) Å, α = 90°, β = 101.2555(15)°, γ = 90° and volume = 2212.19(13) $Å^3$ are based upon the refinement of the XYZ centroids of 4370 reflections above 20 σ(I) with 4.837° < 2θ < 53.03°. For **2**, a red block-like specimen of $C_{22}H_{27}N_7NiO$, approximate dimensions 0.140 mm×0.280 mm×0.360 mm, was used for X-ray crystallographic analysis. The crystals were mounted onto quartz fibers, and the X-ray diffraction intensity data were measured in a similar way as described for **1**. The final cell constants of a = 9.5652(2) Å, b = 9.8556(3) Å, c = 12.5580(3) Å, α = 71.0853(15)°, β = 78.5024(14)°, γ = 80.4849(15)° and volume = 1090.96(5) $Å^3$ are based upon the refinement of the XYZ-centroids of 9914 reflections above 20 σ(I) with 4.708° < 2θ < 61.13°. Crystal data, data collection parameters, and refinement data have been calculated.

7.2.5 Protein binding study

Binding interaction of **1** and **2** with BSA and HSA was carried out using standard Trp fluorescence by excitation at 295 nm and monitoring the corresponding emission at 340 nm using a Fluoromax-4p spectrofluorometer from Horiba JobinYvon (Model: FM-100) with a rectangular quartz cuvette of 1 cm path length. A buffered stock solution of BSA and HAS protein in Tris-HCl (pH 7.4) was used. Concentrated stock solutions of **1** and **2** were prepared by dissolving them separately in Tris-HCl buffer to get required concentrations. An aqueous solution (2 mL) of BSA or HSA (10 μM) was titrated by successive addition of complexes (0 to 100 μM) which was monitored by measuring the increment of the absorption band at 278 nm in UV-vis spectroscopy.

7.2.6 Catecholase activity

3,5-Ditertbutylcatechol (3,5-DTBC) was used to monitor the catecholase activity of the complexes. A 10^{-4} M solution of complex was treated separately with 100 equivalents of

3,5-DTBC in methanol under aerobic conditions. Absorbance of resultant solution was plotted against wavelength (300 to 500 nm) in a regular interval of 10 min. The dependence of rate on various concentration and different kinetic parameters were obtained by treatment of a 10^{-4} M solution of complexes with 25 to 200 equivalent of the substrate and monitoring the upsurge in absorption at 402 nm as a function of time in 30 min intervals. The peak at 402 nm indicates the formation of oxidized product *viz.* quinone.

7.2.7 Detection of hydrogen peroxide in the catalytic reactions

The reaction between ferrous sulfate and 1,10-phenanthroline, which formed a red-orange Fe^{2+}-tris-phenanthroline complex that absorbed at 509 nm was followed to detect the formation of hydrogen peroxide during the catalytic reaction.[15] A 1:3 ratio between Fe^{2+} and 1,10-phenanthroline was used for the experiment. When an equal amount of 10^{-3} (M) solution of **1** and **2** were mixed separately with $FeSO_4$ and 1,10-phenanthroline, there is the formation of an absorption band at 509 nm in the UV-visible spectrum indicating the formation of $[Fe(phen)_3]^{2+}$. With the addition of an equal amount of DTBC to the above solution, the intensity of the band at 509 nm decreases after 10 min. When the reaction mixture was kept for 25 min, there was no absorption band observed at 509 nm, which clearly indicates that all the ferrous ions have been converted to ferric ions due to the formation of H_2O_2 in the reaction mixture.

7.2.8 Supplementary materials

CCDC 1483307 and 1483308 contain the supplementary crystallographic data for **1** and **2,** respectively. These data can be obtained free of charge via http://www.ccdc.cam.ac.uk/conts/retrieving.html, or from the Cambridge Crystallographic Data Centre, 12 Union Road, Cambridge CB2 1EZ, UK; fax: (+44) 1223-336-033; or e-mail: deposit@ccdc.cam.ac.uk.

7.3 Results and discussion

Synthesis and characterization. **HL** was prepared according to the reported method by refluxing equimolar 1-phenyl-1,3-butanedione (0.81 g, 5 mmol) and *N*,*N*-diethylethylenediamine (0.711 mL, 5 mmol) in 30 mL of methanol for half an hour.[14] The resulting mixture gave a yellow solution containing tridentate HL. This methanolic solution was evaporated to dryness to obtain a yellow oil which was used without further purification. Complexes [NiL(N_3)] were also prepared as per the reported method.[14] Both the tetrazolato complexes were prepared by [2+3] dipolar cycloaddition of nickel-ligated azide and benzonitrile and 4-cyanopyridine, respectively, (scheme 7.1). For **1**, a reaction using benzonitrile as a solvent gave a low yield of the product. So, in both cases, DMF was used as solvent and diffusion of diethyl ether in filtered solution produced wine red crystalline compounds [NiL(5-phenyltetrazolato)] (**1**) and [NiL{5-(4-pyridyl)-tetrazolato}] (**2**), respectively. Both complexes have been characterized by elemental analyses, IR, ESI-MS spectroscopy, and single-crystal X-ray crystallography. Two hours of microwave irradiation were found to be required at 130 °C for complete reactions. The formation of product as confirmed by the disappearance of azide stretching band at 2043 cm^{-1}. A new band appears at 1627–1637 cm^{-1}, indicating the formation of tetrazolato (Figure 7.1 and 7.2).[16] The ESI-MS spectra of **1** show molecular ion peak of [NiL(5-phenyltetrazolato)+Na]$^+$ at 487.7 (Figure 7.3); **2** has a peak at 464.5 as [NiL(5-phenyltetrazolato)+H]$^+$ (Figure 7.4).

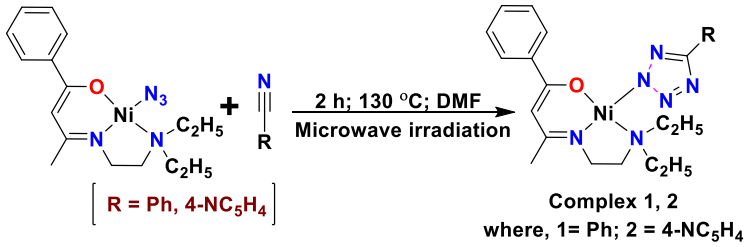

Scheme 7.1. *Synthesis of complexes **1** and **2**.*

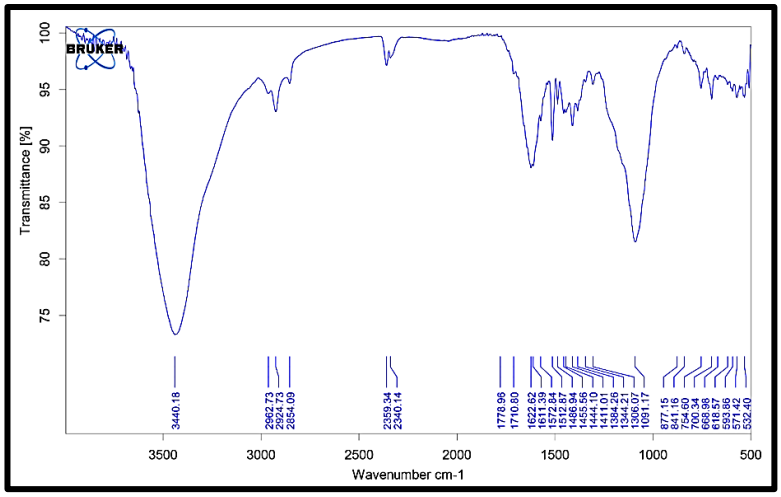

Figure 7.1. *FT-IR of complexes* ***1****.*

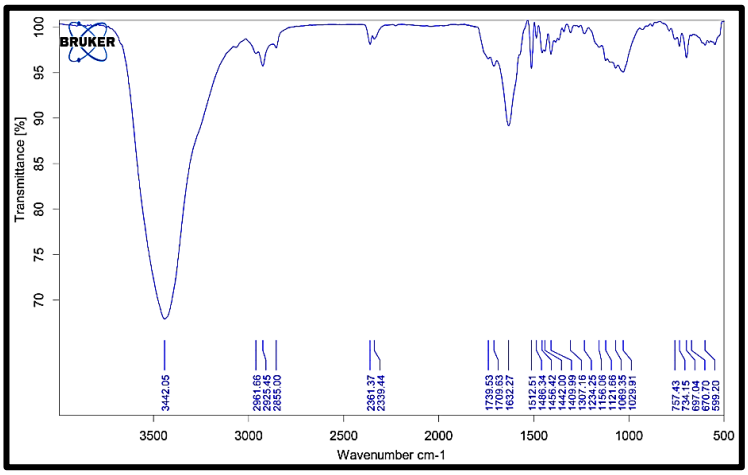

Figure 7.2. *FT-IR of complexes* ***2****.*

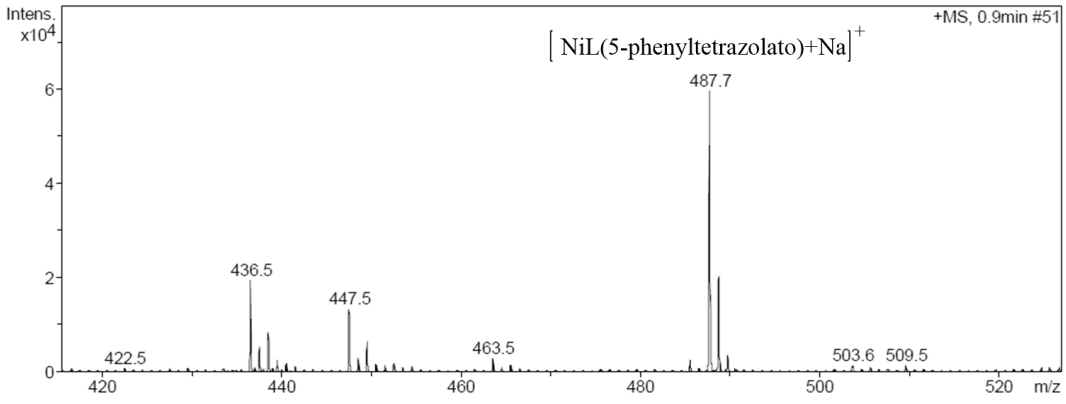

Figure 7.3. *ESI-Mass spectrum of complexes* ***1****.*

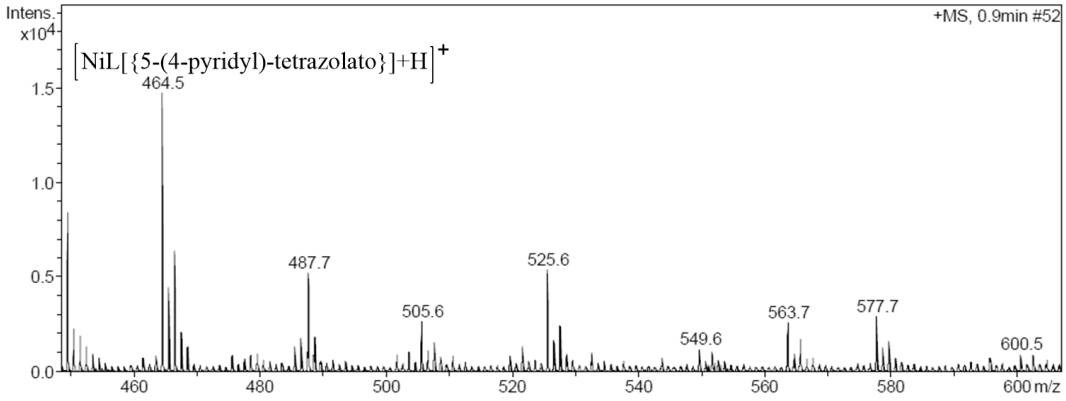

Figure 7.4. *ESI-Mass spectrum of complexes **2**.*

Description of the solid-state structures of 1 and 2. Complex **1** is monomeric and crystallizes in the monoclinic space group P21/n with the square planar environment surrounding the nickel ion (Figure 7.5). HL is tridentate while one tetrazolato group completes the square base. The tetrazolato moiety is attached to nickel through N2-atom. The bond lengths between Ni and N/O-donor centers are within the range of 1.83-1.95 Å, quite similar to those which have been reported.[17] The average coordination bond angles around Ni are around 91.42° (table 7.1). The dihedral angle between phenyl and tetrazolato ring was 8.47°. Hydrogen bond interaction between two adjacent molecules provides a dimeric structure through C14-H14B···O1 and C13-H13B···N6 (Figure 7.5). Complex **2** crystallizes in the triclinic space group P-1. The geometry surrounding nickel is identical to that of 1 (Figure 7.6). The metal-ligand bond distance was between 1.83 and 1.96 Å, the average bond angle is almost 90° (table 7.1), and the dihedral angle between tetrazolato and phenyl ring was 5.2°. Similar hydrogen bonding interactions like **1** are also observed in this structure, giving dimers of the molecules by weak interactions (Figure 7.6).

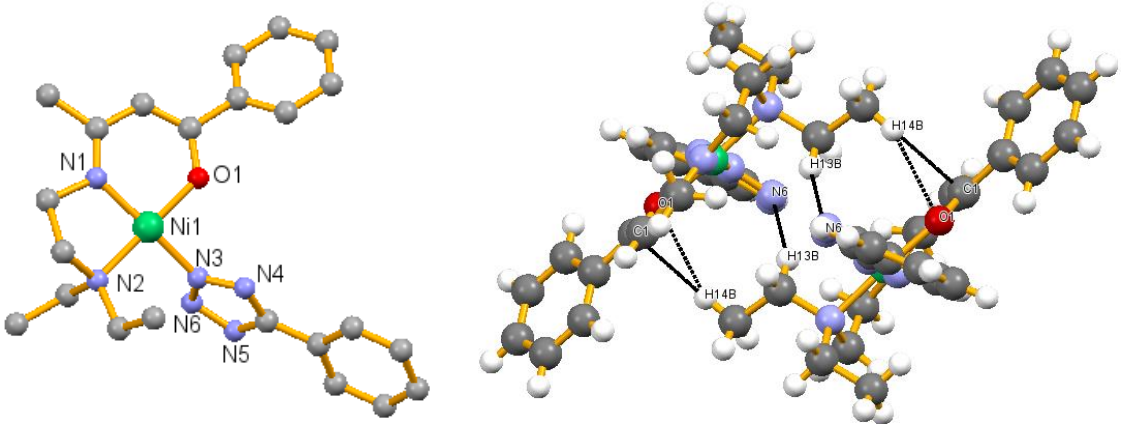

Figure 7.5. *Single crystal structure and hydrogen bonded dimeric structure of complexes* ***1****.*

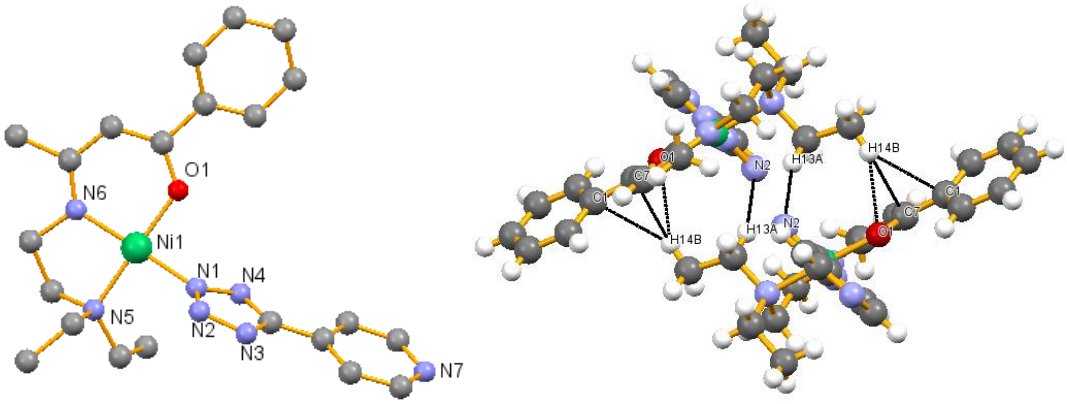

Figure 7.6. *Single crystal structure and hydrogen bonded dimeric structure of complexes* ***2****.*

Table 7.1*. Bond lengths (Å) and bond angles (°) data of complex* ***1*** *and complex* ***2****.*

Complex 1			**Complex 2**	
Bond lengths			**Bond lengths**	
1	N1-Ni1	1.858(2)	N1-Ni1	1.908(1)
2	O1-Ni1	1.836(2)	N6Ni1	1.862(1)
3	N3-Ni1	1.900(2)	N5Ni1	1.958(1)
4	N2-Ni1	1.952(2)	O1Ni1	1.8368(8)

Bond angles			Bond angles	
1	O1--Ni1...N3	85.82(8)	O1--Ni1...N6	94.73(4)
2	N1--Ni1...O1	94.59(8)	N1--Ni1...O1	86.28(4)
3	N1--Ni1...N2	86.44(8)	N1--Ni1...N5	92.88(5)
4	N3--Ni1...N2	93.57(8)	N5--Ni1...N6	86.24(5)
5	N2--Ni1...O1	176.96(8)	N5--Ni1...O1	178.57(4)
6	N1--Ni1...N3	171.72(9)	N1--Ni1...N6	173.34(5)

Electronic spectra and photophysical study. The electronic spectra of these compounds were recorded in methanol. Complex **1** and **2** show bands as shoulders at 425 and 427 nm, respectively, which correspond to the d-d transition in square planar Ni(II) complex (Figures 7.7). One ligand to metal charge transfer peak is observed at 355 and 356 nm, respectively, for **1** and **2** as reported elsewhere for transition metal complexes with Schiff base ligands.[18]

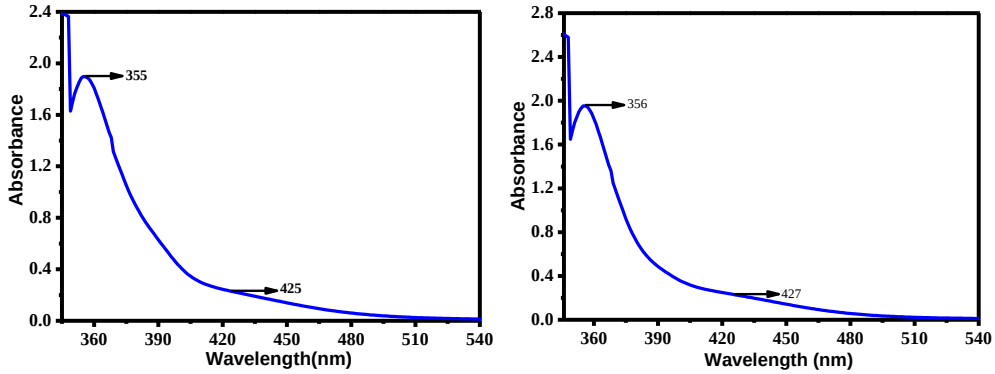

Figure 7.7. *UV-vis absorption spectra for complex **1** and **2**.*

The emission spectral study of the complexes in methanol shows an emission band at 430 and 434 nm for **1** and **2**, respectively, upon excitation at 365 nm. The excited state means lifetimes were 1.19 and 8.90 ns, respectively, at room temperature (table 7.2) (Figure 7.8 and 7.9). This phenomenon can be attributed to the intra-ligand fluorescent 1($\pi \rightarrow \pi^*$) emission of the coordinated ligand.[19]

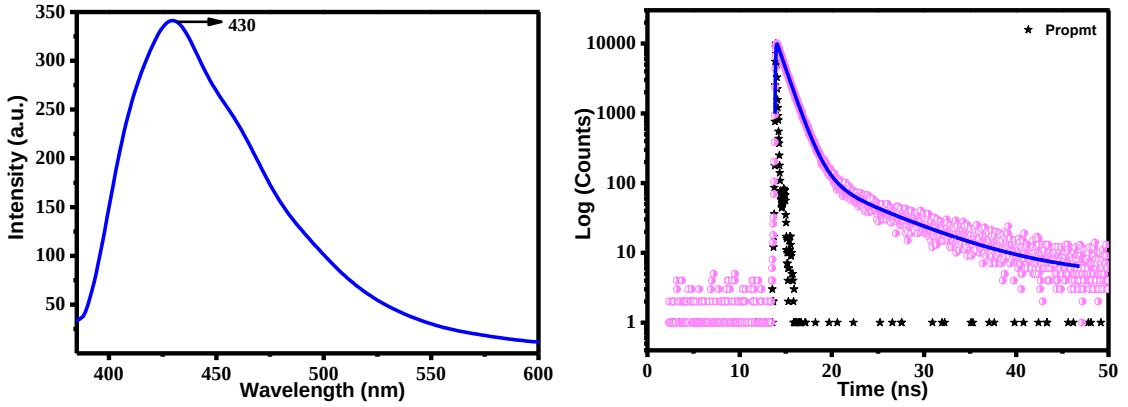

Figure 7.8. *Photoluminescence spectrum (left) and time-resolved photoluminescence decay profile (right) for Complex* ***1****.*

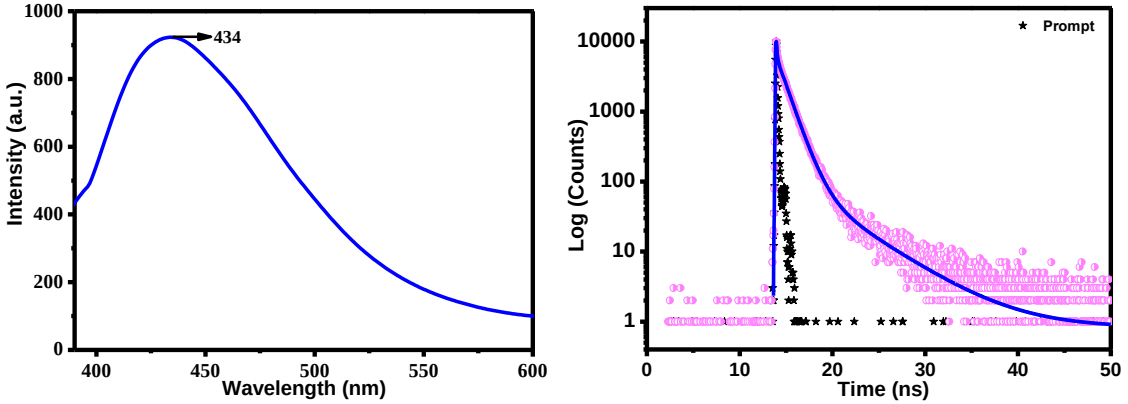

Figure 7.9. *Photoluminescence spectrum (left) and time-resolved photoluminescence decay profile (right) for Complex* ***2****.*

Table 7.2. *Photoluminescence decay parameters of complex* ***1*** *and complex* ***2****.*

System	τ_1 (ns)	a_1	τ_2 (ns)	a_2	$\langle\tau_2\rangle$ (ns)	χ^2
Complex 1	1.09	0.98	7.26	0.02	1.19	1.08
Complex 2	2.37	0.94	1.09	0.06	8.9	1.02

Interactions of complexes with serum albumins by fluorescence quenching study. Binding of prospective molecules to blood plasma is important as transport of drugs happens through the bloodstream after binding with the albumin proteins.[20] To study the

interaction of the synthesized compounds with blood plasma proteins, the quenching of intrinsic fluorescence of the proteins has been monitored. The fluorescence property of BSA is attributed due to tryptophan, tyrosine, and phenyl alanine residues.[20] The fluorescence spectra of **1** and **2** with BSA indicate there is a progressive decrease in the fluorescence intensity accompanied by a significant redshift (Figure 7.10, 7.11).

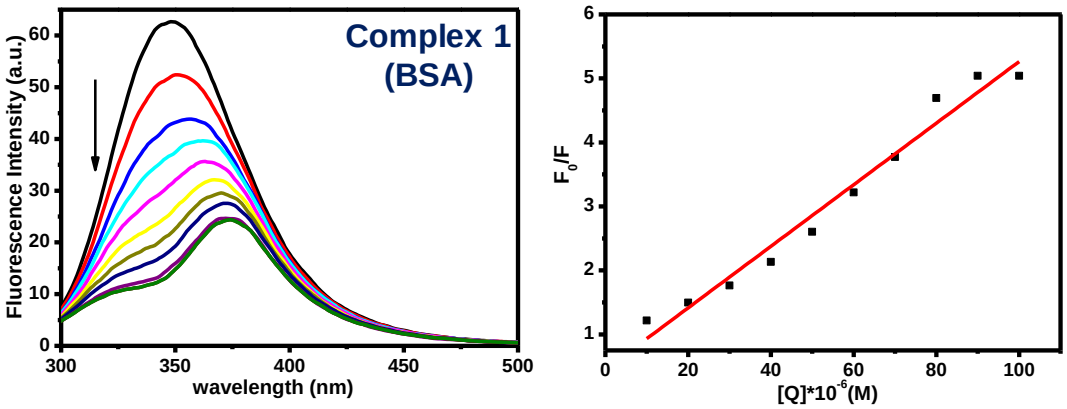

Figure 7.10. *Fluorescence quenching of BSA by complex **1**. The Stern-Volmer plot is show in inset.*

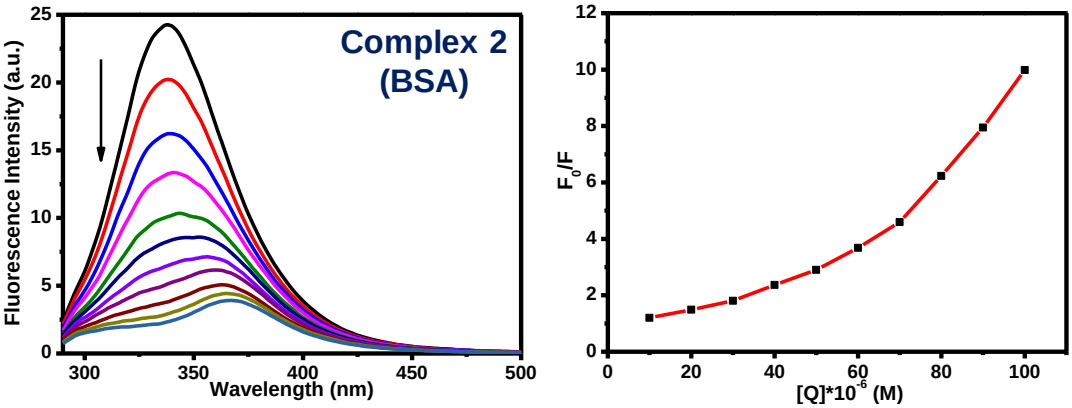

Figure 7.11. *Fluorescence quenching of BSA by complex **2**. The Stern-Volmer plot is shown in the inset.*

Probable energy transfer from indole unit of tryptophan to protein-bound compound may have induced the shift of emission maxima toward lower energy. Analysis of Stern-Volmer plot[21] based on bimolecular quenching rate constant and average time of fluorophore provides more insight into the protein binding. The relationship is given by,

$$\frac{F_0}{F} = 1 + k_q \tau_0 [Q] = 1 + K_{SV}[Q]$$

where F_0 and F are the fluorescence intensities in the absence and presence of a quencher, k_q is the bimolecular quenching rate constant, τ_0 is the average lifetime of fluorophore in the absence of a quencher, and [Q] is the concentration of quencher (metal complexes). A plot of log [F_0-F/F] versus log[Q] provides an upward curve concave toward the y-axis indicating two-way quenching by collision as well as by complex formation with the same quencher. The K_{sv} and k_q values obtained from the curve were 10^4 M^{-1} and 10^{12} $M^{-1}S^{-1}$, indicating the possible role of static quenching and strong binding between BSA and **1** and **2**.[22]

A similar trend is also observable for binding complexes with HSA. The intensity of the fluorescent band is decreased to 5–15% for **1** and **2**, respectively, of its initial intensity, indicating the formation of a stable ground state complex (Figure 7.12, 7.13).

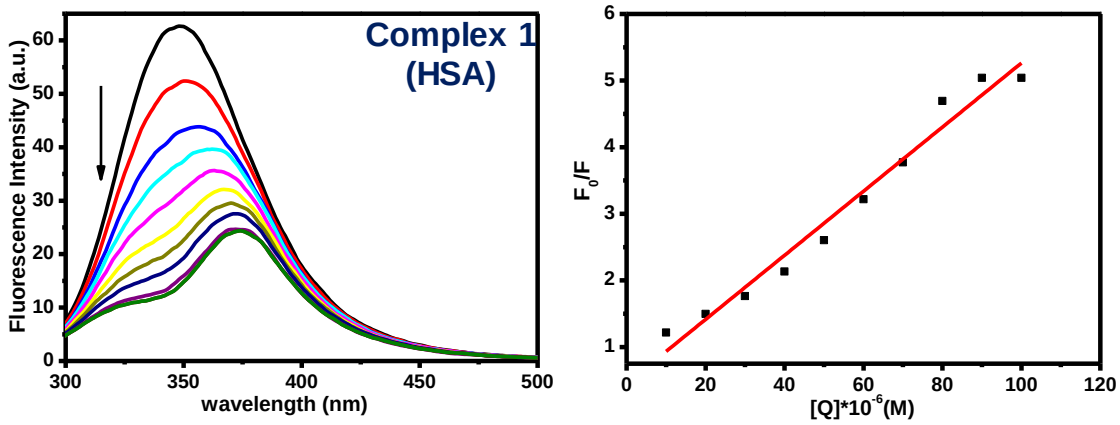

Figure 7.12. *Fluorescence quenching of HSA by complex **1**. The Stern-Volmer plot is show in inset.*

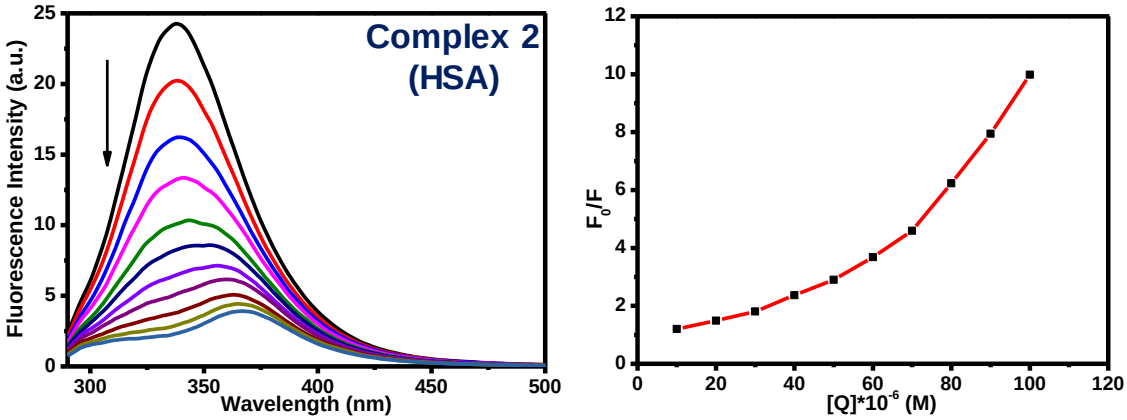

Figure 7.13. *Fluorescence quenching of HSA by complex **2**. The Stern-Volmer plot is shown in the inset.*

The Stern-Volmer plots at lower concentration have linearity; however, at higher concentration an upward bending toward F_0/F axis is observed. To determine the binding constant and number of binding sites, a Scatchard equation was employed which is given by,

$$\log\left[\frac{F_0 - F}{F}\right] = \log K_a + n \log[Q]$$

where K_a and n are the binding constant and number of binding sites, respectively, and F_0 and F are the fluorescence intensities in the absence and presence of the quencher, respectively. A plot of $\log(F_0\text{-}F)/F$ versus log[Q] is used to determine the value of binding constant (from intercept) and number of binding sites (from slope). Calculation shows that the binding constant for HSA complexes is 10^5 $M^{-1,}$ and the n value was found to be around one. All the relevant data are summarized in table 7.3.

Table 7.3. *Stern-Volmer quenching constants, binding constants, and binding sites.*

System	K_{sv} (M^{-1})	K_q (M^{-1})	K_a (M^{-1})	n
Complex-1 (BSA)	4.0×10^5	6.5×10^{12}	1.016×10^6	1.342
Complex-2 (BSA)	6.6×10^5	1.0×10^{12}	2.88×10^7	1.652
Complex-1 (HSA)	3.2×10^5	5.2×10^{12}	2.24×10^5	1.220
Complex-2 (HSA)	92324.980	14939.31×10^9	2.29×10^{-5}	0.632

Catecholase activity study. We were tempted to explore the catecholase oxidation reaction utilizing the synthesized complexes as a probable catalyst as no such studies have been reported with tetrazolato complexes. To evaluate the catecholase activity of the synthesized complexes, 3,5-di-tert-butylcatechol (3,5-DTBC) (Scheme 7.2) was taken as the substrate as it shows a low quinone–catechol reduction potential.

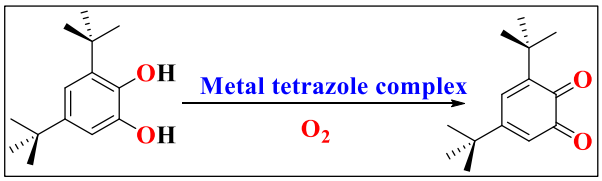

Scheme 7.2. *General representation for the oxidation of catechol into quinone.*

The reactions were carried out under aerobic conditions and monitored by UV–vis spectroscopy. In an experimental setup, 10^{-5} M solutions of the complexes were prepared in methanol and treated with 100 equiv. of 3,5-DTBC. After addition of the substrate into the complex, a new band gradually starts to appear at 400 nm with time due to the formation of the oxidized product 3,5-DTBQ (Figures 7.14).

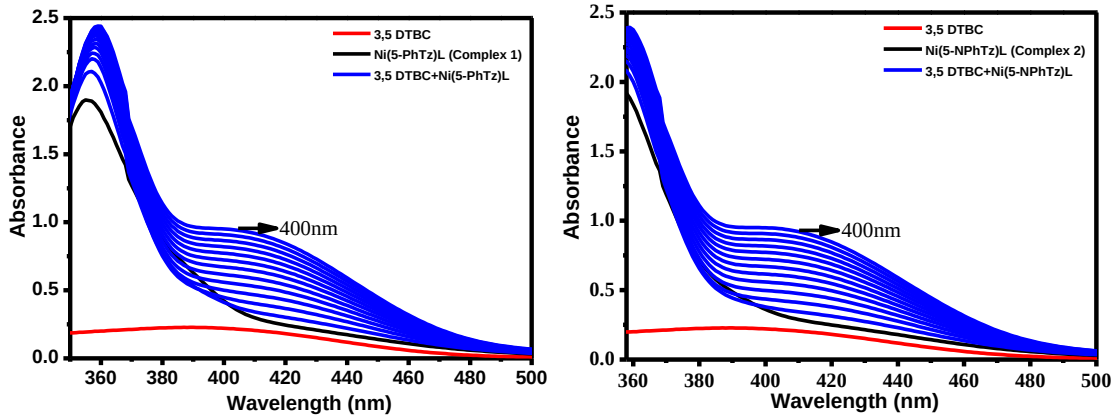

Figure 7.14. *Spectral pattern of catecholase activity over time for complex* ***1*** *and* ***2*** *after addition of 3,5-DTBC.*

To understand the kinetic aspects of catalysis for **1** and **2**, initial rate method was employed to determine the rate constant by analyzing the observed rate versus substrate concentration data based on Michaelis–Menten approach of enzymatic kinetics. The

Michaelis–Menten constant (K_M) and maximum initial rate (V_{max}) were determined by linearization using Lineweaver–Burk plots[23] for **1** (Figure 7.15).

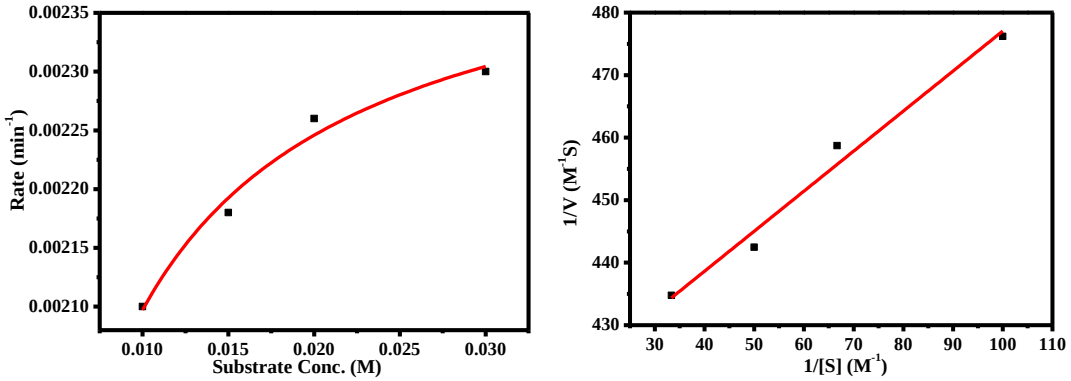

Figure 7.15. *Michaelies-Menten plot and Lineweaver Burk plot for complex **1**.*

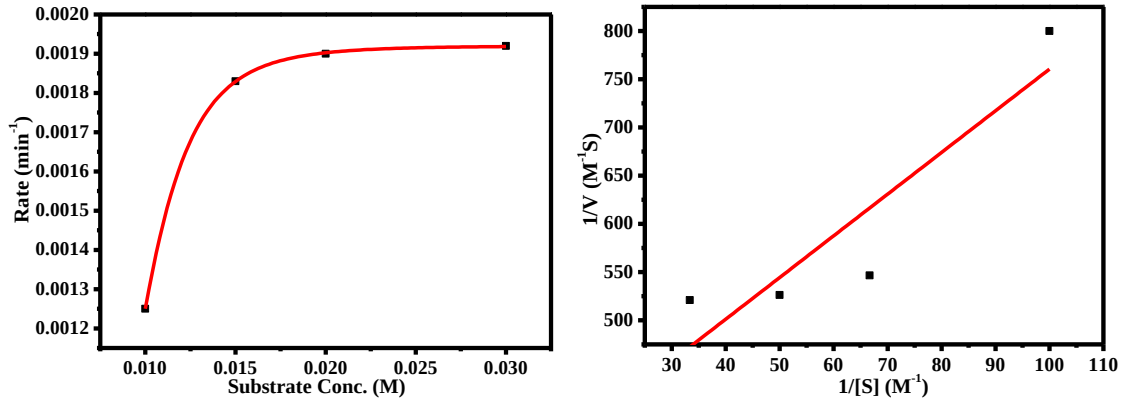

Figure 7.16. *Michaelies-Menten plot and Lineweaver Burk plot for complex **2**.*

The turnover number values (k_{cat}) were obtained by dividing the V_{max} values by the concentration of the corresponding complexes summarized in table 7.4. However, **2** shows marked deviation from simple linear kinetics (Figure 7.16) and a decrease in the rate is observed at higher concentration (150 equivalent or more), making it unfeasible to determine the kinetic parameters. However, all the data demonstrate both the complexes are acting as a catalyst towards oxidation of 3,5-DTBC at lower substrate concentration.

Table 7.4. *Various kinetic parameters of catecholase activity.*

Complex	Fixed complex /catalyst conc. (M)	Vmax (M min^{-1})	Std. error	K_M (M)	Std. error	Kcat/ T.O.N. (h^{-1})
Complex 1	.0001	.00245	2.33227×10^{-4}	0.00132	0.00143	1.470×10^{3}
Complex 2	.0001	.00192	2.72756×10^{-6}	0.00916	0.0000208345	0.115×10^{3}

To examine the probable reaction pathway and intermediate formed during the oxidation reaction, we have investigated the probable complex-substrate intermediate through ESI-MS, the change in d-d transition band of Ni(II) upon interaction with 3,5-DTBC through UV-vis spectroscopy and formation of H_2O_2 during the reaction by oxidation of $[Fe(phen)_3]^{2+}$ complex spectrophotometrically. ESI-MS positive spectrum of a 1:100 mixture of 1 and 3,5-DTBC, recorded after 5 min of mixing, exhibits two major peaks at *m/z* = 243 and 463, respectively, which correspond to quinone-sodium aggregates $[(3,5\text{-DTBQ})Na]^+$ and $[(3,5\text{-DTBQ})_2Na]^+$ (Figure 7.17).[24] Another smaller peak at 515.3 may be due to the formation of complex aggregate "A" (Figure 7.18) with a little deviation which is similar to an earlier report.[25]

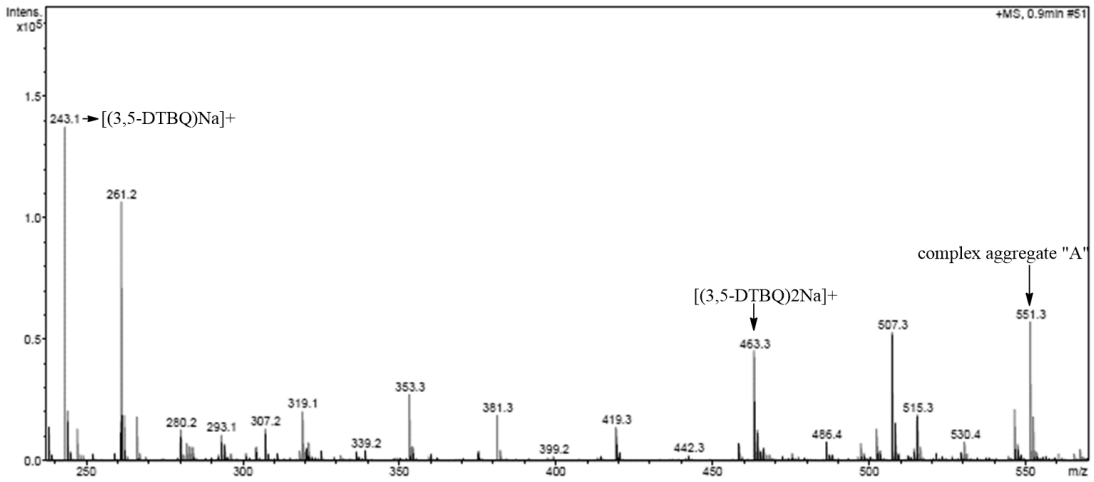

Figure 7.17. *ESI-MS spectra of DTBC after treatment with complex 1 after 10 minutes.*

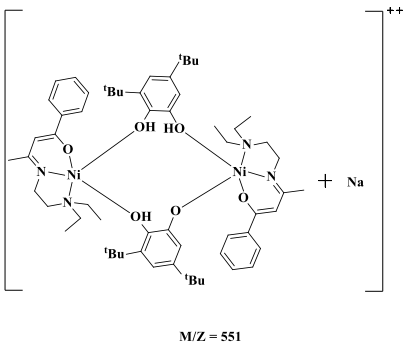

Figure 7.18. *Probable structure of complex aggregate "A".*

Monitoring the catalytic reaction through UV–vis spectroscopy reveals the formation of a very broadband at 700–800 nm gradually (Figure 7.19). This indicates a change of coordination environment around the nickel center from four-coordinate to five- or six-coordinate.[26,27]

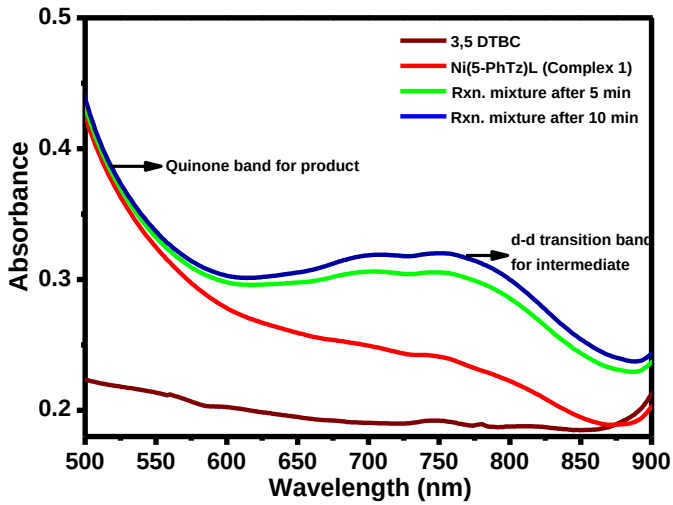

Figure 7.19. *Change in d-d transition band of Ni(II) with time upon reaction with 3,5-DTBC for complex* ***1****.*

Another interesting feature is the formation of H_2O_2 during the catechol oxidation reaction from atmospheric oxygen. To detect the formation of H_2O_2 UV–visible spectroscopy has been utilized. The experiment is based on the reaction between the ferrous ion (Fe^{+2}) and 1,10-phenanthroline in the presence of complex and 3,5-DTBC.

Ferrous ion forms a tri-phenanthroline complex with a reddish-orange color which absorbs at 509 nm. It is known that if hydrogen peroxide is added to the ferrous ion before the addition of 1,10-phenanthroline, then H_2O_2 will oxidize all the ferrous ion to ferric ion inducing no formation of a red-orange complex with 1,10-phenanthroline and a sharp reduction at 509 is expected. This concept has been exploited for the determination of H_2O_2 in the samples as per a previous report.[15] Herein, we took advantage of this experiment such that after adding ferrous ion and 1,10-phenanthroline to the complex solution, its UV spectrum is recorded, which shows an absorption band at 509 nm. However, when the DTBC solution is added to the complex solution along with ferrous ion and 1,10-phenanthroline, a sharp decrease in absorbance spectra is seen after 10 min (Figure 7.20). Moreover, the absorption band at 509 nm completely vanishes after 25 min. This reduction trend clearly indicates the absence of Fe^{+2}-triphenanthroline complex. This is because of the formation of H_2O_2 in catechol oxidation as it converts all the ferrous ion to ferric ion leading to the disappearance of the characteristic band at 509 nm. This result confirms the generation of H_2O_2 from aerial oxygen during the oxidation reaction.

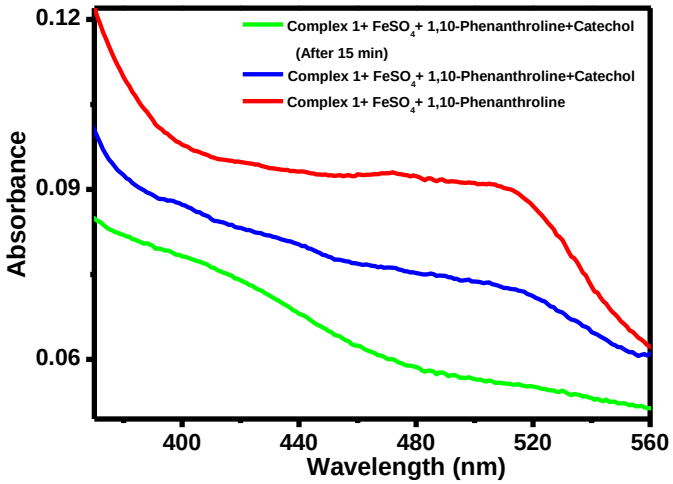

Figure 7.20. Detection of H_2O_2 using 1,10-phenanthroline for complex **1**.

7.4 Conclusions

A [2 + 3] dipolar cycloaddition between nickel ligated azide and two different organonitriles has been utilized to generate two new tetrazolato complexes *viz.* [NiL(5-

phenyltetrazolato)] (**1**) and [NiL{5-(4-pyridyl)-tetrazolato}] (**2**). Both complexes have been characterized by various spectroscopic tools, NMR spectroscopy, X-ray crystallography, and elemental analyses. The serum albumin protein binding and photophysical properties of the complexes have been explored. Furthermore, catecholase-like properties of both complexes have been studied, which is first for the nickel tetrazolato complexes. Both complexes have moderate catechol oxidation properties which tend to decrease at the higher substrate to catalyst ratio. ESI-MS study has been utilized to identify the probable intermediate and role of aerial oxygen during oxidation reaction is also investigated.

7.5 References

[1] Saha M., Das M., Nasani R., Choudhuri I., Yousufuddin M., Nayek H. P., Shaikh, M. M., Pathak, B., Mukhopadhyay, S. (2015), Targeted water-soluble copper–tetrazolate complexes: interactions with biomolecules and catecholase like activities, Dalton Trans., 44, 20154-20167 (DOI: 10.1039/C5DT01471A)

[2] Mukhopadhyay S., Mukhopadhyay B. G., Silva, M. F. C. G. D., Lasri J., Charmier M. A. J., Pombeiro A. J. (2008), Pt (II)-promoted [2+ 3] cycloaddition of azide to cyanopyridines: convenient tool toward heterometallic structures, Inorg. Chem., 47, 11334-11341 (DOI: 10.1021/ic8014223)

[3] Dong R. T., Ma Z. Y., Chen L. X., Huang L. F., Li Q. H. Hu, M. Y., Shen M. Y., Li C. W., Deng H. (2015), Zinc and cadmium metal-directed coordination polymers: in situ flexible tetrazole ligand synthesis, structures, and properties. Cryst. Eng. Comm., 17, 5814-5831 (DOI: 10.1039/C5CE00939A)

[4] Zhong D. C., Wen Y. Q., Deng J. H., Luo X. Z., Gong Y. N., Lu T. B. (2015), Uncovering the role of metal catalysis in tetrazole formation by an insitu cycloaddition reaction: an experimental approach, Angew. Chem. Int. Ed., l54, 11795-11799 (DOI:10.1002/anie.201505118)

[5] Bhattacharya S., Roy S., Chattopadhyay, S. (2016), Tetrazolate bridged dinuclear photo-luminescent zinc (II) Schiff base complex prepared via 1,3-dipolar

cycloaddition at ambient condition, J. Coord. Chem., 69, 915-925 (DOI: 10.1080/00958972.2016.1153078)

[6] Liu Y. Q., Ren, G. J., Zhang, Y. H., Xu, J., Bu X. H. (2015), Constructing novel Cd(II) metal–organic frameworks based on different highly connected secondary building units via alteration of reaction conditions, Dalton Trans., 44, 20361-20366 (DOI: 10.1039/C5DT02987B)

[7] Hou Z. J., Liu Z. Y., Liu N., Yang E. C., Zhao, X. J. (2015), Four tetrazolate-based 3D frameworks with diverse subunits directed by inorganic anions and azido coligand: hydro/solvothermal syntheses, crystal structures, and magnetic properties, Dalton Trans., 44, 2223-2233 (DOI: 10.1039/C4DT03172E)

[8] Liu W. T., Li J. Y., Ni Z. P., Bao X., Ou Y. C., Leng J. D., Liu J. L., Tong, M. L. (2012), Incomplete spin crossover versus antiferromagnetic behavior exhibited in three-dimensional porous Fe (II)-bis (tetrazolate) frameworks, Cryst. Growth Des., 12, 1482-1488 (DOI: 10.1021/cg201569m)

[9] Meng G. X., Feng Y. M., Wang Y., Gao Y. L., Wan W. W., Huang X. T. (2015), Effect of pH on the self-assembly of three Cd(II) coordination compounds containing 5-(4-pyridyl) tetrazole: syntheses, structures, and properties, J. Coord. Chem., 68, 1705-1718 (DOI: 10.1080/00958972.2015.1024668)

[10] Pachfule P., Chen Y., Sahoo S. C., Jiang J., Banerjee R. (2011), Structural isomerism and effect of fluorination on gas adsorption in copper-tetrazolate based metal organic frameworks, Chem. Mater., 23, 2908-2916 (DOI: 10.1021/cm2004352)

[11] Nasani R., Saha M., Mobin S. M., Martins L. M., Pombeiro A. J., Kirillov A. M., Mukhopadhyay S. (2014), Copper–organic frameworks assembled from in situ generated 5-(4-pyridyl) tetrazole building blocks: Synthesis, structural features, topological analysis and catalytic oxidation of alcohols, Dalton Trans., 43, 9944-9954 (DOI: 10.1039/C4DT00531G)

[12] Saha M., Nasani R., Das M., Mobin S.M., Pathak B., Mukhopadhyay S. (2014), The effect of remote substitution on the formation of preferential isomers of

cobalt(III)-tetrazolate complexes by microwave assisted cycloaddition, Inorg. Chem. Front.,1, 599-610 (DOI: 10.1039/C4QI00089G)

[13] Saha M., Nasani R., Das M., Mahata A., Pathak B., Mobin S. M., Carrella L. M., Rentschler E., Mukhopadhyay S. (2014), Limiting nuclearity in formation of polynuclear metal complexes through [2+ 3] cycloaddition: synthesis and magnetic properties of tri-and pentanuclear metal complexes, Dalton Trans., 43, 8083-8093 (DOI: 10.1039/C4DT00378K)

[14] Shit S., Sen S., Mitra S., Hughes D. L. (2009), Syntheses, characterization and crystal structures of two square-planar Ni(II) complexes with unsymmetrical tridentate Schiff base ligands and monodentate pseudohalides, Transition Met. Chem., 34, 269-274 (DOI 10.1007/s11243-009-9189-9)

[15] Mukhopadhyay D., Dasgupta P., Roy D. S., Palchoudhuri S., Chatterjee I., Ali S., Dastidar S. G. (2016), A sensitive in vitro spectrophotometric hydrogen peroxide scavenging assay using 1, 10-Phenanthroline, Free Radicals & Antioxidants., 6, 124 (DOI: 10.5530/fra.2016.1.15)

[16] Mukhopadhyay S., Lasri J., Charmier M. A. J., da Silva M. F. C. G, Pombeiro, A. J. (2007), Microwave synthesis of mono-and bis-tetrazolato complexes via 1, 3-dipolar cycloaddition of organonitriles with platinum(II)-bound azides, Dalton Trans., 45, 5297-5304 (DOI: 10.1039/B709959B)

[17] Mukhopadhyay S., Mandal D., Ghosh D., Goldberg I., Chaudhury M. (2003), Equilibrium studies in solution involving nickel (II) complexes of flexidentate schiff base ligands: isolation and structural characterization of the planar red and octahedral green species involved in the equilibrium, Inorg. Chem., 42, 8439-8445 (DOI: 10.1021/ic0346174)

[18] Das M., Chatterjee S., Harms K., Mondal T. K., Chattopadhyay, S. (2014), Formation of bis (μ-tetrazolato) dinickel(II) complexes with N, N, O-donor schiff bases *via* in situ 1, 3-dipolar cyclo-additions: isolation of a novel bi-cyclic trinuclear nickel(II)–sodium(I)–nickel(II) complex, Dalton Trans., 43, 2936-2947 (DOI: 10.1039/C3DT52796D)

[19] Das M., Ghosh B. N., Rissanen, K., Chattopadhyay S. (2014), Anion modulated structural variations in copper (II) complexes with a semicarbazone Schiff base: synthesis, characterization and self-assembly, Polyhedron., 77, 103-114 (DOI: 10.1016/j.poly.2014.03.027)

[20] Krishnamoorthy P., Sathyadevi P., Cowley A. H., Butorac R. R., Dharmaraj N. (2011), Evaluation of DNA binding, DNA cleavage, protein binding and in vitro cytotoxic activities of bivalent transition metal hydrazone complexes, Eur. J. Med. Chem., 46, 3376-3387 (DOI :10.1016/j.ejmech.2011.05.001)

[21] Zhao P., Wei Q., Dong J., Ding F., Li J., Li L. (2016), Synthesis, structure and spectroscopic studies on DNA binding, BSA interaction of a nickel(II) complex containing L–methionine Schiff base and 1, 10-phenanthroline, J. Coord. Chem., 69, 2437-2453 (DOI: 10.1080/ 00958972.2016.1206657)

[22] Li X. W., Li X. J., Li Y. T., Wu Z. Y., Yan C. W. (2013), Syntheses and structures of new trimetallic complexes bridged by N-(5-chloro-2-hydroxyphenyl)-N′-[3-(dimethylamino) propyl] oxamide: cytotoxic activities, and reactivities towards DNA and protein, J. Photochem. Photobiol., 118, 22-32 (DOI:10.1016/j.jphotobiol.2012.10.009)

[23] Caglar S., Adiguzel E., Sariboga B., Temel E., Buyukgungor O. (2014) Mono and dinuclear copper (II) naproxenato complexes containing 3-picoline and 4-picoline: synthesis, structure, properties, catechol oxidase, and antimicrobial activities, J. Coord. Chem., 67, 670-683 (DOI: 10.1080/00958972.2014.891198)

[24] Sarkar S., Majumder S., Sasmal S., Carrella L., Rentschler E., Mohanta, S. (2013) Triple bridged μ-phenoxo-bis (μ-carboxylate) and double bridged μ-phenoxo-μ1, 1-azide/μ-methoxide dicopper(II) complexes: syntheses, structures, magnetochemistry, spectroscopy and catecholase activity, Polyhedron., 50, 270-282 (DOI: 10.1016/j.poly.2012.10.050)

[25] Banu K. S., Chattopadhyay T., Banerjee A., Bhattacharya S., Suresh E., Nethaji M., Zangrando E., Das D. (2008), Catechol oxidase activity of a series of new dinuclear copper(II) complexes with 3, 5-DTBC and TCC as substrates:

syntheses, X-ray crystal structures, spectroscopic characterization of the adducts and kinetic studies, Inorg. Chem., 47, 7083-7093 (DOI: 10.1021/ic701332w)

[26] Gatteschi D., Scozzafava, A. (1977), Single crystal polarized electronic spectra of a five-coordinate macrocyclic complex of nickel(II), Inorg. Chim. Acta, 21, 223-227 (DOI:10.1016/S0020-1693(00)86265-9)

[27] Adhikary J., Chakraborty P., Das S., Chattopadhyay T., Bauza A., Chattopadhyay S. K., Ghosh B., Mautner F. A., Frontera A., Das D. (2013), A combined experimental and theoretical investigation on the role of halide ligands on the catecholase-like activity of mononuclear nickel(II) complexes with a phenol-based tridentate ligand, Inorg. Chem., 52, 13442-13452 (**DOI:** 10.1021/ic401819t)

Chapter 8

General Conclusions and Future Scope

Chapter 8

General Conclusions and Future Scope

8.1 General Conclusions

Design and fabrication of novel smart materials based on low molecular weight gelators have become a fascinating approach with manifold applications. It is well known that the driving force behind the formation of supramolecular self-assembly in low molecular weight gelators is the non-covalent interactions which enable them to be thermo-reversible, biodegradable, and fabricable with standard routes. The main goal of present work is to design low molecular weight based gelator and investigate their role in various inter-disciplinary fields. With this purpose, here newly synthesized low molecular weight nitrile substituted 1,3,5-benzene tricarboxamide (BTA), and tetrazole derived metal-organic crystalline, and gel materials are reported. The reported molecules have shown aggregation induce enhance emission (AIEE) and in one case self-healing ability which enables them to be utilized in sensing of cations, anions, and biomolecules. Apart from that, the probable utilization of the synthesized gels in bioinspired catalysis, anticancer drug-delivery and as photoluminescence material has been explored.

In **chapter 2** , **3 and 4**, synthesis of 4-cyanophenyl substituted BTA based gelator (**G1**), 3-cyanophenyl substituted BTA based gelator (**G2**), 2-cyanophenyl substituted BTA based gelator (**G3**), 4-cyanomethylphenyl substituted BTA (**G4**) and their metallogels with transition metal ions (Fe^{2+}, Fe^{3+}, Cu^{2+}, Zn^{2+}, Co^{2+}, Ni^{2+}, Ag^{+}, Cd^{2+}) have been presented. All the gelators (**G1**, **G2**, **G3,** and **G4**) show AIEE after gelation and selectively sense **Fe^{2+}/Fe^{3+}** (by **G1** and **G4**), **Fe^{2+}/Fe^{3+}**, **Ag^{+}** (by **G2**) and **Fe^{2+}** (by **G3 and G4**) by turning off the fluorescence. Furthermore, Among all the metallogels, **Cu(II)G1** can sense **SCN^{-}**, **Zn(II)G1** can sense **Br^{-}**, **Ni(II)G1** can sense **CN^{-}**, **Cu(II)G2** can sense of **I^{-}** , **Ni(II)G2** and **Co(II)G2** can sense **S^{2-}** by turning off the fluorescence whereas **Fe(II)G1/ Fe(III)G1** can sense **S^{2-}** by turning on the fluorescence. Apart from that, the

copper-based metallogel [**Cu(II)G2**] mimics as a bio-inspired catalyst for the conversion of catechol to quinone by aerobic oxidation in the gel state at room temperature and pressure (in **chapter 2**). Further, In **chapter 4**, a cobalt metallogel [**Co(II)G4**] has been presented which can sense L-tryptophan selectively among other essential amino acids in gel state as well in a complex structure like BSA protein in nano-molar level by drastic quenching of AIEE. The change is observable even by naked eyes. In **Chapter 5**, [3,5-bis{(4-(cyanomethyl)phenyl) carbamoyl} benzoic acid] (**G5**) and methyl 3,5-bis((4-(cyanomethyl)phenyl)carbamoyl benzoate (**Me-G5'**) (G5' = G5-H) have been synthesized and reported. Treatment of the **G5** gel with $[RuCl_2(\eta^6\text{-}p\text{-cymene})]_2$ leads to the formation of aruthenium-based metallogel [**Ru(II)G5**] by stabilizing ruthenium(II)-arene moiety in gel state *via* coordination through carboxylate donor site. The ruthenium(II) metallogel has been found to be pH sensitive, and treatment of the gel with lactic acid leads to gel collapse, and the ruthenium(II) ion has been found to be released as lactyl-lactato complex which has been found to be cytotoxic against different cancer cell lines. **G5** molecule has shown immense potential to disturb the MCT transport chain in cell division progression through molecular docking study. Furthermore, **Chapter 4** and **5** also reports the role of water as a solvent in sol to gel and sol to crystal transformation.

In **chapter 6**, synthesis of photoluminescent lanthanoids based metallogels *viz.* [**La(III)G6-Cl**, **La(III)G6-NO3**, **Pr(II)G6-Cl**, **Gd(III)G6-NO$_3$**] has been performed by using di(1*H*-tetrazole-5-yl) methane (1,5-DTM) as a ligand (**G6**). Among all lanthanoid based metallogels, the **La(III)G6-Cl** metallogel showed self-healing ability. **Chapter 6** also reports the crystal formation of **Gd(III)G6-NO$_3$** through confined metallogel space. In **chapter 7**, nickel complexes [NiL(5-phenyltetrazolato)] (**complex 1**) and [NiL{5-(4-pyridyl)-tetrazolato}] (**complex 2**) [HL = 3-(2-diethylamino-ethyl imino)-1-phenyl-butan-1-one] have been synthesized by microwave irradiation. These metal tetrazole complex have shown protein binding and bioinspired catechol oxidation.

8.2 Future scope

The addition of metal ion with LMW gelators tune the properties of both like conductivity, color, rheological behavior, adsorption, emission, photophysical properties, magnetism, biological activities, catalytic activities, redox activities, and self-healing. The LMW gelators incorporated with metal and triggered gelation which able them to apply in catalysis, sensing, biomedicine, electronics, and optical devices, nanogels materials, drug delivery, and more to come. As a future prospective, to the continuation of present thesis work, the nitrile substituted 1,3,5-benzene tricarboxamide (BTA) can be converted into tetrazole substituted 1,3,5-benzene tricarboxamide (BTA) which enhance the number of donor sites and able them to coordinated with metals in various ways (Scheme 8.1). The versatility in the coordination of metals with LMW tetrazole based gelators can be tested in various application from materials to biology (Figure 8.1).

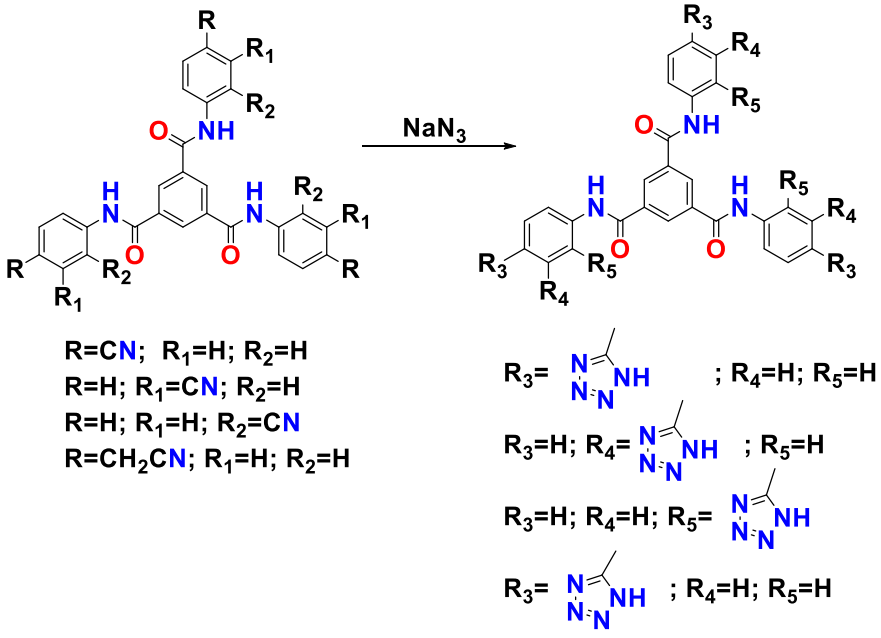

Scheme 8.1. Systematic scheme for the synthesis tetrazole substituted 1,3,5-benzene tricarboxamide (BTA).

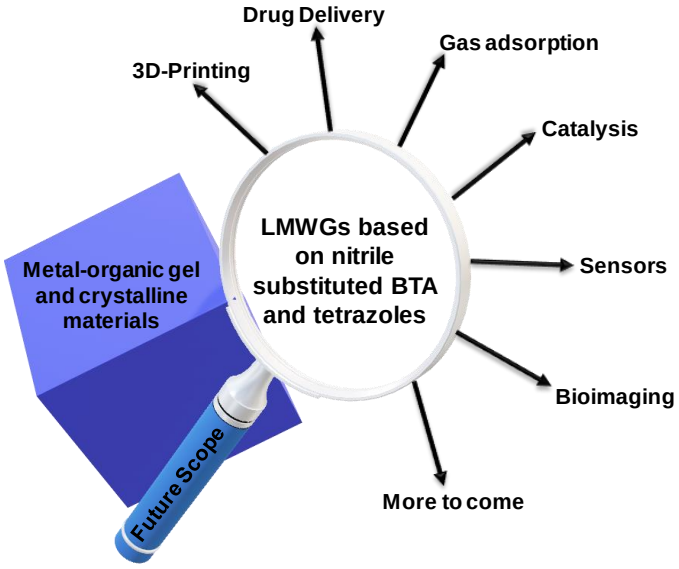

Figure 8.1. Applications of metal-organic gels and crystalline materials.

The investigation of new metallogels formed via LMW gelator with expected functionality is still largely serendipitous, and therefor, it creates major challenges to screen the types of interactions and structure elucidation. Thus, understanding of the metal ion triggered gelation with LMW gelators and tuning the various weak interactions to make the gels favorable for versatile applications are expected to be explored in a more rigorous manner in the near future.